COMBINING KNOWLEDGE AND INFORMATION - GRAPH-BASED DESCRIPTION OF DRIVING SCENARIOS TO ENABLE HOLISTIC VEHICLE SAFETY

Florian Bechler
ZF Friedrichshafen AG & Institute of Engineering and Computational Mechanics, University of Stuttgart
Germany

Jörg Fehr
Institute of Engineering and Computational Mechanics, University of Stuttgart
Germany

Fabian Neininger, Stefan Knöß, Bernhard Grotz
ZF Friedrichshafen AG
Germany

ABSTRACT

Currently, vehicle safety is based on knowledge from injury values, crash pulses, and driving kinematics which leads to intervention strategies separated into isolated domains of active and passive safety. In this contribution, it is shown how vehicle safety can be approached holistically, allowing for human-centered and scenario-based safety decision-making. For this purpose, information from interior and exterior vehicle sensors can be linked by a mathematical framework, combining the knowledge that is already available in the individual domains. A universal graph representation for driving scenarios is developed to master the complexity of driving scenarios and allow for an optimized and scenario-based intervention strategy to minimize occupant injury values. This novel approach allows for the inclusion of sub-models, expert knowledge, results from previous simulations, and annotated databases. The resulting graph can be expanded dynamically for other objects or occupants to reflect all available information to be considered in case of urgency. As input, interior and exterior vehicle sensor data is used. Further information about the driving situation is subsequently derived from this input and the interaction between those states is described by the graph dynamically. For example, occupant attentiveness is derived from measurable eye gaze and eyelid position. From this quantity, reaction time can be estimated in turn. Combined with exterior information, it is possible to decide on the intervention strategy like e.g. alerting the driver. Physical or data-based functional dependencies can be used to represent such interactions. The uncertainties of the inputs and from the surrogate models are included in the graph to ensure a reliable decision-making process. An example of the decision-making process, by modeling the states and actuators as partially observable Markov decision process (POMDP), shows how to optimize the airbag efficiency by influencing the head position prior to an impact. This approach can be extended by additional parameters like driving environment, occupant occupancy, and seating positions in further iterations to optimize the intervention strategy for occupants. The proposed framework integrates scenario-based driving dynamics and existing knowledge from so far separated safety systems with individual activation logic and trigger points to enable holistic vehicle safety intervention strategies for the first time. It lays the foundation to consider new safety hardware, sensor information, and safety functions through a modular, and holistic approach.

INTRODUCTION

Since the 1950s, people have been thinking about how to make driving safer. In [1] and [2] a seatbelt was presented to prevent occupants from being thrown out of the car in the event of an accident. However, it became a legal requirement much later, see Fig. 1. Shortly afterward, it became clear how important it is to manage the energy of a crash properly. It was realized that high accelerations and impacts on the human body have to be prevented. Thus, a crumple zone and a solid passenger cabin became indispensable. In the 1990s, first series-produced airbags were introduced to increase crash mitigation and occupant protection, which further reduced peak loads on the human body by controlling the crash energy even better. With further inventions such as a belt force limiter, a knee airbag, a belt pretensioner, and an activated headrest, the mitigation of the impact, also described as passive safety, for the occupant was optimized.

The development of accident avoidance in addition to accident mitigation, began in the early 1990s to further reduce fatal and serious accidents. Whereas systems were previously only developed to be activated in the event of an impact, at the time of accident t_0, from now on functions were also developed to be activated before a possible accident, i.e. $t < t_0$, also known as active safety systems and advanced driver-assistance system (ADAS). For the first time, systems intervened in the driving dynamics. Following anti-lock braking systems (ABS) and electronic stability control (ESC) other systems like the automated emergency brake and various warning functions were developed in the 2000s, [3]. The development of vehicle safety from crash mitigation to crash avoidance is shown in Fig. 1.

To make this possible and prevent collisions before they happen, it is necessary to sense the environment and collect information. The need for sensors on the vehicle grew. The further ahead of the impact the intervention is required, the more sensor information and knowledge about the current driving situation are necessary [4]. The availability of sensors on and inside the vehicle grows to make active safety functions and advanced driver-assistance systems possible. The development is going further and further in this direction, especially in the interior, sensors are the enabler for comfort functions. For example the interior sensors enable small functions such as gesture control. But also in conditional autonomous driving, changing seating positions is a function made possible by interior monitoring, or also an assessment of how distracted the driver is and whether he can react to a dangerous situation.
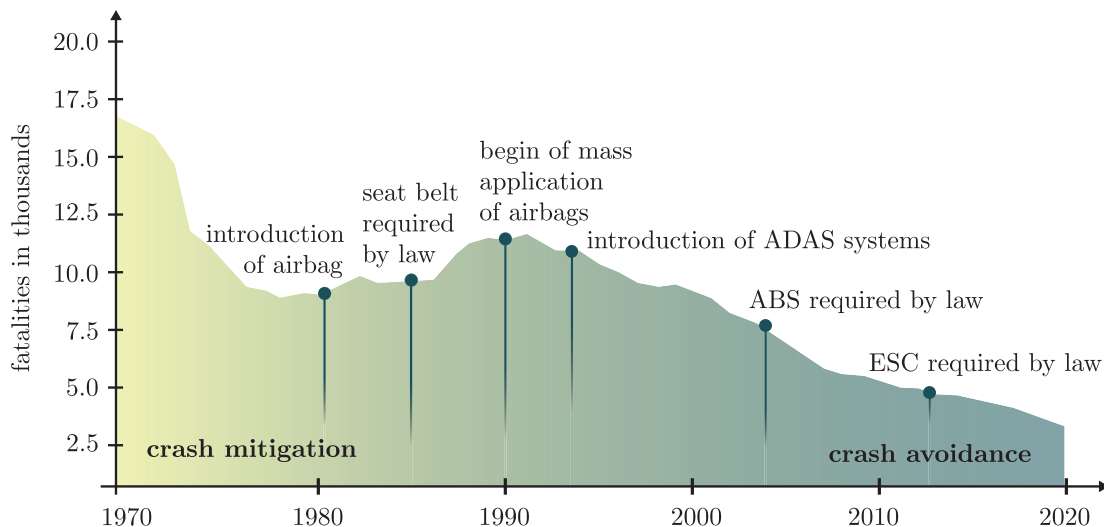

Figure 1: Development of vehicle safety [5] and fatalities on Japanese roads [6].

VISION

Despite those developments, developing safe vehicles and safe traffic is a challenge due to (i) changes in mobility solutions, (ii) the possibility to hand over driving tasks to the automated driver, or (iii) taking new seating positions. Covering the increased parameter space is not easy. Reasons are the increasing complexity but also because previous developments are based on minimizing harm to occupants in standard load cases. Those load cases are defined by national and international authorities and the safety functions are optimized to solve these load cases as reliably as possible.

To target the increased complexity and to increase vehicle safety to protect occupants better, the next step is the combination of all existing system knowledge with the information available due to the growth in sensor and data availability. In this work, a novel graph-based approach for such a holistic vehicle safety is presented. In Fig. 2 a small example scenario is depicted to show how complex decision-making can be facilitated in a presumably simple driving scenario. It also demonstrates what needs to be taken into account to protect the occupant in the best possible way in dangerous driving situations. The example exhibits a driving car with increasing road traffic. As time passes, the vehicle in front begins to decelerate and the driver would have to brake in order to prevent an accident. The driver misses the chance to brake because of distraction and the question is, how is it now possible to optimally protect the occupant in the given situation? The first step is to determine which variables are of interest at which point in time.

The vehicle under test (ego vehicle, E) is colored in green, whereas potential accident opponents ($B_{\{1,2,3\}}$), referred to as bullets hereinafter, are in black. Figure 2(a) describes the uncritical driving of the ego vehicle on an empty two-lane road with only one occupant, the driver, in the car. In the next time step Fig. 2(b) the road becomes more crowded. Besides a leading vehicle B_1 in front of the ego, another vehicle B_2 is driving in the second lane. If the B_1 decelerates, shown in Fig. 2(c), ideally detectable via the taillights, the ego vehicle needs to react and has different options. If the time-to-collision (TTC) is larger than the time-to-brake (TTB), it is still possible to stop before a collision occurs. However, if the TTC is smaller than the TTB, it has to be evaluated if a rear-end collision could be worse and should be avoided. For this evaluation, the head position and seating position of the driver is important because it determines how effective passive safety systems can be in the event of a collision. The driver in Fig. 2 is not in an ideal position for a full-frontal impact. As the left lane is blocked (B_3) and there is also an obstacle (O) on the right side, an evasive maneuver also influences the safety strategy. To exploit the safety potential of the airbag, the driver should be moved towards the center. This can be achieved by a collision on the passenger side of the vehicle, as shown in Fig. 2(d), which would be possible since the passenger seat is not occupied, making this particular scenario less critical.
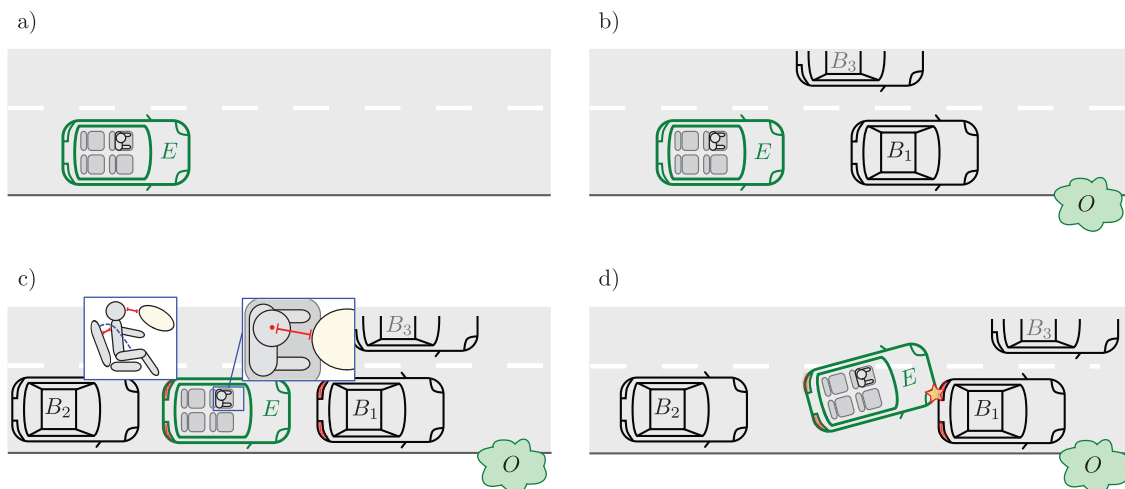

Figure 2: Evolution of a driving scenario (a)-(c) with ego vehicle (green) and bullet vehicles (black).

This small scenario shows that for each phase of the sequence specific input is required for safety decisions, both directly measurable and derived from sensor data, e.g. the TTB or the TTC are calculated from the ego vehicle dynamics and the bullet's velocity and position. However, there is a lot of research and development in the different domains, and scenarios like this can't be solved with separated and isolated systems and models. For example, there are already many physical approaches to describe and predict the movements of other vehicles [7]. Surrogate models exist to estimate the driver's head movement as a function of vehicle acceleration [8]. Furthermore, expert knowledge and data-based approaches exist to describe, for example, the driver's attention [9]. So a variety of mathematical descriptions of different contexts already exists at different levels of quality. But these models exist and many things can already be sensed, there is for example, no autonomous emergency braking system that takes the driver's drowsiness into account.

The challenge is combining the sensor information and all the knowledge already available in the domains to make an optimal safety decision for the occupant and tackle the problem holistically. The crucial point in such an approach is to know and take into account the uncertainties in the sensors and the limitations of the surrogate models so that the decision-making becomes reliable. In addition, the safety strategy must be traceable in retrospect, which precludes the use of black box models. To reach the goal and move towards a function that can optimally control driving safety actuators and fulfill the requirements, a simulation environment is set up that makes it possible to test different approaches. The simulation environment makes it possible to synthesize sensor signals and identify the most crucial parameters and relations. Furthermore, the virtual microscope simulation tells use which decision methodology is useful and how the gained information can be reused in further safety functions. Last but not least the information acquisition is highly dependent on available sensors and the proposed safety strategy on available safety actuators in the car, which requires a modular framework. Conversely, the modular approach makes it possible to integrate new security functions, new surrogate models, or new actuators directly into the framework.

FRAMEWORK

To achieve this a simulation framework is set up. The first step is to simulate and formulate a driving scenario. Based on the driving scenario and the vehicle, sensor models can then be used to simulate the data that the vehicle's sensors would provide. This augmented sensor data is then forwarded to the mathematical model of the driving scenario. Here, further information is derived from the sensor data, and the calculated variables and their dependencies are set in context. The mathematical description consists of several sub-models to calculate states. The exact structure is described in the following. The calculated states are then passed on to a decision-making process and a driving safety strategy is developed based on the mathematical description of the scenario. The safety intervention decision and its timestamp are then fed back to the driving scenario. The simulation framework described is depicted in Fig. 3.
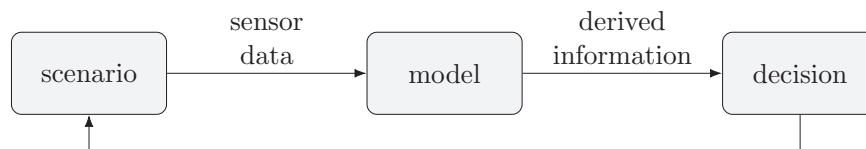

Figure 3: Simulation framework from scenario generation to decision-making.

Scenario Simulation and Input Data

When creating the driving scenario pool, scenarios in which only vehicles participate in traffic are currently being examined. For the dynamics of the vehicles, single-lane models are used. Subsequently, the ego vehicle is equipped with sensor models of cameras-, LIDAR-, or radar-modules. The use of sensor models is very important, as it is essential to take into account uncertainties that occur in reality

in order to make a reliable decision later. In addition to the external perception, it is also important to consider the information about the occupants based on interior sensors. The ability to simulate the behavior of occupants is still rather limited, which is why annotated data from databases are used and merged with the appropriate simulated driving scenario. In Table 1 the simulated and used quantities are listed. It is important to note that the sensors in the vehicle have different measuring frequencies. In this work, the signals are all sampled to the same frequency before further processing, and it is therefore assumed that all signals are in sync for the time steps.

Table 1:
Measurable quantities interior and exterior of the vehicle.

exterior data		interior data	
objects	· type	driver	· eyeglance
	· size		· hands-On
	· position		· eye closure
	· velocity		· head position
	· yaw		
setting	· environment	Other Occupants	· Seat occupancy

Mathematical Description of the Driving Scenario - Combining and Deriving Information

With the simulated sensor information now collected, the goal is to derive as much information as possible about the current driving situation. In doing so, it should be possible to use existing mathematical or data-based and expert knowledge to estimate or calculate non-measurable variables. To meet these requirements and in addition allow dynamic reaction to objects that appear in the driving scenario a graph description [10], [11] of the driving scenario is chosen. The graph description is based on the concept of a bipartite graph. The nodes of the graph represent the different states of the driving scenario. The edges represent the dependencies between these states. The edges are directed, which means that the direction of the edge indicates the direction of the dependency. In Fig. 4 the definition of the nodes and the edges are given. The state objects inherit attributes from the type objects. State objects are for example the position, velocity, and yaw of an object. Type objects are, e.g. a car, a pedestrian, or a bicycle. For example, if another car is detected by the sensor and the activation condition is met being a potential bullet, all states belonging to that bullet vehicle are added dynamically to the graph.

The edges contain the function that describes the relationship between two states. In the functions, already-known relationships are applied. For example, physical models, such as motion models [7], data-based models, such as behavioral models of road users [12], or models that reflect expert knowledge, such as the Karolinska sleepiness scale (KSS) [9], are used to define the edge functions.

In order to explain how the representation appears as a graph and what it actually can contain, the representation of the example scenario from Fig. 2 is shown in Fig. 5.

Starting with Fig. 5(a) on the top of the setting in which the vehicle is driving is represented, in (orange). It only has one sensor input describing if the car is driving in a rural environment, on a highway or in a highly dynamic city environment. Below the setting, the ego vehicle (green) is defined. The measurable input values for the ego vehicle are typically the acceleration and the steering angle. From those, other kinematic states can be calculated a trajectory can be derived afterward with the help of a motion model. Below is a description of the last object that occurs in the first frame of the driving scenario, the driver, in (red). The measurable input variables are head position, hands-on detection, head position, and eye closure detection, according to Table 1. It can be seen that the driver has a connection to both the vehicle and the environment. The connection to the vehicle is necessary to predict the head position, as this is strongly related to the trajectory being driven [8]. The connection to the environment describes the

relationship between the driver's attentiveness and the setting in which the driver is currently driving. For example, in highly dynamic urban traffic, a high level of attentiveness is more important than on a quiet country road. Those three objects (driver, ego vehicle, environment) are always active assuming we consider vehicles, where a driver is still needed. The small section in Fig.5 shows that a trajectory can be determined with the help of a constant turn rate and acceleration (CTRA) motion model, the accelerations and the velocities. In the next frame Fig. 2(b) another vehicle appears in front of the ego. This potential bullet vehicle is reflected in (blue), in Fig. 5(b). In the simulation, the activation e.g. the relevance of the bullet object is checked.
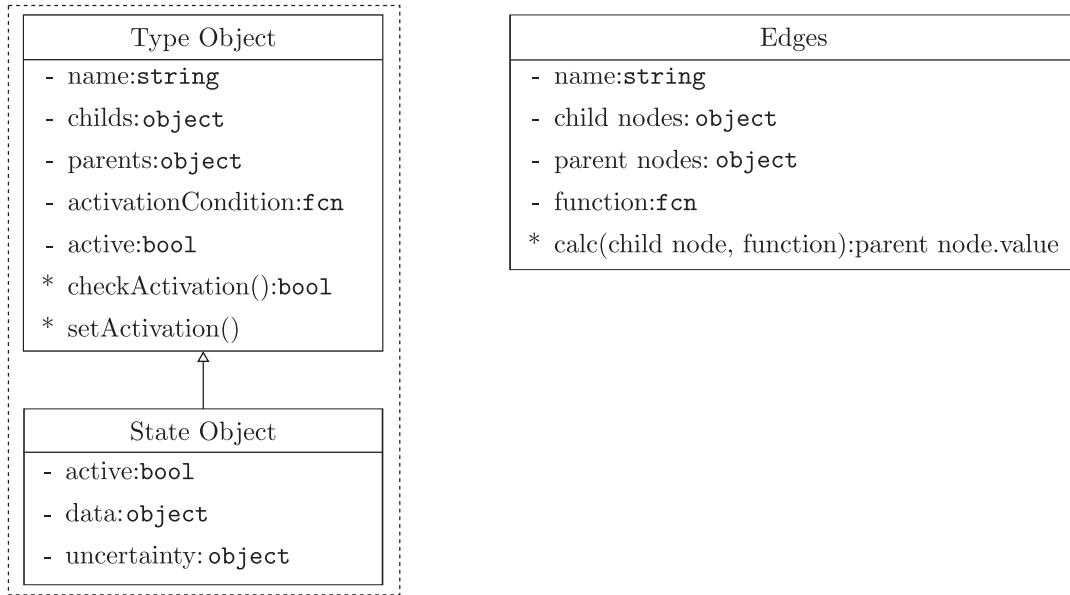

Figure 4: Definition of the node and edge objects of the graph including attributes and function.
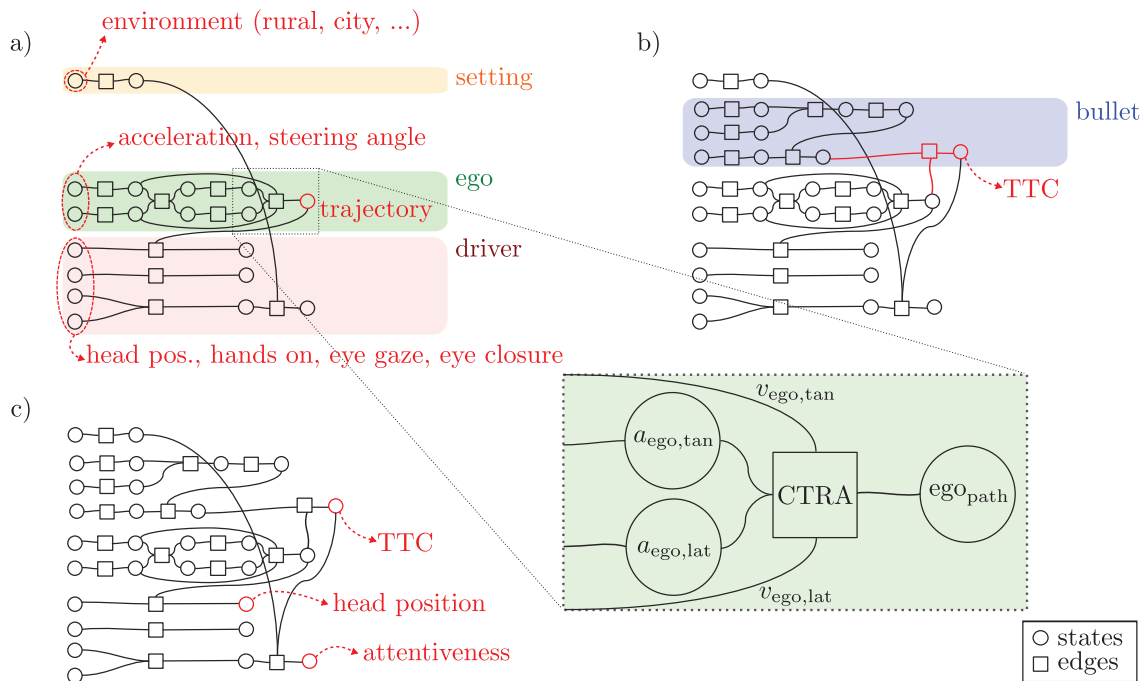

Figure 5: Graph representation of the evolving driving scenario presented in Fig. 2.

For this purpose, it is evaluated whether the activation condition is fulfilled, e.g. the bullet moves below a certain distance from the ego the object with its states is added to the graph. The basis of the kinematic characterization is the measurable states: position, velocity, and yaw angle. Similar to the ego vehicle, a potential driving trajectory can be determined from them with the help of a motion model. Together with the trajectory of the ego vehicle, a time to collision can now be calculated, which is highlighted in red. In the example scenario, the leading vehicle is now decelerating and states like the head position, the attentiveness, the surrounding area, and the TTC are important values to develop a safety strategy to optimally protect the occupants. Now the question is how to make a decision based on the information gained.

With this modeling and implementation, it is now possible to describe a scenario mathematically over time. It is possible to describe the development of the scenario dynamically and thus also take changes into account. Derived from this, the variables relevant to vehicle safety are calculated. With the information gained about the driving scenario, the next crucial step is reliable decision-making.

Decision-Making

In an attempt to make the right decision for the occupant, the problem is formulated as a Markov decision problem. A Markov decision process is a combination of states and actions but with a probability distribution over the outcome of the actions. For example, one wants to travel from state A to state B ($\{A, B\} \in \mathcal{S}$) in the shortest possible time and has the choice between the actions: taking the train, walking or cycling, ($\{\text{train,walk,bike}\} \in \mathcal{A}$). The probability of heavy traffic or of the train being late can be modeled as a probability distribution. The Markov decision process considers the probabilities and chooses the best action.

Since many important states of the safety decision problem cannot be measured directly, but are derived from measurable parameters, it is generalized as a partially observable Markov decision problem (POMDP) [13]. The POMDP is formulated as a tuple

$$\{\mathcal{S}, \mathcal{A}, O, T, Z, R\}, \tag{1}$$

with the state space $\mathcal{S}$ describing all states of the scenario and $\mathcal{A}$ representing the possible actions, e.g. the actuators of the car that could be triggered. To reflect the uncertainties the decision are based on the so-called observation space O, which describes the observable states. The observation function Z describes the probability of observing o when being in state s and taking action a. The transition function T describes the probability of transitioning from state s to state s' when taking action a. The reward function R describes the reward for being in state s and taking action a. The reward is a scalar value and is defined as the expected value of the reward function.

To make this approach a little more accessible, an example implementation is described below. In this example, the aim is to influence the driver's head position before the collision so that the airbag is as effective as possible. Figure 2 shows a sketch of the driver in bird's eyes view.
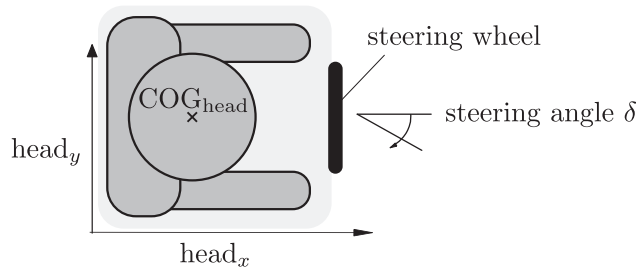

Figure 6: Outline of the POMDP scenario from a bird's eye view.

From this the state space is defined as $\mathcal{S} = \{\text{head}_x, \text{head}_y, a_{\text{ego}}, \delta_{\text{ego}}\}$ representing the head position of the occupant, the acceleration a of the vehicle, and the steering angle δ. The action space $\mathcal{A} = \{a_{\text{ego}}, \Delta\delta_{\text{ego}}, \text{BP}\}$ represents a deceleration a_{ego}, a steering intervention $\Delta\delta_{\text{ego}}$, and the activation of a two

staged belt pretensioner BP to restrain the occupant. Two-stage means that the belt pretensioner can activate an electronic retractor with a limited force and a pyrotechnic retractor with a stronger force. It is defined as $BP \in \{0, 1, 2\}$, with 0 = no activation, 1 = electronic retractor, 2 = pyrotechnic retractor. While the electronic retraction can be used several times, the pyrotechnic retraction is depleted after one firing. The steering intervention and the deceleration are also discretized, which makes the whole action space discrete. The observation space $O = \{head_{O,x}, head_{O,y}, a_O, \delta_O\}$ reflects the uncertainties between the actual states and the sensor data. Both, state and observation space are continuously defined. The transitions from state s and an action a to the new state s' are given by $T(s, a, s')$. The assumption is made, that the steering angle only influences the y-position of the head, whereas the belt pretensioner and the deceleration only influence the x-position. Pseudo-physical formulas are used for the transition function, which describes the relationship between vehicle acceleration, steering angle, and belt pretensioner to head position. To reflect the uncertainties in the sensors the observation probabilities $T(s, a, o)$ represent the dependency between the observation o and the real state s, which can be derived from sensor specifications or model validations. Finally, a reward function $R = (s, a, s')$ tells the algorithm which actions will bring the head closer to the desired target position, which is assumed to be $head_{tar} = [30\,cm, 35\,cm]$. Additionally, deceleration is always rewarded to minimize the crash energy. Choosing a feasible reward function and weighting the target correctly is not an easy task and requires further investigation, especially if more states and more actions are considered.

Figure 7 shows the results of the POMDP for the example scenario in the x-direction on the left column and in the y-direction on the right column. The black dashed line represents the desired head position, the blue line the actual head position, and the pink line the observation of the head position. The time decreases as it represents the time to collision, so the collision occurs at $t = 0\,s$.
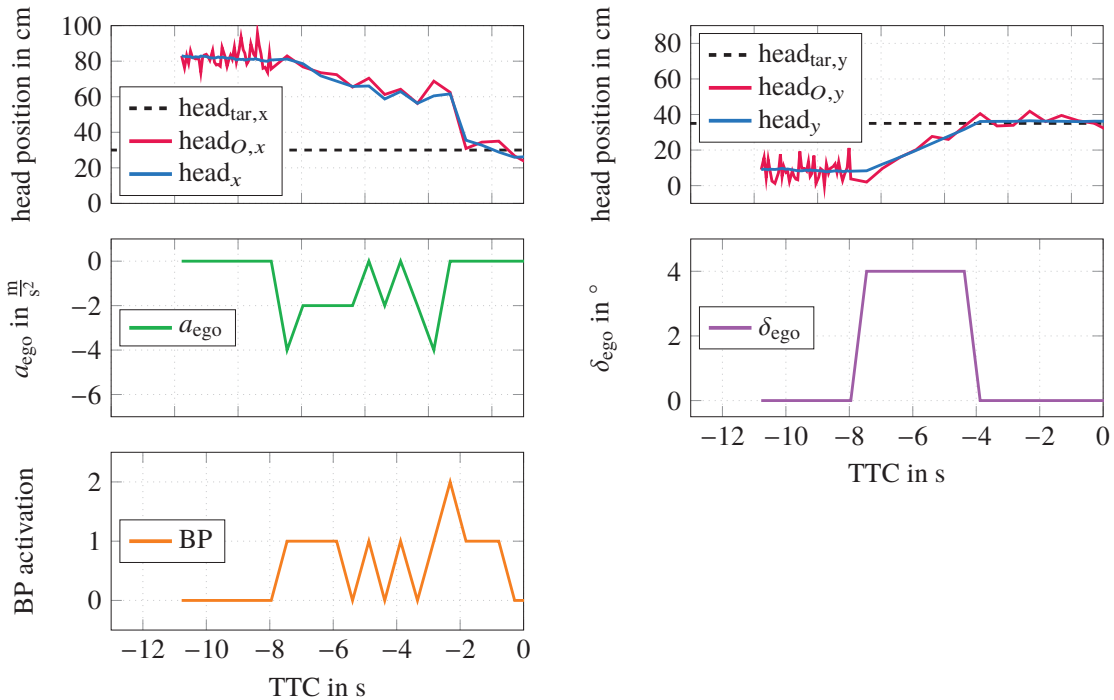

Figure 7: Results of a POMDP to optimize the head position before a collision.

The green line shows the chosen deceleration of the vehicle and the orange line the activation of the belt pretensioner. It is shown that the pyrotechnic belt tensioner is activated shortly before impact and the deceleration is set as high as possible. The algorithm is therefore able to find the solution. In y-direction the head position is influenced by a steering intervention, which is shown with the purple line. However, the methodology is not yet directly linked to the graph description, it is the goal to do this in the next

step. Then the observable states would come directly from the graph. Another challenge is currently the computation time. The solution of the POMDP was calculated with a sample-based approach, where 200 samples are calculated per time step. All samples search a tree to a predefined depth and look at which combination of actions maximizes the reward. The described model calculates about 0.2 s for a 50 ms time step, on a 4 x 3.4 GHz CPU, which is too slow for a real-time application. Especially when even more states and even more actions case to be considered, the computation time becomes even longer. However, it is necessary to optimize the POMDP for computational efficiency.

Tools

Within this framework, different tools are used. The scenario simulations run in Matlab using a proprietary toolbox in which single-track models are used for the vehicle dynamics and sensor models to augment the sensor data. The results are forwarded in `csv`-format to the graph which is implemented in Julia [14], to meet the more object-orientated requirements. The decision-making process, e.g. the POMDP, is also defined and solved in Julia using the `POMDPs.jl` [15] package and a DESPOT algorithm [16], an optimized tree search, as an online solver to grant fast evaluations and calculations.

INTEGRATION INTO CURRENT DEVELOPMENT PROCESSES

Currently, such a centralized approach can not be included in current vehicle with due to distributed control systems. However, in nearly all vehicle domains is an increase in electrically controlled functions and their complexity increases the number of electrical and electronic modules and the necessary communication requirements. New electrical/electronic (E/E) architectures that will keep the complexity of future vehicle systems manageable are constantly developed. The core element is the change from today's domain-specific to a cross-domain and centralized E/E architecture with a few but very powerful vehicle computers instead of many individual control units. That allows flexibility in the function development but also hardware independence. The developments in the other domains will enable such a holistic driving safety system becoming real. It will not only be possible but also the necessary step to achieve the goal of the software-defined vehicle. This holistic and modular approach allows for adding new functions as well as actuator-sensor combinations for future vehicle sensors and interior designs. The direction described above sets sensed quantities into context and a decision is made based on that. The aim is to be able to use the framework other directions in the future. In doing so, the insight should be used to determine which states have to be changed in order to make the situation safer for the occupant. This allows inferences to be drawn about which actuators are important in which driving scenarios and where there is still potential for actuator and function development.

CONCLUSION, CHALLENGES & OUTLOOK

In this work, an approach was presented to integrate vehicle safety from separated systems into a holistic decision-making process under inclusion of existing knowledge. The development of a holistic approach away from separate systems and load case optimization is the next logical step in the evolution of vehicle safety. A simulation framework was described which contains the whole chain from input data to decision-making. Starting with a simulation of driving scenarios and sensor data, it was described how this data can be further processed and how the existing knowledge and models can be used to link the variables in a meaningful way. Therefore, a graph representation was chosen which allows the application to a dynamically changing driving scenario. It was then described how a partially observable Markov decision process can be used to find a reliable, deterministic, safety strategy based on the mathematical description of the scenario and the available actuators.

However, the system is deterministic, the validation is very difficult for such an approach because of the high complexity. Covering the almost infinite variety of possible driving scenarios, and interactions between road users, humans, and machines and passing them on in a deterministic decision-making process is not an easy task. Another challenge is the computational efficiency of the microcontrollers

currently used in vehicles. Actuators in passive safety, such as the airbag, have activation times in the millisecond range. A decision computation in such a small time span would not be possible with current vehicle technology. Nevertheless, the computational performance in vehicles is constantly increasing, which also makes more complex evaluations possible. Last but not least, one has to think about what happens in case of a system failure. The dynamic modeling of the problem can well cover the failure of individual sensors and actuators, but not if the central system that makes the decisions and triggers the actuators is not working. It would be a possibility to have a redundant system running as a backup. Overcoming these challenges is the crucial step for the cross-system evaluation of driving scenarios and the further development of driving safety. When the software-defined vehicle with actuators becomes a reality, it will be the next step toward increased road safety for all stakeholders.

ACKNOWLEDGEMENTS

REFERENCES

[1] Shelden, C. H. (1955). Prevention, the Only Cure for Head Injuries Resulting from Automobile Accidents. Journal of the American Medical Association, 159(10), pp.981–986. DOI: 10.1001/jama.1955.02960270001001

[2] Bohlin, N. I. (1961). Patent No. DE1101987B, Germany.

[3] Winner, H., Hakuli, S., and Wolf, G. (2009). Handbuch Fahrerassistenzsysteme: Grundlagen, Komponenten und Systeme für aktive Sicherheit und Komfort. Springer, Wiesbaden. DOI: 10.1007 978-3-8348-9977-4

[4] Grotz, B., Straßburger, P., Huf, A., and Roig, L. (2021). Predictive safety - Preception-Based Activation of Pre-Crash Systems. ATZ worldwide, 1, pp.18–24. DOI: 10.1007 s38311-020-0620-3

[5] Hay, J. (2022). A Surrogate Model-Enhanced Simulation Framework for Safety Performance Assessment of Integrated Vehicle Safety Systems. Schriften aus dem Institut für Technische und Numerische Mechanik der Universität Stuttgart, Ph.D. Thesis, Vol. 75. Shaker, Aachen. ISBN 978-3-8440-8727-7

[6] National Police Agency, Traffic Bureau (2022). Traffic Accidents and Fatalities Over Time (from 1966); https://www.npa.go.jp, accessed: 2022-02-11.

[7] Schubert, R., Richter, E., and Wanielik, G. (2008). Comparison and Evaluation of Advanced Motion Models for Vehicle Tracking. pp.1 – 6. DOI: 10.1109/ICIF.2008.4632283

[8] Cyrén, O. and Johansson, S. (2018). Modeling of Occupant Kinematic Response in Pre-Crash Maneuvers. Master's thesis, Department of Mechanical and Maritime Sciences, Chalmers University of Technology, Gothenburg, Sweden.

[9] Shahid, A., Wilkinson, K., Marcu, S., and Shapiro, C. M. (2011). Karolinska Sleepiness Scale (KSS). In STOP, THAT and One Hundred other Sleep Scales, pp.209–210. Springer. DOI 10.1007 978-1-4419-9893-4_47

[10] Gienger, A. (2021). Combining Model- and Data-based Methods for Process Monitoring and Fault Diagnosis (in German). Universität Stuttgart, Ph.D. Thesis. Shaker, Aachen. ISBN 978-3-8440-8461-0

[11] Bechler, F., Jörg, F., Neininger, F. T., Grotz, B., and Knöß, S. (2022). Bipartite Graph Modeling of Critical Driving Scenarios - an Occupant Safety Perspective. In MATHMOD 2022 Discussion Contributions, ARGESIM Report, No. 17, Vienna, Austria. DOI: 10.11128/arep.17.a17060

[12] Robin, T., Antonini, G., Bierlaire, M., and Cruz, J. (2009). Specification, Estimation and Validation of a Pedestrian Walking Behavior Model. Transportation Research Part B: Methodological, 43:36–56. DOI 10.1016/j.trb.2008.06.010

[13] Åström, K. (1965). Optimal Control of Markov Processes with Incomplete State Information. Journal of Mathematical Analysis and Applications, 10(1), pp.174–205. DOI 10.1016/0022-247X(65)90154-X

[14] Bezanson, J., Edelman, A., Karpinski, S., and Shah, V. B. (2017). Julia: A Fresh Approach to Numerical Computing. SIAM review, 59(1), pp.65–98. DOI 10.48550/arXiv.1411.1607

[15] Egorov, M., Sunberg, Z. N., Balaban, E., Wheeler, T. A., Gupta, J. K., and Kochenderfer, M. J. (2017). Pomdps. jl: A Framework for Sequential Decision Making Under Uncertainty. The Journal of Machine Learning Research, 18(1), pp.831–835.

[16] Somani, A., Ye, N., Hsu, D., and Lee, W. S. (2013). DESPOT: Online POMDP Planning with regularization. Advances in neural information processing systems, 26. DOI 10.48550/arXiv.1609.03250

COMPARISON OF INJURY SEVERITY PREDICTION USING SELECTED VEHICLES FROM REAL -WORLD CRASH DATA

Susumu Ejima,
Tsukasa Goto
SUBARU Corporation
Japan

Peng Zhang,
Kristen Cunningham,
Stewart Wang
University of Michigan, International Center for Automotive Medicine
USA

Paper Number 23-0034

ABSTRACT

Advances in automotive telemetry technology have the potential to predict occupant severity from vehicle conditions at the time of an accident, and appropriate triage, as well as transport to a trauma center, can greatly improve subsequent treatment. The National Automotive Sampling System Crashworthiness Data System (NASS-CDS: 1999-2015) was used to filter for new case selection criteria based on vehicle type and matched to Subaru vehicle categories. We have proposed four types of injury severity prediction algorithms that were matched with the categories of Subaru vehicles. Specifically, 1) ISP model that categorized the principal direction of force (PDOF) into four impact directions (front, left, rear, and right) , 2) ISP-R model that considers the effect of the right-front passenger in addition to the four impact directions, 3) ISP-f1R model that represents PDOF as a continuous function using periodic basis splines, called functional data analysis, and 4) ISP-f2R model in which the knot position was modified in 3). In this study, five-fold cross-validation was performed within the training data (NASS-CDS 1999-2015) to evaluate the performance of these four models. In addition, external validation was performed using the National Automotive Sampling System Crash Investigation Sampling System (NASS-CISS: 2017-2019). The results of the cross-validation showed that the area under the receiver operating characteristic curve (AUC) was used to evaluate the model performance, which was 0.854 for the ISP model and 0.862 for the ISP-R model, indicating that the ISP-R, which considered the influence of the right-front passenger, was more accurate. The AUC values were 0.847 for the ISP-f1R model and 0.856 for the ISP-f2R model using a continuous function for the direction of impact, indicating that the ISP-R model had the highest AUC value among the models. On the other hand, the validation results with NASS-CISS were 0.817 for the ISP model and 0.828 for the ISP-R model, and 0.831 for the ISP-f1R model and 0.828 for the ISP-f2R model, indicating that all models had AUC values above 0.8. The important factors for the occupant injury prediction algorithm were delta-V, belt use, age, and crash direction, and the presence of a right-front occupant was a significant injury risk modifier, especially in side impact crashes.

INTRODUCTION

Advanced Automatic Collision Notification (AACN), which determines the severity of possible injuries to occupants in traffic accidents, was expected to not only shorten the time to initiate patient care, but also save patients' lives by selecting the hospital to which they will be transported based on appropriate triage [1]. According to a report [2] by the Centers for Disease Control and Prevention (CDC) Field Triage Task Force, the triage process consists of four stages (physiological, anatomic, mechanical, and special considerations). In the third, "mechanics," the effectiveness of predicting severity based on data transmitted from telematics has been demonstrated.

Research on injury severity prediction algorithms for automobile occupants [3-8] has been conducted in the United States since around 2000. As mentioned above, the background of this research was the appropriate triage decision during emergency medical care, which started with the determination of the injury level of the occupants based on the damage to the exterior and the interior of the vehicle during an accident. The existence of an underlying traffic accident database was essential to the development of the injury severity prediction algorithm, and the contribution of the extensive traffic accident database conducted in the United States [9-10] was extremely significant.

The CDC report [1] recommends that a patient with a predicted probability of serious injury of more than 20% was considered to be at high risk of serious injury and should be taken to an appropriate trauma center and treated accordingly. The severity used in injury prediction algorithms was mainly the Maximum Abbreviated Injury Scale (MAIS), which is the maximum value of the Abbreviated Injury Scale (AIS) [11], and the Injury Severity Score (ISS) [12], an index used to evaluate multiple trauma. Augenstein et al. [3] constructed the URGENCY algorithm using MAIS as the severity and several effective variables, which has been applied to BMW vehicles and verified using actual accidents [13]. Kononen et al.[5] developed a vehicle-level injury severity prediction model for each of the four impact directions using ISS, which was applied to the GM OnStar service. Subsequently, Wang et al. [14] improved the model and proposed a method to replace the crash direction with a continuous function using Principle Direction of Force (PDOF), which has been verified in actual accidents as an algorithm for each passenger seating position. Various injury prediction algorithms [15-17] have also been studied in Japan, and an injury prediction algorithm [18] has been integrated into the AACN called D-Call Net [19], which was now in practical use. The severity of injury was calculated based on the injuries (fatal, serious, minor, and non-injury) listed in the Japanese traffic accident database (Institute for Traffic Accident Research and Data Analysis: ITARDA) [20], and the injury probability of the occupant was calculated based on pseudo-delta-V, crash direction, belt use, age, and other factors.

In this study, the ISS, which has a high correlation with the fatality rate, was used as the severity of injury as an algorithm for predicting injuries to Subaru vehicles in the United States. Specifically, we focused on the vehicle category to which Subaru vehicles belong and conducted logistic regression analysis based on NASS-CDS [9] data to develop four ISPs models. The algorithms were based on NASS-CDS (1999-2015), and these algorithms were validated using the cross-validation with NASS-CDS and the latest dataset, NASS-CISS (2017-2019) [10], to clarify the characteristics of injury prediction by different models. We believe that the AACN provides a baseline for vehicle safety performance and post-accident safety (including emergency medical care) in actual accidents. By continuously improving this injury severity prediction algorithm, we can contribute toward "zero" traffic fatalities, one of the pillars of a safe transportation system.

METHODS

Data Source

Although there were various vehicle damage situations included in NASS-CDS, from a practical point of view, the variables used in the algorithm were based on the information transmitted by vehicle telematics, i.e., information obtained from the EDR (Event Data Recorder). As for the information about the occupants, the variables were age and gender, which may be obtained by the telematics service provider operators during an emergency call. The reason for setting these restrictions on variables was to reflect the current state of information available from current vehicle telematics systems.

For NASS-CDS (1999-2015) and model years 2000 or later were filtered using new case selection criteria based on vehicle type to match Subaru vehicle categories. Since limiting the sample to Subaru-make vehicles would result in a smaller sample size, we expanded our scope to investigate the vehicle belong to Subaru vehicle categories. The vehicle category was defined by limiting the study cohort to only the vehicle types recently produced by Subaru. We used the NHTSA standard definitions of passenger cars and sport utility vehicles (SUVs) as defined in the NASS-CDS coding [21]. The cohort was selected using the following specific vehicle codes: 02, 04, 05, and 06 are passenger cars and 14, and 15 are SUVs (Table 1).

An additional inclusion criterion for this study was that the principal direction of force (PDOF) was known. The PDOF was the direction of force input during a collision and was calculated from the longitudinal and lateral delta-V measured from the EDR. Then, the PDOF was used to classify four impact directions as shown in Figure 1(a): Frontal (11,12 or 1 o'clock), Left-side (2-4 o'clock), Rear (5-7 o'clock), and Right-side (8-10 o'clock). Furthermore, instead of classifying the PDOF into four impact directions, we used a statistical analysis called functional data analysis [14] where cyclic basis splines were used to model the PDOF curve as shown in the Figure 1(b). Vehicles that sustained a non-horizontal event, such as a rollover, were excluded. The number of collisions was classified into single or multiple.

The occupant and injury parameters were based on the following criteria. Belt status was available as "all front-occupants belted" vs. "at least one front-occupant unbelted", since the injury severity prediction was created at the vehicle level. We did not consider the belt status of rear-seat passengers because current Event Data Recorders (EDRs) might not sense presence or rear-seat occupants. The age threshold was set at 55 years [14], and the presence of elderly passengers was defined as whether there was one passenger aged 55 years or older. The presence of female passengers was defined as if there was one female passenger. In addition, the presence or absence of a right-front passenger was taken into account in this analysis, so the front-right

passenger was also categorized as either "present" or "absent".

ISS, defined as sum of the squares of the AIS of the three most significantly injured body regions, were available. The models were designed to predict ISS at the vehicle level. We chose highest ISS among the any of occupants. The total number of identified NASS cases that matched these conditions was 7,351. Table 2 lists the variables used in the analysis.

Table 1 Select body type from NASS-CDS

NASS-CDS Code	Body type	SUBARU Category
02	Car	2-door sedan, hardtop, coupe
04		4-door sedan, hardtop
05		5-door/4-door hatchback
06		Station Wagon (excluding van and truck-based)
14	Utility	Compact Utility (Utility Vehicle Categories "Small" and "Midsize")
15		Large utility
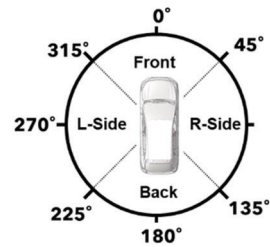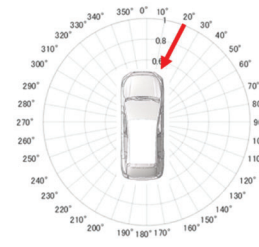
(a) Four impact directions   *(b) PDOF as continues curves*

Figure 1 Two different methodology using PDOF

Injury Prediction Model

In this study, four different algorithms were proposed. First, an algorithm that categorizes PDOF into four impact directions (front, right, rear, and left) according to Kononen et al.[5] and predicts whether someone in the vehicle has a high probability of being seriously injured using vehicle and occupant factor was developed. In addition, an algorithm that takes into account the influence of the right-front passenger was also developed. Next, following Wang et al.[14] statistical analysis, called functional data analysis, was employed to represent the PDOF effect as a continuous function, and periodic basis splines were used to model the PDOF curves. The key factor here was the number of basis splines (degrees of freedom). The greater the number of splines, the finer the PDOF curve can be obtained, which depends on the number of data. In defining the PDOF curve, two models with different knot positions were proposed. The knot position can "shift" the basis curve to focus on a specific region. Two methods were used here: the traditional method of choosing knots where there were many data points, i.e., according to the quantile of the data, and the forced method of setting knots because 0, 90, 180, and 270 degrees were known to be transition points. Note that the effect of the right-front passenger was taken into account in both models.

The four different algorithms were developed here using logistic regression models to predict the probability of sustaining ISS 15+ injuries.

1. ISP: Model without consideration of presence of right-front passenger.
2. ISP-R: Model with consideration of presence of right-front passenger.
3. ISP-f1R: Functional data analysis using PDOF and quantile-based knot selection using PDOF.
4. ISP-f2R: Functional data analysis using PDOF and knot selection based on impact direction.

Restricting the vehicle category from Subaru might also limit the usefulness of certain predictors. For example, the majority of the Subaru were passenger cars and small to midsize SUVs. Vehicle type was less heterogeneous

and thus might or might not be strongly associated with injury risk. The stepwise procedure was used to select a subset of more relevant features to construct the final algorithm. The concept of using a statistical approach was to predict a 20% probability of ISS 15 or greater and the importance of each variable defined within a predictive model. Logistic regression models were fitted under the NASS sampling schema to investigate ISS 15 or greater injury with different configurations of the variables which was defined Table 2. In this study, the algorithm using the NASS-CDS, was developed as the basis to predict injury. The logistic regression equations are as follows:

$$P(ISS\ 15+) = \frac{1}{(1 + exp(-z))} \qquad\qquad Equation\ (1)$$

$$z = \beta_0 + \sum_{i=1}^{n} \beta_i x_i \qquad\qquad Equation\ (2)$$

where *P (ISS 15+)* is the probability that the ISS is 15 or greater (considered to be a serious injury level), β_0 was the intercept, β_i were the coefficients of the predictors x_i, and *n* is the number of predictors. These coefficients were shown in Table 2. It is necessary to have a cutoff value for *P (ISS 15+)*. The CDC Expert panel's recommendations for development of an injury risk algorithm specified a probability cutoff value of 0.2 using ISS. In another word, probability of 0.2 was defined as a serious injury at the crashes. In this study, this cutoff value was used with *P (ISS 15+)*.

Selection of variables for inclusion in the predictive models was done using forward and backward stepwise regression [22] to determine a final model. Starting from the null model, in each step, the criteria to add or remove one variable minimize Akaike information criteria (AIC) [23]. AIC was an information criterion that addresses the trade-off between the goodness of fit of the model and the complexity of the model. AIC was used in the stepwise variable selection in developing the predictive model. AIC includes a penalty that increases when the number of estimated parameters increases. Therefore, this penalty discourages over-fitting. The procedure stopped when AIC cannot be improved, and the final model was outputted. The performance of regression models was assessed with AIC and area under the curve (AUC) characteristic [24] which represents the model sensitivity as a function of specificity. The data analysis was conducted using R 4.1.1[25] with packages survey, pbs, and MASS.

Table 2 Predictor variable used in models that are able to be measured from vehicle telemetry or call center from the vehicles belong to Subaru category.

Variables	Categories
Delta V (mph)	Change in velocity (logarithm of Delta V)
Direction of impact	Four directions (Front/Left/Right/Rear) or
	PDOF (0 to 350 degree in 10-degree increment)
Vehicle Type	Car, Utility (MY 2000 and new car)
Number of Events	Single, Multiple
Belt Use	Belted, Unbelted
Right-front Passenger	Presence of right-front passenger
Age	At least one greater than 55 years
Gender	At least one female

Validation

Model validation was important to evaluate the expected prediction accuracy in the field. Five-fold cross validation [26] was performed within the training data (NASS-CDS 1999-2015) to evaluate model performance. The cross-validation delivered a merged version of all five validation data sets. By merging them, one summary was presented. Furthermore, we also externally validated the developed algorithms using the Crash Investigation Sampling System (CISS) cases. NASS-CISS is the improved NASS sampling scheme which better reflects the current population, newer vehicles, and enhanced injury coding. The number of cases by Subaru vehicle type identified from NASS-CISS was 1,163. NASS-CISS has a higher weighting than NASS-CDS, which means it represents more cases. Performance measures such as AUC were used to assess the accuracy of the developed predictive model.

RESULT

Statics Analysis

A statistical analysis was applied to the databases used (NASS-CDS, NASS-CISS) to quantify the contribution of each variable related to injury. Table 3 shows the comparison of each predictor between ISS 15+ vs. ISS 15- by each database. The numbers indicate the mean value of delta-V, and percentages for other categorical variables. In addition, t-test and Chi-squared test were used respectively for delta-V and other categorical variables for statistical comparison. The proportion of frontal impact was high as the direction of impact. The ISS 15+ in particular has a higher percentage of side impact from the left side. In terms of vehicle type, both categories have high percentages of Car. As for multiple collisions, ISS 15+ tended to have a higher rate, and the rate of seat belt use was higher for ISS less than 15. The proportion of right-front passenger was higher in ISS 15+, and the proportion of elderly occupants was higher in ISS 15+. Gender was not significantly different between the two groups. On the other hand, for NASS-CISS, a similar trend to that of NASS-CDS was observed, however, for each direction of impact (ISS 15+), the percentage of rear-end impact was higher than that of NASS-CDS, while the percentage of right-side impact was lower. Furthermore, the percentage of multiple collisions (ISS less than 15) was smaller than that of the NASS-CDS.

Table 3 Means and standard deviations of key variables stratified by ISS 15+ vs. ISS 15-. in NASS-CDS and NASS-CISS.

Variables		NASS-CDS(1999-2015) n=7,351			NASS-CISS(2016-2017) n=1,163		
		ISS 15+	ISS 15-	p-value	ISS 15+	ISS 15-	p-value
Delta V (mph)		29.0	20.4	<0.001	23.7	20.7	<0.001
Direction of impact	Front	55.3%	72.1%		59.9%	75.9%	
	Left	23.0%	7.1%	<0.001	13.1%	5.5%	0.013
	Right	17.8%	9.6%		8.6%	7.6%	
	Rear	3.9%	11.3%		18.4%	11.0%	
Vehicle type	Car	84.5%	79.7%	0.009	84.2%	81.3%	0.607
	Utility	15.5%	20.3%		15.8%	18.7%	
Number of Multiple Events		65.8%	54.1%	0.002	61.9%	29.1%	0.020
Seatbelt usage		63.3%	84.1%	<0.001	57.0%	83.9%	0.123
Presence of right-front passenger		38.5%	21.6%	<0.001	35.2%	18.5%	0.032
Presence of passengers older than 55 years		39.3%	17.5%	<0.001	27.4%	24.5%	0.069
Presence of female passengers		64.8%	60.6%	0.115	55.3%	58.5%	0.449

Logistic regression analysis was performed using the subject vehicles defined in the previous section to create ISPs and determine their contribution to each predictor variable. Table 4 shows the results of the coefficients of each variable in the logistic regression models (ISP, ISP-R, ISP-f1R, and ISP-f2R) using the stepwise variable selection method. p-values less than or equal to 0.05 were shown in bold. The most significant variable in the analysis was delta-V, which was common to all models. For each impact direction, ISP and ISP-R showed a relatively higher risk than the other impact directions from "left-side" impact. On the other hand, ISP-f1R and ISP-f2R, which approximate the PDOF effects with continuous functions, were represented by periodic curves (C1, C2, C3, C4) and have four degrees of freedom. The coefficients in the table approximate the effect of PDOF by combining the four curves and indicate the optimal degree of fitting. In addition, belt use was found to be a significant variable in all models. Age was found to be the most important variable among the factors related to the occupants. For ISP-R, in which the effect of the right-front passenger was taken into account, the variable for right-side impact (far side) was found to be significant. Although ISP-f1R and ISP-f2R were not significant, the selection of variables by AIC was an important factor to improve the accuracy of the model. On the other hand, only the ISP model selected gender differences as a predictor.

Table 4 Estimation of coefficients for variables from the ISPs (ISP, ISP-R, ISP-f1R, ISP-f2R).

Parameters		ISP	ISP-R			ISP-f1R	ISP-f2R
Intercept		-15.900	-16.559			-13.842	-12.754
ln Delta-V (mph)		**4.049**	**4.125**			**4.229**	**4.171**
Direction of impact	Front	0.481	0.470	PDOF	C1	-5.642	-6.076
	Left	**2.245**	2.586		C2	1.969	1.347
	Right	1.617	1.382		C3	**-2.989**	**-3.238**
	Rear	0.000	0.000		C4	**-2.588**	**-3.908**
Belt use	Belted	**-1.350**	**-1.250**			**-1.283**	**-1.256**
	Unbelted	0.000	0.000			0.000	0.000
Vehicle type	Utility	**-0.467**	-0.459			-0.499	-0.472
	Car	0.000	0.000			0.000	0.000
Number of events	Multiple	0.382	0.391			0.351	0.356
	Single	0.000	0.000			0.000	0.000
Presence of older occupants	55 or greater	**1.516**	**1.477**			**1.517**	**1.534**
	Under 55	0.000	0.000			0.000	0.000
Presence of right-front passenger	Front	-	0.847	PDOF	C1	2.222	1.026
	Left	-	-0.326		C2	-1.138	-0.220
	Right	-	**1.262**		C3	1.322	0.519
	Rear	-	0.648		C4	0.495	1.123
Presence of females	At least one female	-0.257	-			-	-
	No female	0.000	-			-	-

Algorithms were compared by their sensitivity and specificity the NASS-CDS with the five-fold cross-validation and the NASS-CISS. The sensitivity and specificity of the models when the cutoff values were varied from 0.10, 0.15, 0.20, 0.25, and 0.30 were shown in Table 5-6. The area under the receiver operating characteristic curve (AUC) results were also shown as a measure of the model's performance.

When the PDOF was categorized into four impact directions, the ISP-R model showed higher sensitivity than the ISP model by taking into account the influence of the right-front passenger, and there was no significant difference between the two models in terms of specificity. The models with PDOF represented as continuous functions (ISP-f1R, ISP-f2R) showed lower sensitivity values than ISP-R. No significant differences in specificity were observed for all models. The AUC, which evaluates model performance, was highest for the ISP-R model, followed by ISP-f2R, ISP-f1R, and ISP. On the other hand, validation using NASS-CISS showed that the ISP and ISP-R models, which were modeled with four impact directions, showed different trends depending on the value of the cutoff. Compared to the ISP model, the sensitivity of ISP-R varied depending on the cutoff value. The model using a continuous function for PDOF showed a similar trend, with ISP-f2R showing a slightly higher sensitivity than ISP-f1R. There was no significant difference in specificity among all models. The AUC was higher for ISP-f1R, followed by ISP-f2R, ISP-R, and ISP.

Table 5 Comparison of sensitivity and specificity with the five-fold cross-validation with the ISP, ISP-R, ISP-f1R and ISP-f2R.

NASS-CDS (Five-fold cross-validation)

cutoffs	ISP		ISP-R		ISP-f1R		ISP-f2R	
	sensitivity	specificity	sensitivity	specificity	sensitivity	specificity	sensitivity	specificity
0.10	0.580	0.903	0.586	0.900	0.581	0.906	0.579	0.899
0.15	0.493	0.946	0.518	0.943	0.461	0.945	0.474	0.946
0.20	0.430	0.965	0.451	0.966	0.389	0.968	0.406	0.967
0.25	0.370	0.976	0.401	0.978	0.349	0.979	0.360	0.977
0.30	0.324	0.986	0.353	0.983	0.316	0.984	0.320	0.983
AUC	0.854		0.862		0.847		0.856	

Table 6 Comparison of sensitivity and specificity with the NASS-CISS with the ISP, ISP-R, ISP-f1R and ISP-f2R.

NASS-CISS

cutoffs	ISP		ISP-R		ISP-f1R		ISP-f2R	
	sensitivity	specificity	sensitivity	specificity	sensitivity	specificity	sensitivity	specificity
0.10	0.658	0.896	0.652	0.909	0.652	0.899	0.653	0.894
0.15	0.533	0.928	0.444	0.929	0.465	0.931	0.512	0.934
0.20	0.389	0.953	0.376	0.954	0.385	0.944	0.414	0.953
0.25	0.289	0.963	0.333	0.969	0.342	0.964	0.347	0.967
0.30	0.230	0.969	0.240	0.971	0.282	0.969	0.284	0.972
AUC	0.817		0.828		0.831		0.828	

DISCUSSION

In this study, four different algorithms were developed using the NASS-CDS (1999-2015) to predict injuries focused on vehicles belonging to the Subaru category. The results showed that all algorithms showed higher risk curves for front, right, rear, and left impacts than Kononen et al.[5]. The main reason was the effect of limiting the vehicle body types in the NASS-CDS coding to 2, 4 to 6 for passenger cars and 14 and 15 for utility vehicles among the Subaru vehicle types. Subaru vehicles were relatively small or medium-sized, and the difference in vehicle body weight may have resulted in the higher risk curves.

The contribution to each predictor was determined from the results of the logistics regression model using the stepwise variable selection method. Delta-V, belt use, and age were common to all models as factors with high contribution, and in particular, delta-V was found to be the factor with the highest contribution rate. In the models (ISP and ISP-R) for the four impact directions, the contribution from the left-side impact was large, which was similar to other literature [27-28]. For the models that represent PDOF as a continuous function (ISP-f1R, ISP-f2R), the maximum number of degrees of freedom was four (C1, C2, C3, C4), even when the number of data was over 7,000 cases. In the end, a primary effect with PDOF as a continuous function and a secondary effect due to the presence of the right-front passenger were modeled with four degrees of freedom. Wang et al. [15] used 10 degrees of freedom for the PDOF periodic function and five degrees of freedom for the effect of the right-front passenger. For the four impact directions (front, right, rear, and left) model, the degree of freedom was three, indicating that the advantages of the functional data analysis were not fully demonstrated compared to the impact direction model.

The effect of the secondary effect was determined for the case with a right-front passenger in each crash direction (ISP-R) and for the models with continuous PDOF functions (ISP-f1R and ISP-f2R). The results for each impact direction (ISP-R) showed that the secondary effect for the case with a right-front passenger was larger in the case of right-side impact. Similarly, for the models representing PDOF as a continuous function (ISP-f1R, ISP-f2R), the secondary effects were observed, although the effects were not significant due to the limited number of samples.

Newland et al.[29] noted that drivers with a front seat passenger present were more at risk than drivers without a passenger as a risk factor for drivers. Thus, passenger interaction, which represents contact with adjacent occupants in the same seating row, was found to be more severe when a right-front passenger was present. The effect of gender difference was only chosen for the ISP in the stepwise variable selection method.

According to the AUC results using the NASS-CDS dataset, ISP-R, which categorized PDOF into four impact directions, was higher than the models that represented PDOF as a continuous function (ISP-f1R and ISP-f2R). The reason for this may be that, as stated previously, the functional data analysis was limited to Subaru vehicle categories from NASS-CDS, which narrowed down the number of cases, and therefore could not demonstrate sufficient performance. Wang et al.[15] reported that the AUC value was improved by using a continuous function for PDOF. In order to improve the performance of the algorithm, it is necessary to collect data on a larger number of accidents, and data consistency is important. There was no significant difference in the specificity of the models, while ISP-R performed better than the other models in terms of sensitivity.

On the other hand, the AUC results using the NASS-CISS dataset showed that the model with PDOF as a continuous function produced better results. For sensitivity, ISP-f2R showed the highest results when the cutoff value was 0.2 (the value recommended by the CDC). It is important to set an appropriate cutoff value for the NASS-CISS because it includes relatively new vehicles and the safety performance of vehicles in a crash has been improved. Sensitivity and specificity were in a trade-off relationship, and it is important to balance sensitivity and specificity in setting cutoff values, and it is necessary to discuss appropriate triage decisions based on field data. In addition, NASS-CISS has larger weights than NASS-CDS and represents more cases. The median weight of the NASS-CDS was 75. In contrast, the median weight of NASS-CISS was 193. The larger weight for NASS-CISS was likely due to the greater number of crashes per year compared to when NASS-CDS was implemented. The new weighting of the NASS-CISS addresses this issue and thus has a larger weight. A larger sample was needed to evaluate the safety performance of newer vehicles of a given year, which

also plays a role in improving the performance of the algorithm.

CONCLUSOIN

In this study, the Subaru vehicle category was selected as the vehicle body type from the NASS-CDS, and four different algorithms were used to predict the severity of injuries. All algorithms were able to predict the risk of serious injury (ISS 15 or higher), confirming that the injury prediction method was useful for on-site triage of occupants in the event of an accident. The area under the receiver operating characteristic curve (AUC) was used as a measure of model performance, and cross-validation using NASS-CDS showed that the ISP-R model had the highest result at 0.862. Additional validation using NASS-CISS resulted in AUC values above 0.8 for all models. The major predictors were delta-V, direction of impact, seatbelt use, and age, and the presence of a right-front passenger was found to be an important injury risk modifier, especially for side impact crashes. These models need to be continually improved with the collection of crash data.

The model that most predicted injury outcomes was at the occupant level, not at the vehicle level. However, in practically crash scenario, a vehicle's telematic system would make the initial contact and Emergency Medical Services (EMS) would respond to the vehicle as a unit. Therefore, this paper proposes an injury severity prediction model that aims to predict crash vehicle categories that may include serious injuries at the vehicle level. Many automakers are attempting to collect rear seat occupant information as well as front seat occupant information. Thus, by understanding the status of occupant information collection, the injury severity prediction model can be extended to the occupant level.

Reference
[1] MacKenzie, EJ., Rivara, FP., Jurkovich, GJ., et al. A national evaluation of the effect of trauma-center care on mortality. The New England Journal of Medicine, 354:366–378. 2006.
[2] Sasser, SM., Hunt, RC., Sullivent, EE., et al. Guidelines for field triage of injured patients: recommendations of the National Expert Panel on Field Triage., MMWR Morbidity and mortality weekly report, 58:1–35. 2009.
[3] Augenstein, J., Digges, K., Ogata, S., Perdeck, E., and Stratton, J., Development and validation of the URGENCY algorithm to predict compelling Injuries. Proceeding of the 17th ESV Conference 2001, Paper No. 352
[4] Bahouth, GT., Digges, KH., Bedewi, NE,. et al. Development of URGENCY2.1 for the prediction of crash injury severity. Top Emergency Medicine. 26:157–165. 2004.
[5] Kononen, DW., Flannagan, CA., Wang, SC., Identification and validation of a logistic regression model for predicting serious injuries associated with motor vehicle crashes. Accident Analysis and Prevention, 43:112–122. 2011
[6] Ayoung-Chee, P,, Mack, CD., Kaufman, R., Bulger, E., Predicting severe injury using vehicle telemetry data. Journal Trauma Acute Care Surgery. 74, 190–194; discussion 4–5. 2013.
[7] Kusano, KD., Gabler, HC., Comparison and Validation of Injury Risk Classifiers for Advanced Automated Crash Notification Systems. Traffic Injury Prevention, 15, S126–S133, 2014.
[8] McMurry, TL., Cormier, JM., Daniel, T., et al. An omni-directional model of injury risk in planar crashes with application for autonomous vehicles. Traffic Injury Prevention, DOI: 10.1080/15389588.2021.1955108, 2021.
[9] National Highway Traffic Safety Administration. National Automotive Sampling System. Washington, DC: National Highway Traffic Safety Administration; Available at:
https://www.nhtsa.gov/crash-data-systems/national-automotive-sampling-system. Accessed May 15, 2020.
[10] National Highway Traffic Safety Administration. National Automotive Sampling System. Washington, DC: National Highway Traffic Safety Administration; Available at:
https://www.nhtsa.gov/file-downloads?p=nhtsa/downloads/CISS/ Accessed May 15, 2020.
[11] Association for the Advancement of Automotive Medicine. "Abbreviated Injury Scale (AIS)": Available at: https://www.aaam.org /abbreviated-injury-scale-ais/. Accessed May 1, 2020.
[12] Baker, SP., O'Neill, B., Haddon, WJr., Long, WB., The injury severity score: a method for describing patients with multiple injuries and evaluating emergency care. *Journal of Trauma.*14:187–196. 1974.
[13] Rauscher, S., Messner, G., Baur, P. Augenstein, J., Digges, K., Perdeck, E., Bahouth, G., and Pieske, O., Enhanced automatic collision notification system -Improved rescue due to injury prediction- First filed experience. Proceeding of the 21th ESV Conference 2009, Paper Number. 09-0049
[14] Wang, SC., Kohoyda-Inglis, CJ. et al., Second Generation Aacn Injury Severity Prediction Algorithm: Development and Real-World Validation. Proceeding of the 25th ESV conference, Paper Number: 17-0133-O, 2017.

[15] Kuniyuki, H., A Study of Injury Prediction Method and Influential Factors in Frontal Collision Using Accident Data, JSAE Transaction Vol.43. No. 2. p.261-267. 2012

[16] Tominaga, S., Nishimoto, T., Motomura, T., Matsumoto, M, Lubbe, N., and Kiuchi, T., Injury prediction algorithm for AACN based Japanese road accident data, JSAE Transaction Vol.46 p.925-930. 201

[17] Kubota, K., Nishimoto, T., Tominaga, S., and Miyoshi, T., Development of Injury Prediction Algorithms Based on Seating Positions, Impact Directions and Injury Regions. JSAE Spring Annual Conference. Paper Number 20175518. 2017

[18] Nishimoto, T., Mukaigawa, K., Tominaga, S., Motomura, T., Lubbe, N., Kiuchi, T., Matsumoto, M, and Matsumoto, H., Serious Injury Prediction Algorithm based on large-scale data and under-triage control. Accident Analysis and Prevention, Vol 98, p.266-276. 2017

[19] D-Call Net https://www.helpnet.co.jp/. Accessed Nov 24, 2022.

[20] Institute for Traffic Accident Research and Data Analysis (ITARDA). https://www.itarda.or.jp/english/ Accessed Nov 24, 2022.

[21] National Highway Traffic Safety Administration, National Automotive Sampling System (NASS) Crashworthiness Data System Analytical User's Manual 2007 File. National Center for Statistics and Analysis, NHTSA, U.S. Department of Transportation, Washington, DC.

[22] Hocking RR,: The Analysis and Selection of Variables in Linear Regression. Biometrics, 32, (1976).

[23] Akaike H,: A new look at the statistical model identification, IEEE Transactions on Automatic Control,19(6):716–723, doi:10.1109/TAC.1974.1100705, MR 0423716, (1974).

[24] Fawcett T,: An Introduction to ROC Analysis. Pattern Recognition Letters. 27 (8): 861–874. doi:10.1016/j.patrec.2005.10.010, (2006).

[25] R software, https://www.r-project.org/. Accessed May 2020.

[26] Stone M,: Cross-validatory choice and assessment of statistical predictions. J. Royal Stat. Soc.,36(2),111 147, (1974).

[27] Farmer, CM,. Braver, ER., Mitter, EL., Two-vehicle side impact crashes: The relationship of vehicle and crash characteristics to injury severity. Accident Analysis and Prevention, 29, Issue 3, Pages 399-406, 1997.

[28] Stigson, H., and Kullgren, A,. Effect of Side Impact Protection in Reducing Injuries. 22nd International Technical Conference on the Enhanced Safety of Vehicles (ESV), Washington, D.C., June, Paper Number 11-0319, 2011

[29] Newland, C., Belcher, T., Bostrom, O. et al., , Occupant-to-occupant interaction and impact injury risk in side impact crashes. *Stapp Car Crash J,* 52**,** 327-47. 2008.

STUDY ON THE IMPROVEMET OF PEDESTRIAN'S VISIBILITY BY GEOMETRIC PATTERNS PROJECTION LIGHTING

Masayoshi Takori

Yuji Tsuchiya

Kei Oshida

Honda R&D Co., Ltd.

Safety and Human Factor Research Domain Innovative Research Excellence

Japan

ABSTRACT

A growing proportion of traffic accidents with pedestrian fatalities are occurring at night. With conventional lighting technology, using stronger illumination to increase the visibility of pedestrians contrarily causes the issue of increasing glare.

The present research therefore devised geometric pattern projection lighting that is aimed at extending the distance at which drivers can detect pedestrians while at the same time reducing glare for pedestrians. Test subject verification regarding visibility of pedestrians by drivers was performed and the effectiveness of the devised lighting was made clear.

1. INTRODUCTION: ISSUE AND AIMS

Accidents with pedestrian fatalities make up 36% of traffic accidents in Japan. By road status, 35% of such accidents are on straight roads. Looking at time of day, 29% of such accidents occur during the day and 71% at night, so more accidents with pedestrian fatalities on straight roads occur at night (Fig. 1).

As current nighttime lighting technology, there is the auto high-beam (AHB) system that detects whether or not

there are vehicles in the surrounding area and automatically switches between low beam and driving beam.

Development is underway of variable light distribution-type headlight systems (adaptive driving beam (ADB))

that detect the location of vehicles in the surrounding area and mask the lights so as not to expose them to glare.

These conventional systems have an issue, which is that because they try to prevent glare for pedestrians, they

do not adequately illuminate pedestrians.

Geometric pattern projection lighting was therefore devised and its effectiveness was made clear.
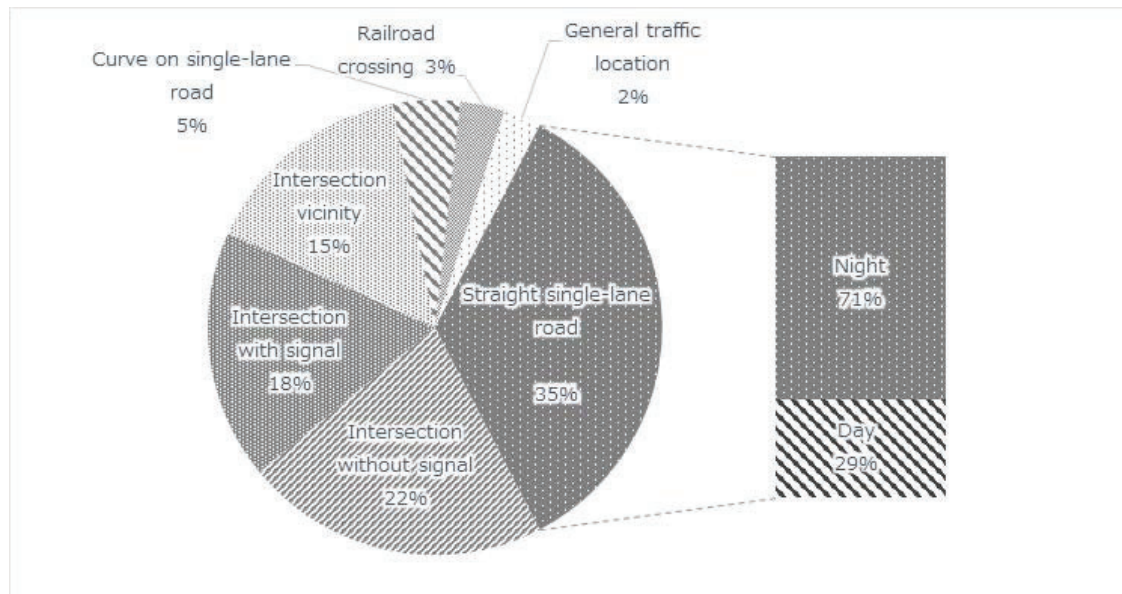
Figure 1. Pedestrian fatalities in Japan in 2021 in percentages by road state and in percentages of pedestrian

fatalities on straight roads by day and night [1]

2. PROPOSAL: LIGHTING WITH GEOMETRIC PATTERNS

The present research made use of projection technology, which has made evolutionary advances in recent years,

to study how projecting illumination with geometric patterns could enhance visibility of pedestrians while at the

same time acting to reduce glare for pedestrians. Advance study was made regarding geometric patterns and

illuminated area.

First, regarding geometric patterns, the following three patterns were studied.

The first pattern, as shown in Fig. 2, illuminates with vertically banded light in order to reduce glare.

When pedestrians cross through an area that is illuminated with vertically banded light, the light in the bright lines in the banding is a powerful stimulus, whereas the stimulus of light in the dark lines is weakened. It was confirmed that movement is made more conspicuous by this variation in light stimulus. Since the bright lines in the vertical banding are emphasized, however, it was found that pedestrians appear like sticks and are not easily recognized as pedestrians.

Therefore the second pattern studied as a way to enhance the visibility of pedestrians was a grid pattern, as shown in Fig. 3, that adds horizontal bands to the first pattern. It was confirmed that the visibility of pedestrians was enhanced over the first pattern because the light is in a grid pattern. However, depending on the body type of the pedestrian, this pattern ends up continuing to shine the powerful light into the pedestrian's eyes with the horizontal bands, so it was found that this pattern was not able to reduce the glare.

The third pattern studied as a way of enhancing the visibility of pedestrians, therefore, was the diamond-shaped pattern made up of diagonal lines shown in Fig. 4. This would reduce the amount of light on pedestrians regardless of differences in their body type. As a result, it was found that this could emphasize the movement of pedestrians, enhance the visibility of pedestrians, and reduce the glare on pedestrians, as shown in Fig. 5. This diamond-shaped illumination pattern was used in the testing of subjects to confirm its effectiveness.
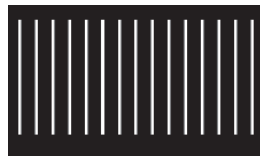
Figure 2. Vertically banded pattern
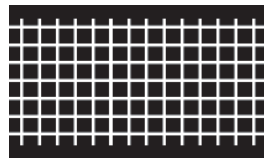
Figure 3. Grid pattern

Figure 4. Diamond-shaped pattern

Figure 5. How pedestrians appear

The area illuminated by this diamond-shaped pattern is shown in Fig. 6. Assuming that a driver driving a vehicle at a speed of 40 to 60 km/h finds a pedestrian trying to cross the road and stops, we decided to illuminate the

sidewalk of 40 to 80 m. As shown in Fig. 7, we decided to illuminate the pedestrian's whole body with the diamond-shaped pattern.
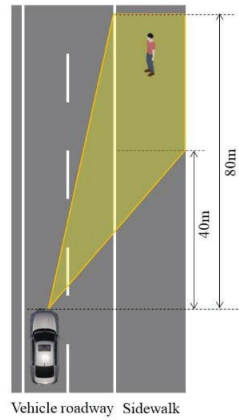

Figure 6. Illuminated area

Figure7. Conceptual image of illumination

3. CONTENT OF TEST

3.1. Evaluation Method

The distance on a straight road at which a driver using geometric pattern projection lighting will notice a pedestrian was determined by testing with human research subjects.

For convenience, the geometric pattern projection lighting will be referred to in the following as projection lighting.

3.2. Human Research Subjects and Informed Consent

There were 40 human research subjects aged 20–60 years. They were selected randomly by an in-house call for applications.

The human research subjects participated of their own free will. The parties responsible for the testing gave them full spoken and written explanations in advance of the purpose of this research, its content, and the right of participation, and their written consent was obtained.

This testing was conducted with approval (98HM-076H) from the Bioethics Committee of Honda R&D Co., Ltd.

3.3. Status of Vehicle Lighting

The following two patterns were determined for the lighting modes.

(1) Low-beam lighting

(2) Low-beam lighting and projection lighting

3.4. Pedestrian Clothing

The object of visibility in this research is defined as pedestrians crossing the road. The pedestrians crossing the road are defined as wearing upper and lower clothing that is black. Testing was conducted with this reduced visibility condition.

Figure 8. Pedestrians crossing the road wearing black upper and lower clothing

3.5. Test Environment and Procedure

The test location was an outdoor test course. Testing was conducted in clear weather in an environment without nighttime lighting.

The test used a 200-m-long section of straight road with one lane on each side. The test layout had the positional relationship shown in Fig. 9.

For the test procedure, the test vehicle was positioned at a sufficient distance from the pedestrian. The human research subjects were instructed to board the test vehicle and look toward the front to simulate ordinary driving. The test vehicle was driven forward and the distance at which the human research subjects perceived the pedestrian was measured. The test vehicle was driven at a speed of 6 km/h or lower. The pedestrian that was the object of perception walked back and forth on the sidewalk at a normal walking pace (1 m/sec).

After the distance at which the subject of perception recognized the pedestrian was measured, the test vehicle

was positioned at a location 43 m away from the pedestrian and sensory evaluation of the visibility of the pedestrian was conducted. The distance of 43 m is the stopping distance envisioned for a vehicle at the speed of 40 km/h decelerating at 4 m/s^2. The sensory evaluation was scored on a five-point scale with the following criteria.

5   Clearly saw that it was a person

4   Though hard to see, it was visibly a person

3   Though not certain, there was an impression of seeing a person

2   There was an impression of seeing an object of some kind

1   Nothing was visible
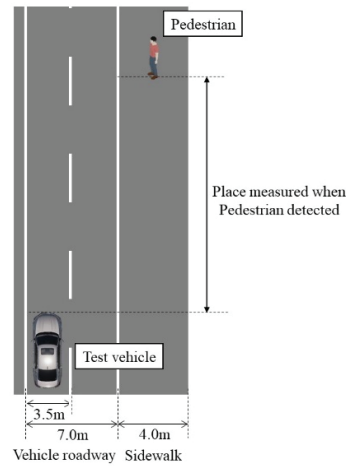
Figure 9. Test layout

4. TEST RESULTS

Average values were calculated for the results from measurement of the distance at which the human research subjects perceived a pedestrian. The results are shown in Fig. 10.
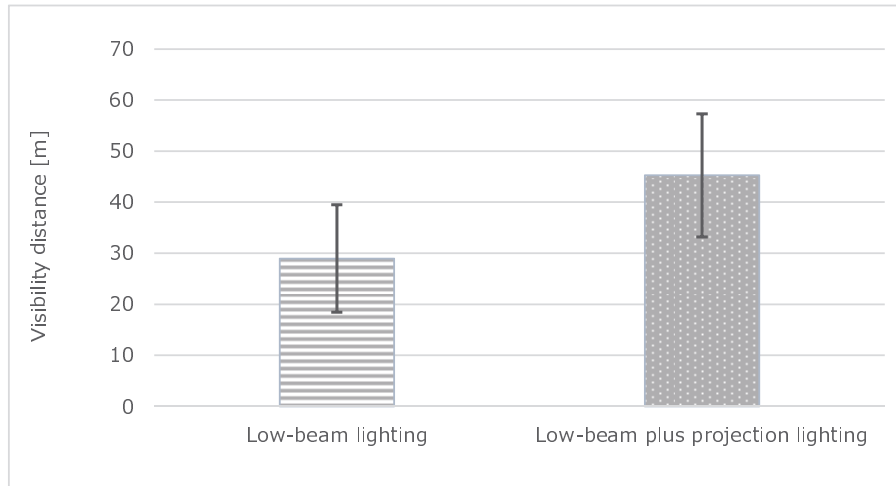
Figure 10. Average value of pedestrian perception distance on straight road

It is apparent from Fig. 10 that where the average distance with low beam is 28.9 m, the average distance with projection lighting is 45.2 m. The perception distance was extended by 16.3 m. No difference by age of the human research subjects was observed in the results. These results were recognized as showing a significant difference as determined by significance testing (t test).

Figure 11 shows the results of sensory evaluation.
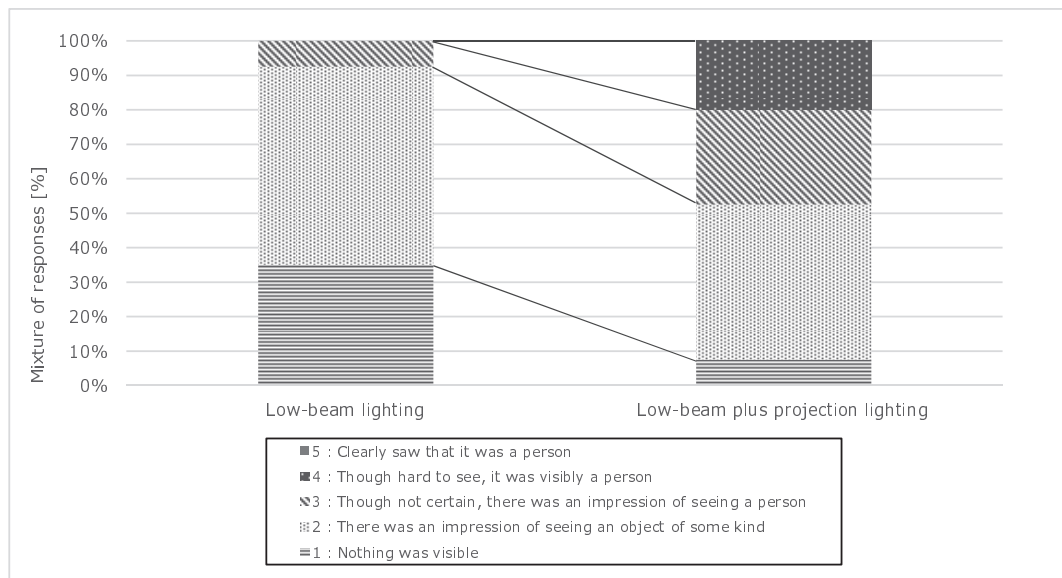
Figure 11. Sensory evaluation of pedestrian visibility on straight road

Responses of "There was an impression of seeing an object of some kind" or higher can be expected to have an accident reduction effect. These responses amounted to 65% of the total with the low-beam lighting and 93% with the projection lighting, an enhancement of 28 percentage points. No difference by age of the human research subjects was observed in the results.

5. DISCUSSION

Pedestrian accidents on straight roads at night are thought to be caused by drivers overlooking crossing pedestrians and delay in detecting them. In the road environment in Japan in particular, where vehicles are driven on the left side of the road, accidents involving pedestrians crossing from the right side at night make up a larger percentage.

The test results showed that where the average perception distance at which drivers detected the pedestrian crossing from the right was 28.9 m with the low-beam lighting, with the projection lighting the average perception distance was 45.2 m, a 16.3-m extension of the perception distance. Envisioning deceleration at 4 m/s^2 from the point where the crossing pedestrian was detected, the distance with the low-beam lighting corresponds to the stopping distance at a speed of 35 km/h, whereas the distance with the patterning beam corresponds to the stopping distance at a speed of 45 km/h. This suggests that an accident reduction effect can be expected up to a higher speed range.

Similar testing was also conducted in a scenario of a vehicle waiting to turn right (i.e., across traffic) at an intersection, with the pedestrian crossing from the same side. Those results confirmed that with the projection lighting, drivers perceived pedestrians crossing from the same side at a point on average 2.9 m before perception with the low-beam lighting. This suggests that projection lighting has an effect even in the area that is in the driver's peripheral vision. When the pedestrian is walking at a pace of 1 m/s, the driver is able to perceive the pedestrian approximately 3 seconds sooner. This can be expected to help keep drivers from starting to move forward when they have overlooked the approaching pedestrian.
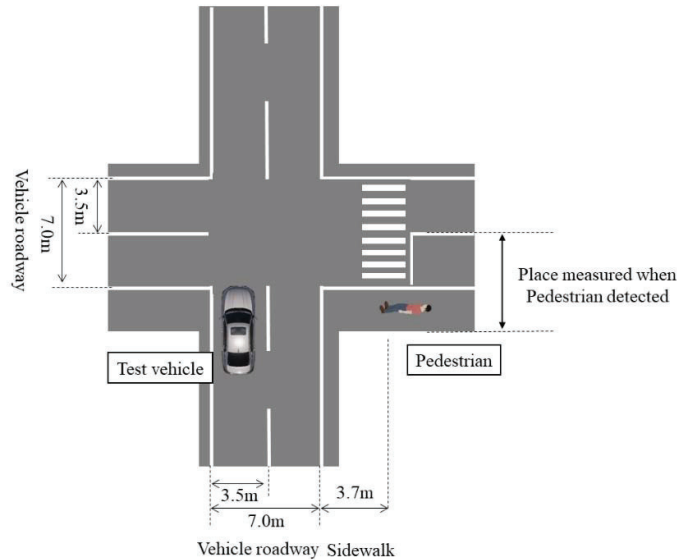
Figure 12. Layout of test at intersection

6. CONCLUSION

In this research, geometric pattern projection lighting was devised with the aim of extending the distance at which drivers detect pedestrians while reducing the glare for pedestrians. Verification of the test subjects conducted with respect to visibility of pedestrians by drivers made clear the effectiveness of the lighting.

As a result, the following results were obtained.

(1) Where the pedestrian perception distance on a straight road was an average of 28.9 m with the low-beam lighting, it was an average of 45.2 m with the projection lighting, a 16.3-m extension of the perception distance.

(2) In sensory evaluation of the visibility of pedestrians on a straight road, responses of "There was an impression of seeing an object of some kind" or higher amounted to 65% of the total with the low-beam lighting, whereas it was 93% with the projection lighting, an enhancement of 28 percentage points.

(3) It was confirmed that the pedestrian perception distance in a scenario of right turn at an intersection with projection lighting was on average at a point 2.9 m before detection with the low-beam lighting.

It was found from these results that it is possible for the proposed projection lighting to extend the distance at which drivers perceive pedestrians beyond the distance with low-beam lighting while also reducing the glare for pedestrians.

Going forward, efforts will be made to clarify the effectiveness of increasing the visibility of automobiles as seen by pedestrians, and to conduct an evaluation of the reduction of glare felt by pedestrians.

7. **REFERECE**

[1] Institute for Traffic Accident Research and Data Analysis

[2] Yoshiro Aoki and Masato Gokan and Nobuaki Tanaka and Shinichi Todaka and Teruhito Moriya and Ryo Goto and Ryo Chijimatsu and Daisuke Takahashi and Hirohiko Oshio and Ippei Yamamoto.2019. "Glare reduction and influence of behavioral characteristic for pedestrian by glareless-ADB light distribution" Society of Automotive Engineers of Japan Spring Meeting

[3] Yoshiro Aoki and Kazumoto Morita and Michiaki Sekine and Nobuhisa Tanaka.2013. "Visibility of Pedestrian by the Headlight in Consideration of the Glare to the Driver on the Oncoming Vehicle" Transaction of the Society of Automotive Engineers of Japan,Inc. 44(1),pp131-136

[4] Institute for Traffic Accident Research and Data Analysis.2010. ITALDA INFORMATION 83,pp1-12

[5] Institute for Traffic Accident Research and Data Analysis.2022. ITALDA INFORMATION 140,pp1-8

DYNAMIC TESTING WITH PRE-CRASH ACTIVATION TO DESIGN ADAPTIVE SAFETY SYSTEMS

Kai-Ulrich Machens
Lars Kübler
ZF Automotive Germany GmbH, Industriestr. 20, 73553 Alfdorf
Germany

Paper Number 23-0067

ABSTRACT

Pre-crash occupant dynamics change more and more with the broad usage of advanced driver assistance systems (ADAS) and automated driving (AD) functions. Occupant interaction with pre-crash activated seatbelt systems (SBS) represent a challenge and an opportunity at the same time for providing restraint solutions tailored to the individual passenger and to the actual driving situation. To fully understand the dynamics, and to design robust control parameters, the increased complexity can eventually only be assessed by means of a virtual approach. Consequently, this requires compulsory realistic advanced physical tests and development targets to ensure that integrity and functionality of all system components are fully understood and modeled appropriately. Focusing on the most frequent crash types: frontal and rear end crashes, allows to use a specially designed, stripped-down Anthropomorphic Test Device (ATD) to dynamically load the seatbelt system in a representative way. In addition, a high-precision surrogate with different selectable upper body moments of inertia, seated on a generic steel seat with an adjustable backrest is available to extend the range of the applicable load. In both cases the retaining effect caused by friction on a real vehicle seat is accounted for by an adjustable viscous damper, retarding the motion of the lower body. These reduced setups guaranty by design a direct and accurate positioning of the ATD, minimizing test setup variability.

As a novum, a seamless transition from initial pre-crash dynamics to the final crash pulse loading can be realized when mounting these ATDs on an innovative test bench using closed-loop controlled electric linear motors to accelerate a linear ball bearing guided carbon sled along a 6-meter track for achieving a maximum in reliability and in repeatability. This physical bench test represents the foundation not only for demonstrating benefits of pre-crash activation on seat belt systems but also for validating functional SBS simulation models, so that numerical simulations become its digital twin. Reliable digital SBS simulation will be the key to generate more and advanced seat belt functions. However, the capability to measure efficiently and accurately via physical tests the performance of these SBS products throughout the entire range of their functional design space, will promote not only the product, but further raises the credibility of simulation. A new rating criterion *Characteristic Shoulder Force Level* (CFL) evaluating the SBS performance virtually is proposed, which assess the performance of the SBS intervention up to *force-closure* and demonstrates the strength of a hybrid approach. Different vehicle configurations, crash pulses, load scenarios and SBS activation strategies can be rated and directly compared to each other. This supports improved integrated safety systems solutions and allows detailed analyses of active safety pre-crash interventions as triggered by ADAS or AD. The combined virtual-physical approach is illustrated via load cases combining braking intervention with conventional and actively controlled seatbelt systems. The potential benefit to occupant safety of different combination of braking and SBS activation is measured and discussed.

INTRODUCTION

Plankermann [1] states that about 90% of all road traffic accidents can be assigned to the human factor. Full autonomous driving will eventually take the principal factor out of the equation, being the reason why this vision is so appealing in terms of road traffic safety. However, before this becomes reality, the next step forward to enhance vehicle safety is expected to be driven by new technologies in onboard sensors and electronic control units, enabling adaptive safety systems and advanced driver assistance systems (ADAS) to improve occupant real-world safety. Autonomous emergency braking (AEB), which is obligatory from 2024 for all new registered vehicles in the European Union [2], for example can help to prevent accidents, or at least reduce the severity of an accident, as described by Graci et al. [3] and the benefit of AEB for occupant safety is already acknowledged by Euro NCAP [4] and NHTSA [5].

The next safety level for occupant safety systems (OSS) will be reached when feeding back, data collected by the vehicles' surrounding and interior sensors, into an adaptive safety system for selecting the appropriate strategies and activating the protection devices accordingly, case by case. Interlinking active and passive safety allows a sooner, and case sensitive activation of the OSS, reducing the occupant injury risk.

Scenario-based verification with high accuracy bench tests

The evaluation and validation of complex case sensitive OSS functions is a challenging task since these systems must perform accordingly to all possible situations and under all possible conditions. As discussed for example by Spitzhüttl et al. [6] and

Wågström et al. [7], innovative, so-called scenario-based verification and validation approaches, combining virtual and physical testing, are considered most suitable for this task. This appreciation is also shared in the Euro NCAP Working Group paper on AEB/AES from Schramm [4], reflecting on the need to "be able to validate the OEM performance, by a combination of vehicle in the loop tests and simplified tracks". According to Reuter [8] they equally recognized within their roadmap 2030 to extend not only the number of variants of sled tests but also to incorporate virtual testing to enhance the robustness of safety system towards crash severity variance and towards occupant physis. The need for adaptive occupant safety systems is emphasized by investigations such as from Hu et al. [9]. They carried out a sensitivity study on injury risks for a wide range of the US adult population. Occupants generated from parametric human models were installed in a validated generic vehicle driver compartment and an U.S. NCAP frontal crash was simulated. Their results suggest that safety systems, that adapt to passenger stature and body shape may improve crash safety for all occupants.

The present authors addressed in [10] the need to improve on repeatability for system - or for subsystem tests to be able to identify and validate accurately functional models of seatbelt components thoroughly over the full design space. Fully validated functional models are necessary to build a reliable base to assess virtual holistic safety ratings by scenario based full vehicle simulations. For connecting physical and virtual testing they suggest in [10] to use a specifically designed test bench called Hyper Dynamic Response Actuator (HyDRA) with a generic, well defined test setup. Accurate measurement systems, enhanced control of test parameters and bench efficiency yield in reduced setup time for each test, making HyDRA the perfect tool for performing large number of load case variations, essential for the identification and validation of functional simulation models of SBS components.

The expected demand to rate and verify SBS functionality in subcomponent testing with precrash activities, motivated the development of an additional, more complex test setup on HyDRA test bench, presented in this paper, with either an ATD being accelerated under ADAS activity or under a precrash activation of an actively controlled SBS.

The chosen ATD-like kinematics to load the SBS is geared to a fundamental investigation on the influence of pre-crash activation on restraints' effectiveness. Outcome of this study is a proposition how to rate the contribution of the SBS under precrash action to real-world safety. The approach is based on the technical understanding of the classical in-crash SBS functionality which needs to be adapted to add precrash activities. An appropriate functional segmentation of the in-crash phase is presented in the next section.

CRASH PHASES FOR CLASSICAL AND INTEGRATED SAFETY

Discussions on how to mitigate the consequences of a crash, the crash sequence itself is commonly divided into three phases, the pre-crash-, the in-crash-, and the post-crash-phase, as described by Kramer et al. [11]. The shortest phase in time is the in-crash phase lasting about 100-200 ms dependent on the crash scenario, being commonly described as a velocity alignment of vehicle and occupant. Linear in-crash velocity alignment as used by Zellmer et al. [12] averages out important effects during this phase and is consequently not suited to distinguish in a meaningful way between different pretensioner systems. Voigt et al. [13] subdivide the in-crash phase, based on the shoulder belt force readings from sled tests, into the following segments: *Pretensioning – Coupling – Load Limiting*. In this paper a split of the in-crash phase into the functional segments: *crash-detection, force-closure* and *ride-down* is suggested and motivated for classical passive and integrated safety as illustrated in Figure 1, as *pretensioning* must be regarded as a sub-task to improve coupling.

Classical passive safety

The in-crash-phase in classical passive safety as depicted in Figure 1 in the upper row, starts with a constant speed situation and an occupant in its nominal position. Ideally, in case of an optimal fast sensory system (or a sufficiently soft crash pulse) the crash detection is completed before a significant occupant displacement relative to the vehicle has taken place, since such a displacement reduces the remaining safety space in the vehicle cabin, needed for the *ride-down* with the lowest possible forces. During the crash-detection the seatbelt is unlocked and does not decelerate the occupant - no forces are built up in the seatbelt. The quality of a vehicle sensory system is rated on how fast an incoming crash can be reliably identified after occurrence of the first physical contact, so that a Time-to-Fire (TTF)-signal can be routed to trigger the SBS.

The second in-crash-phase is called *force-closure*. It includes SBS pretensioning and locking, as well as the force build up to the load limiting level initially set. Since the SBS being locked, the relative forward displacement of the ATD is building up the belt forces. In classical passive safety phase 2 is regarded functionally as the most dynamic phase. The functional tasks of slack removal, retractor locking and building up of belt forces is influenced by various factors. The SBS performance depends on the actual in vehicle situation (available belt slack, compressibility of occupant including clothing, belt friction in D-Ring, belt contact to occupant, elasticity in fixation points, etc.) and dynamics (dynamic load on the belt system, vehicle pulse, ...) as well as the subsequent retractor locking, which may be accompanied for example by a more or less pronounced belt force drop, discussed later. Depending on the geometry of the SBS anchor points and the instantaneous ATD kinematics the kinetic belt forces are building-up until the predefined limiting force level is reached, and *force-closure* is completed.
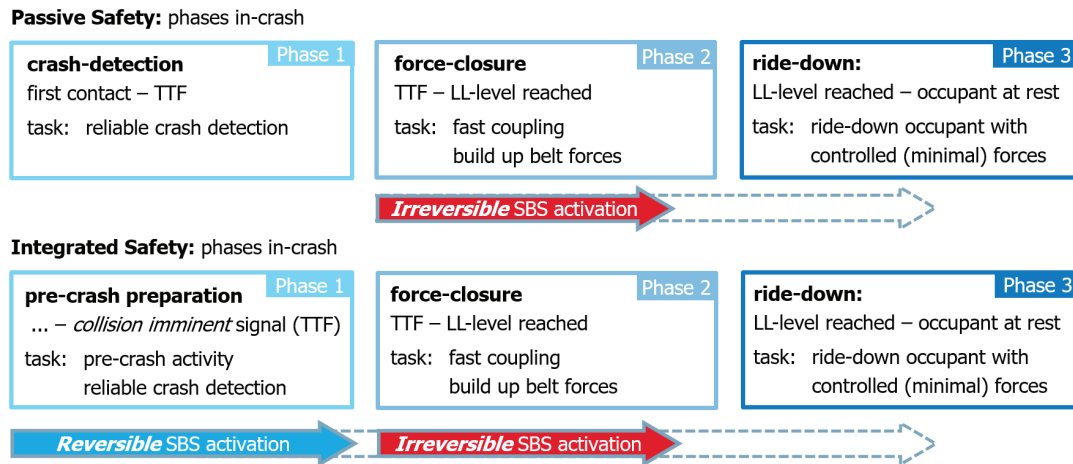
Figure 1 In-crash phases:
first row: The in-crash scenario splits classical passive safety into three distinctive functional segments: Crash-detection, force-closure and ride-down. When assuming a fast crash detection sensory system, only a minor displacement of the occupant relative to the vehicle is expected in phase 1.
second row: Integrated safety pre-crash vehicle maneuvers and reversible SBS activation might move the occupant out of its nominal seating position prior to Time-to-Fire (TTF)-signal, the deployment of irreversible SBS action. Phase 2 starts with initial conditions depending on the pre-crash intervention applied before. Therefore, SBS performance in phases 1 and 2 depend on each other and need to be evaluated together. The ride-down task – phase 3 – utilizing the maximum of the remaining cabin space to ride-down the occupant with minimal forces is identical as in classical passive safety.

The third in-crash-phase describes the *ride-down* of the ATD with controlled minimal forces acting on the dummy through the seatbelt, via friction forces to the seat and to the floor, and if present via airbag systems. During the in-crash phase the relative ATD forward displacement yields in a monotonic, continuous reduction of deceleration distance available in the cabin. The remaining space after *force-closure* shall be completely used to stop the relative motion with controlled forces applied to the ATD, defining the optimum load limiting level for an individual occupant. The handover of the ATD loaded from the belt system into the ATD-airbag contact and the stable capturing of the head is regarded as the major challenge of this phase. Even though the ride-down is a challenging task, it is proportional to the kinetic energy of the ATD entering into the *ride-down* phase and proportional to the available space, hence the combination of both parameter is suggested to measure and to rate the performance of SBS systems.

Integrated safety

As stated by Kramer et al. [14] in chapter 4, within the framework of integrated safety, a clear separation between pre-crash and in-crash phase is no longer possible. One might postulate a "new" starting point for the in-crash phase, as when the vehicle safety electronic control unit (ECU) has decided on an imminent collision. This point in time is either before or after the first physical contact, defined as t=0 s in this paper, depended on the crash prediction / detection algorithm of the SBS ECU. This "new" starting point would exclude reversible, preventive actions, for instance the pre-safe operation of an actively controlled retractor, from the in-crash phase. These types of actuations are triggered by signals interpreted as instable driving situation. If this situation is on top autonomously changed by ADAS intervention it can modify the occupant position via direct forces (example: repositioning of the occupant by belt forces) and / or via indirect forces (inertia forces caused by evasive maneuvers or by emergency braking). Consequently, the initial condition of the occupant in terms of position, velocity, and seatbelt tension forces can become less well defined at the in-crash phase starting point. This will be discussed in more detail on the example of emergency braking. On one hand emergency braking before impact reduces the velocity delta between vehicle and crash target, and thus reduces the crash pulse or even at best avoids the impact altogether, mitigating the safety risk. On the other hand, the occupant's chest forward displacement caused by braking maneuvers as reported by Mages et al. [15] is likely to reduce the efficiency of SBS pretensioning to remove belt slack, and the *ride-down* could start with an occupant in a less advantageously displaced position. Reversible pre-crash actions can be either assigned to driver assistance or to pre-crash preparation. But all dynamic maneuvers until *force-closure* together represent a continuous transition, which impact the severity of the subsequent force-controlled *ride-down*.

Depicted in the lower row of Figure 1, it is suggested to treat the first relevant deviation in speed between vehicle and occupant as starting sequence for the *crash-preparation* phase. This makes it accessible to physical and virtual testing. A scenario approach combines phase 1 and 2 until the occupant is coupled to the vehicle as *force-closure* is reached. From a functional point of view only the *ride-down,* phase 3 remains unchanged for classical passive and for integrated safety (see Figure 1), thus it can be used to rate on the efficiency of different SBS with the approach suggested in the following section.

HOW TO RATE SEATBELT SYSTEM PERFORMANCE

Component contribution depends upon integral scenario

The performance of a safety system cannot be judged independent from a load case, which is composed of:

1. *Crash scenario:* delta velocity between ego and bullet vehicle, vehicle overlap, impact direction, crash pulse, …
2. *Occupant*: mass, size, feet (fixed to ground or loose), belt routing, …
3. *Vehicle sensory system*: Time-to-Fire delay, ignition strategy for seatbelt & airbags, …
4. *Vehicle*: anchor point geometry, seat adjustment (back rest angle, position), available safety space, crash stability cabin, …
5. *Vehicle seat & environment*: crash-performance seat, pelvis seat immersion (seat stiffness), energy dissipation by seat deformation, friction ATD-seating area, energy dissipation instrument panel, steering column compliance, …
6. *Seat belt system*: retractor-pretensioner (reversible, irreversible, type of pretensioner suitable for load case?), buckle pretensioner, anchor pretensioner, retractor load limiter (constant, switchable, multi-stage, …), buckle load limiter, anchor load limiter, belt webbing, dynamic locking tongue, D-ring (coating), seat integrated SBS, …
7. *Airbag system*: front airbag, knee airbag, seat airbag, airbag in or on belt, …

Therefore, a certain safety target definition is either met or not met by the assessed SBS including ignition and load level switching strategy, i.e., occupant safety is a holistic property of the full load case, and it cannot be attributed to just a single component or sub-system. Although optimal ATD injury risk values are the ultimate goal, it is considered helpful to introduce a metric with a heuristic character. This metric allows to benchmark both – a SBS as well as vehicle attributes like crash pulse severity – separately for each crash phase. It is designed more like the heuristic rating criteria in chess i.e., how to judge on the contribution of a single chess move in an evolved match, to achieve the final goal "checkmate".

A fast crash detection – as an example – is generally favorable for occupant safety as the TTF-signal, which triggers the irreversible emergency activation, is send out shortly after the first physical contact. This is particularly important in scenarios with hard crash pulses, slow pretensioning systems or small safety spaces. Here the loss of precious safety space of the cabin through unrestricted ATD forward displacement i.e., without decelerating belt forces from a restrained and locked SBS applied is even more important to reach set occupant safety targets. A slower crash sensor may be tolerable in a vehicle with soft pulses and/or large safety spaces.

A more complex question is to rate the efficiency of seatbelt activation (pretensioning, locking, belt force build-up to load limiting level) prior to *force-closure*, reducing partially the kinetic energy of the ATD which coincides with the consumption of safety space, not any longer available in the subsequent *ride-dow*n of the ATD by controlled forces applied via belt and via airbags systems. The next subsection discusses SBS efficiency prior to the *ride-down* phase and introduces a metric to evaluate it.

SBS efficiency to the point of "force-closure"

When replacing the passenger seat by a generic steel seat with a seating surface inclination of 10° and a backrest position adjusted for the ATD to conserve the initial chest and pelvis position from the analyzed vehicle, the simulation reveals that the ATD crash kinematic in phase 1 and 2 is hardly effected by the seat change (see example of load case LC0 in the appendix A). Consequently, the *force-closure* performance of the SBS can be gauged by means of a generic ideal constant load limiter (CLL) retractor system, which substitutes the original seatbelt system during *ride-down* (phase 3). This transposes the ATD dynamic behavior of the full vehicle setup to a simplified setup where the ATD kinematic can be virtually continued without affecting the natural ATD crash kinematics. The "computed" ideal generic CLL load limiter level required to *riding-down* the energy stored in the ATD at the beginning of phase 3 over a fixed total distance to reach maximum chest forward displacement can be used as metric to quantify the SBS *force-closure* performance.

The procedure is illustrated in Figure 2. The full vehicle configuration has a deformable vehicle seat and a safety system with a switchable load limiter (SLL) and a passenger airbag, which starts to load ATD's chest and head region at about 55 ms after TTF. Also, at this moment the retractor switches to the lower load level, reducing the occupants shoulder belt force from about 5 kN to 2 kN in order to establish a smooth load onto the ATD during its transition from the seatbelt to the passenger airbag, illustrated in Figure 2 by the black line. The intended first shoulder belt force load limiting level of 5 kN is reached at 40 ms – with *force-closure* being established. When applying the full vehicle system equivalent SBS parameters to the simplified performance measurement setup named "Torso at Seat" (T@S), all relevant dynamic parameters from phase 2 are respected and conserved (green plot Figure 2). To measure the SBS force-closure performance the initial SBS is replaced with the beginning of phase 3 by an ideal generic (CLL) load limiter SBS. All other energy management systems like airbags, switchable load limiters, deformable passenger seats, feet to floor contact friction are taken off, only the non-linear damping characteristics of the deformable passenger seat is modelled on the steal seat by attaching a linear viscous damper to the artificial lower leg to realize comparable generic damping during phase 2. The constant load limiter level in the generic SBS is set in a way, that the chest forward displacement of the ATD stops precisely at 300 mm within ±1.5 mm tolerance. Even though different vehicle configurations do provide more or less safety space to *ride-down* the ATD, the fixed distance allows to better compare SBS configurations in different vehicles.
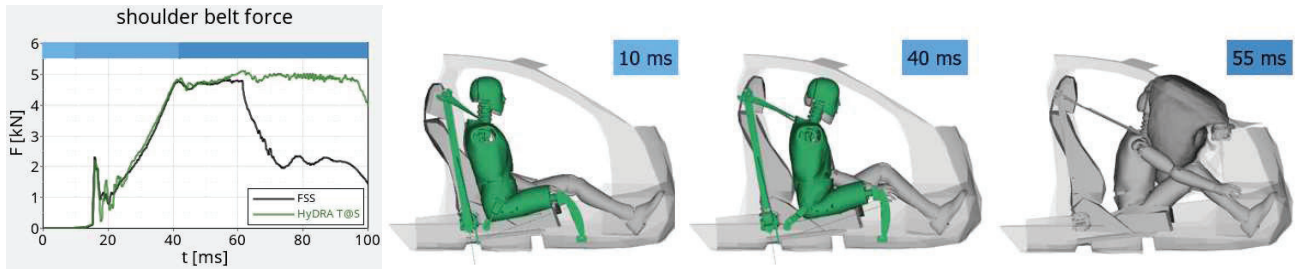
Figure 2 In-crash phases 1-3: Crash-detection, force-closure and ride-down based on shoulder belt force. When using full vehicle system equivalent SBS parameters in the performance measurement setup D.0 (see appendix A), the results from both setups match in terms of shoulder belt force and ATD kinetic for in-crash phases 1-2. For ride-down in phase 3, airbag and load limiting system is replaced by an equivalent CLL system to stop the ATD forward motion at a chest displacement of 300 mm. The simplified T@S-ATD (green) on a steal seat improves repeatability and precision in physical and virtual testing. This load limiting level is used as single value metric to measure the SBS system performance for a given load case.

The ATD preserves its typical kinematic in a vehicle environment, as it depends mainly on the vehicle configuration, which is considered by the metric. Also, the ATD kinematic is not expected to be significantly modified when the ATD interacts with airbags, as these devices are predominantly geared to protect head and neck during late stage of the ride-down phase and to decelerate the ATD by applying pressure over a larger ATD contact area than the belt. Therefore, the occurred kinetic energy reduction of the ATD is well described by its effect on chest forward displacement. When defining the total chest forward displacement for the ATD to come to a halt after ride down at 300 mm the theoretically required CLL level of the generic seatbelt system can be computed. This derived CLL level is called *characteristic shoulder force level* (CFL) and is used as single value metric: A lower absolute CLL level indicates a better SBS performance prior to *force-closure*. Cause and effects relative to a reference system become easily accessible by simple force level comparison.

Fortunately, by means of this metric, the parameters of the vehicle configuration can be transferred onto a simplified set-up with *reusable* rigid seat with *stable* dynamic system characteristic, yielding in more efficient testing as well as more efficient simulation. The transfer from a validated full vehicle system model to the simplified setup, as well as sensitivity studies on geometrical parameters with the simplified setup, are shown and discussed in detail in the appendix A. From there it can be derived that it is adequate to characterize any vehicle configuration in the simplified setup by *eight* adjustable quantities.

Simplified generic load case described by "The BIG 8"

To summarize the findings from the example configurations in the appendix A, the load case is fully characterized by the following eight parameters, and the *force-closure*-performance can be assessed appropriately with simplified setups like D.0:

1. *Vehicle pulse:* SBS fixation point deceleration time sequence in for-aft direction
2. *Time-to-fire delay:* earliest point in time an imminent crash is safely detected
3. *ATD:* mass & stiffness distribution, kinematics, feet sliding / footrest, ...
4. *Initial Torso inclination:* H-angle dependent on backrest orientation
5. *SBS fixation points:* D-ring, buckle, and anchor relative to seat
6. *Pelvis damper force:* deceleration through seat friction in phase 2, restraining forces due to deformation, and geometric interlock in phase 3, defined in the simplified T@S-setup by a damper characteristic to provide damping of a generic seat
7. *System slack:* webbing on spool, configuration slack (chest & pelvis), buckle head movement, chest compression, …
8. *Available safety space:* max chest forward displacement without body to interior impact

These parameter-set is designated "The BIG 8". Assuming vehicle specific recommended values for item 2-8, item 1 - *vehicle pulse* heavily depends on the load case vulgo crash scenario. This list of items could be extended where appropriate by two robustness parameters.

  I. *Part temperature*
 II. *New / aged parts*

Using an identical SBS (3-PGA) and an identical control strategy in different vehicle configurations defined by "The BIG 8" it is possible to compare these configurations by the metric introduced in Figure 2, to be discussed in the next section.

Vehicle load case benchmark and quantification

"The BIG 8" characterize a vehicle configuration, and by applying an identical SBS mounted in different vehicle configurations the single value metric "CLL level maximum 300 mm chest forward displacement" allows to compare and eventually to rate different vehicle load cases. The resultant CLL level is referred to as *characteristic shoulder belt force* level (CFL). This is done exemplarily for the configurations from Figure 14 and from Figure 17 i.e., under load case CL0 without pre-braking. The absolute

Machens 5

(CFL), the delta (dCFL) and relative (rCFL) characteristic shoulder belt force levels are printed in

Table 1. The first row shows the absolute force level, and the second row the difference between the individual configuration and the *Pretty Good Vehicle* (PGV) - configuration (D.0), the chosen reference vehicle as delta (in N) and as percentage, calculated according to

$$dCFL_{D.x} := CFL_{D.x} - CFL_{D.0} \quad ; \quad rCFL_{D.x} := \frac{CFL_{D.x} - CFL_{D.0}}{CFL_{D.0}} \quad , for\ x = 1,2,3,4. \tag{1}$$

Table 1
Characteristic shoulder force levels (CFL) for configurations of Figure 17 using SBS-1 and SBS-2 when subjected to LC0 - no braking load case. Relative CFL for SBS-2 and SBS-1 show about same percentage.

Seatbelt System SBS	Vehicle Configuration LC0 T@S			D.0 HyDRA T@S baseline	D.1 anchor slack +40 mm	D.2 backrest +5°	D.3 anchor & buckle fixation - 100mm	D.4 D-ring -200mm
SBS-1	absolut characteristic shoulder force level	CFL_D.x	in N	10000	10600	8600	6200	7400
	relative characteristic shoulder force level	dCFL_D.x	in N	0	600	-1400	-3800	-2600
		rCFL_D.x	in %	0,0%	6,0%	-14,0%	-38,0%	-26,0%
SBS-2	absolut characteristic shoulder force level	CFL_D.x	in N	8800		7700		6400
	relative characteristic shoulder force level	dCFL_D.x	in N	0		-1100		-2400
		rCFL_D.x	in %	0,0%		-12,5%		-27,3%

The results indicate that the SBS shows significant differences between configurations. Configuration D.3 is most advantageous followed by D.4 and D.2. The added slack at the anchor in Configuration D.1 leads to a rating inferior to that of D.0 (PGV), which is consistent to the fact, that the pretensioner is not able to remove all slack added at the other end of the belt. These results displayed graphically in Figure 3 confirm well the conclusions derived from the detailed analysis in appendix A. The SBS with a different pretensioner type, SBS-2, subsequently used as reference seatbelt system *Pretty Good Seatbelt System* (PGS) was evaluated for vehicle configuration D.0, D.2 and D.4. The absolute CFL levels for vehicle configuration D.0 differ between SBS-1 and SBS-2 but the relative characteristic forces from Figure 3 show the same trend for both SBSs, allowing the classification of vehicle configurations.
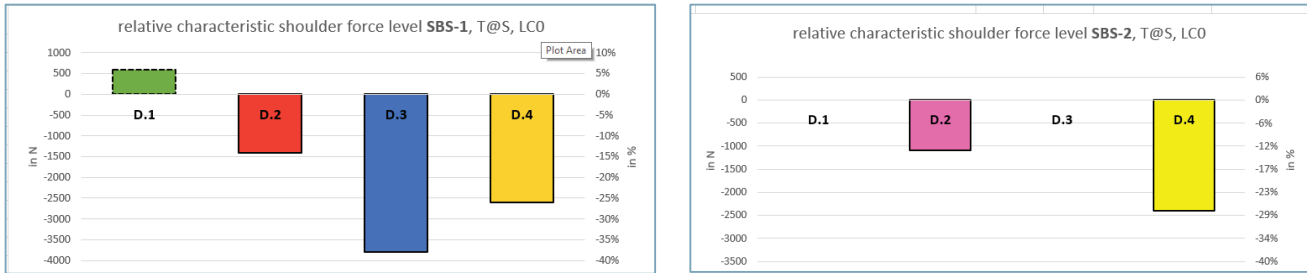

Figure 3 Vehicle configurations D.1-D.4 relative to D.0 compared by relative characteristic shoulder force (see Table 1) for seat belt system SBS-1 (left picture) and for SBS-2 (right picture D.0, D.2, D.4) with ATD T@S under load case scenario LC0

This investigation is an example of how different vehicle configurations (defined by "The BIG 8" parameter set) can be compared with this metric, simply by using an identical SBS (3-PGA system and activation strategy). Alternatively, this approach can be used to rate different SBS systems or/and different SBS control strategies in each target vehicle configuration, which will be discussed in detail in the following section.

SBS PERFORMACE BENCHMARKING

In this section three different SBS systems with their individual control strategies are mounted and assessed in the PGV geometry and three different vehicle load cases are applied: Load case LC0 consists of the US NCAP pulse for the PGV, whereas load case LC1 and LC2 incorporate the effect of two different pre-braking load cases, as illustrated in Figure 4.
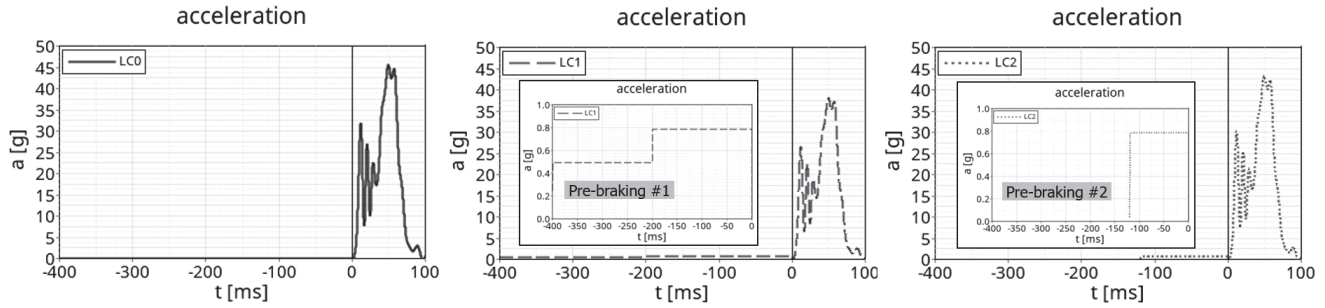

Figure 4   Left picture - LC0: US NCAP pulse of the PGV for FWFI at 56 km/h.
Center picture – LC1: Long pre-brake pulse, starting at 400 ms before the crash with plateaus of 0.5 g and 0.8 g, each lasting for 200 ms, followed by actual crash pulse. Pre-braking reduces the impact velocity by 2.6 m/s, accounted for by applying a factor of 0.833 to the pulse.
Right picture – LC2: Short pre-brake action starting at 120 ms before the crash, with a plateau of 0.8 g lasting for 120 ms, followed by the US NCAP pulse multiplied by a factor of 0.94.

Since t=0 s is defined as physical start of the crash i.e., time of first vehicle to obstacle contact, pre-crash activation shows a negative timestamp. The first pre-braking load case LC1 - consists of stepping up from 0.5 g level to 0.8 g level, with each level being maintained for 200 ms, which slows down the velocity of the target vehicle by 2.6 m/s. This is accounted for by applying a factor of 0.883 (see equation (2)) to the pulse. The second pre-braking load case LC2 consists in immediate maximum braking with 0.8 g for 120 ms prior to the crash, with the original crash pulse scaled by a factor of 0.94. Here-in it is assumed that the reduced delta velocity between barrier and target vehicle can be accounted for by simply downscaling the US NCAP pulse of the PGV for FWFI subsequent crash pulse by a factor of

$$\frac{v_0 - \Delta v_{braking\_\#1}}{v_0} = \frac{15.56 - 2.6}{15.56} = 0.833 \quad \text{and} \quad \frac{v_0 - \Delta v_{braking\_\#2}}{v_0} = \frac{15.56 - 0.96}{15.56} = 0.94 \quad . \tag{2}$$

The following three different SBS systems were selected for this investigation:

SBS-1:   Pretensioning via spool-coupling, CLL 3 kN, TTF 10 ms, Standard D-Ring, Standard buckle

SBS-2:   *Pretty Good Seatbelt System* PGS: Pretensioning via torsion-bar-coupling, CLL 3 kN, TTF 10 ms, Standard D-Ring, Standard buckle

SBS-3:   Actively Controlled Retractor ACR, CLL 3 kN, TTF 10 ms, Standard D-ring, Standard buckle with two different start *reversible pull-in activation* (RPA) times:
   RPA1: Activation at $t = -400\ ms$
   RPA2: Activation at $t = -120\ ms$

The dynamic ATD response is described by time sequences of three force / displacement pairs: Recording quantities are, at the retractor; retractor force / webbing pay-out, at the upper body; shoulder belt force / chest forward displacement, and at the lower body; anchor belt force / tongue slip. Figure 5 to Figure 7 display the results gathered for the load cases LC0, LC1, and LC2.

The design of the two retractor pretensioners, SBS-1 and SBS-2, differ significantly in their torque loading path from the pretensioning unit into the spool. Regardless of this fundamental difference, it has barely an impact on pretensioner force peak levels and on pretensioning pull-in speeds, but it yields in a different locking behavior, resulting in different slopes to finalize the *force-closure*. In comparison to SBS-1, SBS-2 pulls-in a significantly larger amount of webbing and the force drop accompanying the inversion of the spool rotation being less pronounced. SBS-2 reaches the CLL level slightly earlier than SBS-1. Other than expected from their close chest forward displacement curves in Figure 5, all these advantages of the SBS-2 do lead to a significant change in the characteristic shoulder force levels (CFL) in Table 2 which differ by 1200 N between SBS-1 and SBS-2 i.e., 13.6%. The absolute CFL values are related to the energy (work) of the shoulder belt force and to the displacement remaining after *force-closure* as discussed in appendix B.
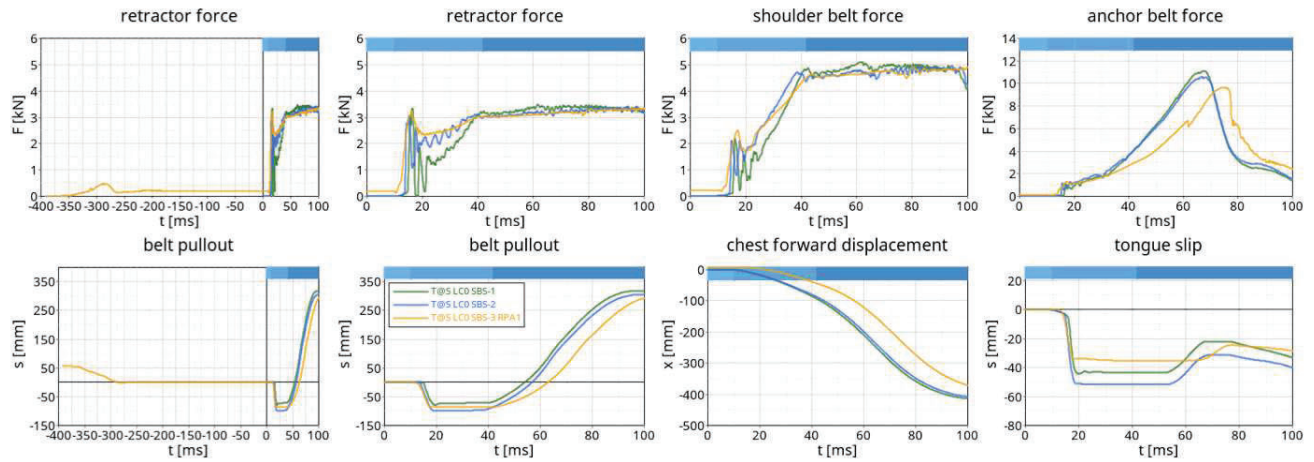
Figure 5 Dynamic T@S-ATD response when subjected to LC0 (US NCAP pulse of the PGV for FWFI at 56 km/h as shown in Figure 4 (left picture)) for three SBS configurations. Standard pretensioners SBS-1 and SBS-2 differ in the transition to force-closure, apparent on the force readings at the retractor and at the shoulder. Their small difference in chest forward over 400 mm displacement constitutes a considerable difference in CFL of 1200 N. SBS-3 with early activation (RPA1) causes the chest forward displacement to be reduced by 79 mm at t=60 ms, advantageous to unfold a frontal airbag. CFL refer to Table 2.
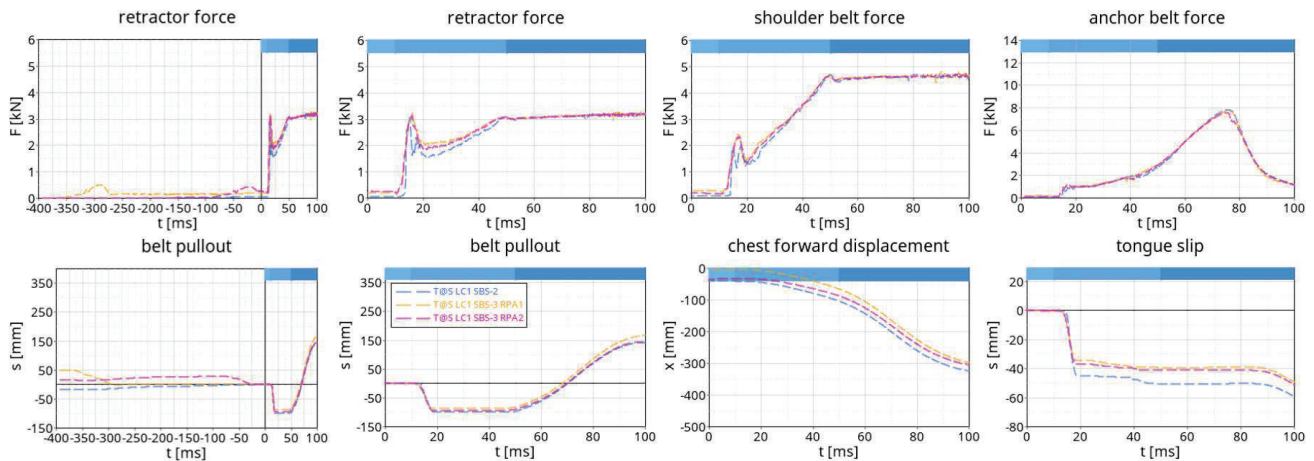
Figure 6 Dynamic T@S-ATD response for LC1 for three different SBS configurations. Early SBS-3 activation with RPA1 is of advantage compared to RPA2, chest forward displacement at t=60 ms is reduced by 38 mm, and by 18 mm respectively to standard non-active pretensioner SBS-2. Corresponding CFL refer to Table 2.
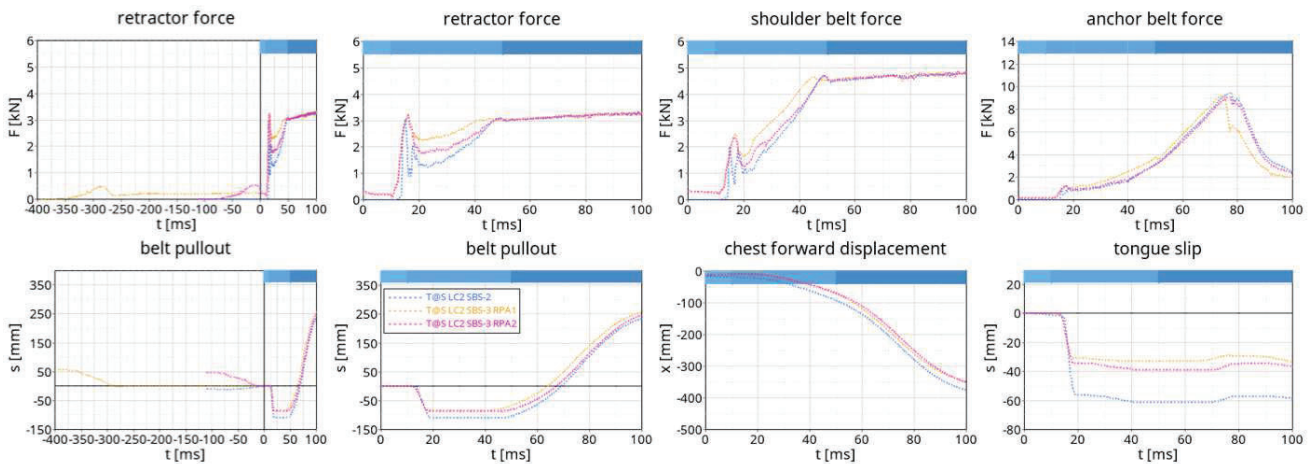
Figure 7 Dynamic T@S-ATD response for LC2 for three different SBS configurations. Simultaneous pre-braking and activation of SBS-3 (RPA2) results in similar CFL rating compared to early ACR activation (RPA1). Both ACR activation strategies show a similar benefit, the chest forward displacement at t=60 ms is reduced by 18 mm and 26 mm compared to a traditional pretensioner system. Corresponding CFL refer to Table 2.

However, the actively controlled retractor (ACR, SBS-3) shows, due to the early intervention, a consistent improvement for all load cases. In the pre-braking scenario, LC1 displayed in Figure 6, the effect of the active intervention is as expected more pronounced than for LC2 shown in Figure 7, as the braking induced ATD chest forward displacement in LC1 has more time to evolve for standard pretensioners i.e., without active intervention. With the conventional pretensioner SBS-2 the chest shows already a forward displacement of 40 mm (LC1) respectively 17 mm (LC2) prior to the crash. The RPA1 pre-activation from SBS-3 generates a shoulder belt force of about 200 N in the pre-braking scenario, which is apparently strong enough to prevent ATD forward displacement under braking deceleration for all load cases LC0-LC2. Late activating of SBS-3 (RPA2) in load case LC1 with early braking (see pink line in Figure 6) results in a chest forward displacement prior to crash of 34 mm. The reversible pre-crash activation, latest simultaneously with the pre-braking operation, of SBS-3 reduces significant slack by aligning the belt system at moderate forces before the crash. The belt pull-out is set to zero at t=0 s, start of the actual crash pulse to ease the comparison of pretensioning and crash dynamics for different systems. Consequently, for ADAS activation, before t=0 s, pre-crash webbing pull-in shows up above and pre-crash belt pull-out shows up below the neutral axis. Although the pretensioning of SBS-3 works on an already slack reduced seat belt system, the SBS-3 is able to pull-in almost the same amount of belt as SBS-2, with both systems using an identical pretensioning mechanism. The higher retractor force level between pretensioning and *force-closure* for SBS-3, results from lower belt system slack due to the pre-crash belt slack removal. The shallower slope to *force-closure* of the shoulder belt force from SBS-3 correlates with a slower ATD chest forward displacement, indicating that the impulse passed from the 200 N pre-tensioning force onto the ATD upper body is high enough to retard the chest forward displacement. At t=60 ms the difference in chest forward displacement between SBS-2 and SBS-3 amounts to 79 mm for LC0, 38 mm for LC1 and 18 mm for LC2, not only in a lower total chest forward displacement, but more importantly the *retarded* chest forward displacement allows a frontal airbag system to safely unfold in front of the ATD chest.

Also of advantage, the early slack reduction with low forces modifies the anchor belt force vs. time characteristics visible in Figure 5 when comparing SBS-1 and SBS-2 to SBS-3. Figure 6 and Figure 7 reveal that the advantageous anchor belt force behavior is conserved as well for LC1 and for LC2. The slow pre-crash belt slack removal, even by pre-braking without ACR activation transduces into the pelvis region. This is not equally accomplished by the irreversible highly dynamic retractor pretensioning operation. The analysis suggests that a contact with beneficial significant friction forces between seat area and ATD is realized by the pre-crash slack removal.

On one hand, pre-braking reduces the vehicle velocity before the impact, i.e., the crash pulse becomes softer and softer, the longer the braking interval lasts - being in general of advantage to improve occupant safety. On the other hand, the chest forward displacement at *force-closure* is prone to be larger with pre-braking than without pre-braking, yielding in a reduction of safety space for the ride-down phase.

Whether an AEB intervention is likely to mitigate a crash event does not only depend on the length of the braking interval and the availability of an actively controlled safety system, but it also depends on the level of the braking deceleration in combination with the individual occupant reaction - to be discussed in the following section.

PRE-CRASH ANALYSIS UNDER LOW G

Limited suitability of ATD for low g pre-crash analysis

Traditional crash ATDs are not suited to predict occupant reaction for decelerations below 1 g. Mages et al. [15] compared experimentally the chest displacement of an H350 ATD with the chest displacement of human test persons during physical drive tests, whereas Schilling et al. [19] approached this subject by simulating virtual load cases comparing the response of an active SAFER-HBM with the response of H350- and THOR-ATD models. Both publications conclude that there is a significant difference in the chest forward displacement at low g levels between the human body and the ATDs. The ATDs tend to show significant lower upper body displacements compared to human occupants, being related to a stiff non-biofidelic pelvis region.

Recent preliminary braking tests on tarmac and on gravel were performed with a compact class vehicle to simulate the behavior of a sleeping front passenger on the basis of three different occupants only (including the authors). When subjected to deceleration levels below 0.5 g occupants react individually, depending on the individuum and its alertness, being warned or unwarned of the impending braking, either the upper body will be thrust into the locked seatbelt, or the upper body will be stabilized by tightening pelvis muscles. When being in a relaxed initial status, without consciously tightening the pelvis muscles, dynamic chest forward displacement into the locked seatbelt is assumed to occur for vehicle decelerations exceeding 0.75 g. The impressions gained from these first-off braking tests can be summarized to: once the dynamic chest forward displacement is initiated the motion is more governed by the inertia distribution of the human occupant, muscle activities do not play a major role any longer. To simulate this effect, a simplified generic ATD geometry was developed and machined to be discussed in the upcoming section.

Simplified ATD with instant response time

The simplified generic ATD substitute named "Rebound Guy Mk I" (RBGI), with two major Degrees of Freedom (DOF) only, as depicted in Figure 8, is designed to generate for impacting crash pulses a kinematic response that compares to the H350-ATD shown on the right picture of Figure 8. The moment of inertia of the upper body relative to the swivel-joint, connecting upper to lower body as well as the position of the lower body itself are the key parameters for this kinematic. The basic configuration with H350-ATD like moment of inertia can be easily changed with lump masses either by adding to or by removing from the upper

body. Slack is accounted for by two elements one in the chest and one in the pelvis region, and the amount of slack is adjustable. The initial inclination of the upper body can be varied from 0° - 45° to the vertical. Bump stops visible in Figure 8 limit the back-and-forth rotation of the upper body and the linear transition of the lower body. Loading SBSs with this simplified RBGI geometry increases test efficiency, accuracy, and repeatability.
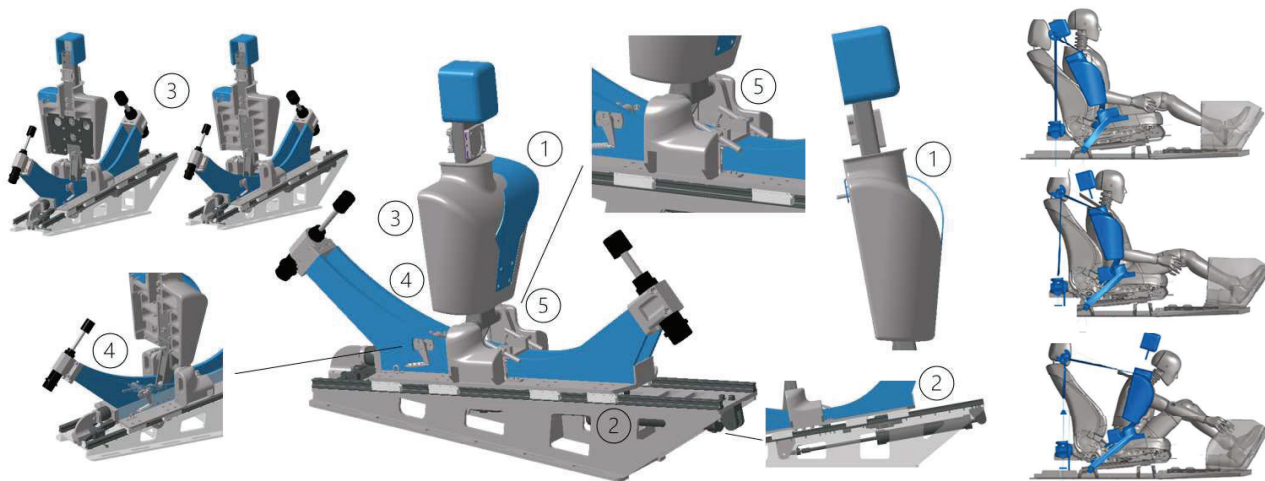

Figure 8 *CAD (left picture) and kinematic (right-hand picture) of generic ATD "Rebound Guy Mk I" (RBGI) with two major DOF: DOF 1, upper body connected via swivel-joint to lower body; DOF 2, lower body railed on ball bearings sliding up a 10° slope. Bump stops limit the chest rotation and the pelvis displacement. Features: ① chest slack, ② lower body viscous damper, ③ variable moment of inertia adjustable by trim masses, ④ adjustable initial upper body inclination, ⑤ pelvis slack. The RBGI is placed inside a frame to attach the seatbelt system, which represents the PGV configuration. Recording damper force, lower body displacement and upper body rotation angle provides accurate monitoring of the RBGI kinematic useful for Digital Twin validation. Right-hand picture: Comparison of RBGI kinematic relative to H350 ATD subjected to LC0.*

The reduced DOF allows a faster and more accurate initial ATD positioning. Altogether the setup guarantees a more stable and repeatable system behavior (no fatigue of rubber components, defined slack, etc.) and the kinematics is precisely monitored by an integrated sensing system (damper force, lower body displacement, upper body rotation angle). This build-in motion monitoring system allows a direct forward-backward transfer of kinematic results between the physical and the virtual world, offering a major benefit to identification and validation work. With regards to pre-crash activation at low g-levels the undamped, inertia dominated rotation of the upper body causes an instant response, considered to be closer to the reaction of an unwarned occupant not tightening the pelvis muscles, than to the response of the H350-ATD. The stiffness of the RBGI slack elements under SBS pre-crash activation can be further improved to better correspond to a H350-ATD slack resistance.

The simulation results with RBGI-ATD subjected to LC1 are displayed in Figure 9 and Figure 10 shows the results for LC2 accordingly. The results are displayed in the way as the results gathered with the T@S-ATD (Figure 6 and Figure 7) allowing a directly response comparison between the different ATDs for identical load cases. At crash contact (t=0 s) for LC1, without ACR pre-crash activation whilst braking, the RBGI-ATD chest forward displacement reaches 100 mm compared to 40 mm only for the T@S-ATD. This is illustrated in Figure 11 via a side view of the ATDs, T@S (green) and RBGI (red) and SBS-2 subjected to LC1 for the time stamps: t=-0.4 s, t=-0.2 s and t=0 s. An early ACR activation like RPA1, starting with the pre-brake maneuver, can prevent chest forward displacement in the pre-crash phase for both ATDs. The advantage of the ACR (SBS-3, RPA1) is more pronounced for the agile ATD RBGI showing 100 mm less chest forward displacement at t=60 ms than the standard SBS-2 pretensioner (see Figure 9) whereas the difference when using the T@S-ATD reaches only 40 mm (see Figure 6). Reduced chest forward displacement at t=60 ms is beneficial as the frontal airbag can unfold more freely.
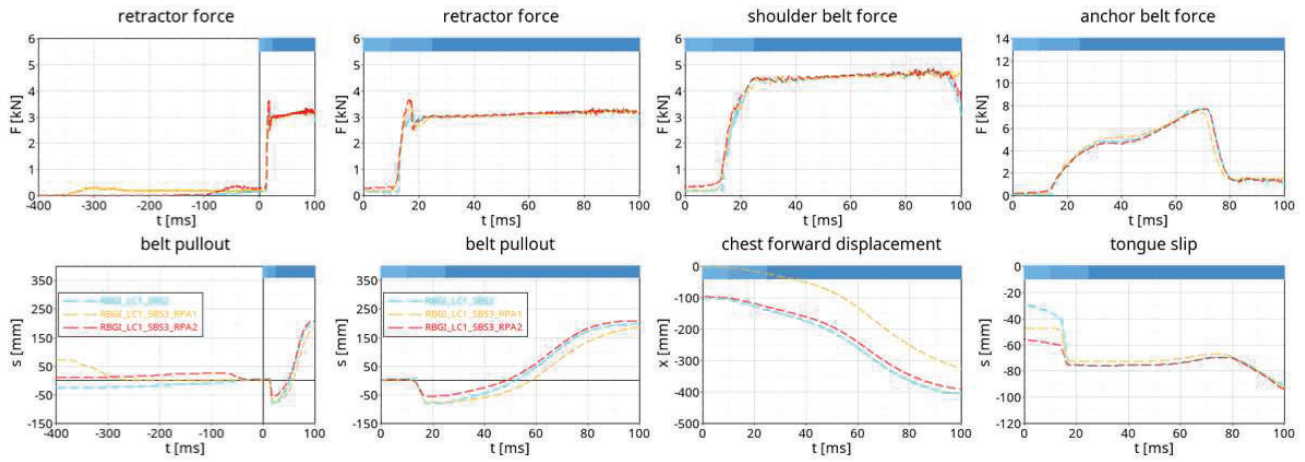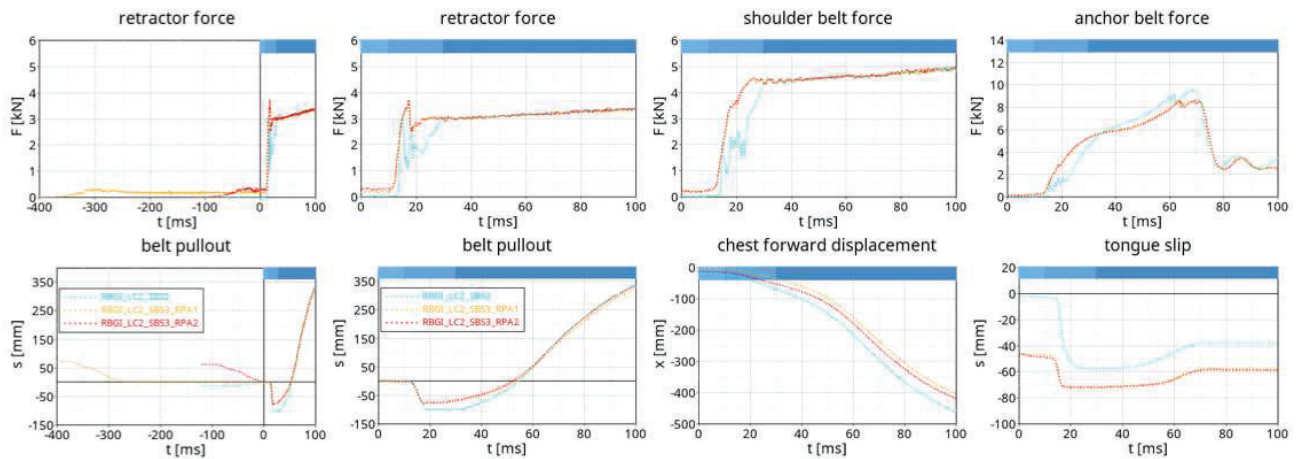
Figure 9 Dynamic response of RBGI subjected to load case LC1 with long pre-braking pulse described in Figure 4 (center picture) for SBS-2 and SBS-3. Comparison with Figure 6 illustrates, that RBGI-ATD shows a higher sensibility to braking action than T@S ATD, suggesting that RBGI-ATD can be regarded as a worst-case scenario representing a sleeping hence relaxed occupant. Pronounced differences in anchor force readings for RBGI-ATD and for T@S ATD will be addressed by further optimization work on the lower body.

Figure 10 Dynamic response of RBGI subjected to load case LC2 with short pre-braking pulse described in Figure 4 (right picture) for SBS-2 and SBS-3. Comparison with Figure 7 illustrates, that RBGI-ATD shows a higher sensibility to braking action than T@S ATD. Differences in anchor force readings for RBGI-ATD and for T@S ATD analogous to LC1.
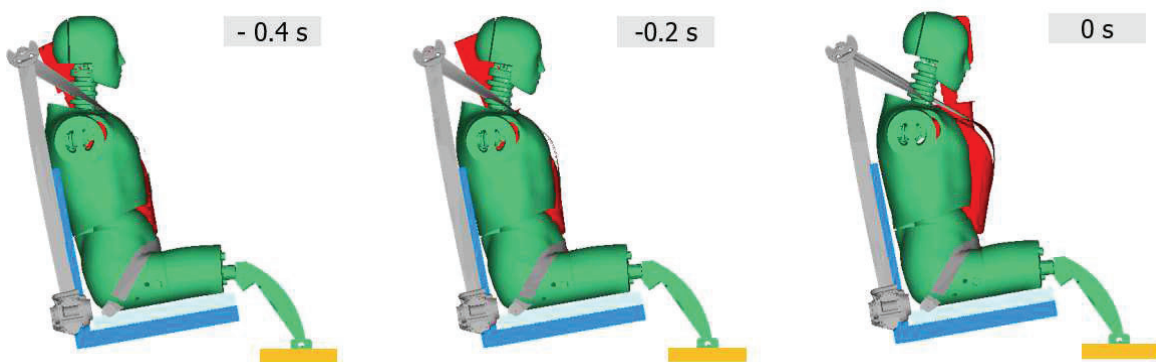
Figure 11 RBGI-ATD (red) compared to T@S-ATD (green) for LC1 initial (left picture), subjected to 0.5 g deceleration (middle picture), and subjected to 0.8 g deceleration (right picture). RBGI more sensitive to low g activation due to higher mobility at upper hip when deceleration level exceeds 0.5 g.

Characteristic shoulder force levels for different SBS systems in PGV vehicle configuration with two different occupants: T@S-ATG and RBGI-ATG subjected to crash pulse LC0, LC1 and LC2 (as illustrated in Figure 4). The difference between T@S and RBGI response are best observed under LC1, with extended braking time. RBGI chest forward displacement response for low g acceleration might be considered as worst-case scenario for human occupants.

Vehicle Configiguration	Seatbelt System SBS T@S D.0 = PGV		SBS-1 TTF+10ms	SBS-2 = PGS TTF+10ms	SBS-3 RPA1 & TTF+10ms	SBS-3 RPA2 & TTF+10ms
T@S D.0 LC0	characteristic shoulder force level	in N	10000	8800	7100	
	relative characteristic shoulder force level	in N	1200	0	-1700	
		in %	13,6%	0,0%	-19,3%	
T@S D.0 LC1	characteristic shoulder force level	in N		5400	4800	4800
	relative characteristic shoulder force level	in N		0	-600	-600
		in %		0,0%	-12,5%	-12,5%
T@S D.0 LC2	characteristic shoulder force level	in N		7800	6300	6600
	relative characteristic shoulder force level	in N		0	-1500	-1200
		in %		0,0%	-19,2%	-15,4%
RBGI D.0 LC0	characteristic shoulder force level	in N		10650	8000	8000
	relative characteristic shoulder force level	in N		0	-2650	-2650
		in %		0,0%	-24,9%	-24,9%
RBGI D.0 LC1	characteristic shoulder force level	in N		7400	5200	6350
	relative characteristic shoulder force level	in N		0	-2200	-1050
		in %		0,0%	-29,7%	-14,2%
RBGI D.0 LC2	characteristic shoulder force level	in N		10150	6900	7350
	relative characteristic shoulder force level	in N		0	-3250	-2800
		in %		0,0%	-32,0%	-27,6%

Since the RBGI kinematic is more sensitive to inertia effects Table 2 reveals a significant difference between the results obtained with RBGI and the results obtained with T@S. The results with RBGI-ATD highlight even more the benefit of early reversible-restraint activation (LC1 30 % improvement compared to 13 %, LC2 32 % improvement compared to 20 %). The design intended removed stiffness in the RBGI's "pelvis region" causes with braking a direct chest forward displacement (being inertia related it needs time to build up) relative to the fixation points, and the associated belt pull-out takes place without generating significant belt forces. This chest forward displacement represents a loss in safety space and it cannot be recovered i.e., by pretensioning, once lost. This explains why the seatbelt system without active pre-safe option yields an inferior performance with RBGI than with T@S-ATD: With active controlled retractors (ACR) and an early pre-safe activation, ideally before pre-braking, the initial safety space can be conserved before the actual crash occurs.

Rating various contributions to occupant protection

A comparison of the absolute characteristic shoulder force levels between load case LC0 (impact without pre-braking), LC1 (long pre-braking) and LC2 (short emergency pre-braking) in Table 2 for T@S-ATD and equally for RBHI-ATD reveals, that pre-braking – the longer the better – is beneficial for occupant safety independent of the seatbelt system. This is especially remarkable for LC2. Even in the case where the impact occurs shortly after the emergency braking is initiated, the loss in safety space by an unrestricted chest forward displacement accompanying the braking deceleration is still sufficiently compensated by a softened pulse due to the reduced impact velocity.

Following the strategy to use the *Pretty Good Vehicle* (PGV) configuration and *Pretty Good Seatbelt-System* (PGS) as references allows to compare even the effect of different dimensions from "The Big 8" on occupant safety. I.e., the results from Table 2 permit to conclude, that the safety improvement with an active controlled retractor (T@S D.0 LC0 SBS-3 RA1: CFL=7100 N) relative to the reference (T@S D.0 LC0 SBS-2: CFL=8800 *N*) is somehow comparable to the improvement by pre-crash braking. The ACR result is bracketed by the results gathered with the PGS for long (T@S D.0 LC1 SBS-2: CFL=5400 N) and for short emergency braking (T@S D.0 LC2 SBS-2: CFL=7800 N) maneuvers. An effect in the same order of magnitude can be achieved by changing the vehicle configuration. The ACR benefit can be rated, according to Table 1, between a 5° steeper backrest (T@S D.2 LC0 SBS-2: CFL=7700 N) and D-ring fixation point moved by 200 mm to the rear (T@S D.4 LC0 SBS-2: CFL=6400 N), provided that the result is not biased by a changed ratio of chest to shoulder belt displacement as discussed in appendix B.

In principle each of the "The Big 8"-parameters can be optimized using the proposed CFL-metric. Crash-pulses for example can be rated to optimize the crashworthiness of vehicle structures by comparing the CFL measured in PGV configuration with PGS restraint system for different crash pulses. This way a much more specific rating is obtained, than by applying some of the crash pulse criteria discussed by Kuebler et al. [16], which are derived either directly from the pulse by means of simple mathematical operations or based on simplified mechanical models e.g., Occupant Load Criterion (OLC).

From the validated reference simulation model based on PGV and PGS the rating based on CFL are readily obtained and can be verified by testing as to be discussed in the next section.

HARDWARE TO TEST SBS PERFORMANCE ON SLED FOR SIMULATION ANCHORAGE

The simplified generic ATD substitute also referred to as "Rebound Guy Mk I" (RBGI) depicted in Figure 9 is built in hardware to be run on a test bench called "Hyper Dynamic Response Actuator", shown in Figure 12 (photo left), and presented in detail by Machens et al. [10]. The test bench consists of a rail guided carbon sled driven by nine closed loop controlled electric linear motors running along a 6-meter track. Active control of sled acceleration and deceleration opens the field of experimentally analyzing effect of pre-crash and in-crash dynamics - incorporation of ADAS operation and ACR activation during the test sequence.

Figure 12 "Rebound Guy Mk I" (RBGI) on HyDRA® (see [10]) test bench (photo left). Close up before the test (photo center) and after the test (photo right). The SBS is fitted on a lightweight aluminum frame structure, designed to represent the PGV vehicle coordinates but it allows also to vary fixation points. Viscous damper with force load cell hidden underneath lower body rail.

The seatbelt system is connected to a lightweight frame structure out of aluminum, which is mounted onto the carbon sled. Although standardized testing with the generic PGV configuration is recommended to assess SBS performance, SBS fixation points can be varied within a certain range. With a maximal propulsion power of 120 kN on HyDRA® test bench a typical RBGI setup can be accelerated up to 30 g. This allows to combine dynamical effects from pre-crash ADAS activation, typically below 1 g acceleration, to be followed by a significant crash-pulse, allowing to assess and to optimize SBS functionalities on these important real-world safety load cases. To simulate different backseat inclinations the initial angle of the RGBI's upper body can be set between 0-45° degree to the vertical (Figure 8).

A second simplified test-bench setup called Torso@Seat (T@S) consists of an adapted H350-ATD as illustrated in Figure 13. This setup serves to link bench results to actual standardized crash test results and is particularly versatile, when reproducing test results from a full-scale vehicle crash or from a sled test configuration with H350-ATD to analyze and optimize effects on the HyDRA® bench. This simplified bench test setup, already used as a simulation model in Figure 3 consists of a H350-ATD with the under legs replaced by a hinged stiff gear, connected to a viscous damper. The H350 arms are replaced by lumped masses with different weights fitted to the shoulder hinges. In this configuration the backrest of the rigid seat can be adjusted between 0°-45°
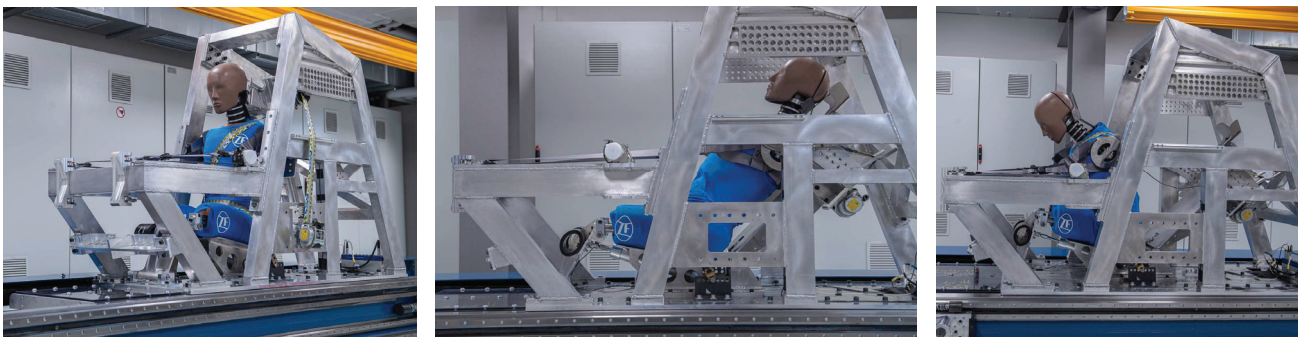

Figure 13 HyDRA® H350 Torso@Seat (T@S) setup before test with 10° (left picture) and with 45° (center picture) back rest angle and after test (right picture). The ATD is trapped in the forward position by a SBS with a pair of retractors especially designed for fast belt pull-in. ATD is placed inside a lightweight aluminium farme structure with PGV SBS coordinates. Setup details: hinged stiff gear substituting the under leg, adaptive viscous damper, bump stops, arm mass substitutes, backrest adapter plates to mount seat integrated retractors, adjustable backrest inclination.

from the vertical as well, and it incorporates an adapter for mounting seat integrated retractors. An adjustable neck-rest provides support to the ATD-head during the acceleration phase of the sled. The neck-rest also helps to efficiently position the ATD on the aluminum seat with high precision. In addition, a specially designed harness wrapped around the ATD-back and connected to a belt driven safety stop, prevents the ATD from getting damaged when stopping the sled after crash-pulse acceleration by a highly dynamic braking deceleration.

LIMITATIONS AND DISCUSSION

HyDRA® test bench with its RBGI (Figure 12) and T@S (Figure 13) setups are intended to apply a realistic load to the seat belt system up to the beginning of *ride-down* phase, for identifying and validating this most important sequence for innovative seatbelt restraint systems. The ATD like devices are not instrumented for assessing injury values, but for recording precisely the kinematic when they are simultaneously subjected to crash pulses, restrain forces from the SBS, seating surface friction forces, etc…, as well as possible seat belt activation (pretensioning). Once all Digital Twin parameters of the physical HyDRA® test bench are fully derived and identified, the setup kinematics is deemed to be validated, and can be used to gauge the quality of the functional models from which the virtual SBS is build up.

Injury risk assessment is not intended to be done on the physical test bench, but it could be estimated by means of a subsequent full vehicle simulation with Human Body- or ATD-models. The late stage of the ride down phase, where the ATD interacts with the seat and the airbag systems, depends highly on the actual vehicle environment. The deformable passenger seat and other vehicle interior parts for example can significantly influence this late phase. Towards the end of the last in-crash phase, HyDRA®'s ATD kinematic will deviate more and more from the ATD kinematic in a full vehicle setting. The analysis and interpretation of results of the *ride-down* phase from physical tests on the generic bench relative to the in-vehicle behavior would be questionable. Particular effects associated to deformable vehicle seat i.e., "submarining" is not accounted for by the standardized setup and can also not be tested for on a stiff seat bench. Oblique crash scenarios, often encountered in real-world vehicle crashes, often start off with a strong impulse in driving direction followed by growing lateral accelerations as the vehicle is forced into a rotatory motion cannot be represented either. These scenarios cannot be assessed on a one-directional, linear test bench. Also, the two presented simplified ATD kinematics are not geared to predict lateral forces; compared to a biofidelic behavior the pelvis region of HyDRA®'s ATD is per design much stiffer. In all these cases it is more appropriate to assess the occupant dynamics via full scale vehicle simulations with Human Body Models (HBM), with dynamically validated functional seatbelt subsystem models.

CONCLUSION

Reviewing the in-crash phases of classical passive safety a functional segmentation into three distinct phases: *Crash-detection, force-closure* and *ride-down* is appropriate, with the SBS key-functionality to establish *force-closure* of the belt to the vehicle being connected to phase 2. Once *force-closure* is completed the *ride-down* phase with controlled forces in seatbelt and in airbag systems can take over. When transferring this segmentation to integrated safety, phase 1 is transformed to a *pre-crash preparation* phase characterized by significant vehicle ADAS dynamics and /or pre-crash activation of reversible seatbelt systems before a crash event is classified as eminent. The handover to phase 2 is defined by the moment in time, where the irreversible SBS activation is triggered when the SBS-ECU has decided on an imminent crash. This can be either before or after the first physical contact of the ego-vehicle with a bullet vehicle or an obstacle and it is dependent on the quality of the available crash-detection system. The analysis concludes that for Integrated Safety phase 1 and phase 2 cannot be assessed and evaluated individually, as the vehicles and/or SBS pre-crash activation is inseparable linked to the efficient force coupling of the passenger to the vehicle.

The performance of the SBS and its activation is load case i.e., vehicle dependent and can be rated by the single value metric "characteristic shoulder belt force level" illustrated in and discussed following Figure 2. It combines the consumption of safety space and the reduction of kinetic energy on the ATD by a single number: "CLL level".

Most interestingly, by defining a reference vehicle configuration, the *Pretty Good Vehicle* (PGV), and by defining a reference seatbelt system, the *Pretty Good Seatbelt System* (PGS), it becomes possible not only to identify and to rate relative improvements in the seatbelt configuration and in its activation strategy, but also to classify load case scenarios and to optimize on vehicle constellations, provided that the target vehicle does not deviate too much from the PGV.

The presented methodology has the potential to develop and classify a suitable seatbelt system for a target vehicle, and to judge on late changes to the SBS in development program on vehicle level (example different pulse, altered fixation points, …) in a quick and reliable way, without the need of precise information on the passenger seat and on the airbag system used. Potential passenger injury risks for vehicle load cases depend undeniably on the interaction of all system parameters. But when the analyzed SBS with its control strategy performs equally or better than the "gold standard" - *Pretty Good Seatbelt System* – a SBS pre-sign off might help to focus on improving other contributors like seat structures or dashboards, etc.

Using an identical SBS in the target vehicle and the reference vehicle PGV allows to classify the target vehicle. When the target vehicle configuration is rated less advantageous than the PGV, it is from a technical point of view obvious that a more sophisticated SBS, seat, or airbag system is needed to compensate for the deficiency to reach an equivalent safety rating.

Finally, pre-crash scenarios incorporating ADAS or SBS activation can be assessed and rated via the defined metric by the comparison of different activation strategies.

In this paper the derived methodology is presented for the first time in public. Starting from the validated full vehicle simulation model of the PGV the methodology is illustrated via a parameter study applied to this model, and the general application for this methodology is discussed. The test hardware presented in the last section is ready at hand, to validate and backup simulation results assessing vehicle and load case specific SBS qualification including their control strategy. Correlation of physical test data to virtual prediction is beyond the scope of this paper and is first to be revealed in real-world vehicle application projects with our partners in the automotive industry.

OUTLOOK

The prevalent usage of ADAS functionality intend to mitigate or at best avoid an impending crash, utilizing information from outboard sensory systems. The expected earlier classification of an actual driving situation as unavoidable imminent crash will foster the performance and impact of pre-crash activated SBS, although the decision making using environmental sensing still have some challenges to be overcome as described by Straßburger et al. [17]. Pre-crash activated SBSs, including their control strategy, are designed to provide an optimum solution for the momentaneous load case. This will significantly raise the number of elementary load cases to account for during the development process to be eventually only manageable by a virtual approach and efficient coding. Out of the need to assess relevant crash configurations, not addressed by today's regulations or consumer crash tests, virtual assessment methods are required and in development as reported by Dobberstein et al. [18], sharing their standpoint at the EU project OSCCAR. A recently published approach by Schilling et. al. [19] couples MATLAB Simulink to LS-Dyna to describe mechatronic pre-crash activated seat belt systems accurately and efficiently seems promising, and it matches perfectly to the digital twin approach favored by Machens et al. [10].

The simplified setups and the focus to validate the SBS by assuring identical ATD kinematic on the physical and on the digital twin, presented in this paper, intend to broaden this approach, and to be also able to rate the safety benefit of SBS pre-crash activation. The virtual model of the simplified setup with reduced Degrees of Freedom speeds up considerably calculation time and yields in higher numerical stability, making these modes suited for numerical optimization methods, as more variants can be treated in the same amount of time. The ability to validate simulation models on sub-system level for load cases with a seamless transition from low g to high g crash acceleration is seen as a major advantage of the presented device. The results from this paper suggest that the sub-system SBS can be validated and optimized with the HyDRA T@S or - RBGI based on "The Big 8" approach i.e., independent of passenger seat and airbag system. Once the CFL metric is established and widely accepted, the effect of late changes in the vehicle project, which alter the initial "The Big 8" SBS parameter set, can be rated, and evaluated accurately and fast with regards to occupant safety at subsystem level. This performance rating intends to identify suitable SBS more accurately, rather than looking for differences in ATD injury values in a few load cases. In addition, robust results are obtained by using parameter variations in the setup like different lump mass distributions on the ATD to account for occupant diversity.

Reversible pre-crash activation of seatbelt system can start earlier i.e., as soon as the crash detection system has preliminarily identified a rough driving situation or a potential crash event. Belt slack reduction and even occupant repositioning through the SBS can be performed already at moderate forces. Hence reversibility is a major strength of mechatronic SBS. The SBS intervention can be ramped up stepwise according to likelihood of a crash, identified by the crash detection system to provide an optimal occupant protection for the actual driving situation without driver and passenger consciously noticing the intervention. In the joint task to mitigate occupant injury risk seatbelt systems are today already considered as very significant contributor. When developing an adaptive safety functionality, SBS will gain further in importance.

REFERENCES

1. Plankermann, K.," Human Factors as Causes for Road Traffic Accidents in the Sultanate of Oman under Consideration of Road Construction Designs", 2013 Dissertation Universität Regensburg, https://epub.uni-regensburg.de/29768/1/Dissertation%20Kai%20Plankermann.pdf
2. Official Journal of the European Union, L 325/1, 16.12.2019, EUR-Lex - 32019R2144 - EN - EUR-Lex (europa.eu)
3. Graci, V., Douglas, E., Seacrist, T., Kerrigan, J., et.al., "Effect of automated versus manual emergency braking on rear seat adult and pediatric occupant precrash motion", Traffic Injury Prevention, Peer-Reviewed Journal for the 26th International Technical Conference on the Enhanced Safety of Vehicles (ESV), 2019, https://doi.org/10.1080/15389588.2019.1630734
4. Schramm, R., "Euro Ncap'S First Step Towards Scenario-Based Assessment By Combining Autonomous Emergency Braking And Autonomous Emergency Steering", Conference: 26th ESV Conference 2019, Endhoven, Paper Number 19-0128, https://www-esv.nhtsa.dot.gov/Proceedings/26/26ESV-000182.pdf
5. NHTSA Announces Update to Historic AEB Commitment by 20 Automakers, https://www.nhtsa.gov/press-releases/nhtsa-announces-update-historic-aeb-commitment-20-automakers, 3.02.2022
6. Spitzhüttl, F., Liers, H.," Calculation of the point of no return (PONR) from real-world accidents", Conference: 26th ESV Conference 2019, Endhoven, Paper Number 19-0141, https://www-esv.nhtsa.dot.gov/Proceedings/26/26ESV-000141.pdf
7. Wågström, K., Leledakis, A., Östh, A. et al.," Integrated safety: Establishing links for a comprehensive virtual tool chain", 26th ESV Conference 2019, Endhoven, Paper Number 19-0177 https://www-esv.nhtsa.dot.gov/Proceedings/26/26ESV-000177.pdf
8. Reuter, R. „Roadmap 2030: Euro NCAP entwickelt neue Kriterien für Crashtests", https://www.automobil-industrie.vogel.de/euro-ncap-entwickelt-neue-kriterien-fuer-crashtests-a-1113849/, 28.04.2022
9. Hu, J., Zhang, K., Reed, M., Wang, J.-W., Neal, M., Lin, C.-H. "Frontal crash simulations using parametric human models representing a diverse population, Traffic Injury Prevention", (2019), 20:sup1, S97-S105, DOI: 10.1080/15389588.2019.1581926
10. Machens, K.-U., Kübler, L.:" Physical & Virtual Dynamic Test-Bench to Approach Integrated Safety", Proceedings Airbag 2022, 15th International Symposium and Exhibition on Sophisticated Car Occupant Safety Systems, 2022, Mannheim, Germany
11. Kramer, F., "Passive Sicherheit von Kraftfahrzeugen." Springer Vieweg, 2009, ISBN 978-3-8348-9254-6.
12. Zellmer, H., Kahler, C., Eickhoff, B.," Optimised pretensioning of the belt system: A rating criterion and the benefit in consumer tests", 19th ESV Conference 2005, Washington, D.C., Paper Number 05-0004, https://www-esv.nhtsa.dot.gov/Proceedings/19/05-0004-O.pdf
13. Voigt, T., Schrenk, W., Zellmer, H., "Enhanced seat belt modelling process to improve predictive accuracy of dummy response in frontal impact", 22nd ESV Conference 2011, Washington, D.C., Paper Number 11-0151, https://www-esv.nhtsa.dot.gov/Proceedings/22/isv7/main.htm
14. Kramer, F., Franz, U., Lorenz, B., Remfrey, J., Schöneburg, R. "Integrale Sicherheit von Kraftfahrzeugen.", 4. Auflage, SpringerVieweg, 2013, ISBN 978-3-8348-2608-4
15. Mages, M., Seyffert, M., Class, U.," Analysis of the pre-crash-benefit of reversible belt pre-pretensioning in different accident scenarios", 22nd ESV Conference 2011, Washington, D.C., Paper Number 11-0442, https://www-esv.nhtsa.dot.gov/Proceedings/22/isv7/main.htm
16. Kuebler, L.; Gargallo, S.; Elsaesser, K.: Characterization and Evaluation of Frontal Crash Pulses with Respect to Occupant Safety, Proceedings Airbag 2008 – 9th International Symposium and Exhibition on Sophisticated Car Occupant Safety Systems, 2008, Karlsruhe, Germany
17. Straßburger, P., Grotz, B., Heiß, S., Arbter, B., Hachmann, K., Metzger, J., Ocelić, N., "Predictive safety: towards holistic top-down systems engineering for pre-crash systems", 27th ESV Conference 2023, Yokohama, Paper Number 23-0234
18. Dobberstein, J., Mayer, C., Kleinbach, C.," Results oft he EU project OSCCAR from Mercedes Benz perspective", VDI-Berichte Nr. 2387, 13. VDI-Tagung Fahrzeugsicherheit, VDI Verlag GmbH Düsseldorf 2022, ISSN 0083-5560, E-ISBN 978-3-18-102387-7
19. Schilling, S., Soni Anurag, Hinrichs H., Verheyen C., Lucht A., Eickhoff B.,"Evaluation of motorized seatbelts in the Euro NCAP AEB-CCFtap scenario: Application of a feedback control loop model in Simulink coupled to a finite element model in LS-Dyna", VDI-Berichte 2387, Proceedings 13. VDI-Tagung Fahrzeugsicherheit, VDI Verlag GmbH Düsseldorf 2022, E-ISBN 978-3-18-102387-7
20. Regulation No 16 of the Economic Commission for Europe of the United Nations (UNECE) Supplement 2 to the 07 series of amendments — Date of entry into force: 19 July 2018, Official Journal of the European Union 27.4.2018, page L 109/1-99 http://www.unece.org/trans/main/wp29/wp29wgs/wp29gen/wp29fdocsttts.html

CONTACT INFORMATION

Dr.-Ing. Kai-Ulrich Machens, Manager SBS Core Engineering, Test Methodology & Acoustics, ZF Automotive Germany GmbH.
Email : kai-ulrich.machens@zf.com ; phone: +49 7172 302-2286

Dr.-Ing. Lars Kübler, Director SBS Core Engineering, ZF Automotive Germany GmbH.
Email : lars.kuebler@zf.com ; phone: +49 7172 302-2230

ACKNOWLEDGMENTS

APPENDIX A

Evaluation from full vehicle to equivalent bench setup

A validated full vehicle safety system simulation model is best suited to study the effects of model reduction. In contrast to physical tests, it shows no variability in terms initial and boundary conditions, i.e., ATD seating position, belt routing and slack, etc. Sensitivity analyses with this "full safety system" (FSS) model are used to evaluate the effect of model simplifications on kinematics and forces characterizing the ATD dynamics. Figure 14 illustrates this process by means of four basic vehicle environments derived from a midsize sedan with a 5-star rating in current U.S. NCAP as reference vehicle, designated *Pretty Good Vehicle* (PGV). The safety system of the FSS consist of a Switchable Load Limiter (SLL) switching the shoulder belt force from 5 kN to 3 kN at 62 ms and a passenger airbag, the other three configurations are equipped with a retractor-pretensioner and a constant load limiter (CLL) with 5 kN shoulder force and no airbag.

All setups are equally subjected to US NCAP pulse of the PGV for Full Width Frontal Impact (FWFI) at 56 km/h (designated as load case LC0) starting with an H350 ATD model seated on the front passenger seat. The four configurations from Figure 14 show the model complexity is stepwise reduced, from (A) full vehicle SBS, (B) airbags removed, (C) vehicle seat replaced by steel seat and finally (D) ATD arms replaced by lump masses of 3 kg and the under legs substituted by a hinged gear with a 1 kN-damper. The dynamic response of the ATD is described by the three force / displacement pairs displayed in Figure 15: at the retractor; retractor force / webbing pay-out, at the upper body; shoulder belt force / chest forward displacement, and at the lower body; anchor belt force / tongue slip.
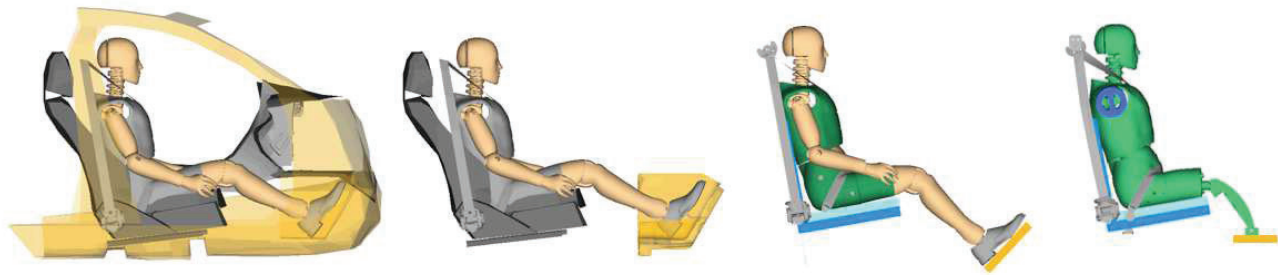

Figure 14 (A) Validated full safety system (FSS) from a midsize sedan (PGV) with (left picture, result in Figure 15: black continuous line) and (B) without airbag system (center left picture, result: black dashed line) is transferred to a configuration with identical anchor point geometry, same H350 (H-angle) (C) but seated on a steal seat with a seating surface tilted by 10° and fixed foot rest position as in FSS (center right picture, result: green dotted line). (D) Simplified bench test setup called "Torso at seat" (T@S) with under legs replaced by a hinged stiff gear and a viscous 1 kN damper, H350 arms substituted by lumped masses of 3 kg fitted to the shoulder hinges (right picture, result: green continuous line).

In phase 1 and 2 the full vehicle configuration and steel seat correlate well for retractor and for the ATD upper body, they diverge only for the anchor belt force. The linear damper at the shank in setup D reduces the anchor belt force in comparison to setup C, but it is not able to cover all effects starting from sliding feet pulling on the tibia up to the feet encountering an obstacle resulting in a complex motion and force sequence. However, the anchor belt force matches in phase 2 adequately with the FSS. The largest deviation in anchor belt force results from the significant restraint performance of the deformable passenger seat at about 70 ms, when the ATD buttocks dives into the seat, causing large contact forces. Fortunately, this effect occurs in phase 3 and hence the simplified setup called Torso @ Seat (T@S) (green continuous line) is able to predict phase 1-2 accurately and independently from the real passenger seat. However, it should be emphasized, that the absolute characteristic force level calculated by using a constant load limiting level to stop the chest forward displacement from T@S configuration at 300 mm is influenced by the lower leg damper characteristics, since the damper dissipate energy from the system, intended like a real vehicle seat.

When comparing the horizontal shear forces acting on the *collarbone* with ATD arms and with lump mass substitutes, shown in Figure 16, it can be concluded that 3 kg lump masses, attached to the shoulders of T@S-ATD represent adequately the dynamic interaction of ATD arms to the torso. As replacing the ATD arms does hardly alter the ATD dynamics in phase 1 and 2, the ATD with lump masses is considered an adequate representation of an H350-ATD. Also, the variant with lump mass improves on test setup repeatability, and prevents damage from uncontrolled moving arms during the test.
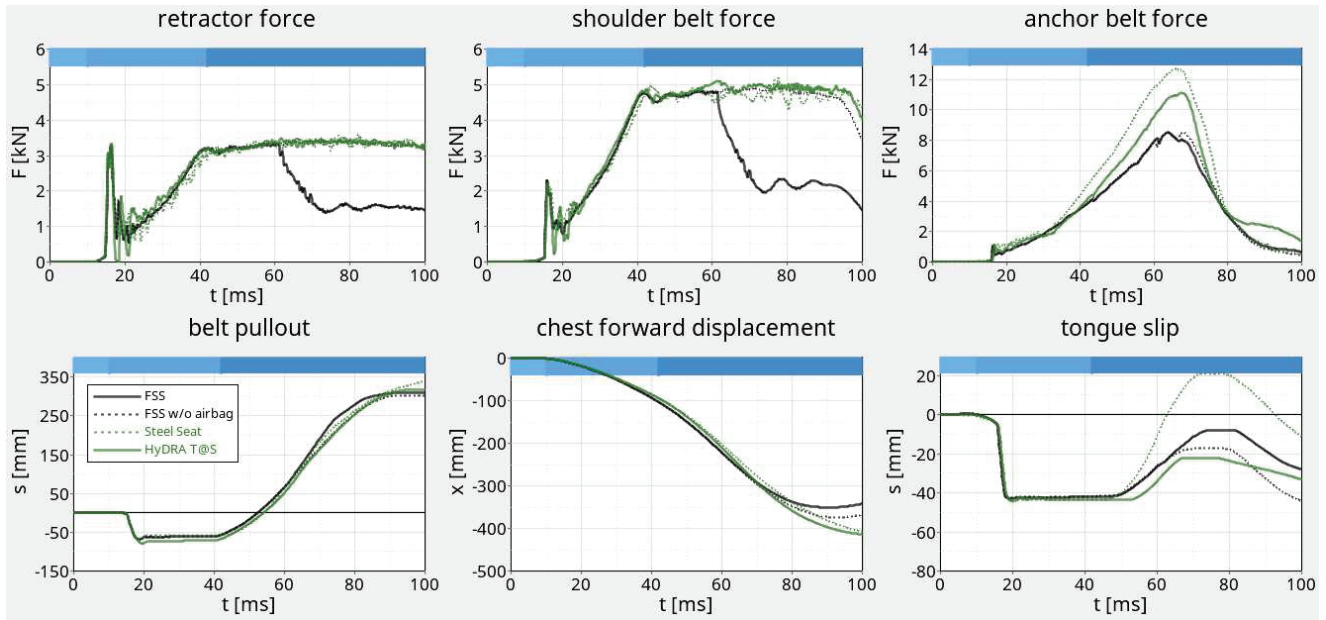
Figure 15 Dynamic ATD response (PGV subjected to LC0: US NCAP pulse for FWFI at 56 km/h with an H350 ATD) for four configurations with stepwise reduced complexity presented in Figure 14 (including scenario associated colors / style definition) expressed by force/displacement pairs for pretensioner, for upper and for lower body. The color banner above the graph differentiates between the in-crash phases 1-3. Comparable results prior to force-closure for all measures except the pelvis force. The misfit (green dotted line) results from low steel seat friction, which is in the final reduction step compensated by a damper added to the hinged gear system substituting the ATD legs (green continuous line).
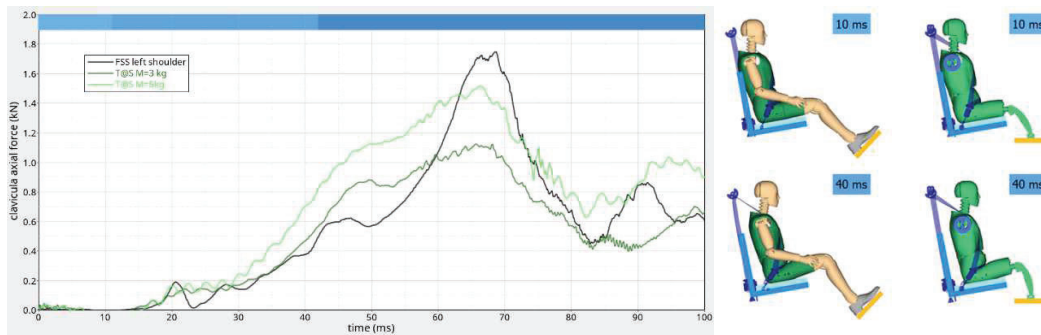
Figure 16 Comparing the horizontal shear force in the left collarbone for the FSS configuration with H350-ATD arms (black line) to its shear force in T@S configuration with lump masses of M=5 kg (light green line) and M=3 kg (dark green line) substitute identifies 3 kg as adequate dynamical replacement. Left picture: Both ATD kinematics shows good agreement for example at the begin of in-crash phase 1 and at the begin of phase 2.

Sensitivity to configuration parameters

Baseline for this investigation is the simplified bench test setup D.0 as presented in the previous section. Figure 17 depicts the different parameters analyzed: D.1: pelvis slack (40 mm added at anchor), D.2: backrest orientation steeper by 5°, D.3: fixation points (anchor and buckle moved by 100 mm to rear) and D.4: D-ring position shifted by 200 mm to rear. The corresponding dynamic ATD responses are displayed in Figure 18.
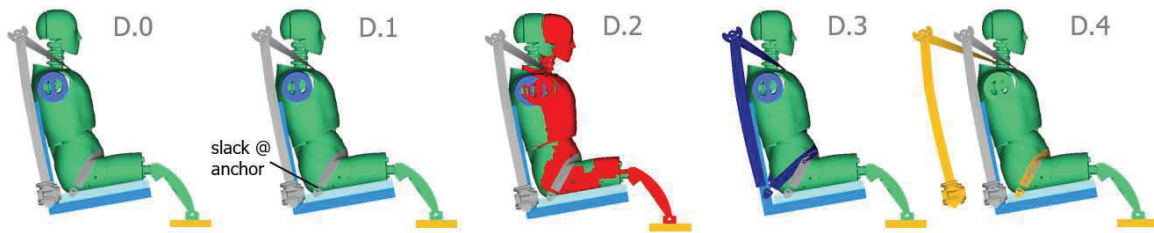

Figure 17 Illustration of four single parameter variations on the simplified bench test setup (D.0) from Figure 15 (from left to right) by D.1: adding 40 mm belt slack at the anchor, D.2: backrest rotated by 5° to the vertical, D.3: anchor and buckle fixation points moved 100 mm to the rear, D.4: D-Ring fixation moved 200 mm to the rear.
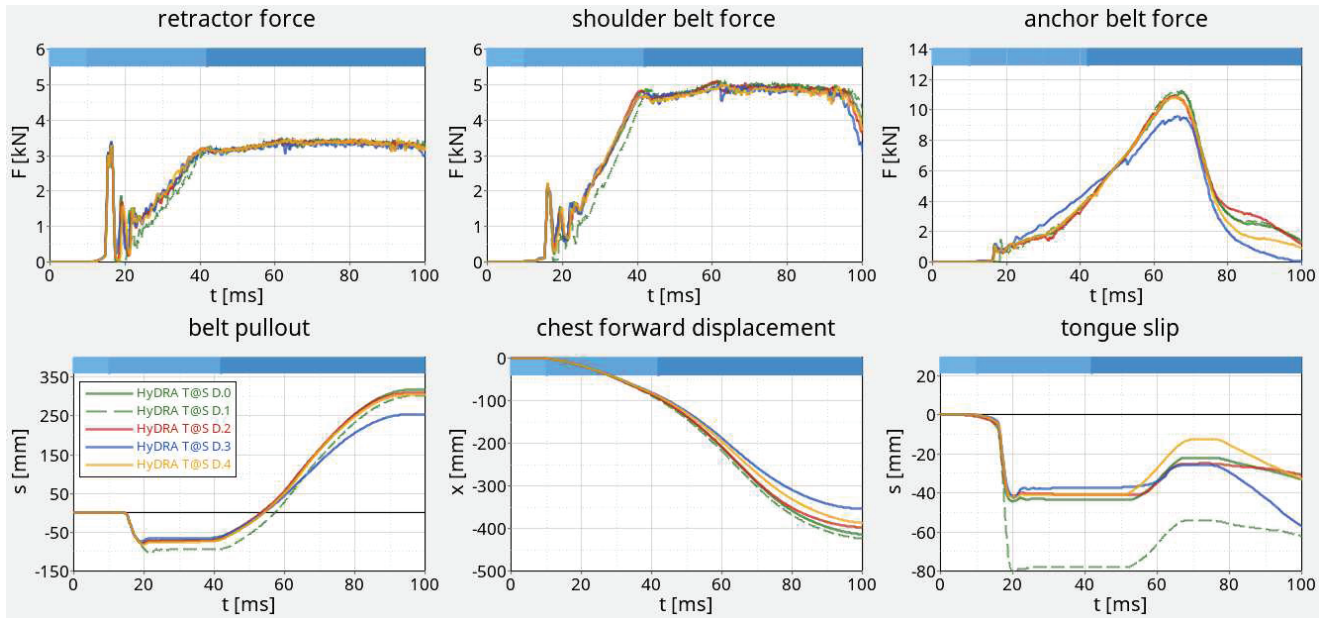
Figure 18 Dynamic ATD response (subjected to LC0: US NCAP pulse of the PGV for FWFI at $56\ km/h$ *with an H350 ATD) for the baseline and four single parameter variations. The added pelvis slack hidden in D.1 (dashed line) at the end of the belt is not fully absorbed by the larger pretensioner pull-in. The changes in the belt geometry D.2-D.4 are not visible in retractor and shoulder force neither in belt pull-in but affect the chest forward displacement.*

The added 40 mm belt slack in D.1, being a significant amount of slack, introduced at the anchor furthest away from the retractor pretensioner is not fully compensated by extra pretensioner pull-in, consequently it affects the ATD chest forward displacement. Modifying the ATD initial condition to a 5° more upright seating position (D.2), as well as modifying the webbing orientation at the fixation points (D.3 and D.4) do not significantly affect the force vs. time behavior. However, the altered belt inclination from ATD to SBS fixation change the force vector in driving direction and sum up to significant differences in the displacements. Chest forward displacement and retractor belt pull-out are closely correlated whilst tongue-slip is less predictive, as it is more sensitive to the changed ATD pelvis kinematic.

The configuration D.3, resulting in the shortest maximal chest forward displacement differs in anchor force vs. time behavior from the other configurations in Figure 18. The changed webbing orientation, predominantly in the lap belt, is assumed to be responsible for a faster slack removal in the pelvis region by the natural pelvis forward displacement, such that pelvis belt forces and friction forces between seating surface and ATD become larger. Therefore, the higher forces acting between seating surface and ATD buttocks restrain the pelvis region. Particularly the changed belt pull-out characteristics of configuration D.3 indicates that the ATD kinematics has been changed, which might influence the ratio of shoulder belt force to energy present in the ATD, as discussed in Appendix B. Consequently, a comparison via CFL of kinematically different configurations like D.3 might be biased.

An analogous kinematic consideration can be applied to configuration D.2 and D.4. Both show a belt routing from ATD to fixation points that are directed more to the rear, and consequently both yield in reduced chest forward displacements. These geometric effects are expected to be perfectly captured by simulation models.

The chest deflection results from this parameter study are displayed in Figure 19, comparing chest deflection for a fixed CLL level in the upper row and different CLL levels (Characteristic shoulder force level – CFL) in the lower row, so that the different configurations yield the same maximal chest forward displacement of 300 mm. Maximal chest deflection is linked to injury assessment ratings like in EU NCAP and it is used as protection criteria for frontal impact in legal requirements. The smallest maximal chest deflection for equal shoulder belt forces and for equal maximum forward displacement is achieved with D.4. The different belt rooting may also contribute to this result, as the belt might be routed further away from the chest deflection sensor point, or closer to the stiff "non biofidelic" clavicle of the H350 ATD deflecting the belt more, thereby reducing the amount of the shoulder belt forces and compressing the chest. Gauging these effects for real-world safety, the ranking deduced from the characteristic shoulder force level reported in

Table 1, the configuration D.3 comes out best, followed by D.4 and D.2. When analyzing the systems with respect to maximal chest deflection with equal maximum chest forward displacement, as illustrated in the lower row of Figure 19, configuration D.4 and D.3 are comparable followed by D.2. D.1 is rated less preferable than D.0.
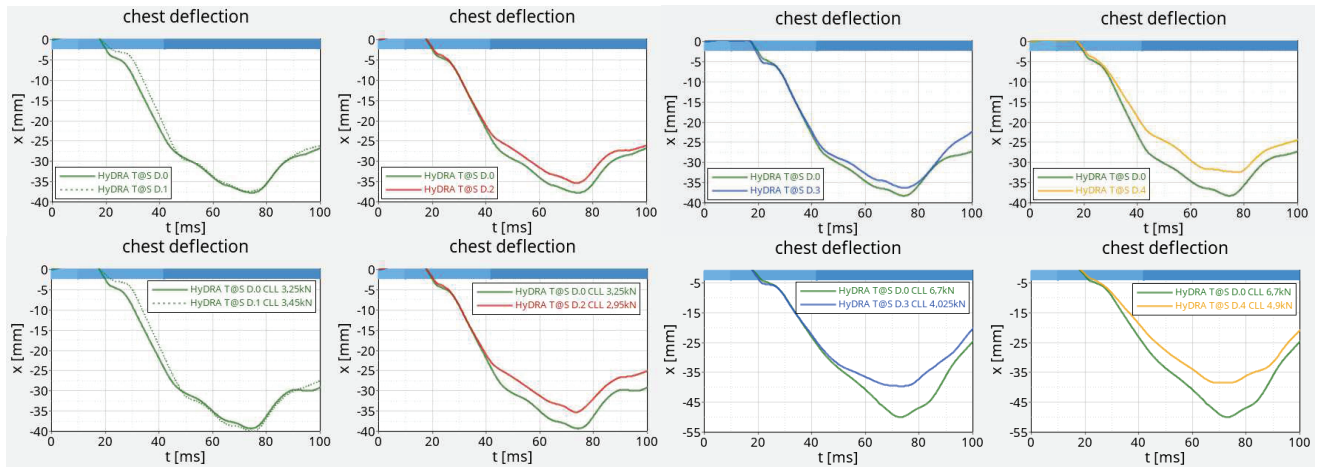
Figure 19 First row: Chest deflection results for the parameter study with configurations in Figure 17 D.1, D.2, D.3, D.4 are compared from left to right with the baseline D.0. The baseline D.0 (apart from D.1 with added slack) remarkably combines largest chest deflections with largest chest forward displacement. Second row: Chest deflection by using the characteristic shoulder force CFL as CLL level, resulting in an identical maximal chest forward displacement in all configurations.

APPENDIX B

Energy Considerations for CFL with maximal chest forward displacement set to 300 mm

The quantity *characteristic shoulder force level* (CFL) introduced and illustrated in Figure 2 is linked to a maximal chest forward displacement distance offset, set to 300 mm, and this quantity coincides with the dynamic test requirement for UNECE regulation R16 [20] to homologate standalone seatbelt systems. The CFL is per definition the *constant* force level needed to stop the ATD chest forward displacement over the *remaining* length, i.e., 300 mm minus the displacement already consumed for *force-closure*. During the *ride-down* phase the ATD kinematics is almost predictable. The pelvis forward displacement is stopped around t=67 ms, coinciding with the maximum peak in the anchor belt force. The maximum chest deflection, regarded as most relevant injury risk quantity, directly associated to seatbelt action, occurs shortly after this point in time (see Figure 19), as the stopped hip introduces an angular moment to the upper body, rotating around the hip joint. Herein the mechanical chest impedance of the ATDs skin vest-foam-rib arrangement, identified by Machens et. al. [10] (in Appendix A Figure 8) to correspond to a mass-spring-damper system with a natural frequency of about 66 Hz, accounts for a delay of 4 ms before a maximum normal chest force results in a maximum chest deflection.

The magnitude of the normal chest force caused by the belt depends on the distance of the routed belt to the chest displacement sensor as well as on the friction coefficient between chest and belt. A rough estimate of typical vehicle configurations in [10] indicates, that less than 50% of the shoulder belt force is directed normal to the chest. This ratio depends on the bend angle of belt around the shoulder, namely on the direction the belt is leaving the shoulder to the D-ring. This should be kept in mind, when directly comparing characteristic shoulder force levels (CFL) from different vehicle configurations i.e., for example changed seating or backrest positions or changes in D-ring positions.

The shoulder belt force, apart from the fact of causing chest deflection, is of major importance to limit the chest forward displacement by dissipating the energy stored in the system. In a system without airbags, ATD energy is presumably dissipated to a minor degree by seat friction, but mainly by shoulder belt force. The work carried out by the shoulder belt force can be calculated by multiplying it with the shoulder belt displacement i.e., belt pull-out from the D-ring.

In most real-world safety systems, the frontal airbag takes over presumably before 300 mm chest forward displacement to trap as soft as possible the upper body and head of the occupant. Therefore, the introduced quantity CFL shoulder force levels are logically significantly higher as the ones observed in actual safety systems with airbags. CFL should be simply regarded as metric, not as meaningful physical quantity for seatbelt systems. This becomes apparent when transferring SBS-1 and SBS-2, both in full vehicle environment using a CLL system (shoulder belt force 5000 N), to a system without airbags. For load case LC0 in Figure 5 both systems stop the chest forward displacement of the T@S slightly beyond 400 mm (SBS-1: 416 mm, SBS-2: 410 mm). In order to stop the ATD at 300 mm maximum chest forward displacement CFL of 10000N (SBS-1) and 8800 N (SBS-2) respectively are required, see Table 2.

It is interesting to compare and discuss these results. In Figure 20 the simulation results for shoulder belt force and *shoulder belt displacement* (i.e., pull-out from the D-ring) for SBS-1 (green) and SBS-2 (blue) are shown for load limiting with different CFL (continuous line) and for identical CLL (dashed line). For same CLL levels (dashed line) the more efficient SBS-2 (larger belt pull-in, no locking dip) reaches *force-closure* (see Figure 20 upper left picture) about 3 ms earlier than SBS-1 but features an similar shoulder belt displacement *after* locking (see Figure 20 lower right picture, small difference may be related to differences in pretensioner design), revealing that the integral from shoulder belt force over shoulder belt displacement (see Figure 20 lower

left picture) and hence the work executed by both systems to stop the chest forward displacement is very similar. Both systems need the same time and displacement to stop chest forward displacement *after* locking and therefore is the difference of 6 *mm* in maximum chest forward displacement visible in Figure 5 (SBS-2: 410 *mm*, SBS-1: 416 *mm*) resulting from a larger belt pull-in of SBS-2, 98 mm compared to 72 mm for SBS-1.
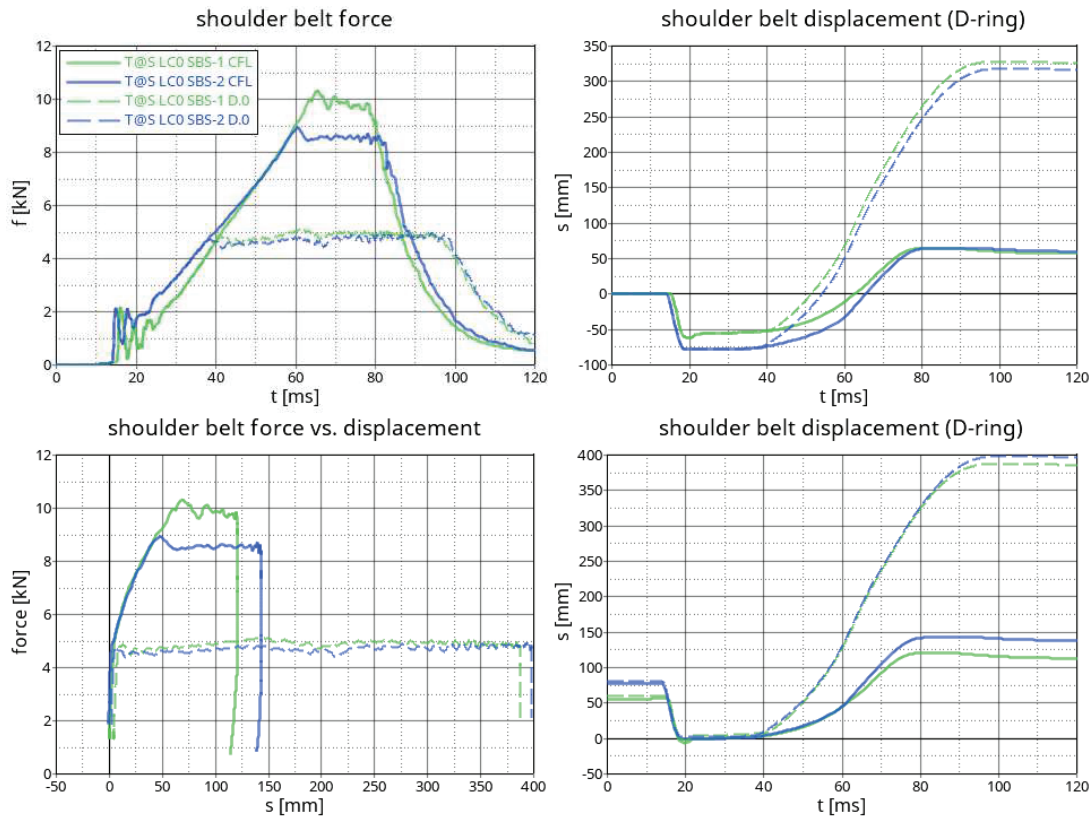

Figure 20 Dynamic T@S response when subjected to LC0 for two different SBSs as in Figure 5: SBS-1 (green) and SBS-2 (blue) with equal CLL (dashed line) and with individual CFL (continuous line). Displaying shoulder belt force vs time (upper left picture), shoulder belt displacement after crash start (t=0) (upper right picture) and after locking (t=22 ms) (lower right picture), shoulder belt force vs. shoulder belt displacement after locking (lower left picture). Shoulder belt displacement after locking is almost equal for same CLL level and different for different CFL, while equal shoulder belt displacement after crash start is observed for same CFLs. Amount of dissipated energy for lower CFL of SBS-2 multiplied by a larger distance similar as the higher CFL of SBS-1 over shorter distance as integral of the over shoulder belt force vs. displacement represents work done by shoulder belt force. Identical force onset for SBS-1 and SBS-2 point to exclusive crash pulse influence (lower left picture).

Limiting the maximum chest forward displacement to 300 mm as defined by the CFL metric is almost equivalent to limit the absolute shoulder belt displacement to 64 mm (at t=80 ms) visible in Figure 20 (upper left picture). The gain in belt pull-in after retractor locking (at t=22 ms), which amounts to a total difference of 22 mm (SBS-2: -78 mm, SBS-1: -56 mm) in shoulder belt displacement is fully used to extend this displacement in the load-limiting phase (Figure 20 lower left picture: SBS-2: 142 mm, SBS-1: 120 mm). To dissipate the same amount of energy with less shoulder belt displacement the characteristic force level needs to be higher for SBS-1. The CFL is almost the ratio of energy (work of the shoulder belt force), needed to stop chest forward displacement at 300 mm, to the rest shoulder belt displacement (available after force-closure) and therefore combines both quantities meaningful for the scenario under investigation.

The relative benefit of the saved shoulder belt displacement to the available *rest* displacement after *force-closure* naturally depends on specified maximum chest forward displacement distance. Referring to Table 2, SBS-1 is for T@S LC0 13.6% less favorable than SBS-2. If 400 mm instead of 300 mm would have been defined as limit to calculate the characteristic shoulder force level, a CFL* of 5200 N (SBS-1) and 4900 N (SBS-2) would be obtained, which corresponds to a disadvantage of only 6% for SBS-1 respectively SBS-2 (PGS). CFL based on 300 mm maximum chest forward displacement is deemed suitable to distinguish the performance of seatbelt systems in a meaningful way, as it reflects reasonably well average vehicle configurations on the market, and also reflects the UNECE R16 homologation requirement.

PEER REVIEW PAPER

This paper has been peer-reviewed and published in a special edition of Traffic Injury Prevention 24(S1), by Taylor & Francis Group. The complete paper will be available on the Traffic Injury Prevention website soon. To access ESV Peer-reviewed papers click the link below
https://www.tandfonline.com/toc/gcpi20/24/sup1?nav=tocList

PROPOSED SPEED LIMITS FOR THE 2030 MOTOR VEHICLE

Matteo Rizzi
Swedish Transport Administration
Sweden

Ola Boström
Veoneer, Chalmers University of Technology
Sweden

Rikard Fredriksson
Swedish Transport Administration, Chalmers University of Technology
Sweden

Anders Kullgren
Folksam, Chalmers University of Technology
Sweden

Nils Lubbe
Autoliv Research, Chalmers University of Technology
Sweden

Johan Strandroth
Strandroth Incorporated
Sweden

Claes Tingvall
AFRY, Chalmers University of Technology
Sweden

Paper Number 23-0166

ABSTRACT

Vision Zero builds on the aspiration to keep kinetic energy below human tolerance to prevent fatalities and serious injuries. In this work, a Swedish expert group within the SAFER arena estimated the maximum safe speed limits for the 2030 motor vehicle based on the boundary conditions of vehicles, road infrastructure and human crash tolerance to achieve close to zero road fatalities and serious injuries.

The present work was based on expert consensus, rather than a retrospective quantitative analysis of crash data. Different load cases were discussed separately, with the involvement of a passenger car being the common denominator. The passenger car and its collision partner were assumed to be of model year 2030, thus reflecting the base safety level of the Swedish car fleet by approximately 2050.

The boundary conditions were set based on pre-crash autonomous braking ability and the maximum acceptable impact speeds that would result in a very low risk of death or serious injury among the car occupants and the car's collision partner. In the case of car to pedestrian impacts, the acceptable impact speed was set to zero, as any impact with pedestrians can lead to serious injuries as a result of ground impacts. It was expected that the responsibility to comply with speed limits will move from the driver to the car itself, and that travel speeds will be autonomously reduced when low road friction, sight obstructions, and other challenges in the traffic environment are detected. This function was expected to be non-overridable. Lateral control was also expected to be further enhanced with lane support technologies, although it was assumed that it will be still possible to override such technologies.

Over time, increased performance of vehicle safety technologies will likely be able to prevent an increasingly large proportion of crashes in all load cases. However, in line with Vision Zero design principles, human crash tolerance will always be the ultimate boundary condition to guarantee a safe outcome in a crash. As a result, the recommended maximum travel speeds in the road transport system containing motor vehicles only of model year 2030 and beyond are:

- 5-7 km/h in pedestrian priority areas,
- 40 km/h in mixed traffic urban areas, if there are no obstructed sensor sightlines, e.g. due to parked vehicles along the sidewalk,
- 50 to 80 km/h on roads without mid- and roadside barriers,
- 100+ km/h on roads with continuous mid- and roadside barriers,
- 40 to 60 km/h in intersections, depending on vehicle mass differences.

The results from this work can be used to inform the development and amendment of transport planning guidelines when moving away from the economical paradigm into Safe System boundary conditions in the setting of speed limits.

INTRODUCTION

Vision Zero, the policy framework for traffic safety introduced in 1995, builds on the aspiration to control kinetic energy and keep the amount of kinetic energy below the threshold of human biomechanics tolerance for severe injuries (Tingvall and Haworth, 1999). In the introduction of Vision Zero, kinetic energy was simply a function of travel speed, but was later defined as impact speed. The strong relationship and the high sensitivity of speed versus injuries has been known for a long time. The early works by Nilsson presented in 1981 (Nilsson 1981, 2004) and later by Elvik (2009) show that travel speed versus fatalities and serious injuries are non-linear relationships and are sometimes described as power functions (Elvik et al., 2019). The relationship between impact speed, or sometimes delta V (change of velocity), and injury risk has been described using many methods.

Injury probabilities are typically quantified with regression models applied to large representative samples of real-world crashes (McMurry et al., 2021; Lubbe et al., 2022). Of particular importance is a good estimation of delta V, for example available from on-board crash recorders (Kullgren et al., 1995; Funk et al., 2008), to show a clear and strong relationship between delta V and serious injury as demonstrated by Doecke et al. (2021). Studies have clearly shown that the relationships are non-linear, but that the threshold for an injury and the slope of the non-linear relationships are complex to estimate by statistical methods (Kullgren and Stigson 2010; Rosén and Sander 2009).

The first attempt to estimate the maximum travel speed and associated speed limits to fit with an aspiration of zero fatalities was done in 1996 (Tingvall et al., 1996). This was later followed up in a paper by Tingvall and Haworth in 1999, with a focus on pedestrians and car occupants.

Table 1.
Possible long-term maximum travel speeds related to the infrastructure, given best practice in vehicle design and 100% seat belt use. Source: Tingvall and Haworth (1999)

Type of infrastructure and traffic	possible travel speed (km/h)
Locations with possible conflicts between pedestrians and cars	30
Intersections with possible side impacts between cars	50
Roads with possible frontal impacts between cars	70
Roads with no possibility of a side impact or frontal impact (only impacts with the infrastructure)	100+

The indicative speed limits were based on a few boundary conditions; car occupants using seat belts and complying with speed limits, and the car being rated four stars at the time Euro NCAP presented the results (at the time, the maximum Euro NCAP rating was just four stars). Even though road user age was known to strongly influence injury outcome, this aspect was not explicitly considered. The limits were said to be relevant long-term. Given the boundary conditions, empirical data to validate the result of the chosen boundary conditions were not available at the time; rather they were seen as aspirations of a number of desired safety performance factors and how they can interact to allow for a certain speed limit. There have been a few attempts to investigate the effect of fulfilling these boundary conditions but they failed due to incomplete speed data and the fact that the safety of individual car models can vary substantially (Stigson 2009).

Later, more boundary conditions were set up, in line with the development of vehicle technologies. Eugensson et al. (2011) presented a speed limit chart based on the fitment and performance of safety technologies on a car of model year (MY) 2020 and beyond (Figure 1).

In contrast to the earlier boundary conditions set by Tingvall and Haworth (1999) which assumed travel speed and impact speed being identical, the new boundary conditions set by Eugensson et al. (2011) took into consideration pre-impact braking. This resulted in lower impact velocities but higher acceptable travel speeds due to the availability of pre-impact braking. The other boundary conditions, like using seat belts and not exceeding posted speed limits, were identical between the two studies. Frailty of elderly road users was not specifically addressed. The safety performance of the car would be in line with the expected safety level for a five stars car of MY 2020 - without precisely knowing what safety features five stars car of MY 2020 would have.
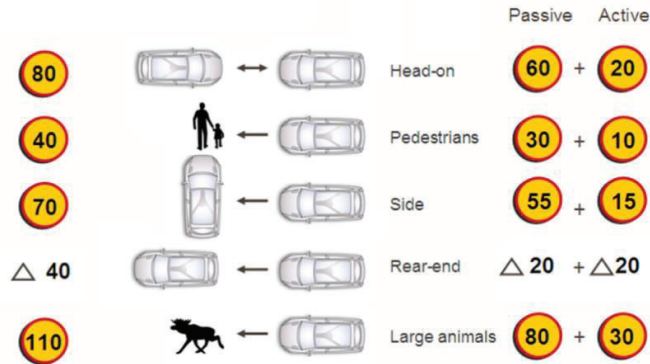

Figure 1. Examples on how the responsibilities can be divided between vehicles (active and passive safety) and requirements for infrastructure (speed limits). Source: Eugensson et al., 2011.

Apart from pre-impact braking, there are other pre-crash technologies intervening prior to crashes, such as Lane Keep Assist (LKA) and Emergency Lane Keeping (ELK), that have been shown in a number of studies to be effective for safety (Leslie et al., 2022). Utilizing a technique to predict the future outcome of technologies, Strandroth (2015) showed that such technologies would substantially reduce the number of fatalities in car crashes and change the pattern of crash types. In research of motorcycle crashes, Rizzi (2016) showed that combinations of safety technologies can interact to produce a higher level of safety where one safety technology is dependent on another safety technology. Leg protection was dependent on an upright crash configuration, which in turn was provided by Antilock Braking Systems (ABS). Similarly, Fredriksson has shown in several studies the benefit of combining active/auto-brake and passive/deployable countermeasures for both pedestrians and bicyclists (Fredriksson and Rosén 2014, Fredriksson et al., 2015). In all, there are many examples of technologies that can not only protect a road user at a given crash severity or change the crash severity by pre-impact braking, and also reduce the risk of a crash or an injury. Therefore, it could be argued that there is a need to update the results shown in Eugensson et al. (2011) to consider the increasing potential of vehicle safety technologies to reduce the risk of death and injury.

The aim of the present study is to update the boundary conditions of vehicles and road infrastructure and to estimate speed limits that would result in a very low risk of death or serious injury. The boundary conditions would mirror the expected safety technologies and performance of a car of MY 2030 and beyond. It would also involve a number of other requirements explained in the next section.

GENERAL APPROACH AND MAIN ASSUMPTIONS

Similar to Eugensson et al. (2011), the general approach of the present work was to form a consensus group to discuss boundary conditions for a number of load cases involving passenger cars. It is therefore important to stress that the present work was mostly based on a rationale using logical deduction, rather than the analysis of crash data. A working group was formed including seven road safety experts with different backgrounds and associations. Most participants were selected within the SAFER arena (www.saferresearch.com) and agreed to be a part of the working group on a voluntary basis and without any monetary compensation. The process was facilitated by discussing different load cases separately, with the involvement of a passenger car being the

common denominator between the cases. The car's collision partner was also assumed to be of MY 2030, thus reflecting the base safety level of the Swedish car fleet by approximately 2050. Similar to Eugensson et al. (2011), the boundary conditions were set based on pre-crash autonomous braking and maximum acceptable impact speed to make long-term injuries and fatalities unlikely among the car occupants and the car's collision partner. The group agreed to not include pre-crash autonomous emergency steering in the boundary conditions as its reliability and relation to injury outcome is still unclear (Robinson et al., 2020).

In this work, it was acknowledged that striking a pedestrian with a passenger car will always be associated with a risk of long-term injury or fatality, since hitting a pedestrian can result in serious injuries as the pedestrian hit the road surface. Therefore, in the boundary conditions for pedestrian impacts, the acceptable impact speed was set to zero km/h.

It was also acknowledged that the maintenance of the road infrastructure has become more relevant with advanced pre-crash technologies like Electronic Stability Control (ESC), Autonomous Emergency Braking (AEB) and lane support technologies. It was therefore anticipated that the road maintenance will be kept to a standard where the vehicle's Advanced Driving-Assistance Systems (ADAS) can operate with no reduction in functionality. It was also anticipated that the road friction would either be at the optimum level, or that the vehicle can detect the available road friction and consequently adjust its travel speed. Accurate and instantaneous road friction estimation is a current topic in research and development (Sander et al., 2019). Hence, we acknowledged that road conditions will not always be optimal, but we expect the vehicle to be able to adjust to them. Basically, it is up to the infrastructure provider to guarantee good maintenance and road friction to deliver the intended mobility on the road.

Vehicles' ability to detect other road users was anticipated to be improved compared to the present performance. The average time between detection and full autonomous braking was assumed to be about 0.5 seconds, which the working group believed to be reasonable based on the current sensor performance. The development of pre-impact safety technologies also includes connectivity and the vehicle's ability to adapt to factors that influence safety. The gradual introduction of ADAS nowadays also includes support for not exceeding the posted speed limit (e.g. Intelligent Speed Assistance, ISA). In general terms, it is anticipated that by 2030, a new car will not allow the driver to travel above the speed at which the car would be able to stop within its sensor horizon with maximum autonomous braking (based on available friction). More specifically, it is anticipated that cars will detect objects and potential crash partners in the sensor horizon and predict potential and possible maneuvers and crash risks. However, sudden, hard-to-predict maneuvers and sensor imperfections might still lead to collisions. Here, the sensor horizon was considered to be about three seconds headway distance, which seems feasible due to the "ground rule" in a car-following situation.

Similarly, we expect vehicle crashworthiness to improve further, with improved structural integrity at high speeds and softer, more forgiving responses at low speeds. This would be enabled, for example, by adaptive front-end structures (Wågström et al., 2005), adaptive occupant restraints (Mackay et al., 1994; Zhao et al., 2019) and better protection of road users outside the vehicle (Fredriksson and Rosén 2014, Fredriksson et al., 2015).

The main assumptions of the present work can be summarized as follows:
● Compared to Eugensson et al. (2011), a new main assumption was added; a passenger car of MY 2030 cannot be driven faster than the speed at which it can stop using maximum braking within its sensor horizon (3 seconds headway distance). It would not be possible to override this functionality. Therefore, the boundary condition of not exceeding the speed limit is moved from the driver to the car itself, and it is a function of the road environment, available road friction, sight conditions etc. Lateral control is enhanced with lane support technologies, although it will be possible to override such technologies.
● Based on that assumption, the boundary conditions are given by pre-crash autonomous braking and maximum acceptable impact speeds that would pose a very low risk of death or serious injury. In the case of pedestrians hit by cars, the acceptable impact speed is set to zero km/h.
● The other boundary conditions, i.e. proper use of seat belts and other protective equipment, is unchanged compared to Eugensson et al. (2021).
● When the passenger car's counterpart is another motor vehicle, it is assumed that that vehicle is also of MY 2030. This is expected to reflect the lowest safety performance of the Swedish vehicle fleet by approximately 2050.

The chain of events leading to a crash (Rizzi 2016) can be used to further illustrate the main differences between Eugensson et al. (2011) and the present work (see Figures 2 and 3). The potential contribution of ADAS in

reducing the number of crashes was also considered in the present work, and conceptually illustrated by a "funnel" between the safe driving phase and the actual crash. The size of such a funnel varies across different load cases, as further described in later sections.
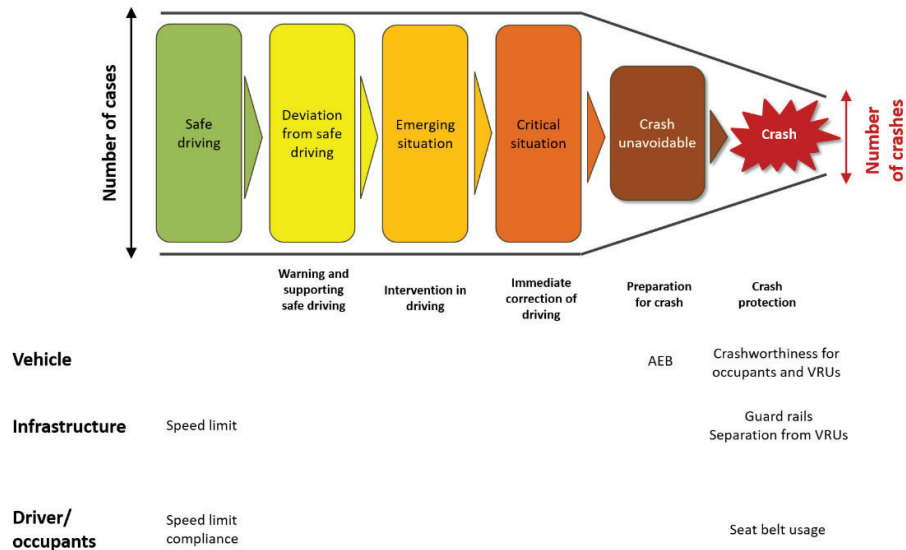

Figure 2. Previous work (Eugensson et al., 2011) illustrated with the chain of events leading to a crash.
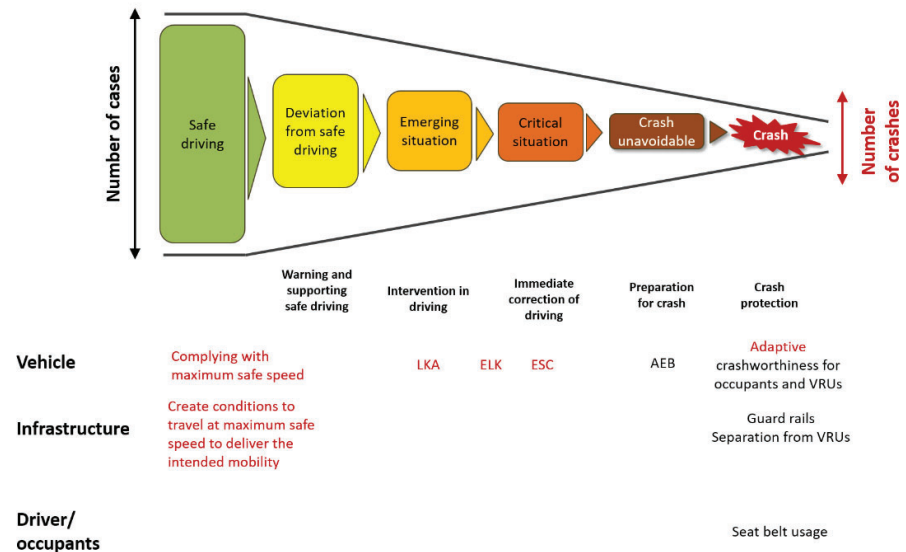

Figure 3. Present work illustrated with the chain of events leading to a crash. Differences with Eugensson et al. (2011) are highlighted with red text.

LOAD CASES

Rear-end collisions

The vast majority of rear-end crashes occur between an approaching vehicle and a still standing or a moving vehicle. In order to study the ability of vehicle seats to prevent long-term whiplash symptoms, rear-end crash tests are conducted by Euro NCAP at a delta V of 16 km/h using a triangular pulse shape. Most vehicle models perform well in these tests. Studies of real-world crashes have shown that the majority of rear-end crashes occur at relatively low speeds and with a low resulting delta V, below 10 km/h (Kullgren and Stigson, 2011). It has also been shown that crashes resulting in long-term whiplash symptoms among the occupants of the struck vehicle usually occur at a delta V above 15 km/h. Also, 15 km/h has been reported to correspond to a 10% risk of long-term symptoms (Kullgren and Stigson, 2011). If the threshold for acceptable risk is set at 10%, the

relative speed between vehicles (of the same mass) in rear-end crashes should be kept below 30 km/h. However, it should be noted that the mentioned results show average risks for the population. The literature shows that many variables may influence the risk of sustaining long-term symptoms after rear-end crashes such as age, gender, stature, weight, seating position, vehicle or seat type, occupant head orientation etc. (Jakobson 2004, 2005; Krafft et al., 1996; Kullgren and Stigson, 2011).

In addition to seats designed to prevent whiplash symptoms, AEB systems fitted to the striking vehicles are expected to be the most important safety technology to avoid injuries in rear-end crashes, either by preventing the crash or by mitigating the crash severity. In 2030 all new passenger cars in Europe are expected to be fitted with AEB technologies aimed to avoid or mitigate crashes with other vehicles travelling in the same direction, both for low-speed and high-speed crashes. The AEB systems can detect both still standing and moving vehicles in the same direction. In 2030, new heavy vehicles (HV) and buses are also expected to have better detection of stationary and moving vehicles compared to the situation today. Studies have shown that first generation AEB technologies, implemented in the last decade, reduce the risk to strike the rear of another vehicle by 38% (Fildes et al., 2015; Rizzi et al., 2014).

An important aspect regarding avoiding rear-end crashes between vehicles travelling in the same direction is that the approaching vehicle must keep the distance of at least the sensor horizon of three seconds to give the AEB system a possibility to react if an unexpected hazardous situation should occur. It is expected that cars of MY 2030 will also have digital maps and GPS positioning that provide the possibility to have a three second headway distance, even in the case of sharp road curvatures and road crests. Cars are also expected to have radar sensors in the vehicle corners.

Hereby, predictable rear-end collisions are expected to be prevented leaving only a very small number of unpredictable rear-end crashes, e.g. scenarios with sudden maneuvers due to system override and sensor errors. A study based on the performance of current advanced vehicle safety technology showed that after full implementation, rear-end crashes will approximately account for 5-10 % of all crashes leading to an injury (Östling et al., 2019a; Östling et al., 2019b). Even though it is expected that this residual will be even further reduced by 2030, the relative velocity in case of a hazardous situation should be kept within the effective envelope of whiplash protections, not exceeding 30 km/h.

Frontal car-car and car-HV collisions
Head-on collisions are expected to occur with MY 2030 vehicles. Narrow undivided roads without mid-separation will allow for sudden and unforeseeable lane departures into opposing traffic, even with advanced lane support and AEB systems, for example on icy roads, as a consequence of technical failures or drivers overriding lateral control systems.

Recent studies estimating residual crashes confirm the expectation of the persistence of head-on collisions. Östling et al. (2019b) found head-on collisions to currently account for 10-12% of crashes leading to AIS2+ injuries; after introduction of ADAS including Driver initiated Evasive Steering Assist (ESA) and Lane Keep Assist (LKA), head-on collisions are still expected to account for 7-12%. Östling et al. (2019a) similarly estimated AIS 2+ injuries occurring in lane departure - opposite direction crashes to reduce from 11% to 6% with ADAS, but not be eliminated.

While steering is in principle more effective in avoiding head-on crashes at high speeds (Brännström et al., 2014), the available road space may not always be sufficient. Roads may simply not be wide enough to avoid an oncoming vehicle on either side. With emergency steering not always being effective, emergency braking appears the avoidance maneuver of choice, which is expected to mitigate crash severity rather than avoid head-on collisions altogether.

Full width frontal impacts against a rigid barrier in consumer ratings are conducted at 50 to 56 km/h. Offset deformable barrier tests are commonly conducted at 64 km/h, replicating a head-on collision at 50 km/h impact speed for both collision partners (Euro NCAP, 2022) and the Insurance Institute for Highway Safety (IIHS) small overlap test is also conducted at 64 km/h. Many passenger cars get good to excellent safety ratings in the IIHS tests. Higher test speeds in IIHS crash tests correspond to an increase in injury risk, with a 15% risk of AIS3+ injury at 64 km/h impact speed and increasing to 59% at 80 km/h and 78% at 90 km/h (Kim et al., 2021).

Doecke et al. (2021) suggest a 10% risk of serious injury at 53 km/h impact speed (calculated as half the closing speed between the two vehicles meeting head-on) based on US field data, and a 1% risk at 28 km/h and a 50%

risk at 76 km/h. Stigson et al. (2012) estimated a 10% MAIS2+ injury risk at a delta V of 28 km/h based on analysis of Swedish on-board crash recorder.

It is anticipated that crashworthiness and restraint systems will get better (Kullgren et al., 2019), to the level where we believe that an impact speed of 60 km/h (a closing speed of 120 km/h) in a head-on collision with an equivalent and compatible passenger car of MY 2030 will be safe enough to avoid serious injuries.

AEB is expected to reduce impact speeds in imminent head-on crashes. However, trajectories can change suddenly and turn a harmless passing scenario into a crash scenario very quickly, especially considering small overlap crashes. The TTC at which a collision becomes unavoidable and triggers AEB, if detected correctly, can be very small even for the simpler rear-end crashes (Spitzhüttl and Liers, 2019). Short TTCs at activation translate into small speed reductions. It was expected that a reasonable performance for head-on AEB in vehicles of MY 2030 is a 20 km/h speed reduction, for reasonably large overlaps and as assuming a TTC judgment of 1.0 second in average (Hasegawea et al., 2017). Aggressive AEB systems with sensitive threat assessment and performance brakes may very well reduce more speed in large overlap situations. For small overlaps and systems optimized to prevent false positive activations, substantial speed reductions will be hard to achieve.

Therefore, we suggest a travel speed of up to 80 km/h (60 km/h allowable impact speed + 20 km/h speed reduction by AEB) on roads without mid-separation where passenger cars could crash head-on. Optimal road friction needs to be provided, AEB systems need to be developed and tested for small-overlap head-on collisions to prove their ability to reliably reduce speed by 20 km/h, and crashworthiness and occupant protection needs to improve particularly in small overlap crashes to provide protection at speeds of 60 km/h and above in case AEB fails to sufficiently mitigate or avoid the collision.

Head-on crashes with incompatible and divergent vehicles, such as heavy vehicles (HV), remain challenging. In crashes with HV, a delta V of 60 km/h for the passenger car is assumed manageable; therefore, both the HV and the car can be allowed to impact at 30 km/h each, only. Strandroth et al. (2012) analyzed car-to-HV crashes in Sweden concluding that an average delta V reduction for the passenger car of 18 km/h with braking only on the HV and 30 km/h with braking also on the passenger car can be achieved. The performance is expected to increase to a speed reduction of 20 km/h before impact for both the car and the HV. We suggest a travel speed of 50 km/h for both the passenger cars and HV where they can meet in opposing traffic without suitable mid-separation given that both are equipped with performant AEB.

Side collisions
Side collisions car-car and car-HV: in Sweden crashes at intersections are the third most common crash type for passenger car fatalities (Trafikanalys 2020). In the European Union, 18% of fatal crashes occur in intersections (ERSO 2021). In the United States, side impacts accounted for 23% of all passenger vehicle fatalities in 2020 (IIHS 2021).

Due to the basic design of a car, today and for the foreseeable future, an occupant is least protected when the car is impacted from the side. Theoretically, with infrastructure measures such as roundabouts, traffic-signs or signal controls at intersections, and with vehicles designed to obey the signals (i.e. connected vehicles) and not lose control due to ESC, vehicles would only impact in the longitudinal direction. However, in situations where vehicles need to leave or enter a main road without the safety measure of a roundabout, further development of ADAS is needed and the sensor set needs to monitor 360 degrees. Side impacts occur typically in intersections (straight crossing path, SCP), in left turns across path (LTAP) and in loss of control.

Loss of control (LOC) crashes have decreased dramatically with ESC systems, and especially the LOC type where the vehicle oversteers, and the side is exposed to other vehicles (Lie 2012). When we move towards more assisted driving and connected vehicles (vehicle to vehicle - V2V, vehicle to infrastructure - V2I) where unsafe speeds due to a mismatch between speed and road friction can be avoided, it is believed that LOC crashes with other vehicles can more or less be eliminated.

In LTAP crashes, the struck vehicle typically decelerates close to or to a full stop on a rural road, before initiating a left turn. If drivers fail to recognize the oncoming vehicle, they may proceed the left turn from this low speed to expose the right side to the oncoming car. There are already systems in production that can detect an oncoming vehicle (including Powered Two Wheelers, PTW) up to 60 km/h for a still standing ego vehicle and brake the car to prevent the turn. This is also driven by AEB test protocols in Euro NCAP.

The SCP is the remaining scenario and likely the most challenging one in the future. Straight crossing path will be difficult even with advanced sensors due to limited sight lines and also because of the large sensor field of view necessary. Besides, vehicles obeying a stop sign, for example, will still have a risk entering an intersection exposed for an oncoming vehicle from either side. From a timing perspective it is challenging for the oncoming vehicle to reduce the speed automatically to a large extent (AEB with forward looking sensors). On the other hand, it is less challenging for the straight crossing vehicle to be automatically stopped from entering the intersection due to sensors looking to the sides. It seems this technology is possible to scale at least for speeds up to 60 km/h of the oncoming vehicles. This is also supported by a new upcoming test in Euro NCAP with this scenario and speed range.

Regarding the maximum impact speeds, it seems that a delta V of 30-40 km/h may be acceptable, based on crash data with modern cars with high NCAP adult occupant rating (Lubbe et al., 2022). In today's best cars it seems that a delta V of 40 km/h is not feasible, but with almost ten more years of development and increased test requirements in NCAP, it is reasonable to believe that this should be achievable for car-to-car impacts. With an acceptable delta V of 40 km/h and the fact that the cars being considered here are ranging in weight from 1500 to 3500 kg, it seems feasible that a 60 km/h travel speed for cars could be managed. As for HVs the weight difference to cars means that they can never travel faster than 40 km/h through a 3 or 4-way intersection.

Side collisions PTW-to-car: worldwide at least half of the 1.35 million traffic fatalities yearly are vulnerable road users. The largest group of these are Powered-Two-Wheeler (PTW) riders, which make up 28% of all road traffic fatalities (WHO 2018). In Europe, this group makes up 15% of fatalities in road traffic, and although there has been a reduction in PTW fatalities in Europe, it has been a slower decline than for overall traffic fatalities (ERSO 2021). Sweden has a similar trend to Europe (STA 2021).

Crashes at intersections are among the most common scenarios with severe and fatal injuries (Fredriksson and Sui 2015, 2016; Puthan et al., 2021). Impact speed, alongside other factors, has been shown to strongly influence injury and fatality outcomes for motorcyclists (Ding et al., 2019). With regard to car-to-PTW collisions in Sweden, crashes at intersections are the most common crash type. In 85% of these, a car crosses the PTWs path in the SCP or LTAP scenarios (STA 2016a).

Compared to other vehicle types, it is more difficult to predict potential new safety systems for PTWs implemented by 2030. Although the implementation of airbags on PTWs is still very limited, the technology seems to be mature (Aikyo et al., 2015) for full-scale implementation. Similarly, research on rear-end AEB for PTWs has been ongoing for several years (Savino et al., 2020; Lucci et al., 2021). We do not expect non-overridable Intelligent Speed Assist will be standard by natural evolution. We foresee that PTWs of MY 2030 may be equipped with a frontal airbag and AEB for rear-end scenarios, but the implementation rate remains unclear.

In intersection crashes, the PTW typically impacts the side of a crossing vehicle. Using risk curves based on traditional motorcycles (Ding et al., 2019) with a helmeted PTW rider, and even with the best-case added protection from a PTW airbag we estimate that 40 km/h is the maximum acceptable impact speed. It is therefore suggested that maximum speed for a PTW through an intersection should be 40 km/h, although this may not confer a very low fatality and injury risk.

Collisions with pedestrians and bicyclists
Collisions between cars and pedestrians are to be avoided altogether. Injuries and even fatalities can occur at very low collision speeds (Hussain et al., 2019) and it appears necessary to emphasize the need to guarantee the freedom from danger for pedestrians. Pedestrians pose very little hazard to other road users, and in collisions between cars and pedestrians it is typically the pedestrian that gets injured, not the car occupant. Thus, the need for pedestrians to be protected from cars over the demand for mobility of cars must be emphasized.

In areas where cars and pedestrians mix, inner city streets or pedestrian streets, and the movements of pedestrians cannot be predicted with certainty, walking speed, i.e. 5 to 7 km/h, appears suitable to guarantee that a driver, or alternatively an automated collision avoidance system, can detect and react to suddenly manifesting collision threats.

Mixed traffic not only includes intentionally mixed traffic on the same surface areas, but also areas where pedestrians can remain undetected while in close proximity to a motor vehicle lane and may suddenly appear when attempting to cross the lane. Besides obstructed sight lines, pedestrian collisions also occur in conditions such as night with glare from streetlights and other participants or rain may impair detection (Wisch et al., 2013).

These sudden appearances may leave very little time to react, with a substantial number of detections below one second TTC and exceeding AEB ability to prevent a collision (Jeppsson et al., 2018). Therefore, in areas with pedestrian traffic and view obstacles such as parked cars along the curb, the car speed must remain at 5-7 km/h to enable the driver or the automated emergency braking system to avoid a collision.

If there is a clear separation between motor vehicle traffic and the view is not obstructed, travel speed may be allowed to increase. If it can be predicted with certainty that pedestrian movements cannot lead to collisions within one to two seconds, a driving speed of 40 km/h should be manageable. That could mean in practice, if the absence of pedestrians within a sufficiently large sensor horizon is guaranteed, then cars can travel at 40 km/h. If the absence cannot be guaranteed, the driving speed needs to decrease proportionally to the possibility of a pedestrian to reach the driving path, and in the end, again to 5-7 km/h.

Collisions between cars and cyclists are more challenging as cyclists can move faster and more often share the same road space with cars. Guaranteeing no cyclist being able to reach the driving path of a car in crossing and turning scenarios requires larger sensor detection areas. When interactions between cyclists and car drivers can occur in longitudinal traffic, lateral distances become crucial. If sufficient lateral distance is not ensured, sudden lateral movements of the bicycle (sudden side winds, the rider attempting to avoid sudden obstacles on the road or starting to turn left not noticing the car) can bring the bicycle quickly in front of the car or directly cause collisions with the side of the car. Guaranteeing absence of collisions appears not feasible; therefore, a mix between speed reduction and injury reduction measures are needed.

We expect that at 20 km/h closing speed, appropriate measures on the car (softened front and side structures; external airbags) (Hu and Klinich, 2012; Fredriksson et al., 2015), and protective equipment for the cyclists (e.g. helmets; Oliver and Creighton (2017)), ideally in combination, can prevent serious injuries (Pipkorn et al., 2020). Forgiving road surfaces for secondary impacts may also be needed. Euro NCAP assesses AEB for cyclists up to a car speed of 60 km/h in straight-crossing scenarios and up to 20 km/h in turning scenarios. We expect that AEB on cars can reliably reduce crash speed by 20 km/h in all intersection scenarios if visibility is assured. Therefore, a 40 km/h traveling speed for cars (and no limit for cyclists) in intersections with good visibility appears suitable also to protect cyclists.

In longitudinal scenarios, pre-impact kinematics appear more complex, and collisions are perhaps harder to predict. While Euro NCAP assesses AEB in longitudinal scenarios where the cyclist is lined up to be hit by the center of the car front, smaller overlaps (i.e., the cyclist more on the side) are not assessed for AEB, but Forward Collision Warning (FCW) only. In line with the complexity assumed for head-on collision between cars, a speed reduction of 20 km/h appears to be a realistic performance for AEB in longitudinal car and bicycle encounters. Therefore, car speed should be limited to 40 km/h if absence of a cyclist on the road cannot be reliably concluded by the car's sensors.

Lateral control systems may further alleviate risks but require sufficient lateral space to be available to steer away from collisions. It appears impossible to guarantee sufficient space, especially on narrow roads with oncoming traffic. If speeds higher than 40 km/h are desired, it appears necessary to physically separate car and cycle lanes.

There is no safe speed for HVs running over vulnerable road users in a first or subsequent impact; collisions must either be avoided altogether or the vehicle geometry must be altered, with gaps either closed permanently or with deployable structures on impact (TRL 2018). With automated collision avoidance systems, for longitudinal and turning scenarios, and run-over protection implemented for HVs, walking speed, i.e. 5-7 km/h, is expected to be manageable.

Collisions with fixed objects/run off road crashes
Single vehicle run off road crashes are, together with head-on crashes, the most common crash scenario involving passenger cars. The proportion of fatal single vehicle crashes varies in the EU countries between 22% and 41% with an average of 31%, while the proportion of single vehicle crashes with MAIS 3+ injuries vary between 22% and 49% (ERSO 2018). While the absolute number of severe single vehicle crashes has decreased over the last 10 years in the EU, the proportion has been rather constant (ERSO 2018). Predictive analysis undertaken in the review of the Swedish road safety targets also suggests that single vehicle crashes will continue to represent a majority of the overall road trauma in the coming decades, even when considering the benefit realization of current and emerging vehicle safety technologies (STA 2016b).

Single vehicle crashes normally start in a lane departure due to loss of control, an evasive maneuver, a vehicle failure, or just an unintentional deviation from the lane. Given the fitment of LKA, Emergency Lane Keeping (ELK) and ESC, the conservative approach would be to assume that scenarios with evasive maneuvers, vehicle failures and unreadable road edge lines would still be in the residual. Following the lane departure, single vehicle crashes come with a variety of crash scenarios including rollovers as well as front and side collisions with frangible and fixed objects. Hence, it is challenging to reproduce a representative single vehicle crash due to the large variation. The unpredictable nature of single vehicle crashes is also depicted by the comparatively flat risk curve in Doecke et al. (2021), that seeks to illustrate the relationship between travel speed and risk for a fatal or serious injury (MAIS 3+).

The safe travel speed with regards to single vehicle crashes will depend on two aspects primarily.
First, the availability of infrastructure elements aimed at preventing run off road crashes. Paved shoulders in combination with line markings and Audio Tactile Line Markings (ATLM) have shown to be effective in reducing run off road crashes by 20-30% (Turner et al., 2010). However, to effectively reduce the majority of all run off road crashes, including those involving loss of control, flexible roadside barriers may be the only viable option with a reduction of serious injuries in this crash type on high-speed rural roads of approximately 90% (Candappa et al., 2011). Hence, even with ADAS technologies, from a single vehicle run off road perspective the speed limit could be set to at least 100 km/h on routes with continuous flexible roadside barriers installed.

Second, in the case with no roadside barriers installed, the travel speed must be adjusted according to the characteristics of the roadside area and the vehicles' ability to read or predict the roadside area. One approach in deriving the boundary conditions would be to design them around the worst-case scenario, which is represented in the Euro NCAP test protocols by a pole side impact at 30 km/h. Side collisions with fixed narrow objects naturally come with specific challenges due to the concentration of energy and the high level of intrusion to the occupant compartment. A strict boundary condition could therefore be based on the acceptable impact speed for side impacts against fixed narrow objects, typically trees and poles. The same rationale could be applied to rollovers resulting in collisions with fixed narrow objects.

A more common scenario though, would be for mid to high volume rural roads to comply with road design guidelines suggesting a roadside area to have a few meters of clear zone, accompanied by a slope of 1/3 or 1/4 depending on the desired degree of mobility. If the stricter boundary condition including rollovers into narrow fixed objects close to the road edge would require an impact speed not higher than 30 km/h, a rural road complying with most road design guidelines could probably allow for the vehicle to leave the road at around 60 km/h. The rationale behind this would be the vehicles' ability to protect the occupants in a rollover at this speed, or the vehicles' ability to use the clear zone to reduce the travel speed at least 30 km/h before potentially hitting a fixed object.

An intermediate scenario could be represented by an undivided road with a roadside area free from hazardous objects, with a slope designed to prevent rollover crashes, and with predictable friction and a non-obstructed view in the sensor horizon. In this case the speed limit could be set with the boundary conditions for the head-on crash load case in mind, i.e. a maximum travel speed of 80 km/h.

Collisions with moose/large animals
Passenger cars are generally not designed to withstand an impact with a moose or other larger animals at high speeds. Moose collisions involve high loads on the vehicle structure and are not included in standardized crash tests. Furthermore, these collisions do not engage the main structure of the car front-end: the moose often directly hits the windscreen area, which is a weak part of the car structure (Björnstig et al., 1984; Lövsund et al., 1989; Williams and Wells 2005). The crash severity in terms of delta V is generally low in these collisions, typically 8-15 km/h even at high speeds (Jakobson et al., 2015). In this delta V range, the probability of an airbag deployment is low (Hussain et al., 2006). Moose crash tests with cars show that interior intrusion can be extensive (Krafft et al., 2011; Jakobson et al., 2015).

An effective countermeasure to reduce collisions with moose and other large animals is a fence aimed at preventing their access to the road. Studies have shown a crash reduction of up to 80% on roads with such fences (Lavsund and Sandegren 1991). The use of road fencing has so far been prioritized on high volume and high-speed roads.

It is anticipated that further development of crashworthiness in this load case is not likely to be significantly pushed by legislation or NCAPs in the near future. Previous crash tests have suggested that the impact speed

should not exceed 70 km/h to be survivable (Ydenius et al., 2017). Based on this conclusion, the maximum acceptable impact speed against a moose might be set at 60 km/h to also help prevent severe injuries.

Previous studies report that 90% of fatal crashes with a moose occur in darkness or twilight (Ydenius et al., 2017). By 2030, it is expected that AEB detection of moose and other large animals will be improved in difficult lighting conditions and that the maximum pre-crash speed reduction could be 20 km/h. The 20 km/h is based on the same rationale as the pre-crash speed reduction in head-on crashes also with low TTC. This would also require sufficient sight lines in the roadside area to ensure a timely AEB triggering.

In summary, the maximum traveling speed should be 60 km/h on roads without wildlife fencing or without sufficient sight lines on the roadside. If the roadside area is sufficiently cleared from obstructing objects, thus increasing the chance of AEB triggering, the traveling speed could be increased to 80 km/h. This would also be beneficial for the maximum traveling speed for run off road crashes.

Summary of results
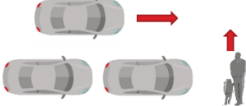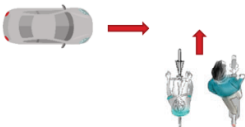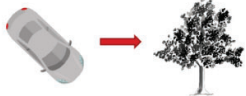Figure 4 summarizes the maximum traveling and impact speeds for each specific load case.

	Maximum acceptable impact speed (km/h)	Maximum safe travelling speed with optimal sight and road friction (km/h)
	dV 15	110
	60	80
	30	50
	40	40
	60	60
	40	40
	0	5-7
	20	40
	30	60
	60	80

Figure 4. Summary of maximum impact and traveling speeds for the included load cases.

The load cases in this work, summarized in Figure 4, can be grouped in three main areas of road user interactions similar to Truong et al. (2022):

- Vehicle priority areas where movement of people and goods is main priority, typically rural and semi-rural midblock sections and intersections,
- mixed traffic urban areas where motor vehicle through-traffic interact with intersecting vulnerable road users and active transport,
- pedestrian priority areas.

Starting with pedestrian priority areas, this work supports the idea that motor vehicles in this space will travel unconditionally with pedestrian movements as the limiting parameter. As a result, the travel speed in pedestrian priority areas is still assumed to be very low, 5-7 km/h, even with vehicles of MY 2030 equipped with AEB for vulnerable road users.

As for mixed traffic areas, motor vehicles are expected to be able to travel somewhat faster due to a more controlled interaction with vulnerable road users, primarily through dedicated and separated bike lanes and pedestrian crossings. The suggested maximum travel speed of 40 km/h, however, assumes no obstructed sensor sightlines, e.g. due to parked vehicles along the sidewalk.

Vehicle priority areas include the other five load cases (rear-end, head-on, side impacts, single-vehicle and large animals) and thereby require a more comprehensive system analysis for the road manager to set safe and appropriate speed limits on a route basis. On high functioning routes, speeds can be set to 100 km/h and above to accommodate high movement needs, if vehicles are separated from other oncoming vehicles, the roadside area is fitted with barriers and access points and intersections are grade separated. However, without physical separation, safe traffic needs to be accommodated by adapting travel speeds to the vehicle's ability to protect the occupants.

On a typical mid-block section, applicable for the load cases of head-on crashes, single vehicle crashes, rear-end crashes and collisions with large animals, the maximum common travel speed would be 80 km/h. However, there might be exceptions due to oncoming HVs or a hazardous and unpredictable roadside area that would require temporarily lower travel speeds at 50 or 60 km/h. Naturally, the maximum travel speed would also decrease if the available road friction was not optimal. Vehicle conflicts in uncontrolled intersections, especially between vehicles with large mass differences are expected to be one of the more challenging load cases. Due to the unpredictable nature of crossing vehicles, and the AEB systems' inability to fully detect oncoming vehicles at high speed from the side, a maximum travel speed of 60 km/h was deemed as safe, or 40 km/h if HVs or PTWs are involved.

The expert group concluded that the recommended travel speeds in the road transport system containing only motor vehicles of MY 2030 and beyond would be:

- 5-7 km/h in pedestrian priority areas,
- 40 km/h in mixed traffic urban areas,
- 50 to 80 km/h on roads without mid- and road side barriers,
- 100+ km/h on roads with continuous mid- and roadside barriers,
- 40 to 60 km/h in at grade uncontrolled intersections depending on mass differences to be accommodated.

While these recommended travel speeds are still based on the expected injury risk in the event of a crash, in line with Vision Zero, it is also stressed in this work that the frequency of crashes is expected to decrease due to the further development and implementation of ADAS. However, the reduction of crashes is not expected to be constant across the included load cases. This aspect is conceptually illustrated in Figure 5, with two examples where the "funnel" representing the number of cases between the safe driving phase and the crash has different sizes. Crashes with pedestrians are expected to essentially be eliminated (Figure 5 lower) while head-on collisions will still occur, although at a lower rate than today (Figure 5 upper). Although human crash tolerance will always be the ultimate boundary condition to guarantee a safe outcome in the event of a crash, it is expected that over time increased performance of vehicle safety systems will prevent a larger and larger proportion of crashes in all load cases.
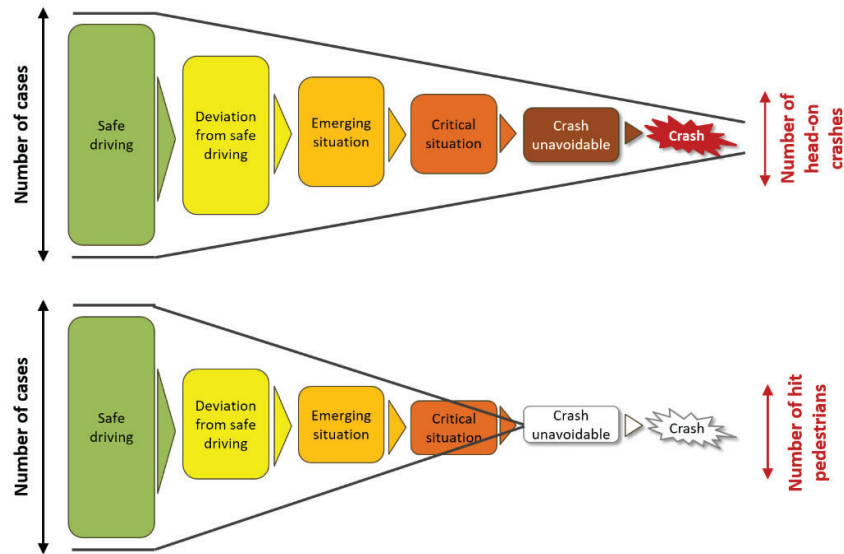
Figure 5. Conceptual illustration of chain of events leading to head-on collisions (upper) or car-pedestrian collisions (lower) with a MY 2030 passenger car.

DISCUSSION

General discussion

Transport policies across the world describe mobility as a function of accessibility and time spent in transport. Time spent in transport is, of course, a function of speed, thus speed limits and speed management form a natural issue to be managed in road infrastructure design and transport planning. The principles in setting speed limits vary across the world and time. The early days saw the "Red Flag Acts" while later, speed choice was solely the decision of the driver. Since many years ago, speed limits have existed more or less everywhere and have been set in accordance with the 85-percentile principle, i.e. the travel speed found appropriate by 85% of drivers. The only significant deviation from this principle has been some sections of the German "Autobahn", where speed limits have not yet been set.

Today, speed and speed limits would be expected to reflect the safety standard of the road infrastructure (AEG 2020), in relation to the vehicle fleet, and the absence or existence of pedestrians and bicyclists. There is, however, no internationally harmonized framework for speed limits. In September 2020, the UN General Assembly endorsed the Stockholm Declaration where a recommendation was accepted for a maximum of 30 km/h in areas where vulnerable road users and vehicles mix, but the UN framework for road rules still does not deal with speed limits. The speed choice is, as a principle, still left to the driver of the vehicle and expressed as "…able to stop his vehicle within his range of forward vision and short of any foreseeable obstruction…" (UN 1968).

In more general terms, there is a recommendation from the UN to adopt the Safe System Principles meaning that the safety of the road transport system should be based on the human biomechanics tolerance for serious injuries. The idea to describe human injuries as a result of kinetic energy is not new, in fact it can be found as the central theme in the work of Haddon (Haddon 1970, 1980). At that time, few preventative methods were available. Still, the principles are used today as the foundation of safety, and they can be seen to include everything from primary to secondary prevention.

The basic principle behind Vision Zero, sometimes called the Safe System Approach, is to keep the amount of kinetic energy below the threshold for the biomechanical tolerance of the human body (Johansson 2009). This is a step further from general prevention principles as it explicitly attempts to control and limit the amount of kinetic energy. While this principle is quite wide and generic, it guides us to speed management and the protection of the human. By adding layers of protection to the human, road users can be exposed to a higher level of mechanical force, i e increase the speed (Corben et al., 2004). These layers can be categorized, where the most inner layer is physical protection of the body in the event of mechanical force directed towards a human. Several layers can be added, and we can also add a layer of reduced mechanical force prior to impact, as well as an overall reduction of kinetic energy by reducing speed (Strandroth 2015; Rizzi 2016).

The first attempt to propose speed limits based solely on the risk of fatality and serious injury which in turn is based on human tolerance to mechanical force, was published in 1996 (Tingvall et al., 1996). In this proposal, the speed limits were based on just a few boundary conditions, in essence the crashworthiness safety standard of a modern passenger car. In 1996, there were no standard cars available with any pre-crash technology that would reduce speed before impact. The road infrastructure safety was limited to separation of oncoming traffic. The next attempt to propose future speed limits was presented in 2011 (Eugensson et al., 2011). With representatives from both infrastructure providers as well as vehicle manufacturers, it aimed at proposing speed limits for future estimated 5-stars cars of MY 2020 or later. In this proposal, the crashworthiness of the passenger car was complemented with pre-crash technologies that would reduce speed before impact. Still, the proposal was based on assumptions of future technology rather than any empirical data, or even availability of the technology that the speed limits were based on. The future safety level of the infrastructure included a widespread use of crash barriers, both medians as well as roadside.

The current proposal of future speed limits goes beyond the two earlier attempts in that 1) it is partly founded in empirical data and 2) incorporates a further layer of safety, impacting the safe driving of the vehicles (see Figures 2 and 3). The assumption that vehicles of MY 2030 would not allow the driver to violate basic road rules could of course be challenged. It is, however, a fair assumption that the safety standard has reached a point that when the vehicle carries information about speed limits, can detect how the driver chooses the traveling speed and would as a consequence support the driver to not violate posted speed limits or even limit the speed, if necessary. The same would apply to drivers not performing in relation to distraction, under influence or fatigue. If, and how, the principle of a vehicle not allowing the driver to exceed fundamental road rules will be introduced is not known. It could be either vehicle regulations or consumer ratings, or both, but it does not seem unlikely that this principle will be well established within the time period up until 2030. While an important step has been taken with mandatory ISA through EU legislation (EU 2021), the development of partly automated driving is ongoing, where basic traffic rules like speed and headway distance would be followed. Thus, the car population would gradually support the driver to at least not exceed posted speed limits and adopt minimum time gaps to other road users.

Another factor related to technical limitation of maximum speed, is geofencing. Such technologies are likely to become more common, both as an initiative from municipalities that wish to control speed within certain areas, but also in organized traffic like freight transport services and public transport. These initiatives would likely stimulate the automotive industry to make non-overridable systems that can react to digital speed data available on the market.

In the boundary conditions for a car of MY 2030, it is considered possible that the car can leave its intended lane into oncoming traffic, or off the road. This might seem unlikely with the technology already existing on today's cars. While it is anticipated that such an event will be rare, it is still included as a load case, as overtaking would still be allowed, and it seems logical that the driver can still override the steering of a car of MY 2030. There are, though, important factors and conditions that reduce the risk of a crash and thus contribute to safety without changing the boundary conditions for speed. One such condition is the availability of machine-readable road signs and road markings. In particular road markings are essential for current and future cars with the ability to stay within the intended lane. Markings with low readability or covered by ice and snow reduce the benefits of lane support technologies.

A more complex condition is road grip, i.e. the result of the interaction of road tires and road friction. This is indeed a critical parameter, as the pre-impact braking is a very significant part of the control of kinetic energy at impact. A reduced road grip as a result of roads covered by snow and ice, and tires with non-optimal characteristics, would have detrimental effects on the ability to brake. This in turn would imply that the road infrastructure provider would have to set a minimum level for road maintenance and the vehicle manufacturer would have to control for the available road friction by autonomously reducing speed if the road grip falls below a specified level.

It is important to stress that the result of this study is to propose safe speeds that seem feasible for a car of MY 2030 or later. It is not a prediction based on empirical data, although such data forms the basis for the assumptions. Empirical data might be based on speed estimates that contain measurement errors and thus impact the quality of the statistical modeling. Still, they offer a useful guide to the current level of understanding of the relationship between speed and injury. They can also be used for finding the effects of reducing speed before impact through technology. For one specific load case, i.e. pedestrians, the biomechanical tolerance has been reduced to zero in the current study. Pedestrians were classified as "objects" that should not be hit at all, meaning

that pre-impact braking should be able to eliminate an impact. This boundary condition is based on the fact that there may not be any harmless collision between a car and a pedestrian. Even at very low impact speeds, the risk of a serious injury is still substantial. The pedestrian can fall to the ground, including being run over by the car. The desire to find a speed that is low enough to avoid hitting a pedestrian does not imply that the pedestrian crashworthiness of the car can be reduced or even removed - there will still be a few crashes where pedestrians will be hit by cars.

Implications
The results of this work show the indicative speeds where safety could be improved significantly through vehicle design and development. This is a guide to the automotive industry, regulative bodies and safety rating bodies, and last but not least, organizations procuring/using cars of different kinds. At the same time, it is also a guide to infrastructure providers and authorities setting speed limits. Roads and streets can be designed and maintained to accommodate vehicles with advanced technologies, and speed limits could be set accordingly. Geofenced limits could set appropriate limits through these indicative safe speeds. The standards of maintenance in terms of friction and readable markings/signs would be highlighted.

It must be stressed, that while the speed limit proposal is built on indicative maximum speed at impact, taking pre-impact braking into the calculation of maximum travel speed, the introduction of a number of other safety technologies would limit the number of crashes that would be relevant for maximum occupant protection. Even technologies like ESC, LKA or ELK greatly reduce the risk of a crash and thus limit the number of cases that lead to the utilization of injury mitigation technologies in a crash. This logic can be clearly seen in the chain of events approach to categorize and analyze the effects of multiple interventions (see Figure 2, 3 and 5). The exposure to potentially serious crashes will clearly be reduced, and this is an important step and development from the first attempt to set logical speed limits based on the safe system principles.

The results should be used to form new guidelines to transport planning, replacing the current practice of setting speed limits based on benefit/cost ratios between travel time and negative impact from safety. These old principles do not seem to be in line with Safe System Principles now adopted across the world (UN 2020). It would even be expected that the regulatory bodies of the UN system (ECE WP1 and alike) set the standards and rules for setting speed limits based on the safety standards conferred by infrastructure and vehicle fleets, alongside regulations for vehicle safety. In the end, speed management is a fundamental metric for the interaction between the vehicle manufacturers and road infrastructure providers.

Limitations and future work
While the present work has a number of important implications for future road safety work, there are a few limitations that are important to note. First, it should be stressed that not all possible load cases involving a passenger car were included (for instance, frontal impacts between passenger cars and PTWs). While several load cases were added, compared with Eugensson et al. (2011), it is still clear that future work should aim at addressing these gaps.

A further limitation is that it is clearly very difficult to know exactly how the road transport system will look like by 2050. A main assumption in this work was that the passenger car, as a means of transportation, will still be part of the road transport system in 2050, one way or another. While this might be debatable, it is also important to stress that this work did not attempt to quantify exposure with passenger cars in 2050 and that the presented results would not be affected by reduced exposure. Therefore, it can still be argued that this work is of relevance as long as passenger cars are used as means of transportation. We do not know to what extent, although we do not need to know that in this particular work.

Finally, it is also important to point out that injury risks are known to increase substantially with age. Crashes at 48 km/h delta V involving male car occupants above 55 years of age, for example, incur a 150% greater risk of producing serious injuries compared to crashes involving younger males (Kononen et al., 2011). High age is associated in particular with increased risk of rib fracture for car occupants and injury risks are known to also increase for cyclists and pedestrians (Wisch et al., 2017). The presented speed limits aimed to ensure a very low risk of fatality or serious injury. This will likely be achievable and achieved for the population of road users with very old individuals still incurring a higher risk of serious to fatal injuries if involved in crashes as a vehicle user.

However, safety for elderly car users must be improved, for example by lowering shoulder belt forces, verified in a regulatory or consumer testing low speed assessment (Digges and Dalmotas, 2007). However, even more drastic measures may be needed to make sure seniors are subject to very low injury and fatality risk similar to mid-aged and younger car occupants. Potentially, the same rearward facing restraint solutions used for children

could be used. Clearly, safety for elderly road users remains a challenge that requires further research into reducing crash and injury risks.

CONCLUSIONS

Human crash tolerance will always be the ultimate boundary condition to guarantee a safe outcome in a crash, in line with Vision Zero and over time, increased performance of vehicle safety systems will be able to prevent a larger and larger proportion of crashes in all load cases. The expert group concluded that the recommended travel speeds in the road transport system containing only motor vehicles of MY 2030 and beyond would be:

- 5-7 km/h in pedestrian priority areas,
- 40 km/h in mixed traffic urban areas, if there are no obstructed sensor sightlines, e.g. due to parked vehicles along the sidewalk,
- 50 to 80 km/h on roads without mid- and roadside barriers,
- 100+ km/h on roads fitted with continuous mid- and roadside barriers,
- 40 to 60 km/h in intersections, depending on vehicle mass differences.

This is a guide to the automotive industry, regulative bodies and safety rating bodies, and last but not least, organizations procuring/using cars of different kinds. At the same time, it is also a guide to infrastructure providers and authorities setting speed limits. Roads and streets can be designed and maintained to accommodate vehicles with advanced technologies, and speed limits could be set accordingly.

ACKNOWLEDGMENTS

REFERENCES

AEG, Academic Expert Group (2020) Saving lives beyond 2020: the next steps. Recommendations of the Academic Expert Group for the 3rd Global Ministerial Conference on Road Safety. Available at: https://www.roadsafetysweden.com/contentassets/c65bb9192abb44d5b26b633e70e0be2c/200113_final-report-single.pdf Accessed on 8th November 2022

Aikyo Y, Kobayashi Y, Akashi T, Ishiwatari M (2015) Feasibility study of airbag concept applicable to motorcycles without sufficient reaction structure. Traffic Injury Prevention 2015, 16:sup1:148-152

Björnstig U, Bylund P O, Eriksson A, Thorson J (1984) Moose collisions and injuries to car occupants. Ann Adv Automot Med. 1984 Oct; 28: 149-153

Brännström M, Coelingh E, Sjöberg J (2014) Decision-making on when to brake and when to steer to avoid a collision. International Journal of Vehicle Safety, Vol. 7; 1: 87-106

Candappa N, D'Elia A, Corben B, Newstead S (2011) Wire rope barrier effectiveness on Victorian roads. Paper presented at the Australasian Road Safety Research, Policing and Education Conference, Perth, Western Australia

Corben B, Senserrick T, Cameron M, Rechnitzer G (2004) Development of the visionary research model – application to the car/pedestrian conflict. MUARC report no 229, Melbourne, Victoria

Digges K, Dalmotas D (2007) Benefits of a low severity frontal crash test. Annu Proc Assoc Adv Automot Med. 2007; 51: 299–317

Ding C, Rizzi M, Strandroth J, Sander U, Lubbe N (2019) Motorcyclist injury risk as a function of real-life crash speed and other contributing factors. Accident Analysis and Prevention, Volume 123, February 2019, Pages 374-386

Doecke S, Dutschke J, Baldock M, Kloeden C (2021) Travel speed and the risk och serious injury in vehicle crashes. Accident Analysis and Prevention, Volume 161, October 2021, 106359 2021

Elvik R (2009) The Power Model of the relationship between speed and road safety, update and new analyses. Institute of Transport Economics, Oslo, Norway

Elvik R, Vadeby A, Hels T, van Schagen I (2019) Updated estimates of the relationship between speed and road safety at the aggregate and individual levels. Accident Analysis and Prevention, Volume 123, 114-122

ERSO, European Road Safety Observatory (2018) Traffic safety basic facts - single vehicle accidents. Available at: https://road-safety.transport.ec.europa.eu/system/files/2021-07/bfs2018_single_vehicle_accident.pdf Accessed on 7th November 2022

ERSO, European Road Safety Observatory (2021) Annual statistical report on road safety in the EU 2020. Available at: https://ec.europa.eu/transport/road_safety/system/files/2021-07/asr2020.pdf Accessed on 7th November 2022

Eugensson A, Ivarsson J, Lie A, Tingvall C (2011) Cars are driven on roads, joint visions and modern technologies stress the need for cooperation. In proceedings of the 2011 ESV Conference, paper 11-0352, Washington DC

Euro NCAP (2022) Offset-Deformable Barrier – ODB https://www.euroncap.com/en/vehicle-safety/the-ratings-explained/adult-occupant-protection/previous-tests/offset-deformable-barrier/ Accessed on 7th November 2022

European Union (2021) Commission Delegated Regulation (EU) 2021/1958 of 23 June 2021. Supplementing Regulation (EU) 2019/2144 of the European Parliament and of the Council by laying down detailed rules concerning the specific test procedures and technical requirements for the type-approval of motor vehicles with regard to their intelligent speed assistance systems and for the type-approval of those systems as separate technical units and amending Annex II to that Regulation. https://eur-lex.europa.eu/legal-content/EN/TXT/PDF/?uri=CELEX:32021R1958&from=EN Accessed on 28th November 2022

Fildes B, Keall M, Bos N, Lie A, Page Y, Pastor C, Pennisi L, Rizzi M, Thomas P, Tingvall C (2015) Effectiveness of low speed autonomous emergency braking in real-world rear-end crashes. Accident Analysis and Prevention, 81, 24-29

Fredriksson R, Rosén E (2014) Head injury reduction potential of integrated pedestrian protection systems based on accident and experimental data – benefit of combining passive and active systems. In proceedings of the 2014 IRCOBI Conference, Berlin, Germany

Fredriksson R, Sui B (2015) Fatal Powered Two-Wheeler (PTW) crashes in Germany – an in-depth study of the events, injuries and injury sources. In proceedings of the 2015 IRCOBI Conference, Lyon, France

Fredriksson R, Rosén E, Ranjbar A (2015) Integrated bicyclist protection systems - potential of head injury reduction combining passive and active protection systems. In proceedings of the 2015 ESV Conference, paper 15-0051-O, Gothenburg, Sweden

Fredriksson R, Sui B (2016) Powered Two-Wheeler accidents in Germany with severe injury outcome - accident scenarios, injury sources and potential countermeasures. In proceedings of the 2016 IRCOBI Conference, Malaga, Spain

Funk JR, Cormier JM, Gabler HC (2008) Effect of delta-V errors in NASS on frontal crash risk calculations. Ann Adv Automot Med. 2008; 52: 155–164

Haddon W Jr (1970) On the escape of tigers: an ecologic note. Am J Public Health Nations Health. 1970 Dec; 60(12): 2229–2234

Haddon W Jr (1980) Advances in the epidemiology of injuries as a basis for public policy. Public Health Reports 1980, 95, 411-421

Hasegawa T, Takahashi H, Udaka S (2017) Clarification of priority factors for reducing traffic accident fatalities in the US and benefit estimation of AEB system for oncoming vehicles. In proceedings of the 2017 ESV Conference, paper 17-0171, Detroit, Michigan, US

Hu J, Klinich KD (2012) Toward Designing Pedestrian-Friendly Vehicles. Report No. UMTRI-2012-19

Hussain A, Hannan M, Mohamed A, Sanusi H, Ariffin A (2006) Vehicle crash analysis for airbag deployment decision. International Journal of Automotive Technology 7(2): 179-185

Hussain Q, Feng H, Grzebieta R, Brijs T, Olivier J (2019) The relationship between impact speed and the probability of pedestrian fatality during a vehicle-pedestrian crash: A systematic review and meta-analysis. Accident Analysis and Prevention. 2019 Aug; 129:241-249

IIHS (2021) Fatality Facts 2020 - Passenger vehicle occupants. Available at: https://www.iihs.org/topics/fatality-statistics/detail/passenger-vehicle-occupants Accessed on 7th November 2022

Jakobson L (2004) Whiplash Associated Disorders in frontal and rear-end car impacts. Doctor of philosophy Thesis for the degree of doctor of philosophy. Chalmers University of Technology, Gothenburg, Sweden

Jakobson L (2005) Fields analysis of AIS1 neck injuries in rear end car impacts – injury reducing effect of WHIPS. Journal of Whiplash & Related Disorders, 3(2), 37-53

Jakobson L, M. Lindman, Carlsson H, Axelson A, Kling A (2015) Large animal crashes: the significance and challenges. In proceedings of the 2015 IRCOBI Conference, Lyon, France

Jeppsson H, Östling M, Lubbe N (2018) Real life safety benefits of increasing brake deceleration in car-to-pedestrian accidents: Simulation of Vacuum Emergency Braking. Accident Analysis and Prevention Volume 111, February 2018, Pages 311-320

Kim W, Kelley-Baker T, Arbelaez R, O'Malley S, Jensen J (2021) Impact of speeds on drivers and vehicles – results from crash tests (technical report). Washington, DC: AAA Foundation for Traffic Safety.

Kononen D, Flannagan C, Wang S (2011) Identification and validation of a logistic regression model for predicting serious injuries associated with motor vehicle crashes. Accident Analysis and Prevention, Jan 2011; 43(1):112-22

Krafft M, Kullgren A, Nygren A, Lie A, Tingvall C (1996) Whiplash Associated Disorders - factors influencing the incidence in rear-end collisions. In proceedings of the 1996 ESV Conference, Melbourne, Victoria

Krafft M, Kullgren A, Stigson H, Ydenius A (2011) (in Swedish) Bilkollision med älg – utvärdering av verkliga olyckor och krockprov. Folksam report, Stockholm, Sweden

Kullgren A, Lie A, Tingvall C (1995) The use of crash recorders in studying real life crashes. In proceedings of the 1994 ESV Conference, Munich, Germany

Kullgren A, Stigson H (2010) (In Swedish) Fotgängares risk i trafiken. Analys av tidigare forskningsrön. Institutionen för folkhälsovetenskap. Karolinska Institutet, Sweden

Kullgren A, Stigson H (2011) Report on whiplash injuries in frontal and rear-end crashes. Folksam report, Stockholm, Sweden

Kullgren A, Axelsson A, Stigson H, Ydenius A (2019) Development in car crash safety and comparison between results from Euro NCAP tests and real-world crashes. In proceedings of the 2019 ESV Conference, Eindhoven, Netherlands

Lavsund S, Sandegren F (1991) Moose-vehicle relations in Sweden: a review. Alces 27:118-126

Leslie A, Kiefer R, Flannagan C, Owen S, Schoettle B (2022) Analysis of the Field Effectiveness of General Motors Model Year 2013-2020 Advanced Driver Assistance System Features. UMITRI report no. 2022-02

Lie (2012) Nonconformities in real-world fatal crashes - Electronic Stability Control and Seat Belt Reminders. Traffic Injury Prevention, 13:3, 308-314

Lubbe N, Wu Y, Jeppsson H (2022) Safe speeds: fatality and injury risks of pedestrians, cyclists, motorcyclists, and car drivers impacting the front of another passenger car as a function of closing speed and age. Traffic Safety Research, 2022, vol. 2, 000006

Lucci C, Marra M, Huertas-Leyva P, Baldanzini N, Savino G (2021) Investigating the feasibility of motorcycle autonomous emergency braking (MAEB): Design criteria for new experiments to field test automatic braking. MethodsX, Volume 8, 2021, 101225

Lövsund P, Nilson G, Svensson M (1989) Passenger car crashworthiness in moose-car collisions. In proceedings of the 1989 ESV Conference, Gothenburg, Sweden

Mackay M, Parkin S, Scott A (1994) Intelligent restraint systems - What characteristics should they have? In proceedings of the 1994 IRCOBI Conference, Lyon, France

McMurry T, Cormier J, Daniel T, Scanlon J, Crandal J (2021) An omni directional model of injury risk in planar crashes with application for autonomous vehicles. Traffic injury prevention. 22(sup1):S122-S127

Nilsson G (1991) Speed limits, enforcement and other factors influencing speed. Chapter 10 in Koornstra, M. J.; Christensen, J. (Eds): Enforcement and Rewarding: Strategies and Effects. Proceedings of the International Road Safety Symposium in Copenhagen, Denmark, September 19-21, 1990. Leidschendam, SWOV Institute for Road Safety Research

Nilsson G (2004) Traffic safety dimensions and the Power Model to describe the effect of speed on safety. Bulletin 221. Lund Institute of Technology, Department of Technology and Society, Traffic Engineering, Lund.

Oliver J, Creighton P (2017) Bicycle injuries and helmet use- a systematic review and meta-analysis. Int J Epidemiol, 2017 Feb 1;46(1):278-292

Pipkorn B, Alvarez V, Fahlstedt M, Lundin L (2020) Head injury risks and countermeasures for a bicyclist impacted by a passenger vehicle. In proceedings of the 2020 IRCOBI Conference

Puthan P, Lubbe N, Shaikh J (2021) Defining crash configurations for Powered Two-Wheelers: comparing ISO 13232 to recent in-depth crash data from Germany, India and China. Accident Analysis and Prevention, Vol. 151 art. nr 105957

Rizzi M, Kullgren A, Tingvall C (2014) Injury crash reduction of low-speed Autonomous Emergency Braking (AEB) on passenger cars. In proceedings of the 2014 IRCOBI Conference, Berlin, Germany

Rizzi M (2016) Towards a safe system approach to reduce health losses among motorcycles. Thesis for doctoral degree (PhD). Chalmers University of Technology, Sweden

Robinson M, Beal C, Brennan S (2020) At what cost? How planned collisions with pedestrians may save lives. Accident Analysis and Prevention. 2020 Apr 16; 141: 105492

Rosén E, Sander U (2009) Pedestrian fatality risk as a function of car impact speed. Accident Analysis and Prevention, 41, 536-542

Sander U, Lubbe N, Pietzsch S (2019) Intersection AEB implementation strategies for left turn across path crashes, Traffic Injury Prevention, 20:sup1, S119-S125

Savino G, Lot R, Massaro M, Rizzi M, Symeonidis I, Will S, Brown J (2020) Active safety systems for powered two-wheelers: A systematic review. Traffic Inj Prev. 2020; 21(1):78-86

Spitzhüttl F, Liers H (2019) Calculation of the point of no return (PONR) from real-world accidents. In proceedings of the 2019 ESV Conference, Eindhoven, Netherlands

Stigson H (2009) A safe road transport system - factors influencing injury outcome for car occupants. Thesis for doctoral degree (PhD), Department of Clinical Neuroscience, Karolinska Institutet, Sweden

Stigson H, Kullgren A, Rosén E (2012) Injury risk functions in frontal impacts using data from Crash Pulse Recorders. Ann Adv Automot Med. 2012 Oct; 56: 267-276

STA, Swedish Transport Administration (2016a) Increased safety on motorcycles and mopeds - combined strategy version 3.0 for the years 2016 - 2020. STA Report 2016:103

STA, Swedish Transport Administration (2016b) Review of interim targets for road safety 2020 and 2030, with an outlook to 2050. STA report 2016:109

STA, Swedish Transport Administration (2021) Analysis of road safety development in 2020. STA publication 2021:099

Strandroth J, Rizzi M, Kullgren A, Tingvall C (2012) Head-on collisions between passenger cars and heavy goods vehicles: Injury risk functions and benefits of Autonomous Emergency Braking. In proceedings of the 2012 IRCOBI Conference, Dublin, Ireland

Strandroth J (2015) Identifying the potential of combined road safety interventions - a method to evaluate future effects of integrated road and vehicle safety technologies. Thesis for doctoral degree (PhD). Chalmers University of Technology, Sweden

Tingvall C; Johansson R, Lie A (1996) Traffic safety in planning, a multidimensional model. In: Traffic Safety, Communication and Health. In Transportation, Safety and Health. Brussels 1996:61-69

Tingvall C, Haworth N (1999) Vision Zero, an ethical approach to safety and mobility. Monash University Accident Research Centre, Melbourne, Victoria

Trafikanalys (2020) (in Swedish) Vägtrafikskador 2019. Available at: https://www.trafa.se/globalassets/statistik/vagtrafik/vagtrafikskador/2019/vagtrafikskador-2019.pdf Accessed on 7th November 2022.

TRL (2018) Bus safety standard – executive summary. Available at: https://content.tfl.gov.uk/bus-safety-standard-executive-summary.pdf Accessed on 7th November 2022

Truong J, Strandroth J, Logan D, Job R, Newstead S (2022) Utilising human crash tolerance to design an interim and ultimate safe system for road safety. Sustainability 2022, 14, 3491

Turner B, Imberger K, Roper P, Pyta V, McLean J (2010) Road safety engineering risk assessment Part 6: Crash Reduction Factors (AP-T151/10)

UN, United Nations (1968) Convention on road traffic, 8th November 1968. Available at: https://treaties.un.org/doc/Treaties/1977/05/19770524%2000-13%20AM/Ch_XI_B_19.pdf Accessed on 8th November 2022

UN, United Nations (2020) Resolution adopted by the General Assembly on 31 August 2020. 74/299 Improving global road safety. Available at: https://digitallibrary.un.org/record/3879711 Accessed on 8th November 2022

WHO, World Health Organization (2018) Global status report on road safety 2018. ISBN: 9789241565684

Williams A, Wells J K (2005) Characteristics of vehicle-animal crashes in which vehicle occupants are killed. Traffic Inj Prev 6(1): 56-59

Wisch M, Seiniger P, Edwards M, Schaller T, Pla M, Aparicio A, Geronimi S, Lubbe N (2013) European project AsPeCSS - interim result: development of test scenarios based on identified accident scenarios. In proceedings of the 2013 ESV Conference, paper number 13-0405, Seoul, Republic of Korea

Wisch M, Lerner M, Vukovic E, Hynd D, Fiorentino A, Fornells A (2017) Injury patterns of older car occupants, older pedestrians or cyclists in road traffic crashes with passenger cars in Europe – results from SENIORS. In proceedings of the 2017 IRCOBI Conference, Antwerp, Belgium

Wågström L, Thomson R, Pipkorn B (2005) Structural adaptivity in frontal collisions: implications on crash pulse characteristics, International Journal of Crashworthiness, 10:4, 371-378

Ydenius A, Kullgren A, Rizzi M, Engström E, Stigson H, Strandroth J (2017) Fatal car to moose collisions: real-world in-depth data, crash tests and potential of different countermeasures. In proceedings of the 2017 ESV Conference, Detroit, Michigan, US

Zhao J, Jakkamsetti P, Katagiri M, Lee S (2019) New passenger restraints with adaptivity to occupant size, seating positions and crash scenarios through paired ATD-HM study. In proceedings of the 2019 ESV Conference, Eindhoven, Netherlands

Östling M, Jeppsson H, Lubbe N (2019a) Predicting crash configurations in passenger car to passenger car crashes to guide the development of future passenger car safety. In proceedings of the 2019 IRCOBI Conference, Florence, Italy

Östling M, Lubbe N, Jeppsson H, Puthan P (2019b) Passenger car safety beyond ADAS: Defining remaining accident configurations as future priorities. In proceedings of the 2019 ESV Conference, Eindhoven, Netherlands

SAFETY OF ELECTRO MOBILITY - WHITE PAPER OF THE FISITA INTELLIGENT SAFETY WORKING GROUP

Kompass, Klaus
KKo4Safety
Germany

Königs, Simon
Euhus, Florian
Fuchs, Franz
Zimmermann, Sascha
BMW AG
Germany

Schöneburg, Rodolfo
RSC Safety Engineering
Germany

Justen, Rainer
Mercedes-Benz AG
Germany

Martin, Saúl
Mensa, Genís
IDIADA
Spain

ABSTRACT

Battery electric vehicles and plug-in hybrid electric vehicles experienced significant increases in sales volume, reaching a worldwide market share of 7% of all newly registered vehicles by the middle of 2021. One of the central challenges of this paradigm shift lies in the safety aspects of electric vehicles and their components. For vehicles with combustion engines, safety aspects have been carefully investigated over decades, standards, regulations, test requirements and system limitations are widely established and acknowledged by vehicle manufacturers, suppliers, government authorities, NGOs and customers. For electric vehicles, this process has just started; yet its objective must be to establish a comparable level of safety taking in consideration the specific needs of those vehicles and their individual risk assessment.

This paper represents a pre-publication of a White Paper on the Safety of Electromobility, to be published by FISITA, the Fédération Internationale des Sociétés d´Ingénieurs des Techniques de l´Automobile. The chapters are designed by dedicated experts from all around the globe and from a variety of institutions within the engineering society under the umbrella of FISITAs Intelligent Safety Working Group ISWG. The White Paper is supposed to be published in autumn, 2023 during the FISITA World Congress in Barcelona and it summarizes the current state of the art as well as new research results for safety aspects during the product lifecycle of electric vehicles and their components. The book will be a precious handbook for all those who develop, produce, use, repair or work otherwise with vehicles with high voltage batteries and powertrains.

The structure of the White Paper follows the product lifecycle and covers the safety aspects for all phases in the following chapters:

- EV-components,
- Manufacturing,
- Use & Operation,
- Repair, Inspection, Maintenance and Service,
- Crash protection,
- Thermal events prevention or control,

- Rescue,
- Cyber Security,
- End-of-Life, Second Life of batteries and Recycling.

In separate chapters the specific Insurance aspects and the use of CAE for safety development, validation and verification are addressed. Last but not least the White Paper will give a forecast on future challenges in this area and also provide references to existing standards and best practices.

In this pre-publication the focus lies on the two chapters "Crash protection" and "Thermal events prevention or control". Other chapters are planned to be pre-published during the time frame between today and autumn 2023.

INTRODUCTION

The Fédération Internationale des Sociétés d´Ingénieurs des Techniques de l´Automobile (FISITA) brings together the global automotive mobility sector to share ideas and advance technological development for the automotive industry. FISITA's mission is to help create efficient, affordable, safe and sustainable automotive transportation, serving a global forum between engineers, industry, government, academia, environmental and standards organizations.

Within FISITA, the Intelligent Safety Working Group ISWG represents a global network of safety engineers, providing a platform for a precompetitive exchange of safety relevant information and experience in order to further improve traffic safety. In 2020 FISITA ISWG published a first White Paper on the safety aspects of Assisted and Automated Driving (Reference OP2020-1 F 0-01) including "Golden Guidelines" for the development and use of automated driving functions. The response to this publication was a motivator for the ISWG to start working on a second White Paper, this time focusing on the safety aspects of electric vehicles.

Battery electric vehicles and plug-in hybrid electric vehicles experienced significant increases in sales volume, reaching a worldwide market share of 7% of all newly registered vehicles by the middle of 2021. One of the central challenges of this paradigm shift are the safety aspects of electric vehicles and their components. For vehicles with combustion engines, safety aspects have been carefully investigated over decades; and so, the standards and limitations are widely acknowledged by original equipment manufacturers (OEM), suppliers, public authorities, and customers. For electric vehicles, this process has only started; yet its objective must be to establish at least the same level of safety.

The purpose of this White Paper is to document and inform the community about all of the potential impacts of Electric Vehicles (EVs) on the global stage, comprehensively covering topics ranging from manufacturing, operation, maintenance, repair, safety, cyber security, end of life and insurance.

Electric Vehicle technology eliminates some of the safety concerns of conventional vehicles powered by internal combustion engines (ICE) like gasoline leakage or fuel tank bursts as a consequence of e.g. a vehicle crash. But yet it brings its own specific safety relevant concerns e.g. due to the high voltage system with 400 V or more, its energy density or the vulnerability of the batteries.

Safety requirements for EVs should consider the differences between the two. The selection of appropriate crash load cases for conventional ICE vehicles strives for a deformation characteristic, which allows for good restraint system performance on the one hand and at the same time assures a sufficient fuel system integrity to avoid car fires. Some of the standard crash load cases are therefore defined to damage sensitive areas where there is a risk to penetrate fuel system components and the integrity of the fuel system is demanded. In the case of electric vehicles the potentially critical areas may be at different locations, the possible measures to protect electric components is different to the protection of e.g. fuel hoses and specific crash tests are required to assure a comparable level of safety for these vehicles. (Plug-In) hybrid vehicles are a mix of both worlds: the safety engineers must protect both the gasoline as well as the electric components.

Another example is the difference in the effort necessary to de-energize the two vehicle variants: for an ICE vehicle it is sufficient to reliably empty the gasoline tank and the subsequent gas hoses from flammable liquids and vapor. In practice it is much more difficult to de-energize an electric battery e.g. on the scene or in a repair shop. A clear guideline is necessary for service technicians, rescue teams, recycling mechanics or even a normal user to ensure a safe operation and handling of this system in every situation.

This White Paper shall serve as a handbook for all safety related topics in the design, manufacturing, use, service, repair, inspection, rescue, and even the re-use of vehicles with electric energy motors. We concentrate on passenger cars in this document, and it describes the state-of-the-art in this topic. To do so, we started from a full vehicle perspective, identified, or defined requirements on this level and then broke them down to

subsystem or component level. In the automotive industry this approach is well known as the V-Model: define the overall objectives, create specific requirements for subsystems or components, develop those with clear and designated specifications and then go back up for the verification and validation on component, subsystem, system to full vehicle level, again.

The White Paper is focused on passenger cars in this edition. Trucks, buses, construction vehicles etc. might have different, specific requirements and options. This is also the case for some parts of Fuel Cell Electric Vehicles (FCEV): the safety aspects of e.g. fueling and the storage of Hydrogen gas is of very high importance and would demand a long and extensive discussion. This discussion was excluded from this White paper and maybe subject to a subsequent edition. The Fuel Cell converts the chemical energy of hydrogen and oxygen into electricity. From this point on an FCEV can be seen like an EV: managing and storing the high voltage power is comparable to the situation in a BEV or a PHEV. The capacity might be smaller, but the basic principle is the same.

Within the ISWG FISITA brought together a group of distinguished experts from all areas relevant to the topic. These experts serve as chapter leaders for their specific areas of expertise, formulate the story line of the chapters, call authors, review their contributions, and edit the full work product. This White Paper is perfect example of the kind of teamwork practiced in FISITA. Academia, industry, legal authorities, member societies, and others work together for the good.

The chapters of the White Paper are based on the life cycle of electric vehicles, from manufacturing all the way to their second life, end of life or recycling. One might miss a chapter on the development of vehicles. In the course of the chapter definition, the editorial team decided against such an explicit development chapter because nearly everything would have landed here: nearly every safety risk can be re-assigned to an inappropriate or missing action during the development. It was decided to allocate these aspects along their most relevant situations of occurrence. Potential risks during the recycling of electric vehicles for example are addressed in the end-of-life chapter.

The publication of the full White Paper is planned for September 2023 during the 39th FISITA World Summit in Barcelona. Two chapters of the full White Paper are published in this contribution to the 27th ESV Conference on the Enhanced Safety of Vehicles, focusing on the aspects of crash safety and the prevention of thermal events in the high voltage batteries. Other pre-publications of individual chapters are planned for the year 2023.

USED ABBREVIATIONS

EV	-	Electric Vehicle, general
xEV	-	Electric Vehicle of any type (BEV, PHEV, …)
BEV	-	Battery Electric Vehicle, pure electric motor
PEV	-	Plug-In Electric Vehicle
PHEV	-	Plug-In Hybrid Electric Vehicle, combination of ICE and EV
ICE	-	Internal Combustion Engine, conventional gasoline or Diesel engine
FCEV	-	Fuel Cell Electric Vehicle, Electricity produced from redox reaction of Hydrogen and Oxygen
FISITA	-	Fédération Internationale des Sociétés d´Ingenieurs des Techniques de l´Automobile
ISWG	-	(FISITA) Intelligent Safety Working Group
HV	-	High Voltage (e.g. 400/800V)
HVS	-	High Voltage System
LV	-	Low Voltage (e.g. 12/24/48V)

PART 1: CRASH SAFETY OF BATTERY ELECTRIC VEHICLES

INTRODUCTION

Current status of E-mobility

In 2020, electric mobility appeared to have made its final breakthrough. Global EV sales reached three million vehicles in 2020 and jumped in 2021 to more than six million vehicles. The global market has reached the level of 7% of all new registrations by the middle of 2021. Such rapid growth in market penetration left both the general public, and to some extent also vehicle safety experts, scrambling for answers regarding real world electric vehicle safety performance and specifics.

Besides reasons such as the offer and costs of vehicles available, vehicle range and charging infrastructure, a further topic discussed very critically in the media up to now has been crashworthiness, leading to pronounced uncertainty on the part of customers and also rescue organizations. Almost every single case where an electric vehicle has been involved in an accident has been reported on in great detail, including speculation about the danger of the occupants and emergency services/ rescue workers receiving electric shocks. Similarly, a significantly increased risk of fire in electric vehicles has been presumed based on some individual vehicle or battery fire events and reports.

At present, the proportion of electric vehicles on the roads is still too low to make many statistically robust observations about EVs in terms of crash safety. However, enough accidents have so far been recorded and evaluated to at least establish that there have been no major or unexpected safety abnormalities specific to EVs. For example, electric shocks as a result of an accident have not occurred yet. For design reasons, they are also fundamentally highly unlikely to occur.

In addition to a still small but growing statistical evidence, the intensive educational work on battery fires is also gradually bearing fruit among the first responders, especially firefighters. The initially strong uncertainty has given way to the realization that during a rescue operation, electric vehicles fundamentally do not need to be dealt with any differently than conventional vehicles. For example, in the event of a fire, water is the most suitable extinguishing agent, and if a vehicle needs to be opened with a cutting tool, there is typically no reason to fear an electric shock.

Confidence in the safety can also be seen in the results of crash safety rating tests. In recent years, a large number of electric vehicles, hybrid vehicles and even fuel cell vehicles have undergone several global consumer metric testings. The results are largely comparable to the tests of conventional vehicles. In fact, the Insurance Institute for Highway Safety (IIHS) in the USA has reached the following conclusion: "With more electric vehicles comes more proof of safety." To quote IIHS President David Harkey [1]: "It's fantastic to see more proof that these vehicles are as safe as or safer than gasoline- and diesel-powered cars." "We can now say with confidence that making the U.S. fleet more environmentally friendly doesn't require any compromises in terms of safety."

These statements are based on an analysis of insurance data carried out by the Highway Loss Data Institute (HLDI), which confirms an analysis conducted back in 2012 that found that the risk of injury and the consequential costs of accidents involving hybrid vehicles are 25% lower than with gasoline vehicles. The analysis compared hybrid vehicles and combustion-engine-only vehicles that were built on the same platform. According to the analysis, the main reason for the apparent better occupant safety performance of the hybrid vehicles is the greater vehicle weight [2]. However, later in this chapter we discuss why this is not the sole reason those electric vehicles provide occupant safety performance that is at least comparable to that of conventional vehicles.

Generally, there is still a permanent improvement of crash behaviour ongoing from vehicle generation to vehicle generation and modern EV's belong to the latest and advanced vehicle designs. That vehicle safety is not a concern of the drivetrain was demonstrated by different OEM's, e.g. Mercedes-Benz at the VDI-Conference in Berlin 2022 [3].

New safety concerns

Compared with gasoline vehicles, electric vehicles have some fundamental technical differences relevant to crashworthiness:

- Battery instead of a fuel tank
- E-Motors instead of a combustion engine

- High-voltage components instead of mechanical or low voltage auxiliary systems
- High-voltage lines instead of fuel lines.

Due to these distinguishing features, the following additional safety challenges have to be considered:

- Packaging, rigidity, weight of new components due to the influence in structural safety and crash characteristics
- The need for prevention of electric shocks and short circuit by the HV system
- The risk of fire generation within electric energy storage systems
- Bursting and explosion risks of gas tanks in fuel cell electric vehicles.

Fire events involving the highly prevalent Lithium-Ion type of batteries have been attracting the attention of mass media. The resulting media reports may have caused concerns among first responders, especially among fire fighters. Thanks to emerging field event studies as well as growing education efforts on part of OEMs and research institutions, these concerns are being addressed.

Beside some others, the National Transportation Safety Board (NTSB) investigated some vehicle fire incidents of electric vehicles in the USA [4] and came to following findings due to safety risks to emergency responders from Lithium-Ion battery fires in electric vehicles:

1. Manufacturers' emergency response guides provide sufficient vehicle-specific information for disconnecting an electric vehicle's high-voltage system when the high-voltage disconnects are accessible and undamaged by crash forces.
2. Crash damage and resulting fires may prevent first responders from accessing the high-voltage disconnects in electric vehicles.
3. The instructions in most manufacturers' emergency response guides for fighting high-voltage lithium-ion battery fires lack necessary, vehicle-specific details on suppressing the fires.
4. Thermal runaway and multiple battery reignitions after initial fire suppression are safety risks in high-voltage lithium-ion battery fires.
5. The energy remaining in a damaged high-voltage lithium-ion battery, known as stranded energy, poses a risk of electric shock and creates the potential for thermal runaway that can result in battery reignition and fire.
6. High-voltage lithium-ion batteries in electric vehicles, when damaged by crash forces or internal battery failure, present special challenges to first and second responders because of insufficient information from manufacturers on procedures for mitigating the risks of stranded energy.
7. Storing an electric vehicle with a damaged high-voltage lithium-ion battery inside the recommended 50-foot-radius clear area may be infeasible at tow or storage yards.
8. Electric vehicle manufacturers should use the International Organization for Standardization standard 17840 template to present emergency response information.
9. Action by the National Highway Traffic Safety Administration, similar to that taken by the European New Car Assessment Program Euro-NCAP, to incorporate scoring relative to the availability of a manufacturer's emergency response guide and its adherence to International Organization for Standardization standard 17840 and SAE International recommended practice J2990 into the US New Car Assessment Program, would be an incentive for manufacturers of vehicles sold in the United States with high-voltage lithium-ion battery systems to comply with those standards.
10. Although existing standards address damage sustained by high-voltage lithium-ion battery systems in survivable crashes, as defined by federal crash standards, they do not address high-speed, high-severity crashes resulting in damage to high-voltage lithium-ion batteries and the associated stranded energy.

REQUIREMENTS AND LOAD CASES FOR THE HV SYSTEM IN ELECTRIC VEHICLES

Requirements and corresponding load cases for crashworthiness are defined by legislators, consumer protection organizations and the individual OEMs.

Legal Crash Tests

There are many laws and regulations regarding crashworthiness that must be fulfilled before a passenger vehicle can be approved for sale in a market. Some of them contain requirements for HV-systems. The overview below lists examples of the most design-determining laws in terms of HV safety during crash.

Table 1.
Examples of laws with HV requirements

Market	Organisation	Law
Europe / United Nations	UNECE	ECE-R 94/137/95/135*/153
USA	NHTSA	FMVSS 305
China	Guobiao	GB/T 31498-2021
Korea	MLIT	KMVSS Art.91 Cl.4
Japan	Jasic	Trias 17(2)-J111(2)

*upcoming: (GRSP) Proposal for the 02 series of amendments to UN Regulation No. 135 (Pole side impact) [5]

The laws contain chemical/thermal, mechanical and electrical requirements for the HV system which are displayed in Table 2.

Table 2.
Examples for legal HV requirements

requirements after crash	Markets				
	Europe (UNECE)	USA (NHTSA)	China (Guobiao)	Japan (Jasic)	Korea (MLIT)
chemical / thermal					
electrolyte spillage (do not exceed a certain amount)	x	x	x	x	x
no fire / explosion (no uncontrolled electric arc or short circuit)	x	x	x		x
mechanical					
REESS retention (no loss of the mechanical connection)	x	x	x	x	x
Electrical (one criteria must be met)					
voltage level (below 60VDC or 30VAC)	x	x	x	x	x
electrical isolation (more than 500Ohm/V)	x	x	x	x	x
physical barrier (IPxxB fullfillment)	x	x	x	x	x
residual energy (less than 0,2J system energy)	x		x		

*REESS – rechargeable electric energy storage system

Figure 1 shows an overview of the required load cases to validate the regulations for the beforementioned markets.
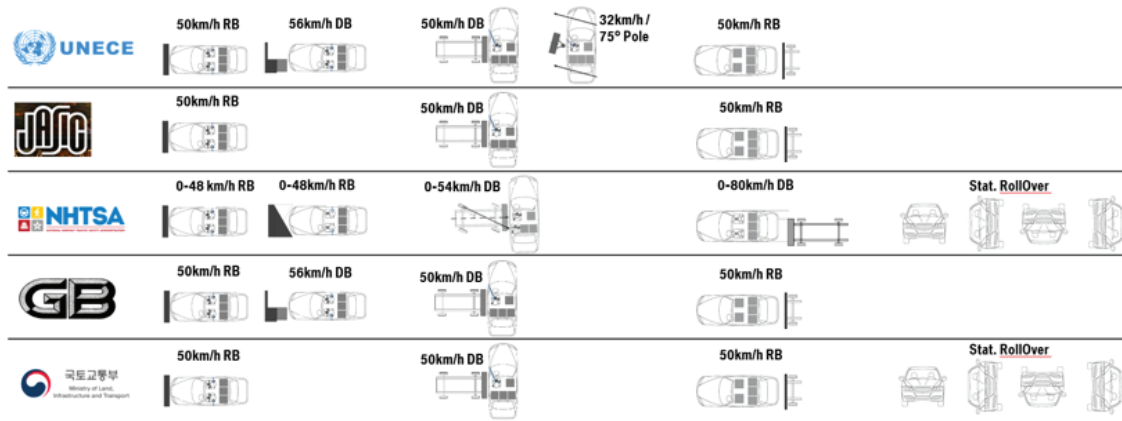
Figure 1. Examples for HV relevant legal load cases (pictograms taken from [6])

Consumer Rating Crash Tests

Most consumer rating organisations use the same or very similar HV requirements to those from the legislators, shown in Table 2. However, load cases can differ significantly in their general configuration and speed. Examples are the 'new car assessment programs' (NCAPs) from USA, Japan, Europe or China. The following table gives an overview about the load case configurations for some organisations.
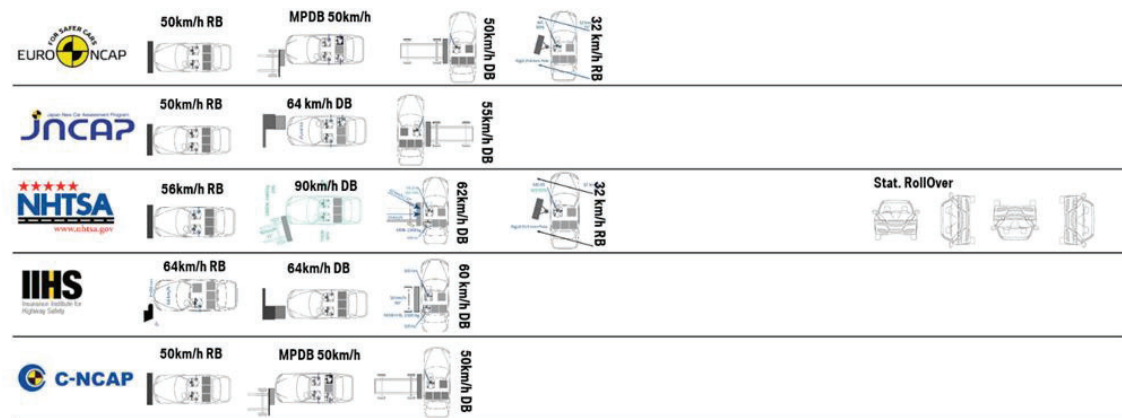
Figure 2. Examples for HV relevant consumer rating load cases (pictograms taken from [6])

Duty of Care Crash Scenarios

The existence of legal and consumer rating crash tests does not abolish the duty of OEMs to carefully observe their products in the field and to define further requirements and load cases if necessary. A Field data analysis can provide the probabilities for an impact with respect to the opponent size, mass, speed, direction, and impact position. Crash scenarios with a certain field relevance must then be assessed in terms of their risk for the occupants which can depend on the vehicle concept. A crash scenario that only implies a low risk within an ICE vehicle might be critical in a BEV and vice versa.

An example for an OEM duty of care crash scenario is the frontal pole impact. For BEVs, many OEMs consider side pole impacts on the entire length of the HV battery.
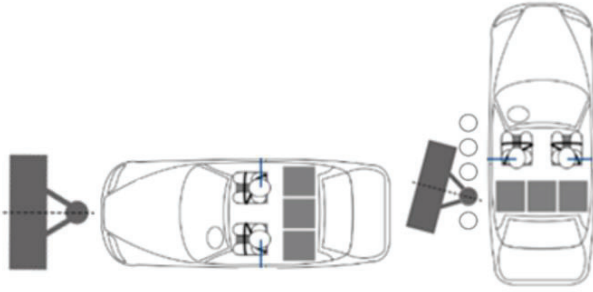
Figure 3. Front and side pole impacts (pictograms taken from [6])

Abuse Tests

A mayor abuse scenario with a high risk for the REESS are bottom impacts when the vehicle runs over, falls on or hits obstacles like stones, lost components from other vehicles or curbs. Figure 4 shows a schematic illustration of how to validate the energy storage device with the aid of various geometric structures that impact the underbody of the vehicle.
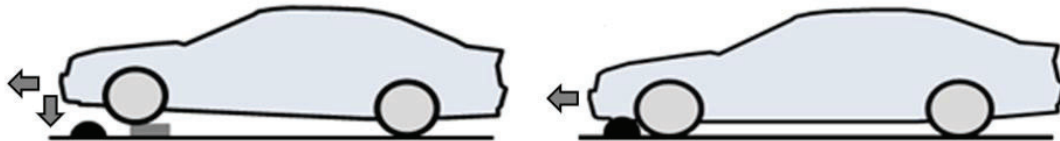

Figure 4: Examples for HV relevant consumer rating load cases

CRASH STRATEGY FOR ELECTRIC VEHICLES

The crash strategy of an electric vehicle has to balance three conflicting objectives:

1. Risks from the HV system shall be minimized. There are 4 major risks that have to be considered:
    - a mechanical load on the battery cell might cause electrolyte spillage or a thermal event in the REESS,
    - a short circuit in the HV system might cause a thermal event,
    - uninsulated live components could be touched by passengers or first responders,
    - a short circuit between HV and LV system could lead to a loss of all critical functions e.q. post-crash functions.

    Those four risks lead to two important design objectives for electric vehicles:

    I. Battery cells must be kept free of mechanicals loads that cause thermal events or electrolyte spillage.,
    II. Components of the HV system must be kept free of mechanical loads that cause insulation faults before they are disconnected from electrical energy supplies (e.g. REESS) and sufficiently discharged.
2. Availability of vehicle shall be maximized. Crashes with low severity should not lead to a breakdown of the vehicle but allow for further usage.
3. Space and material usage for the protection of HV components shall be minimized. Mechanical protections of HV components are heavy and stand in conflict with the objective to design light and efficient vehicles.

Those objectives can be translated to three safety design principles for electric vehicles that help to solve the conflict of goals:

1. Battery cells should be placed in the core zone of the vehicle where lowest mechanical loads appear.
2. All parts of the HV system should be placed as close as possible to the core zone of the vehicle.
3. Components of the HV system that are not placed in the core zone of the vehicle should be disconnected from electrical energy supplies and discharged as soon as possible after detecting a crash with medium or high severity.

The following picture illustrates the relationships of vehicle zones, protection areas, crash severity and HV shutdown within the crash strategy for electric vehicles. The states and terms mentioned here will be described in more detail below.
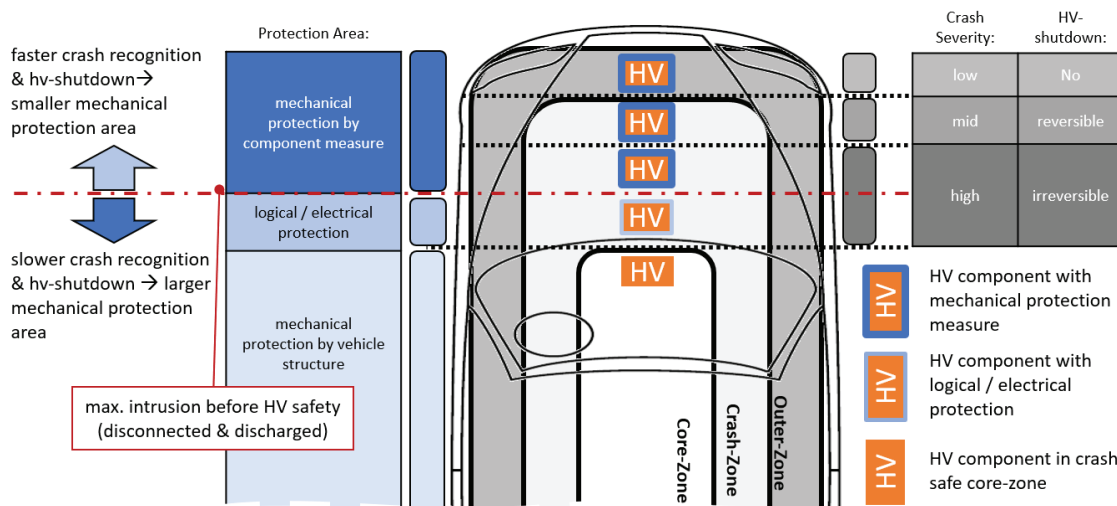
Kompass 8

Figure 5. Crash Strategy for electric vehicles (example frontal crash)

Low Severity Crash:

In a low severity crash without damages to the HV-system, there is no need for a HV-shutdown. In this case, e.g. a low speed bumper damage, the customer is able to drive his car to a save place or even keep using it without further restriction. Deformation only appears in the outer zone of the vehicle. If placed in that zone, HV components need a mechanical protection to avoid electrical risks and to ensure functional availability after crash. Vehicle manufactures try to avoid HV components in that zone.

Medium Severity Crash:

In a medium severity crash with a possible damage of the HV-system, a reversible HV-shutdown is executed. A medium severity crash can also go along with an airbag ignition but must not. In a medium severity crash scenario, e.g. a rear-end collision in stop and go traffic, the customer is able to start the HV-system again, if the automatic HV safety check during restart is ok. The customer has the possibility to drive his car to a save place or to continue his journey and drive to a car workshop. Deformation reaches to the outer part of the crash zone. HV components in that zone need a mechanical protection because they are exposed to load before they are cut of and discharged as well as to ensure further availability after crash.

High Severity Crash:

In a high severity crash with a probable destruction of the HV-system, an irreversible and yet faster HV-shutdown should be commanded. It separates the HV-system from the battery and discharges all remaining energies as fast as possible. A high severity crash normally goes along with an airbag ignition. The vehicle cannot be restarted again. Deformation reaches up to the inner part of the crash zone. HV components in that area might not need a mechanical protection when they are disconnected and discharged before they are exposed to critical mechanical loads (see red line in Figure 5). Depending on the overall damage of the vehicle, the HV-System might be repaired at a workshop.

The OEM implements this strategy by designing an appropriate vehicle structure with concerted geometric locations for the HV components, designing mechanical component protections and by implementing logical as well as electrical safety measures. The following three subchapters explain the mechanical, electrical and logical safety mechanisms in more detail.

Structural / Mechanical safety mechanisms

Architectural implications: Currently, hybrid vehicles are generally based on vehicle platforms for combustion powered vehicles that are then, if necessary, selectively reinforced to account for the additional vehicle weight. Especially beneath the passenger compartment, those load path are not able to ensure broad non-deformation zones for the battery cells while dealing with the significantly higher vehicle weights. Within classical vehicle architectures, battery packs will therefor contain additional load path (lengthwise, crosswise or even both). This reduces the available space for cells which have to be placed between the load path as smaller modules.

Even in the case of many electric vehicles to date, an all-electric drivetrain is still implemented in conventional vehicle structures. One example of such a convertible concept is shown in Figure 6.
With a special tubular frame it is possible to support both the electric motor of the front wheel drive and also the

other HV components while acting as a protective structure for them in the event of a collision. In terms of the bodyshell structure, it is possible to use, among other things, the mounting points of the conventional drive unit including transmission, which is no longer needed in an electric vehicle.

This design means the crash kinematics of a conventional drive unit incl. backward displacement and support in the vehicle tunnel during a frontal impact can be simulated to a very large extent. The load paths present in the basic vehicle can thus also be used effectively in the electrical variant [3].

As the electric drive motor is significantly smaller, there is nevertheless a greater clearance in front of the motor. In the event of a frontal impact, this results in a more harmonious characteristic, an acceleration level that rises in a controlled manner, and 25% more deformation overall.
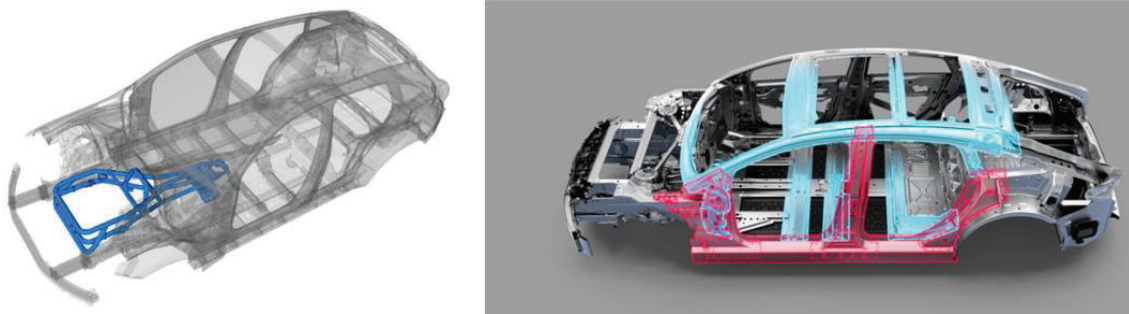
Figure 6. Comparison of Convertible (EQC) vs Purpose Platform (EQS)

In the event of a side impact, the side pole impact represents the main challenge for the accident safety of electric vehicles, as the nature of the battery layout in the underbody makes a direct impact to the battery almost unavoidable. Serious damage to the battery can lead to uncontrolled chemical or electrical reactions in the battery. In the car shown in Figure 6 this challenge is solved by a crash structure integrated in the battery housing that absorbs the impact energy while protecting the interior of the battery from damage.

The crash characteristics of a side pole impact are diametrical to those of a frontal impact. Due to the rigid battery that is firmly fixed to the underbody, the deformation path is reduced almost by half when compared with a conventional vehicle. By contrast, when it comes to the vehicle acceleration, there is a higher acceleration peak in an early crash phase. However, this higher acceleration does not negatively affect the loads on the occupants. The overall outcome is in fact positive since the additional clearance between the occupants and the door permits undisturbed deployment of the sidebags.

The battery itself contains additional energy absorbers that go beyond load conditions in the lab and are intended to provide an additional reserve in the event of potentially greater accident severities in real accidents.

In the future, newer models of electric vehicles will be based on separate electric platforms (Figure 6). Known as the "purpose concept", this has the advantage that the bodyshell structure can be consistently designed for the integration of an all-electric powertrain. In particular, this new architecture takes into account a flat floor concept designed to accommodate an underbody battery in an optimum manner. A center tunnel for housing a transmission and a propeller shaft can be omitted from electric vehicles completely. Two-wheel and all-wheel drive is implemented by the integration of one or two electric motors directly in the front axle/front and rear axles. The large, flat underbody battery can thus be connected to the vehicle structure in a stable and highly integrated manner. This results in significant advantages in terms of durability, rigidity and crashworthiness. The vehicle center of gravity is significantly lower, thus reducing, for example, the risk of rollover in the event of an accident.

In the event of a side impact, and in particular in the event of a side pole impact, intrusions are reduced further as a result of the stable unit of the battery and the underbody. The mounting frame integrated in the battery housing for fastening the battery can be designed as an energy-absorbing crash structure. This allows more installation space to be made available to accommodate battery cells in the battery housing. Due to the highly stable nature of the battery housing, intrusions into the housing during a pole impact can be kept to a minimum.

General Package concept for HV vehicles: Over 50 years of real-life accident research by different OEMs and institutes involving thousands of investigated accidents has led to what is known as a protection zone concept specially developed for electric vehicles. In this concept, the vehicle is divided into three areas:

- Outer zone: Vehicle damage with low accident severity featuring what is known as minor damage, which does not lead to crash recognition and therefore does not lead to an automatic shut-off of the HV system. In this case, the HV system must retain full functional availability in the event of damage.

- Crash zone: The HV system is switched off once the accident severity is sufficient to trigger the occupant protection system. Depending on the accident severity and degree of damage, a distinction could be made between a reversible shut-off (reactivation of the HV system by the customer is possible) and an irreversible shut-off (reactivation of the HV system is no longer possible).

- Core zone: Vehicle areas in which damage is less likely. In crash tests, only very little or no deformation usually occurs here. This area is ideal for accommodating the HV battery and particularly sensitive components.

Inherent stability of HV components: If in individual cases, HV components are accommodated in the outer deformation areas where reliable HV deactivation is not yet ensured, the safety of these components is increased by ensuring that the housings fulfill a minimum requirement for mechanical stability. For this purpose, a damage pattern and load level are derived from the crash simulations and crash tests. For the corresponding HV component parts, the presence of contact protection must be ensured as a minimum. The requirements for the intrinsic mechanical safety of the HV batteries are particularly stringent. Here, alongside the standard crash tests, further load cases are also used to cover real-life accidents to an even greater extent. The need for particular, mechanical protection of HV-components in the crash zone can be reduced by fast cut of times of the battery pack and fast discharge times of the capacitors in the HV-components.

High-voltage line protection: All HV components are connected with each other via high-voltage lines. High-voltage lines are flexible lines that in some cases can be routed inside structural areas. Although this usually involves two separate lines, they can be provided with a shield in particularly sensitive areas in addition to the insulation in order prevent a loss of insulation if crushed. Besides their inherent stability, the degree of protection provided to other HV component parts can also be increased further through the use of deflecting surfaces or protective panels.

Electric Safety mechanisms

Insulation: The high-voltage on-board electrical system (HV system) is fully insulated from the vehicle structure. That means that all HV lines are electrically insulated with a shielding. Hence, there is no possibility that anyone can touch the high voltage live parts. In addition, the orange color of the sheathing indicates that there are HV live parts inside.

Figure 7. HV-lines with orange warning colour

All live parts of HV components are also protected from contact by an appropriate housing. These housings are equipped with a corresponding warning message so that it can be recognized as an HV component.

Figure 8: Warning message on HV components

Electric separation: The galvanic isolation of the HV storage from the rest of the HV system after the HV active state has ended (e.g. driving) ensures that no more electrical energy can flow from the HV storage system

to the HV system. The energy already stored in the intermediate circuit capacities is reduced by a suitable discharge function and there is therefore no longer an electrical hazard in this area. The AC and DC charging lines are also only active in charging mode via HV switches. After charging, they are opened and discharged again. As a result, there is no more energy in the charging lines.

IT-Network: All HV components are connected to each other with both a positive and a negative line. In contrast to conventional 12 V on-board electrical systems, there is therefore no connection to the vehicle body. This type of network is called IT network (Isole Terra, French). Even in the event of damage to the positive or negative line, there is no risk of electric shock or short circuit, as there is not a closed circuit in this case either. So the IT network is error-tolerant against direct contact. There is no electric shock possible by touching the positive or negative side and the car body simultaneously.

Potential equalization: Due to the network type (IT network) used, it is possible to set up potential compensation across all HV lines and HV components via the vehicle body. All housings of HV live components and all the shieldings of the HV lines are connected to each other via a very low resistance across the vehicle body. If both the positive and negative sides of the HV system are damaged, the energy flows off via this low-resistance short circuit. The human body has a much higher transition resistance than the potential equalizer. This ensures that there is no electrical shock hazard for a person when the vehicle is touched in this state.

Logic Safety mechanisms

Monitoring: The entire HV system, especially the battery, monitors itself constantly. Fault currents are detected and displayed at an early stage through continuous temperature monitoring, insulation and short-circuit measurement. For example in the event of serious faults, such as very high short-circuit currents, the system can also protect itself and open the circuit irreversibly via a pyrofuse. All HV components are connected via what is known as an interlock circuit, which monitors whether all the component parts of the HV system are connected correctly. Depending on the fault identified in the HV system, it is either displayed, the component part concerned is prevented from starting again, or the HV system is even switched off.

HV Crash-shutdown: As soon as a certain accident severity is detected in an impact, the HV system is switched off automatically. When this happens, the high-voltage battery relays are opened to prevent further power supply to the HV system. In order to reduce the residual voltage in the high-voltage intermediate circuit to a level of < 60 V DC as quickly as possible (< 5 seconds), HV components with high energy content, e.g. the electric motor or the power electronics, can be actively short-circuited at the same time. This is done by switching on a resistor, through which the current can quickly flow away and be turned into thermal energy. The use of multi-stage occupant protection systems makes it possible to distinguish between reversible or irreversible HV shut-off. If, in the event of less severe accidents, the vehicle still needs to be operational, a reversible shut-off means that the HV system can be switched back on. A reversible shut-off is a precaution triggered by simple shut-down signalling. An insulation test takes place prior to switching the HV system back on. If the insulation test does not detect an insulation fault, the switching back on of the HV system is permitted. In severe accidents, after which there is no way the journey can be continued, the HV system is irreversibly switched off through the ignition of one or several pyrofuses. In addition to the HV crash shutdown via the airbag control unit during normal driving, measures are integrated to trigger a HV shutdown of the high-voltage system in the event of a crash during vehicle standstill (e.g. HV charging, remote software update, use of digital media while standstill).

Manual shut-off points for emergency services: In addition to the automatic crash shut-off, it is possible to switch off the vehicles manually using what are known as rescue shut-off points. For this purpose, redundant options are available via a 12 V switch and an additional 12 V cable loop that can be simply cut. The installation locations are documented in the rescue data sheets. These options are also used during towing away after an accident if the vehicle is only slightly damaged and it cannot determined without doubt if an automatic crash shut-off has occurred.

HVS Intrinsic safety: The above-mentioned safety mechanisms in the event of a crash are supplemented by safety functions that ensure the intrinsic safety of the HV system. These are of course also active in the event of

a crash if crash shutdown detection is defective. These functions , e.g. HV short-circuit monitoring or isolation monitoring, which switches off the HV system in case off fault.

OCCUPANT AND PEDESTRIAN SAFETY

The combination of limited energy density of EV batteries and the demand for increasing driving range leads to large battery installations often dimensionally overlapping with the occupant compartment: the EV batteries can be commonly found in the occupant compartment floor, under the seats, in the floor tunnel, etc., as shown in Figure 9. This overlap, as well as the need to minimize battery intrusion in crash events, typically leads to reduced intrusions into the occupant seating areas if compared to non-EV vehicles, especially in load cases where intrusion is the primary cause of occupant loading, like the side pole impact.

Figure 9: In passenger vehicles, EV battery installations often overlap with occupant compartment footprint

Large EV batteries also often increase mass of EVs when compared to their non-EV peers [7]. Higher vehicle mass has implications for occupant protection. Heavier vehicles tend to have an advantage in car-to-car impacts, providing lower severity crash pulse to its occupants and more severe pulse to the occupants of the lighter vehicle [7]. It remains to be seen if larger penetration of EVs in the global fleet will lead to a more asymmetric distribution of masses in vehicle-to-vehicle crashes.
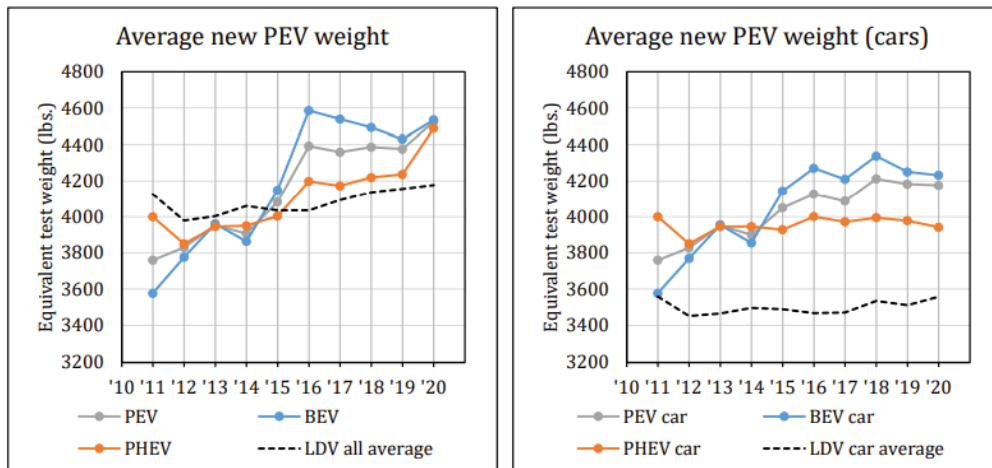
Figure 10: Average new PEV equivalent test weight compared with all LDV. All size classes – left, cars only – right [7]

In conventional vehicles, the internal combustion engine, transmission, drive-shaft and other components can limit the available crush space in severe crashes. The front compartments of EVs typically contain smaller components which may allow designing the vehicle structure for more occupant friendly acceleration pulse in full frontal impacts into a flat rigid barrier. The benefits of such improved pulse characteristics in real world car-to-car collisions needs to be researched and better understood.

The recent rise of EVs coincides with the rise of many new active safety features as well as advanced occupant sensing and occupant restraint technologies. These technologies reduce the risk of a crash event happening as well as the risk and severity of injuries in crash and other events. Even though these technologies are not specific to EVs, they will significantly contribute to overall EV safety performance improvements.

EV propulsion architecture also affects the under-hood compartment layout. Maintaining clearance between the hood and hard components under the hood is important for providing sufficient energy absorption distance for the head of the impacted pedestrian. For example, a sports car with conventional propulsion could face a challenge in this respect because of stacking a large engine under a typically low hood with crank shaft box, engine block, cylinder head and intake manifold taking a lot of space vertically. EVs can bring more flexibility in arranging the under-hood components. On the other hand, some EVs have a luggage compartment under the hood, creating a possibility of hard objects stored there, potentially requiring additional design considerations relevant to pedestrian safety.

Another component of pedestrian safety is related to the low noise emission of the EVs at low speeds when compared to typical ICE vehicles, making them less likely to be noticed by pedestrians and bicyclists. A number of regulatory requirements have emerged around the globe in the past two decades requiring EVs to produce acoustic alerts or warning sounds. Various aspects of this EV feature are still being researched, like optimal sound patterns, intensity and direction, environmental noise pollution, etc.

VERIFICATION/VALIDATION

Even in the age of computer simulations, testing remains indispensable to ensure the high level of occupant safety and partner protection. It became increasingly clear that the development tools for vehicle safety need to be elevated to a new level. Therefore, an increase in the number of load cases that need to be physically crash tested to represent the future road accidents may be expected.

For future car concepts a flexible and efficient crash track concept is needed that not only offers the possibilities of conventional crash tests, but also the prerequisites for new test arrangements such as, for example:

- Crash tests with electric vehicles and other alternative powertrains
- Process optimisation of the entire testing and measuring operation for improving the quality and shortening the preparation and analysis times
- HV battery testing at component and vehicle level

Crash Testing aspects

Electric and hybrid vehicles are assessed and tested as any other transport vehicle of the same category to fulfil with the safety standards. Nevertheless, they have a potential danger in specific cases such as severe crashes due to the risk of electric shock, electrolyte spillage or thermal runaway from the HV battery.

Overall, a huge number of crash test configurations are possible. Testing vehicles equipped with charged lithium-ion batteries or with filled hydrogen introduce very specific requirements for occupational and fire safety and the correspondent testing procedures. In more detail, the laboratory requirements expected for the electric and hybrid crash test performance must include:

- Conventional fire extinguisher at every crash location
- CO2 extinguishing systems at every crash location
- Fireproof blanket to cover the vehicle or HV battery in case of temperature increase or fire
- Smoke extraction flaps
- Gate and door concept for fire and explosion protection
- Depressurization openings for explosion protection
- Jet nozzles at exposed crash points for extreme air mixtures
  to inhibit the formation of explosive mixtures of gasoline, hydrogen, etc.
- Remote-controlled reconnaissance/measurement robots for safe detection of hazards
- Telescopic loader for removing damaged cars
- Water basins for damaged vehicles containing Li-ion batteries
- High-voltage garages for safe, supervised storage of HV crash vehicles after crash testing
- Wireless temperature monitoring systems
- Implications to workshops and laboratory layout (sled setup for ECE R100, battery tear down)
- Hydrogen detectors
- Pressure measurements

- Workshops adaptations – Emergency door to outdoors, extraction system, smoke and fire detection, temperature control
- Crash area adaptation – Emergency door to outdoors, extraction system specially designed for a very fast extraction, smoke and fire detection, temperature control
- Quarantine areas – enclosed areas with flooding system, smoke and fire detection and extinguishing, temperature control
- HV battery storage

According to legal and consumer standards, people safety is guaranteed. The crashworthiness evaluation of EV does not only require preparation of EV measurements, it is also recommended to adapt the layout of the testing facilities but also the deployment of enhanced safety standards during the whole process. Live voltage implies a high risk to all workers involved in the crash test and, therefore, specific safety protocols have to be implemented to guarantee the treatment of vehicle samples to minimize risks in the test preparation, its execution and the post-crash activities.

Main risks of EV are:

- Electric shock
- Fire or smoke

In addition to all the safety procedures described below, the main safety recommendation is the staff training. EV training should be developed by experts and according to the tasks of each worker. Safety training and protocols should be given to all workers without exception.

All EV process should be done considering the two main risks associated to High Voltage and Chemical processes of the lithium-ion batteries. On one hand, Electric shock; all the vehicles should be instrumented with HV harness measurement. Moreover, workers should wear appropriate PPEs and follow internal procedures.

On the other hand, fire or smoke risk; HV batteries temperature should be controlled using appropriate equipment. It is very important to monitor temperature after a crash test to avoid damages in case of thermal propagation. It is also strongly recommended to wear clothes capable to protect against a sudden flame, at least, during crash test and first minutes after crash test. Safety procedures for each test phase are described below.

Test vehicle preparation

Loading / unloading: Vehicle loading/unloading should be done taking into account that most of the HV batteries are located at the vehicle floor, between the wheels. So that, it is very important that, if you use a forklift, to use appropriate separators with the forklift shovels to avoid applying pressure to the HV battery cover. Also, it is recommended to transport the vehicle with the HV system safely disconnected. It is also important to take into account that when disabling HV system, vehicle wheels could be blocked. It is strongly recommended to use trucks with lateral dock.
After unloading the vehicle, it would be important to mark the vehicle as Electric or Hybrid or Hydrogen.

Figure 11: Label used to identify electric vehicles when unloaded into the crash facilities

Vehicle battery charging: Vehicle charging should be done according to the vehicle development stage. When vehicle is a prototype, there could be some safety requirements not 100% operational so the charging should be done under supervision. Also, charging facilities should has some detection and extinguishing mechanisms to avoid fire spread to other facilities.

Vehicle disconnection: Before any preparation, vehicle should be disconnected in such a way that it is impossible to energize powertrain cables. There are two types of disconnection: Mechanical device that separates HV Battery from HV Battery output cables and electric switch that controls High Voltage Battery relays through Low Voltage lines. It is very important to put up poster signalling the vehicle status: connected or disconnected. The vehicle should remain disconnected until the test execution to guarantee workers safety.
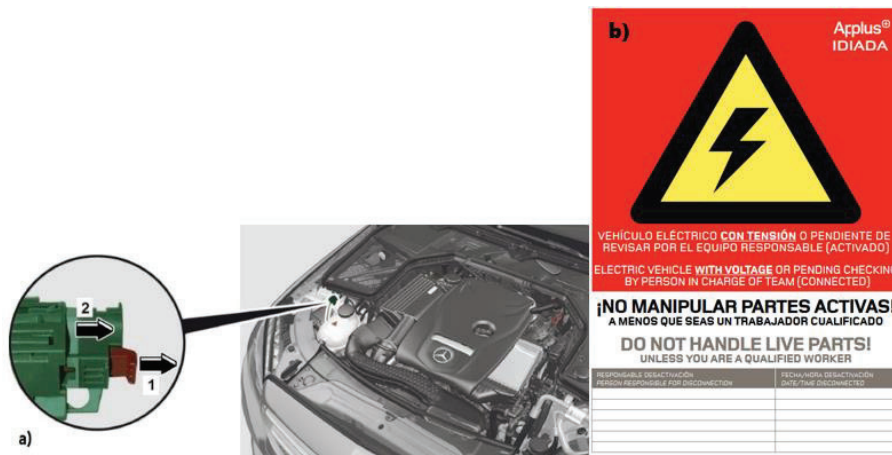
Figure 12: (a) Switch to connect and disconnect the high voltage system of the vehicle [12]. (b) Example poster to be attached on the exterior part of the vehicle indicating the presence of high voltage system activated.

Safety measurements after instrumentation: Previously, legal and consumer standards were explained. Those standard requirements are to measure HV at powertrain lines. For this reason, special instrumentation of HV is necessary. Special cabling should be used to powertrain lines and it is the responsibility of the test facilities staff to verify their correct operation. Also, sensors for data acquisition should be tested and verified.

Activation previous to crash test: Crash test performance: A display is mounted in the outer part of the vehicle to know if the voltage of the HV battery is higher than the 60V allowed. Moreover, an extra switch has to be installed in the vehicle and a temperature monitoring system has to be installed to identify any fire risk.

Safety protocol: The safety protocol is a special procedure for electric vehicles to guarantee workers safety during and after the crash. This protocol is life, meaning that all the time is improving with new experiences.

Before the crash test, a meeting is organized to order all the actions to the people that should be during the safety protocol. During this meeting, it is formed a team of 8 people divided in 4 sub-team:

- Measurement team: 1 measurement leader and 2 measurement assistants. The team mission is to measure voltage values after the crash and verify the vehicle safety.
- Evacuation team: 1 emergency leader and 1 driver. The team mission is to lead the emergency protocol and vehicle extraction outdoors in case the measurement team advise of any problem.
- Car adjustment team: 1 adjustment leader. The team mission is to make adjustments with HV activated in the vehicle.
- Firefighters: 2 professional firefighters subcontracted. The team is supervising the test, analyzing if there is any hazard and, in case of emergency, to lead the fire extinguishing.

During the meeting, all the actions to be performed during standard safety protocol are named and ordered to the workers. It is very important to know which actions should do every worker and the precise order of the actions.

Besides the specified actions, all the workers received EV training related to the protocol, so that, they already know the PPEs and specific tools they should use during the protocol. To summarize it:

- PPEs
    o Fireproof and chemical protection clothes
    o Dielectric gloves
    o Mechanical cover for dielectric gloves
    o Firefighter helmet
    o Isolated shoes
- Protection tools:
    o Dielectric harness
    o Dielectric carpet
- Measurement tools:

- o Thermal camera
- o Voltmeter
- o Megaohmeter
- o Known resistance box

Once all the workers involved in the process are ready, the display is connected to verify its correct operation. Also, temperature monitoring system is turned on to verify the temperature of the HV battery. Finally, the HV system is activated and voltage values and isolation resistance of the vehicle is verified. Once all safety devices are tested, the crash test can be performed.

After the crash, first people to be near to the vehicle are measurement team. Their actions are:

- Verify there is no smoke or fire
- Spread dielectric carpets at the measurement area
- Make voltage and resistance measurements
- Push emergency button to open battery relays (if vehicle has not disconnected after the crash)

Once the measurements are performed, the measurement leader allows to hook the vehicle with the extraction cable. The extraction cable is attached to a forklift outside of the lab. In case of emergency, the forklift can pull the vehicle out of the lab using guiding pulleys. The forklift is driven by evacuation driver.

During 15 minutes after the crash, a quarantine period is stablished. During that 15 minutes, only people using appropriate clothes and tools can be near the vehicle. From crash test until the vehicle is outside of the building, wireless measurement of battery temperature is controlled and monitored through control room staff, specially during the first 15 minutes.

Evacuation team is double checking vehicle temperature using a thermal camera. The team leader is connected with a telephone with the driver and with control room and it is in charge of the vehicle evacuation in case of fire or smoke anomaly.

Emergency protocol: The emergency protocol is the result of some possible problems that can appear and some experiences with EV crash test.

Before mention the different emergencies that can appear, it is very important to know clearly the rescue priority:

1st: PEOPLE

2nd: FACILITIES

3rd: EQUIPMENT

It is also very important to analyze the risks to anticipate the emergency protocol to be performed. The main risks are:

- Electrocution
- Battery temperature increase
- Smoke
- Fire
- Explosion
- Chemical burn because of battery liquids

Emergency protocol cases:

1) No absence of voltage (electrocution)
   After the crash test, it could be possible to detect more than 60 V. If this occurs, there is a risk of electrocution. To avoid any risk, all the people should wear dielectric gloves.
   Once the measurements are performed, it is necessary to push the emergency switch installed at the vehicle. This switch can open the battery relays forcing the voltage drop to 0V.
2) Battery temperature increase (No fire or smoke)
   If the temperature of the battery increase, emergency protocol is activated.
   First, evacuation team with help of firefighters should pull the vehicle outside of the facility. Then, the temperature increase should be evaluated:

$\Delta T \leq 5^{\circ}C/minute$ and T< 60 ºC → Measurement team should try to remove the data acquisition equipment and dummies with help of firefighters

$\Delta T > 5^{\circ}C/minute$ or T > 60 ºC → All the staff not equipped with SBA (self-contained breathing apparatus) should evacuate the crash area and move to Emergency Point. Only firefighters can be near the vehicle.

3) Smoke

   Evacuation driver should pull out the vehicle and move to the Emergency Point. All the staff not equipped with SBA (self-contained breathing apparatus) should evacuate the crash area and move to Emergency Point. Only firefighters can be near the vehicle.

4) Fire

   Evacuation driver should pull out the vehicle and move to the Emergency Point. All the staff not equipped with SBA (self-contained breathing apparatus) should evacuate the crash area and move to Emergency Point. Only firefighters can be near the vehicle.

5) Explosion

   Evacuation driver should pull out the vehicle and move to the Emergency Point. All the staff not equipped with SBA (self-contained breathing apparatus) should evacuate the crash area and move to Emergency Point. Only firefighters can be near the vehicle.

6) Chemical burn because of battery liquids

   In case of a chemical burn because of battery liquids, it is very important to wash the skin or the eyes with Hexafluorine solution. Most of the lithium-ion batteries leakage could be hydrofluoric acid. Only Hexafluorine solution could wash the burn, never use water.

In addition, the possibility of an emergency is very slim, however, crash lab should be prepared for an emergency because the damages of a possible emergency are very high for the facilities and people safety is first.

Figure 13: Equipment and tools needed to deploy the safety protocol within a crash test execution

Post-crash activities: Once the crash test has been performed, extreme care needs to be taken to ensure that there is no high voltage exposed before anybody working with the vehicle. European regulations (R94, R95, Euro NCAP) and American regulations (FMVSS 208, 214 and 301 new, 305), specify some voltage measurements that should be taken and some calculations that must be made after the crash test. However, as EV's can become dangerous when crashing due to electroshock hazard and chemical fire hazard, the addition of extra requirements from the ones defined in official safety standard procedures will help to reduce as much as possible any incident, personal damage risk and its consequences. The post-crash activities and the sample treatment are widely described in Chapter 8 named "Firefighting, Rescue and Post-Crash Vehicle Handling".

Nevertheless, a short introduction to the required workflow for sample treatment and storage can be found hereunder and summarized in Figure 14.
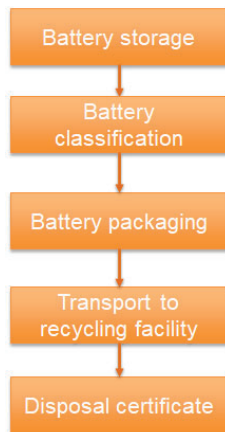

Figure 14: Workflow for high voltage battery treatment after a crash test

Sample treatment: Every EV sample will be treated with extreme care after the test execution to ensure safety of the testing facilities and the workers involved in the vehicle towing and management. Therefore, the crashed samples will be marked with the corresponding label identifying the HV components, the type of test performed and the risk level of the sample.

After participating in a crash test, the EV will stay overnight in the quarantine area where a monitoring system will follow-up any temperature increases of the HV battery, and the fire detectors will inform the firefighters in case of any incidence to intervene and minimize consequences.

Storage: If the HV battery does not show a clear damage after the overnight process it can be stored in isolated containers specially designed to control the temperature of the samples and reduce the risk of fire propagation to other vehicle samples and laboratory facilities. Once the HV battery is not needed for testing purposes it must be correctly packaged and sent to recycling facilities for its dismantling. The recycling facility will provide a disposal certificate ensuring the end-of-life of the HV battery and guaranteeing that post-crash activities are finished.

PART 2: STRATEGIES TO MITIGATE PROPAGATION IN BATTERY ELECTRIC VEHICLES

DESCRIPTION OF THE PHENOMENON

The fire triangle shown in Figure 15 represents a simple model for understanding the necessary conditions to start a combustion reaction (→ fire).
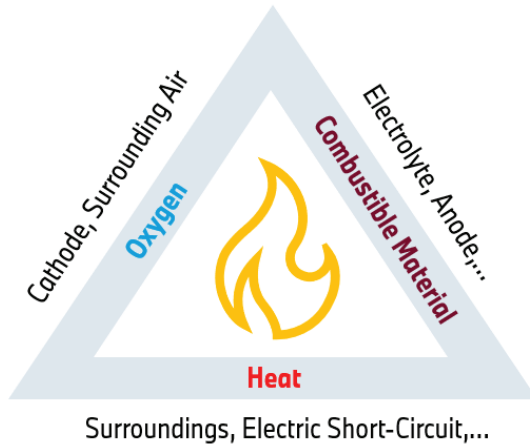

Figure 15: Fire Triangle: The three key elements necessary to start a combustion reaction.

For most fires, the presence of three elements is necessary: A flammable material, an oxidizing agent (most commonly: oxygen), and an initial heat source to trigger the combustion reaction. Modern battery cells consist of flammable materials such as the electrolyte or the anode and bring their own oxygen stored within the cathode material. Conclusively, battery cells typically meet two of three conditions for a fire and already an erroneously high heat input can lead to a strong exothermal reaction, which is commonly called "Cell Thermal Runaway" (TR). Typical errors which can lead to Cell Thermal Runaways are cell-internal short circuits, improper treatment of the battery cell, or heat input from the cell's environment and are presented in detail in the next section. An important key figure to describe a Cell Thermal Runaway is the total amount of heat Q_{tot} released. Figure 16 shows Q_{tot} for state-of-the-art Lithium-Ion battery cells depending on their respective capacity C_{cell}, measured using autoclave calorimetry.
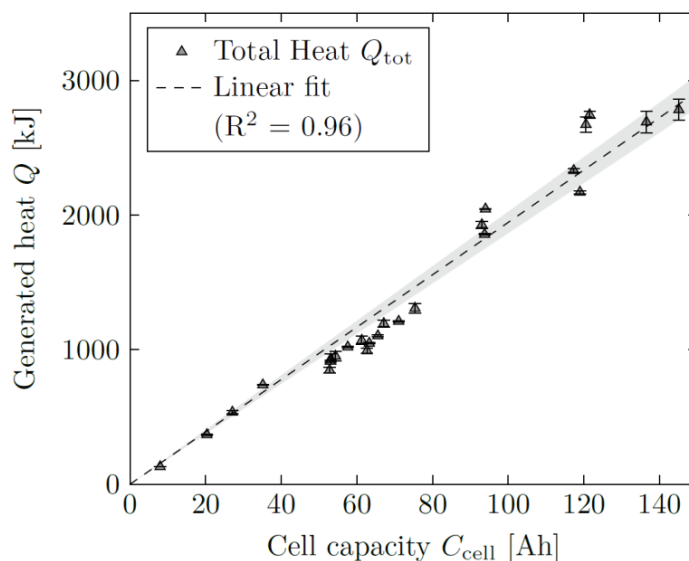
Figure 16: Total amount of heat released during a cell thermal runaway dependent on cell capacity [13].

For the battery cells investigated and depending on cell capacity, the total released energy during a Cell Thermal Runaway can easily exceed 1000 kJ. Furthermore, the data shows a strong dependence of Q_{tot} on cell capacity: a higher energy content typically leads to a higher heat release during a Cell Thermal Runaway. For cell chemistries

enabling high energy densities, TRs typically only last a few seconds. Heat release rates can therefore be expected in the range of hundreds of kilowatts. Obviously, on battery pack level, an error on this scale has the potential to trigger a Thermal Runaway of a neighboring cell which is typically placed millimeters away. A chain reaction in such a worst case scenario is called "Thermal Propagation" and can potentially lead to a fire spreading to the vehicle and imposing a danger to the passengers.

RULES, REGULATIONS AND MOTIVATION TO MITIGATE PROPAGATION

There are different motivations for manufacturers of battery packs or electric vehicles to develop concepts to mitigate propagation. On the one hand, an OEM obviously wants to sell safe vehicles that do not cause situations endangering life and health of the users. On the other hand, regulations and norms concerning battery packs for electric vehicles exist in different countries, which must be obeyed to be able to sell the product in the respective market.

The UNECE (United Nations Economic Commission for Europe), under the "1998 Agreement", releases regulations to create harmonized conditions for the approval & homologation of vehicles. In 2018, Global Technical Regulation (GTR) Nr. 20 phase 1 was published. It includes requirements relating to thermal propagation. Applying a "documentation approach", the OEM must establish a description of the system and its safety concept using a risk analysis. Furthermore, an outline of the validation procedures and results, demonstrating that the customer is not exposed to a dangerous situation, is required. So far, a pure documentation thereof is sufficient and no clearly defined homologation test for a robustness concerning thermal propagation is included. Several countries work on national laws to adopt the UNECE regulations into compulsory regulations, however not always in the same manner.

A very relevant regulation which also includes homologation testing concerning thermal propagation is the Chinese GB 38031-2020. China is the world's biggest electric vehicle (EV) market and wants to play a pioneering role in EV safety regulations. The current GB standard includes, among other things, a thermal propagation homologation test of the battery pack in which a battery cell is brought into thermal runaway by nail penetration or overheating (or an alternative method which the OEM can choose, with some conditions). The thermal event must be detected and for at least 5min after sending out an alarm signal, no explosion shall occur, and no fire must leave the battery system. If the homologation test is performed on the vehicle level, additionally no fire or smoke shall enter the passenger cabin of the electric vehicle for at least 5min.

The GB standard is currently under revision and a new version is being drafted that will possibly replace the current standard in 2025. It may include an increase in requirements concerning thermal propagation with a significant prolongation of the 5min time interval (from detection until fire or smoke inside the passenger compartment would be allowed). If this is implemented, the propagation from cell to cell must be further reduced or even stopped completely to fulfill the homologation requirements.

Besides laws and regulations, the OEM must obey to be able to sell the vehicles in the respective market, also other motivations come into place. On top of all legal requirements and regulatory demands, a product manufacturer has the duty of care. A product shall be failure tolerant and not cause unnecessary harm. But also, economic aspects must be considered. As electric vehicles are a relatively new technology (besides some electric car prototypes at the very early beginning of automotive history), people very closely monitor the abilities and safety performance of this new type of vehicles. A burning electric car will have a many times higher impact in press and customer awareness than a burning internal combustion engine (ICE) vehicle, despite the statistical evidence that electric vehicles do not show any higher probability of car fires compared to ICE vehicles [14] [15]. Additionally, the situations in which EVs and ICE vehicles catch fire are very different. In the rare cases of ICE vehicle fires, the thermal event most often starts during operation due to overheating of the combustion engine and the exhaust system igniting other parts of the vehicle. In the few cases of electric vehicle burns, car fires have been ignited during or after charging the battery pack [16]. The charging situation has a higher potential for escalation because of the proximity to critical areas like garages or houses. For these many reasons, the safety of the electric vehicle including its thermal propagation robustness should always be high priority for every product manufacturer.

STRATEGIES TO HANDLE PROPAGATION

To strongly limit or even to avoid the risk of fire incidents of electric vehicles, a comprehensive safety concept on all levels of the high voltage storage system is essential. Measures only on one level alone will not be sufficient in most cases. The different possible layers of a propagation safety concept are illustrated in Figure 17.
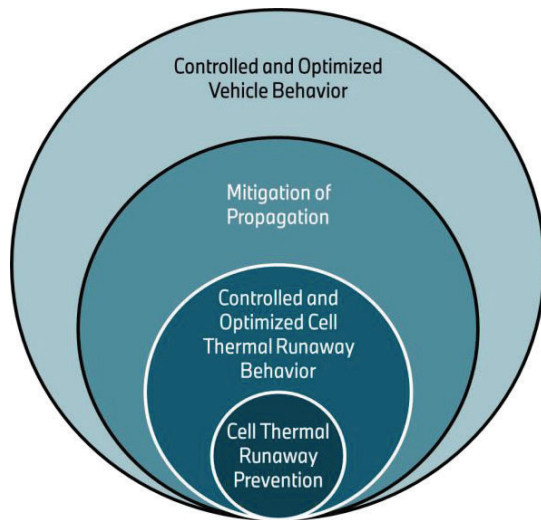
Figure 17: From cell to vehicle level - Four layers to mitigate propagation.

The innermost layers consist of the safety concept on battery cell level. Due to a robust cell design and a mature production process with advanced process and quality measures, safety critical events with a possible cell thermal runaway can be made extremely unlikely or even avoided *("Cell Thermal Runaway Prevention")*. If, nevertheless, a battery cell will undergo a Thermal Runaway, the cell design should allow a controlled and predictable behavior that, for example, does not lead to side-openings or even an explosion-like rupture of the cell housing *("Controlled & Optimized Cell Thermal Runaway Behavior")*. Within the next layer of the safety concept, the battery storage should be able to cope with the controlled thermal runaway of a battery cell and hinder or at least mitigate an uncontrolled chain reaction of consecutive thermal events of neighbor cells (*"Mitigation of Propagation"*). The latter safety layer is for example also reflected in the current Chinese GB norm, which requests no fire outside the battery for at least 5min after detection of a safety critical event. The final layer "*Controlled & Optimized Vehicle Behavior*" includes safety measures on vehicle level to further protect customers and to allow passengers to leave the vehicle safely.

All the described layers of the overall safety concept add up to achieve a high level of safety for the electric vehicle passengers. In the following, possible measures on each level are illustrated in more detail.

SAFETY LEVEL 1: CELL THERMAL RUNAWAY PREVENTION

In the following chapter, an insight is given on possible root causes for cell thermal events and how to avoid or mitigate them.

Cell Thermal Runaway

The thermal runaway of a lithium-ion cell can be described as an uncontrollable, strongly exothermal process through the combustion of the cell-internal materials, in particular electrodes, separator, and electrolyte. To start the combustion reaction, the activation energy of the reactions must be reached. One possibility for the initial heat-up necessary to activate the self-heating of the cell, might be a cell internal short-circuit. Depending on the temperature level the cell material reaches due to such a failure, different exothermal reactions can be triggered. Even at relatively low values above the operating temperatures of typical lithium-ion cells (~70-80°C), the decomposition of the solid electrolyte interface (SEI), marks the entry point to the exothermal heat release and self-heating of the battery cell. The associated heat release is still very low, and the SEI decomposition has a bigger impact on cell lifetime than causing a safety critical event. At temperatures above that point, the electrolyte starts to decompose and even higher up in temperature the decomposition reactions of the anode set in. Those reactions already contribute more significantly to a further self-heating of the cell. Nevertheless, depending on the thermal boundary conditions of the lithium-ion cell, those reactions might not yet lead to the strong uncontrollable exothermal heat release called thermal runaway. If heat is dissipated in a significant way to surrounding cell material or neighbor cells, the temperature threshold for the very critical cathode reactions might not be reached (typically 150°C-200°C for NCM chemistry) and the cell might survive without catching fire. If, however, the cathode reactions are triggered, very significant exothermal reactions, as for example the combustion of the

electrolyte with the released oxygen from the cathode material, can lead to an uncontrollable thermal event with very high self-heating rates (➔ "Cell thermal runaway"). In Figure 18 three different scenarios are depicted with a different initial heat up of the lithium-ion cell.
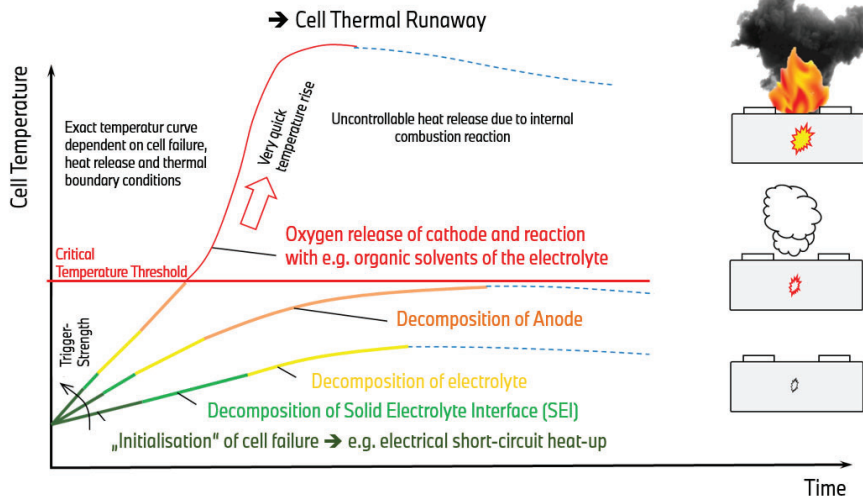

Figure 18: Cell-Temperature over time for different initial failure severity and thus short-circuit-based heat-up of the battery cell. If a critical failure is observed with significant short-circuit power, the different heat release reactions within the cell can be activated. If the temperature threshold necessary to trigger the cathode reactions is reached, an uncontrollable thermal event with quick temperature rise can be observed (figure kindly provided by S. Scharner, BMW)

In Figure 19 the measured temperature-dependent self-heating of a lithium-ion cell under adiabatic conditions is shown. The data has been acquired via ARC (Adiabatic Accelerating Rate Calorimetry). These measurements illustrate at which temperature point exothermal reactions of cells start and at which rate they lead to a self-heating of the cell. With increasing temperature, the self-heating rate increases as additional exothermal reactions are added. The exothermal reactions start with very low rates 0.05°C/min at 70-80°C (➔ SEI decomposition) and go up to very high rates (➔ "Onset of thermal runaway") at temperatures above 170-180°C as soon as the cathode related exothermal reactions kick in.
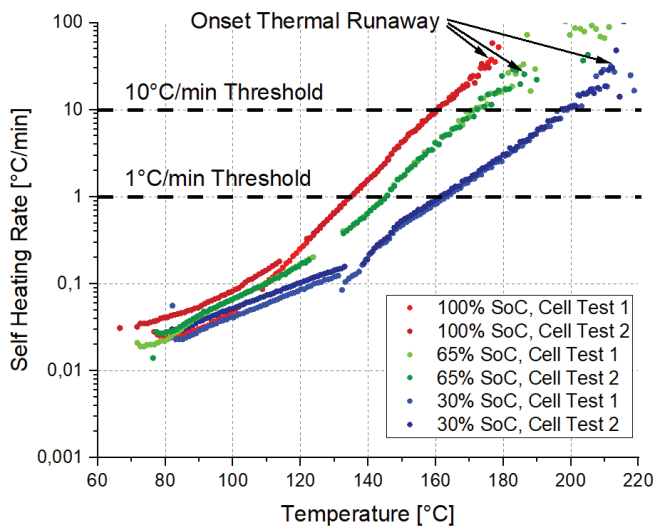

Figure 19: Temperature-dependent self-heating rates in [°C/min] for a Ni-rich NMC cell at three different states of charge (100%, 65% and 30%). The self-heating rate thresholds for 1°C/min and 10°C/min are indicated as well as the temperature regime of thermal runaway. (Data kindly provided by S. Dandl, BMW).

As it can be seen from Figure 19, the self-heating rate curve is dependent on the state of charge (SoC) of the lithium-ion cell. With increasing SoC and thus state of delithiation of the cathode, the cell materials get more unstable and produce the same exothermal self-heating already at lower temperature points (see 1°C/min and 10°C/min thresholds). The thermal runaway onset regime also shifts from about 210°C at 30% SoC to about 175°C at 100% SoC. In conclusion, lithium-ion cells are more thermally stable at lower state of charge.

Similar trends can be seen for different ageing conditions of a battery cell. Over the ageing process of cells and depending on the operational conditions and use case (e.g., percentage of fast-charging cycles and fast-charging power and temperature), lithium plating might occur on the anode. The presence of metallic lithium in the battery cell makes it again more temperature sensitive and will shift the onset of exothermal reactions and thus the self-heating curves towards lower temperatures. In Figure 20, the measured self-heating profiles for different ageing conditions are depicted.
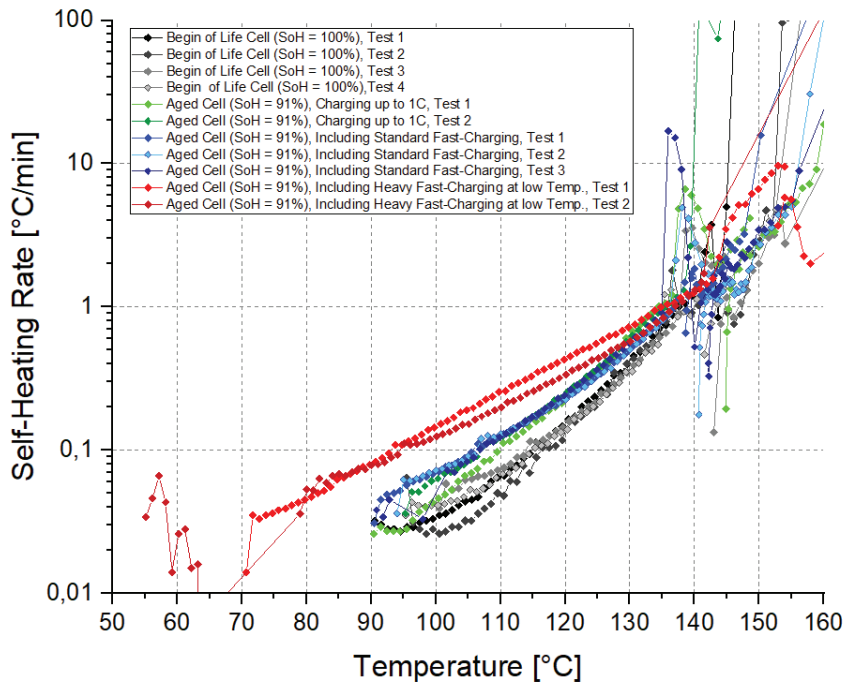
Figure 20: Temperature-dependent self-heating rates in [°C/min] for a NMC cell at four different ageing conditions: begin of life, SoH = 91% & low current charging, SoH = 91% & normal + fast-charging, SoH = 91% & normal + heavy fast-charging at low temperatures. (Data kindly provided by S. Dandl, BMW).

Aged cells show higher self-heating rates and an earlier onset of exothermal reactions in comparison to cells at begin of life. Furthermore, with an increased share of fast-charging cycles and with increasing severity of the charging profile (→ reduced charging time & decreased charging temperatures), the exothermal reactions start already at lower temperatures and show an overall increased self-heating rate.

Cell Internal Root Causes

As described in the sub-chapter above, the precondition required to trigger a thermal runaway of a battery cell is the initial heat input (→ "activation energy") starting the exothermal self-heating of the cell. This initial heat-input might be delivered by different root causes within the cell or from the outside. In the following, a deeper insight to the cell internal root causes is given.

In the table below an exemplary overview over possible cell internal failures and their root causes is given. This table is only a small insight into a comprehensive cell design & process FMEA ("failure mode and effects analysis"). Nevertheless, it becomes clear that cell internal failures, that have the potential to generate enough heat to trigger a thermal runaway, are mainly cell internal short circuits.

Table 3: Exemplary cell internal failures that could potentially lead to a cell thermal runaway. Possible failure root-cause are indicated as well as their potential origins.

Failure	Root Cause	Origin
Cell internal short-circuit via particles	Metal particles (Al, Cu, Steel), non-metallic particles	Welding processes, Particle contamination from the outside, …
Cell internal short-circuit via dendrites	Lithium-dendrites/-plating, Cu-dendrites	Inhomogeneous local charging resistance, electrode misalignment, Cu-particles, inhomogeneous electrolyte wetting,
Cell internal short-circuit via misalignment or deformation	Anode-Cathode electrode(-foil) contact, electrical contact with current collector and cell housing	Bad manufacturing tolerances, cell design errors considering electrode swelling and vibrations
Cell internal short-circuit via damage to isolation layers	Damaged separator, damaged isolation between electrode stack and cell can	Isolation failure in base material, damage of isolation layer during manufacturing

As can be seen, the reasons for cell internal short circuits are various. In the following, a closer look is directed towards the first two failure types – cell internal short-circuits via particles and dendrites.

Particle Short-Circuits: Particles in lithium-ion cells can have many and diverse origins. Besides particles that are introduced to the cell from the outside during the cell manufacturing process or due to the contamination of sub-components, particles can also be generated during the cell manufacturing process. As the cathode and anode current collector and foils are made of Aluminum (Al) and Copper (Cu), all welding processes will produce Al and Cu metal particles when connecting the different electrode layers of same polarity together and joining them to current-collectors and terminals. A possible cap-plate-to-can sealing weld of the housing will generate aluminum or steel- particles depending on the choice of cell housing material. The amount, size distribution and location of the particles will depend on the exact welding process (LASER, resistance, ultra-sonic, …), welding geometry and particle shielding, welding power and size of the connected subcomponents. Also, particles inside the cell might move during the electrolyte filling process if their size and the cell internal space allows that.

If, for example, conductive Al or Cu particles will get to rest at critical locations within the cell and are large enough to penetrate through isolation layers like the polymer separator film (typical thickness in the range of 10-20µm), an internal short circuit can develop. Such internal short circuits (ISC) might have different local heating power $P_{ISC} \propto (U_{Cell}^2 / R_{ISC})$ depending on the momentary cell voltage U_{Cell} and the internal short circuit resistance R_{ISC} (particle resistance plus contact resistances towards electrodes). The larger the particle, the more electrode and separator layers can be penetrated and with each electrode layer contacted, R_{ISC} is further reduced and the short-circuit heating power increased. In Figure 21(a) an electrode plus separator layer is depicted that was locally punctured by a larger particle. If the generated local heating power P_{ISC} is large enough to reach temperatures above the melting temperatures of the polymer separator, the separator between anode and cathode will locally melt and retract further, leading to even a better contact and a stronger short-circuit between the electrodes of opposite polarity (see Figure 21(b))
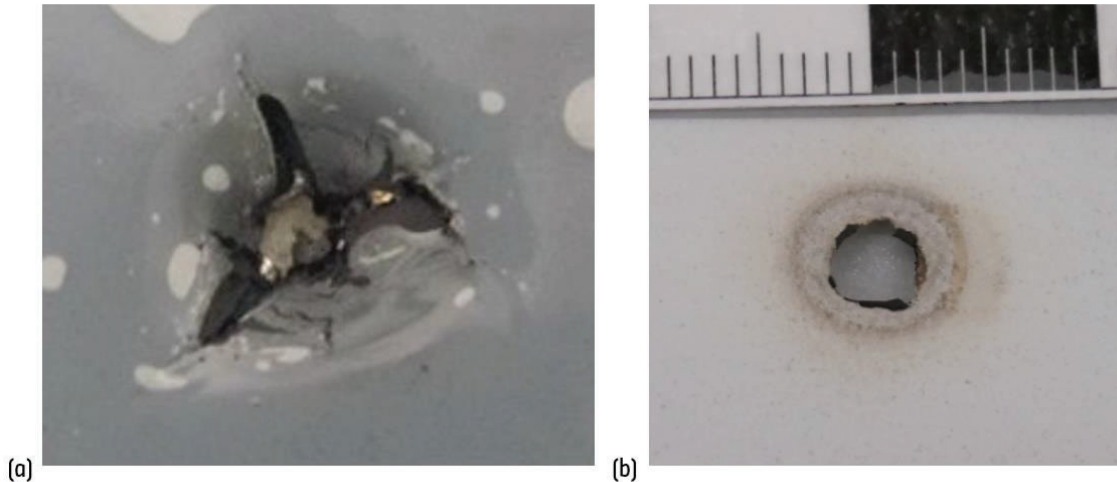
(a)

(b)

Figure 21: (a) Electrode and separator layer mechanically perforated by a cell internal particle. (b) If the local heat up exceeds the melting temperature of the polymer-based separator layer, the isolator film melts around the particle short circuit and enlarges the contact area between anode & cathode.

In case of small particles and high contact resistances or also a weak current carrying capability of the particle, the local particle short-circuit might just lead to an increased self-discharge of the cell without thermal runaway. That latter case corresponds more to a quality issue than to a safety critical state. If, however, short-circuit currents are strong enough and the local heat deposit by the short circuit current is sufficient to trigger the critical exothermal reactions of the cell materials, the cell will go into thermal runaway. Such a scenario can be seen in Figure 22, which shows the measurement data of a partial nail penetration into a lithium-ion cell simulating the case of a very large particle defect penetrating multiple electrode layers (see also exemplary CT image in Figure 22(b)).
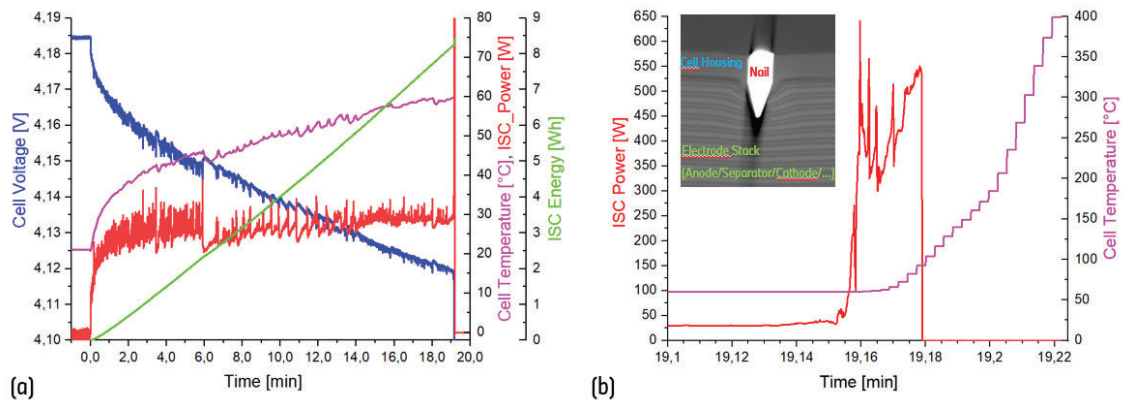

(a)

(b)

Figure 22: (a) Measurement of a partial nail penetration test with a lithium-ion battery simulating a local internal particle short-circuit. The cell discharges over the short-circuit with about 25-30W and heats up. (b) After about 19min and a local heat deposit of about 8.5Wh (ISC Energy), the severity of the short circuit increases suddenly and increases its power to more than 500W locally, leading to the thermal event of the battery cell with a very strong increase of the cell temperature.

Upon activation of the local short-circuit (→ partial nail penetration), the cell voltage breaks down and the cell is discharged over the particle/nail. The measured local short circuit power P_{ISC} is in the range of 25-30W, which leads to relatively strong local heat-up of the cell material surrounding the particle short-circuit. To the outside the cell steadily increases its temperature towards 60°C, however, inside of the cell close to the short-circuit zone, material temperatures well above that point can be expected. After about 19min and a local short circuit heat depot of 8.5Wh (ISC energy in Figure 22(a)), the separator reaches locally its melting temperature, retracts, and causes a sudden increase of the internal short circuit power to values above 500W and a breakdown of the cell voltage.

These very significant heating power values directly lead to a local activation of the very critical cathode reactions and subsequently to the thermal runaway of the battery cell with a drastic increase of the cell temperatures.

Dendritic Short-Circuits: Another potentially critical root cause for cell internal short-circuits which can lead to thermal events are dendritic short-circuits. The two most relevant dendrites that can develop in lithium-ion cells are Cu-dendrites and Lithium-dendrites. Cu-dendrites can for example develop if Cu-particles get to rest on the positive cathode at positive potentials outside their electrochemical stability window. In that case, they are oxidized into Cu^{2+} ions which are positively charged and consequently move through the separator to the negatively charged anode. There they are reduced again to metallic copper which starts to grow and build spikey dendritic metal structures that perforate the separator. Eventually these Cu-dendrites reach the cathode and can create an internal short-circuit between the electrodes.

Also, lithium can form potentially critical dendrites inside the cell. There are various root causes that can lead to Li-dendrite growth, two examples are shown in Figure 23. They all have in common that the lithium, which is initially stored within the cathode, is not homogeneously or to quickly transferred into the anode upon charging and the anodes locally exceeds its capability to fully intercalate the lithium-ions. Metallic lithium then develops on the anode surface in the form of plating or dendrites.
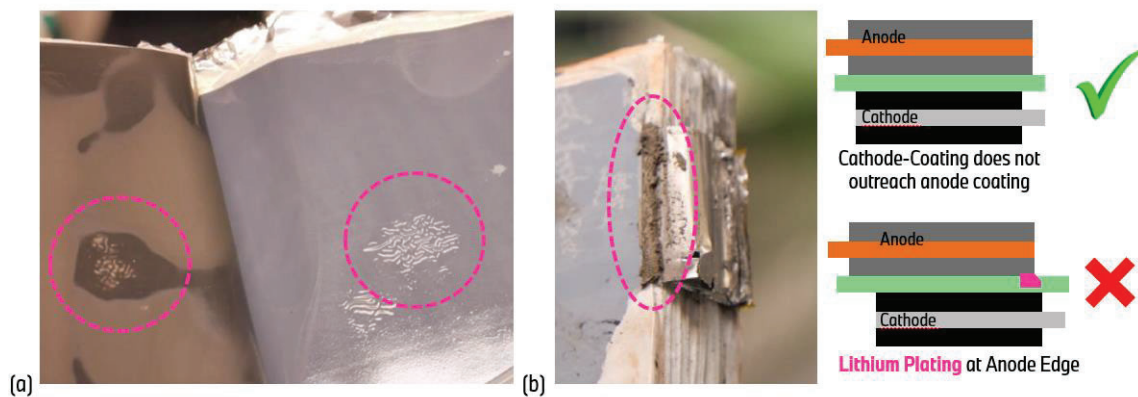

Figure 23: Different cases of lithium plating / dendrite growth. (a) Small lithium plating pattern caused by separator wrinkles. (b) Strong lithium plating due to misalignment of cathode and anode coating.

In Figure 23(a) an opened cell is depicted with local separator wrinkles between anode and cathode. The wrinkles in the separator have led to an alternating distance between anode and cathode and thus to a locally varying charge resistance leading to a reduced charge uptake of the anode at larger distance from the cathode. The anode material in between the separator folds had to take more lithium which then was plated locally onto the anode. As a result, the pattern of the separator wrinkles was transferred into a lithium plating pattern on the anode. This weak lithium plating does most probably not correspond to a large safety risk. In Figure 23(b) however, a more drastic form of lithium dendrite growth can be seen at the edge of an electrode stack due to a manufacturing error. In the latter case, the cathode coating did geometrically outreach the anode coating and therefore did not have a opposite reservoir at the electrode edge to take the lithium upon charging. The lithium from the cathode is then transferred to the outermost edge of the anode which has no sufficient active material to intercalate the lithium. Consequently, a large amount of metallic lithium builds-up locally with the potential to short-circuit the battery cell. Those larger areas of massive lithium dendrite growth can impose a significant safety risk, as they have a much better current carrying capability than the one of individual lithium dendrites and the reactivity of the cell material is locally increased due to the presence of metallic lithium (compare also Figure 20).

Cell External Root Causes

Besides the cell-internal root causes for a thermal event discussed in the previous sub-chapter, also cell external failures are possible that have the potential to lead to a thermal event of a battery cell. Table 4 depicts some exemplary cell-external failures which might lead to a cell thermal runaway, also indicating possible root causes and their origin.

Table 4: Table with exemplary cell external failures that could potentially lead to a cell thermal runaway. Possible failure root-cause are indicated as well as their potential origins.

Failure	Root Cause	Origin
Overtemperature via heat introduction from the outside	Breakdown of or inhomogeneity in cooling/heating system of battery pack, hot-spot upon operation caused by bad contact/welding resistance, short-circuit in HV storage system, fuel-fire from outside, …	Leakage in or breakdown of cooling system, blocking of individual cooling channels, bad busbar welding parameters, HVS-internal short-circuit between cells, external fires, e.g., fuel fires after an accident with ICE vehicles, …
Cell external Short-Circuit	Short-circuit in HV battery pack, battery pack external short-circuit, ...	Particle contaminations, deformation of components, …
Cell internal short-circuit due to mechanical cell deformation	Deformation of battery cell leading to damage to cell internal isolation layers or bringing subcomponents of opposite polarity in contact	Deformation or intrusion of the battery pack, e.g., through an accident.
Overcharge	Failure in battery management system, No or wrong voltage signal available, …	Problems with chipset or software, detachment of voltage sense cables, …
Deep discharge with subsequent continued cell operation	Failure in battery management system, No or wrong voltage signal available, …	Problems with chipset or software, detachment of voltage sense cables, …
Violation of current limits	Failure in battery management system	

As can be seen from non-comprehensive exemplary Table 4, the cell external reasons for a cell thermal event can be various and a more detailed description would exceed the scope of this document.

Cell Design and Manufacturing Process Measures to Avoid Critical Failures

In the following sub-chapter, a more detailed overview is given on potential cell thermal runaway prevention due to process and design measures on cell level. To not exceed the scope of this document, the focus will be on cell internal failures & measures.

Process & Quality Measures – Pushing the failure occurrence to the minimum…

Concerning critical defects or contaminations inside the cell, from process and quality side, there are only two options: avoid the generation or insertion and sort out sub-assemblies and complete cells that possess these contaminations despite all precautions. To avoid the insertion of contaminations, a minimum cleanliness level of subcomponents is required and should be monitored as well as cleanliness of the manufacturing facility. After that, the process control can assure that, for instance, welding processes are well regulated and do not generate larger amounts of particles of significant size. Furthermore, geometric shields, magnetic traps and air-flow systems can hinder the production process particles from entering the cell assembly. In case of electrode misalignments, camera surveillance can help to sort out affected electrode assemblies. If despite all these measures, for instance, critical welding particles enter the cell, there are different means to detect those, at least if they have a critical size. During cell manufacturing, high-potential isolation-failure tests are carried out at different steps. For example, after the stacking or winding of the electrode assembly, the dry electrodes are pressed together, and a high voltage difference (typically above 1kV) is applied to the electrodes of opposite polarity. If larger particles penetrate (partially) the separator, a failure current is measured, and the assembly can be sorted out. Also, camera surveillance can sort out cells with larger contaminations as well as inline X-ray imagining. Finally, at the end of production, the cells undergo an ageing step during which the self-discharge is monitored. An increased capacity loss might be an indication for a discharge over a cell-internal defect. Also, obtained cell capacities and internal resistance values outside the specified tolerance band can be indications for cell internal defects. A reduced cell weight might be an indication for a reduced electrolyte volume or a missing electrode layer. A deviating cell thickness can give an indication for both additionally integrated defects or an insufficient cell

degassing and missing layers in the electrode assembly. It should be noted that the effectiveness of the measures described in this section depends on boundary conditions, such as cell type, chemistry, and the specific manufacturing process.

Design Measures – Avoid failures to occur or mitigate their severity…

Despite the best process and quality control that limit the defect cell rate to a minimum, one must expect a share of produced cells to have an internal defect. By clever cell design measures, however, failures from such defects can be avoided or their consequences at least mitigated.

Starting with the example of a conductive metal particle inside the cell, there are different locations where the particle can come to a rest and potentially cause an internal short-circuit. Three exemplary positions are depicted in Figure 24, one between anode coating and bare cathode current-collector foil (A), one between anode and cathode coating (B) and finally a particle connecting the outermost anode layer and the can of the lithium-ion cell.
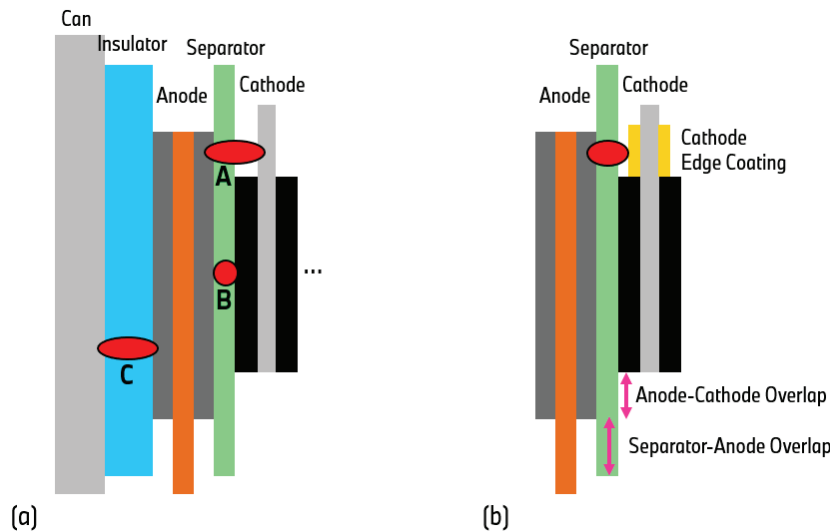
Figure 24: (a) Different exemplary particle positions A, B & C in a lithium-ion battery cell. (b) electrode assembly with cathode edge coating to protect against particles at location A. Indication of anode-cathode overlap and separator-anode overlap.

Of utmost importance are the insulating layers inside the battery cell. The choice of the separator concerning base material (PE, PP, PET, Polyamide, …), potential ceramic coating (thickness, single-side vs. double-side) and thickness resulting in a different mechanical and thermal robustness behavior, strongly impacts the likeliness of a particle pressing through it and creating a short-circuit. The size of the separator-anode overlap and anode-cathode overlap (see Figure 24(b)) strongly influences the possibility of a particle at the edge of the electrode assembly to create a short-circuit. By means of a potential cathode edge coating (from ceramic, polyamide, …) the criticality of a particle at position A can be mitigated (see Figure 24(b)). Particles at that location have the potential to create very low ohmic short-circuits as they connect the bare Al-foil with the anode without the significant ohmic resistance of the cathode coating. Particles at location C short-circuit the outermost anode with the housing of the lithium-ion battery. Depending on the cell format and choice of housing material, internal short-circuits of different criticality can occur. For a pouch-cell, the housing cannot support any severe short-circuit current as it is mostly insulating with only a very thin Al-layer within the composite film used as vapor and electrolyte barrier. For prismatic and cylindrical cells, the polarity of the housing (Aluminum → positive, Steel → negative) strongly influences the particles criticality as well as the ohmic resistance of the connection between housing and terminal. In many cases, a thicker and mechanically more stable insulator layer between can and electrode assembly can create an additional robustness-increase for these short-circuits not to develop.

Obviously, the choice of the cells active material also has an imminent impact on the severity of a potential particle short-circuit. Cathode materials with lower nickel content or lithium-iron phosphate have, for instance, a better thermal robustness. Latter cathode materials, due to their higher temperature stability, can impede a certain internal short-circuit to directly trigger an uncontrollable exothermal heat release in the form of a cell thermal runaway. More information on the choice of the cell active material from a safety perspective can be found in the next chapter.

In some cases, also cell design measures can help to protect the battery cell against failures from the outside. In case of an external short-circuit, a cell internal fuse, realized for example as section of limited cross-section within the Aluminum current-collector, can help to protect the cell from critical short-circuit currents. Another example is the so-called "overcharge safety device" or "current interruption device". In case of an overcharge of the battery cell, the electrolyte is decomposed and larger amounts of gas are released that lead to a cell-internal pressure build-up. The increased pressure is used to tear off or fuse the cell internal electric connection between cell terminal and electrode assembly. By this a further critical overcharge of the battery cell is supposed to be stopped.

Early Detection of Potentially Critical Cell Failures in the Field

No manufacturing process can be 100% perfect. Despite the above-described measures to develop a robust cell design and to avoid failures during production by means of process measures and quality surveillance, one must expect a certain failure rate during cell production. A "Gigafactory" with a production volume of 20 GWh producing for example 21700 cells with ~20Wh, has an output of 1 billion cells per year (enough for 250.000 cars with an 80kWh battery pack each). To have less than one defect car in a year's production, the defect cell rate of the Gigafactory would have to be below the extreme value of 0,001ppm. On top of all product and process quality optimizations, redundant safety measures should be installed to further reduce the risk even in case of single failures.

As described in the previous chapters, not every failure automatically initiates an immediate cell thermal runaway. Many defects will never lead to any safety issue, like for example a metal particle in the cell that is not big enough to penetrate through an isolation layer. Others will only cause weak damages that correspond more to quality defects than a safety relevant failure such as a metal particle creating a weak increased self-discharge without enough heat development to trigger the critical exothermal reactions causing a thermal runaway. Going even further, defects are possible with the potential to create for instance a safety relevant internal short-circuit bringing the cell into a thermal event after minutes to hours or even weeks of operation. If such a defect is slowly developing, there is a chance to detect it and even to react in the form of countermeasures to avoid the thermal event from happening. If we stay in the picture of the cell internal short-circuit created by a particle (simulated by a nail) in Figure 23(a) it took about 19min until the thermal event started. During that period, a sudden initial voltage-drop and voltage reduction due to internal discharge was detectable as well as an increase in cell temperature and a loss of charge (~8.5Wh). Via an advanced battery management system and appropriate safety functions, those signals can be used to detect the critical internal short-circuit caused by the particle already before the event. But it has to be clear that, depending on the failure characteristics and the sensor limitations, not each and every such endeavor can be successful. In case of multiple cells connected in parallel within the battery pack, voltage breakdown due to the internal short-circuit might be reduced and the lost charge visible in the balancing step at the end of a charging process will show less current as it will be small compared to the overall energy of the p-string and not as significant in comparison to balancing inequalities due to cell ageing effects. A temperature sensor on the other hand, might only be helpful to detect the unexpected temperature increase if it is close to the suspect cell.

Despite all these challenges, there is a good chance to sort out a number of critical failures and to initiate reaction mechanisms like a reduction of the maximum SoC ($\rightarrow$ cells with lower SoC are more thermally robust, see Figure 21), a reduction of the maximum charge- and discharge-power and/or an immediate driver warning requesting the customer to drive to the next garage for a check-up.

SAFETY LEVEL 2: CONTROLLED AND OPTIMIZED CELL THERMAL RUNAWAY BEHAVIOR

If, despite all above-described measures, a thermal runaway of a lithium-ion battery occurs, one leaves the first shell of the safety concept. The next layer targets to assure a controlled and optimized thermal runaway behavior, the high-voltage (HV) storage system can support and handle. This includes, among other things, a defined heat release, as well as a controlled gas & mass ejection via a burst membrane to increase the integrity of the cell housing and reduce the risk of ruptures or explosions.

Heat Release upon Thermal Runaway

The heat release upon thermal runaway is, together with the thermal robustness of the battery cell, one of the key-parameters to manage the risk of thermal propagation.

Table 5 shows results of autoclave calorimeter measurements of lithium-ion cells. These measurements allow the determination of the heat release as well as the mass- & gas-ejection characteristics of the battery cell upon thermal runaway.

Table 5: Measurement results of lithium-ion cells in an autoclave calorimeter for the characterization of heat release and mass- & gas-ejection. Comparison of the results for two types of cells with different capacity & energy density in the same cell housing.

Cell Format	Prismatic		Delta [%]
	Batch #1	Batch #2	Identical Cell Housing
Capacity [Ah]	51,0	68,5	
Energy [Wh]	186,7	250,5	→ +34%
Energy Density [Wh/kg]	207	251	→ +21%
Reaction Time [s]	17,4	15,0	→ -14%
Max. Pressure [bar]	1,85	1,88	similar
Gas Release [Liter] @25°C & 1bar	110	125	→ +14%
Cell Mass Loss [%]	47	47	similar
T_Max_Cell_Housing [°C]	433	795	→ +83%
T_Max_Venting [°C]	728	888	→ +22%
Q_tot [kJ]	850	1113	→ +31%

The results are shown for two batches of cells with different capacities but identical cell housings to illustrate the impact of a change in energy density on the thermal runaway behavior. The increase of total heat release Q_{tot} matches well with the increase of the total energy content of the cell from batch #1 to batch #2. At the same time, the increased cell energy density reduces the reaction time of the thermal event and increases the maximum temperature of the cell housing. In other words, the severity of a thermal event increases with energy content and energy density of the battery cell.

The gas release and the resulting pressure peak in the confined space of the autoclave show, however, a smaller impact of the capacity increase from batch #1 to batch #2. Latter could have its origin in the reduced electrolyte/active material ratio for larger capacity cells.

The active mass loss of 47%, defined as the share of mass of the active cell material (→ electrolyte wetted electrode assembly) that was ejected during the thermal event, is similar for both cell batches. By influencing the mass loss ratio via the cell design, the ejection of heat from the cell depending on the overall propagation safety concept can be influenced.

Besides a change in absolute cell size and energy density, another way to strongly impact the thermal runaway behavior and the exothermal heat release, lies in the choice of cell chemistry. In Figure 25, measurements of the specific heat power of different cathode chemistry are illustrated.
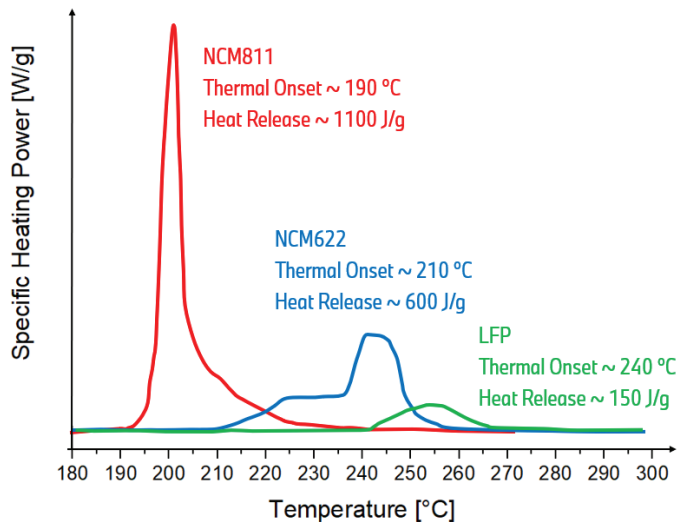
Figure 25: Exemplary differential scanning calorimetry measurements for different cathode chemistries. Specific heat power [W/g], onset of exothermal reactions and heat release [J/g].

In a first step, comparing the different NCM ($Li_xNi_{1-y-z}Co_yMn_zO_2$) variants, it appears that the safety criticality increases with Nickel ratio of the cathode active material. NCM811 (ratio of 8:1:1 of nickel, cobalt, and manganese) shows with 1088 J/g the largest specific heat release ΔH which corresponds to the area underneath the measured specific heat power curve. Also, the exothermal onset is the earliest at about 190 °C. The depicted NCM622 cathode shows with 572 J/g a much-reduced heat release and a higher onset temperature of about 210 °C. With an increase in the nickel content of the cathode, an increase in energy density and cost reductions may be achieved. However, the cells' thermal robustness will suffer, and more heat will be released during a thermal runaway.

Besides the NCM cathodes, also LFP (lithium iron phosphate) is shown in Figure 25. The LFP cathode shows with a specific heat release of 149 J/g and a high exothermal onset temperature of about 230°C the best safety performance, allows however only much reduced energy densities in comparison to NCM cells. The good safety behavior of LFP cells can also be seen in the autoclave calorimeter test results given in Table 6.

Table 6: Measurement results of lithium-ion cells in an autoclave calorimeter for the characterization of heat release and mass- & gas-ejection. Comparison between cells with NCM and LFP cathode chemistry.

Cell Format	Prismatic		Delta [%]
Cathode Chemistry	Ni-Rich NCM	LFP	
Capacity [Ah]	136,6	112,6	
Energy [Wh]	500	333	
Energy Density [Wh/kg]	247	167	➜ -32%
Reaction Time [s]	12,2	126,5	➜ +937%
Max. Pressure [bar]	5,7	0,58	➜ -90%
Gas-Release [Liter] @25°C & 1bar	289	50	
Gas-Release per Capacity [Liter/Ah] @25°C & 1bar	2,11	0,44	➜ -79%
Cell Mass Loss [%]	61	21	➜ -66%
T_Max_Cell_Housing [°C]	992	508	➜ -49%
Q_tot [kJ]	3211	1515	
Q_tot/Energy [kJ/Wh]	6,42	4,55	➜ -29%

The tests have been performed for two prismatic cells with capacities in roughly the same order of magnitude yet different cathode chemistries (Ni-rich NCM vs. LFP). The exothermal heat release per stored electric energy is reduced by about 30% for the LFP cell. Furthermore, cell housing temperatures are cut by about 50% upon thermal runaway. The cell reaction times are increased by one order of magnitude, which explains in combination with the smaller mass and gas release also the significantly lower resulting maximum pressure ($\rightarrow$ -90%) in the closed autoclave chamber upon thermal runaway. In conclusion, the LFP cell shows a much-improved safety performance. However, the achieved gravimetric energy density is reduced by more than 30%.

Finally, another exemplary approach to potentially safe battery cells, is the use of solid-state lithium cells. There are plenty of possible variants of this technology, however most of them have in common that the liquid electrolyte is fully (or at least to a large extend) replaced by a solid electrolyte. This promises improved safety behavior as the organic solvents of the electrolyte contribute strongly to the exothermal reactions of conventional lithium-ion cells. However, also new challenges must be tackled, like for example the safety behavior of metallic lithium anodes.

All in all, it becomes clear that the cell material choice strongly impacts the safety of a battery cell. However, tradeoffs with other cell characteristics as energy density, lifetime and several other parameters must be considered, as well. The safety measures will be different depending on the selection of the cell material. There is no such thing as a one-fits-all safety recommendation.

Integrity of Cell Housing

Another key factor for the overall safety behavior of a lithium ion cell is the thermal and mechanical stability of the cell housing during a thermal runaway ($\rightarrow$ cell housing integrity). On the one hand, the hydraulic diameter of the cell overpressure burst membrane has to be sufficiently large and possess an adequate opening pressure. On the other hand, the stability of the housing should be large enough to reduce the risk of a side-opening of the battery cell or even a rupture or explosion of the cell housing. A rupture or larger side-opening of the cell could cause a significant share of the venting material to be directed towards the neighbor cells and might lead to cell propagation. Furthermore, an explosion like behavior will result in a very large pressure peak within the HV battery storage system risking an undesired opening of the battery pack housing. In Figure 26, different examples for unwanted cell housing side-openings are depicted.
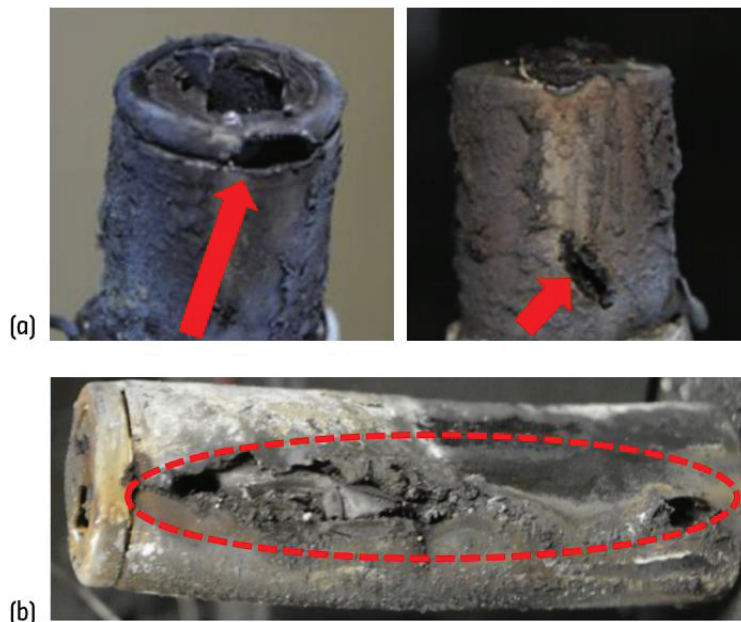

Figure 26: Experiment results to produce unwanted side-openings of 21700 battery cells. (a) Smaller openings due to thermal hot-spots on the cell housing and the internal pressure build-up during thermal runaway. (b) Side rupture of a 21700 cell with an opening over the whole length of the battery cell including strong deformation of the cell housing. Significant exhaust release over the side-opening can be expected. Pictures taken from [17]

For a robust design of the cell housing, the mechanical stress on the housing as well as its ultimate yield strength at the elevated temperature that can be expected during a thermal event need to be considered. In the case of a cylindrical cell, the tangential stress on the housing leading to a possible side-rupture, iscalled Hoop stress. It can be described by the equations in Figure 27.

Hoop Stress of Cylindrical Cell Can:

Tangential stress σ on cell housing

$$\sigma = \frac{P \cdot d}{2t}$$

Necessary housing thickness t to keep housing stability constant ($P/\sigma = const$)

$$t = \frac{P}{2\sigma} \cdot d \quad \Rightarrow \quad t \propto d$$
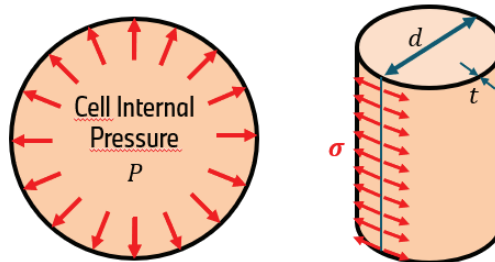
Figure 27: The Hoop stress correlation for a cylindrical cell housing gives the connection between can wall thickness and cell diameter.

In the case of a typical 21700 Ni-plated steel cell housing with a can thickness in the order of 300µm and a vent activation pressure of 28bar, the maximum hoop stress experienced by the cell housing is:

$$\sigma = \frac{P \cdot d}{2t} = \frac{28bar \cdot 21mm}{2 \cdot 300\mu m} = 98MPa \quad \text{Equation 1}$$

The ultimate yield strength of low carbon steel lies in the order of 400MPa at room temperature but decreases significantly with higher temperature. The exact steel alloy, the cell energy density (influencing the maximum housing temperature), the vent activation pressure and the can thickness should be selected in such way that the stress of 98MPa (including a safety buffer) will not be exceeded during the thermal event. For comparison, the ultimate yield strength of 1000 series Aluminum is with about 100MPa only about a quarter of the one of steel. In order to keep the same safety factor between maximum hoop stress and yield strength, an 21700 Aluminum housing would require a four times thicker housing.

SAFETY LEVEL 3: MITIGATION OF PROPAGATION

The entry point to "Safety Level 3: Mitigation of Propagation" is the thermal runaway of a battery cell within the battery pack. To better understand propagation, first, the mechanisms which can lead to the undesirable chain reaction are described. Afterwards, possible measures to mitigate propagation and to ensure passenger safety are presented.

From Cell Thermal Runaway to Propagation – Overview over the Main Mechanisms

Thermal Propagation is defined as the chain reaction which is triggered after a one Cell Thermal Runaway leads to a Thermal Runaway of another cell.
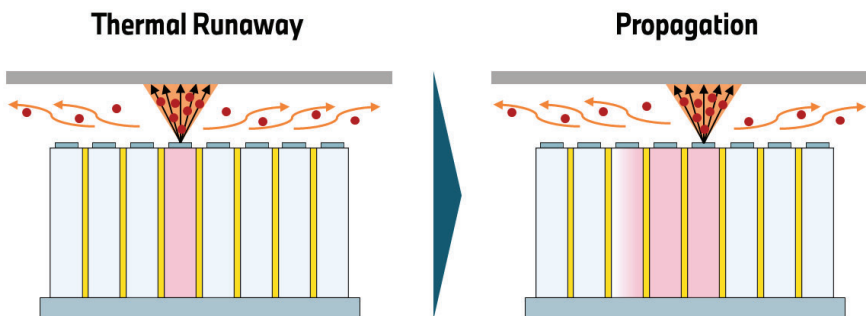

Figure 28: Definition of Thermal Propagation: A Cell Thermal Runaway leads to the Thermal Runaway of another cell.

During and after a cell thermal runaway, differently categorized disturbances are introduced into the battery pack with each having the potential to ultimately lead to Thermal Propagation: Beside the cell internal short circuit within the respective parallel circuit itself, heat diffusion to adjacent battery cells, the emission of hot venting gases, and the emission of electrically conductive particles play a major role.
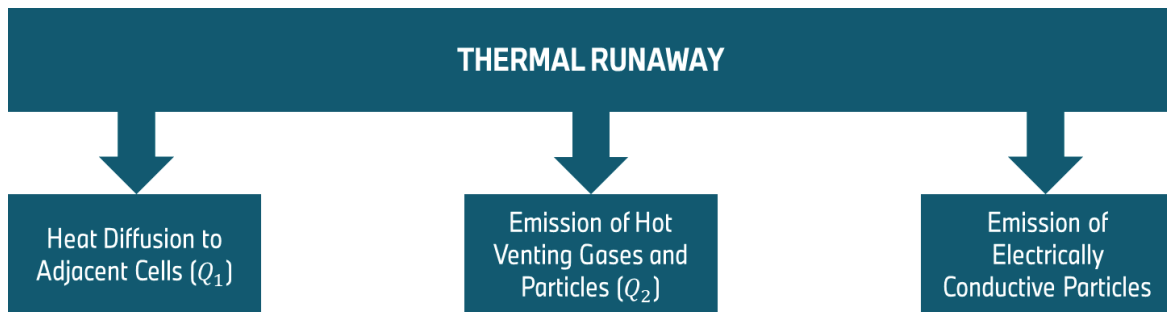

Figure 29: Mechanisms associated with a cell thermal runaway which can lead to Thermal Propagation.

Heat diffusion to adjacent cells (Q1): During and after a cell thermal runaway, the defective battery cell is a source of heat within the battery pack. Exemplarily, Figure 30 shows the temperature profile of a prismatic Li-Ion-Battery Cells during and after a Thermal Runaway in the autoclave test setup.
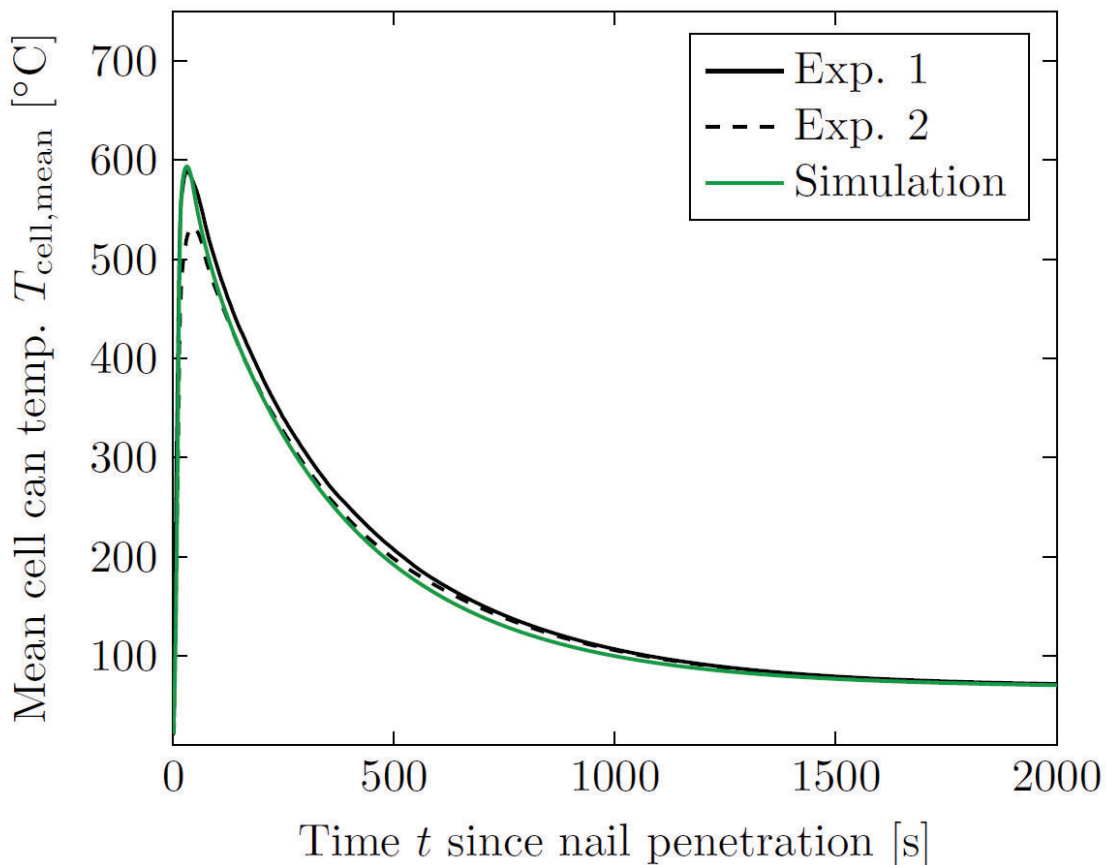
Figure 30: Can Temperature profile of a state-of-the-art 63,5Ah Lithium-Ion Battery Cell during and after a TR [18].

Depending on chemistry and format, battery cells in a Thermal Runaway can reach surface temperatures well above 500°C. Since commonly used insulation materials typically degrade at temperatures around 200°C, a Thermal Runaway holds the potential to lead to secondary short circuits due to degraded insulations.

Furthermore, the heat release also leads to rising temperatures in adjacent cells. As described in Cell Internal Root Causes, this rise in temperature leads to increased self-heating-rates of the cell, which further heat up the adjacent cell. If the cell temperature exceeds its critical value T_{crit}, the thermal runaway and conclusively Thermal Propagation is inevitable. To better understand this interaction, Equation 2 allows to calculate the heat input Q_{crit} necessary to trigger a Thermal Runaway:

$$Q_{crit} = V \cdot (\rho c_p)_{eff} \cdot (T_{crit} - T_{op}) \quad \textit{Equation 2}$$

In the above equation, V describes the outer cell volume, $(\rho c_p)_{eff}$ is defined as the cell's effective heat capacity and T_{op} is the operating temperature. Table 7 summarizes the assumed values for both prismatic and cylindrical cells.

Table 7: Estimation of possible heat intake before reaching the critical temperature T_{crit}.

	Prismatic	**Cylindrical**
Size	180 x 32 x 72,5 mm³	D46 x 95 mm
Volume V	417600 mm³	157881 mm³
$(\rho c_p)_{\text{eff}}$	2400 kJ/m³ K	
T_{crit}	150°C	
T_{op}	50°C	
Q_{crit}	100 kJ	38 kJ

As a result of the conducted calculations, a net heat intake in the order of 100 and 38kJ can lead to Thermal Propagation for prismatic and cylindrical cells, respectively. However, the emitted heat during a Thermal Runaway can be orders of magnitude higher. The design should aim for a possibly direct heat flow to mitigate Thermal Propagation. It should be noted that the calculation in Table 7 only serves as a rough estimation. The exact values naturally depend on various parameters, like the cell's self-heating-rate, and the temperature distribution within the cell. Furthermore, if a battery cell is heated locally above its critical temperature, significantly lower heat inputs can be sufficient to trigger a Cell Thermal Runaway (see Safety Level 1)

Emission of hot venting gases and particles: During a cell thermal runaway, the defective cell emits a hot gas- and particle stream with temperatures up to 1200°C. The rapid rise in both temperature and pressure imposes a high mechanical load on the battery cell and therefore carries the risk of an uncontrolled opening of its housing. Furthermore, the venting mass flow transfers heat to other battery cells through convection and the accumulation of hot particles. This mechanism further increases the net heat input in neighboring cells and can ultimately lead to propagation through the mechanics which are mentioned above. Other consequences include the ignition of surrounding components and cell-external short circuits through degradation of electrical isolations which themselves trigger propagation.

Emission of electrically conductive particles: Battery cells contain highly electrically conductive materials like copper and aluminum, which can be emitted during a Thermal Runaway. The high flow velocities cause a distribution of the conductive particles along their respective flow trajectories, with the risk of bridging air and creeping distances. Conclusively, the emission of electrically conductive particles can cause secondary short-circuits which impose an additional electrical load on other cells within the battery pack and potentially trigger Thermal Propagation. It should be noted, that due to the cell-external heat input, not only low-resistance short circuits and their corresponding high currents, but also long moderate short-circuit currents can potentially trigger propagation.

Measures to Mitigate Thermal Propagation

For the safety of vehicle occupants, to minimize damage, and to comply with all legal requirements, propagation mitigation is essential. In this chapter, measures to handle the hot venting gases, the thermal load on adjacent battery cells as well as measures to avoid secondary short circuits and functional reactions are presented. These categories represent four pillars to mitigate Thermal Propagation.
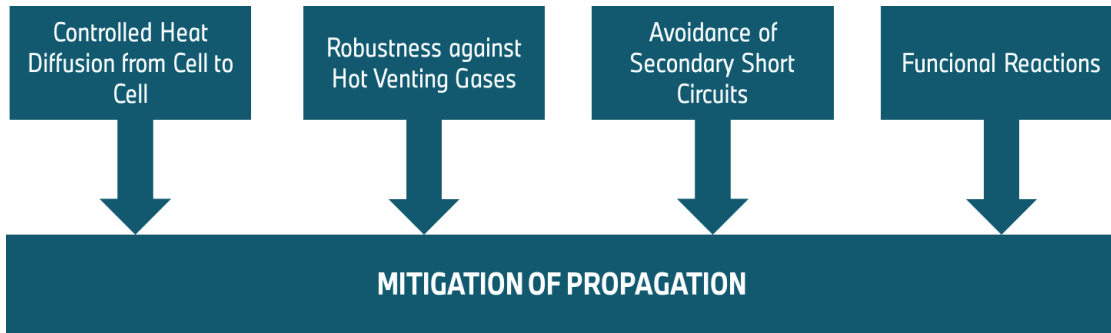
Controlled Heat Diffusion from Cell to Cell

Robustness against Hot Venting Gases

Avoidance of Secondary Short Circuits

Funcional Reactions

MITIGATION OF PROPAGATION

Figure 31: Four Pillars of Measures to Mitigate Propagation

Measures to control heat diffusion to neighboring cells: During and after a cell thermal runaway, the exothermal reactions within the cell lead to a rapid rise in temperature. Heat transfer to the neighboring cells, especially through heat conduction, can lead to critical temperatures in the neighboring cells which can ultimately trigger propagation. From this perspective, it seems obvious to thermally insulate each battery cell as good as possible. However, a sufficient insulation is difficult to obtain since battery packs require a good thermal connection to a cooler which conclusively thermally interconnects neighboring cells. Furthermore, a thicker insulation increases the package space and thus reduces the capacity of the full battery pack. Therefore, a rise in temperature of the neighboring cells cannot be fully prevented. As described in Cell Internal Root Causes, a rise in temperature above T_{ISH} also leads to an increased self-heating (ISH) rate of adjacent cells. If this additional heat input by a neighboring cell itself cannot be fully dissipated to its surrounding, temperature further increases up to the point where the critical temperature T_{crit} is reached. This rises a dilemma: On the one hand, a cell should be thermally insulated as good as possible to strongly limit heat diffusion to its neighboring cells. On the other hand, a good thermal connection between battery cells must be obtained to dissipate heat away from the cell. To further explain these mechanisms, heat diffusion during and after a Cell Thermal Runaway within a battery module of five Lithium-Ion prismatic cells was simulated for two scenarios utilizing the approach presented in [18]: a good ($R_{th} = 4 \cdot 10^{-6} \frac{W}{m^2K}$, scenario 1) and a bad thermal connection ($R_{th} = 0.023 \frac{W}{m^2K}$, scenario 2) between neighboring cells. Scenario 1 represents an ideal heat exchange between the cells. On the contrary, scenario 2 represents a good insulation of the cells; heat dissipation mainly takes place via the bottom-plate-cooler. Figure 32 and Figure 33 show the respective simulation setup and the calculated results, respectively.
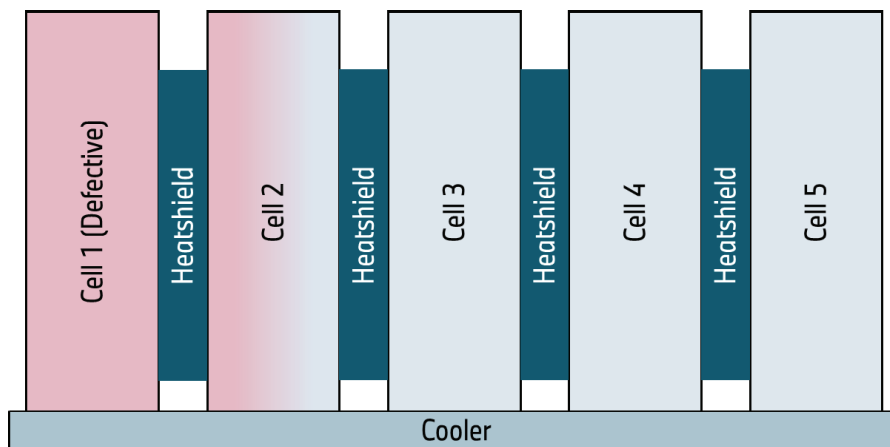

Figure 32: Model setup proposed by Hölle et al. for simulating propagation behavior within a battery pack [18].
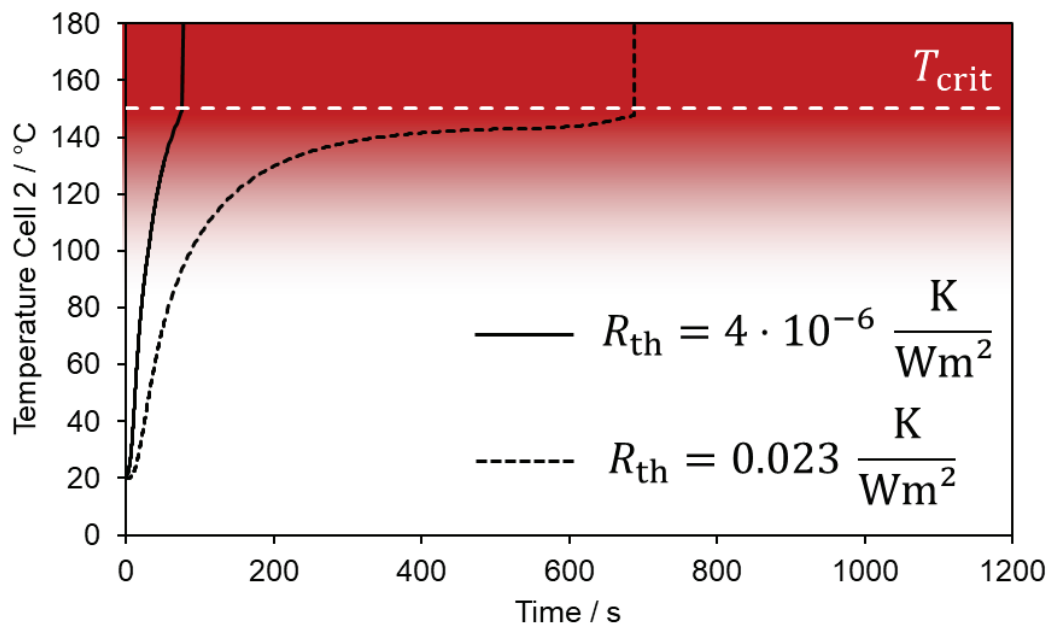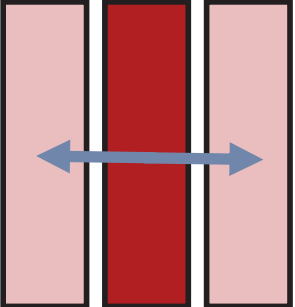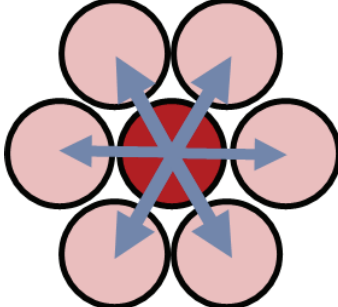
Figure 33: Difference between good and bad insulation. The red region indicates the temperature associated with an increased self-heating rate

Figure 33 shows the temperature of cell 2 adjacent to the TR cell over time. For scenario 1, after only 77 seconds, the average temperature of cell 2 overshoots its critical temperature, leading to another Thermal Runaway thus propagation. However, a good thermal insulation (scenario 2) cannot prevent propagation either. The slow heat input (mainly through the cooling plate) leads to a continuous heat-up of the adjacent cell 2. Once the temperature reaches the area of increased self-heating, the net heat-intake increases over several minutes, eventually heating cell 2 above T_{crit} and leading to a Thermal Runaway thus propagation. Battery manufactures therefore face an optimization problem which must take the following aspects into account:

- <u>Number of nearest neighbor-cells</u>: In this context, a nearest neighbor is defined as a battery cell which is directly thermally connected to the defective cell. To limit the temperature rise of adjacent cells to its minimum, it is crucial to distribute Q_1 as homogenously as possible and thus provide as many nearest neighbors as possible. The number of nearest neighbors strongly depends on the cell format.

Table 8: Cell format and resulting max. numbers of nearest neighbor Cells

Prismatic Cells. Max. Number of Neighbor Cells: 2	Cylindrical Cells. Max. Number of Neighbor Cells: 6
Min Number of Nearest Neighbors Cells: 1	Min Number of Neighbor Cells: 2
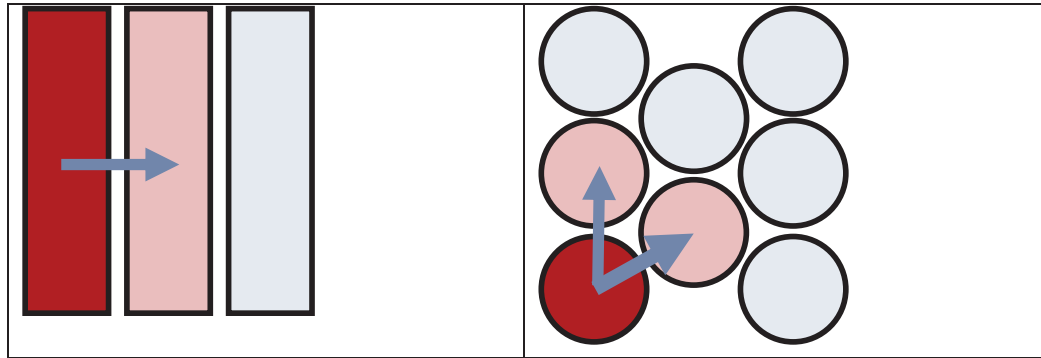
- Thermal connection of neighboring cells. The thermal resistance R_{th} between two cells can be expressed by $R_{th} = \frac{t}{\lambda A}$ where t defines the distance between two neighboring cells, λ is defined as the effective thermal conductivity and A describes the area available for heat transfer. Since today's main goal of battery development is to reach high energy densities, the distance t between two neighboring cells is typically chosen to be as small as possible. Furthermore, the area A mainly depends on cell format and cell arrangement and is also typically constrained by packaging requirements. Therefore, the thermal resistance between cells is typically manipulated through λ by choosing different materials. Since prismatic cells are typically interconnected by their larger side area, heat exchange must be inhibited: In mass produced batteries for automotive use, this inhibition is achieved by heatshields with a comparably low thermal conductivity. For cylindrical cells, however, due to their curved surface and comparably small useable area, it can be preferable to interconnect the cells through higher-conductive materials like aluminum. It should be noted that the thermal behavior also depends on the cells' surrounding like the thermal connection to a cooling plate.
- Thermal coupling of other heat capacities: Heat capacities can smoothen temperature peaks. It can be therefore beneficial to thermally connect the battery cells to surrounding heat capacities or to introduce extra heat capacities into the system.

Measures to Increase Robustness against Hot Venting Gases: As mentioned before, a Cell Thermal Runaway leads to a rapid emission of venting gases with temperatures up to 1200°C. To mitigate propagation, the energy storage needs to implement measures to discharge these venting gases in a well-controlled manner. Energy storages are therefore typically equipped with dedicated degassing units. Degassing units are designed to represent predetermined breaking points in the housing of the energy storage which open a flow cross-section after the pressure within the battery overshoots a certain threshold. After activation, the pressure within the energy storage drops immediately and an uncontrolled opening of the housing can be prevented. Nevertheless, the battery housing must be designed to withstand a certain over-pressure. Once the degassing unit has opened, the hot venting gases and abrasive particles flow from the defective cell to the newly created opening. Highly turbulent flows of high velocity and therefore high heat transfer coefficients are to be expected. Battery packs therefore often use sheet-silicate-materials, also known as Mica shields, to protect the housing from a direct impact of hot and abrasive venting gases to prevent penetration. To prevent ignition of secondary fires, only non-flammable materials should be used within the expected flow path. If flammable materials cannot be fully avoided, it might be possible to use the inerting behavior of the venting gases. Furthermore, heat-proof materials like Mica can be used to protect critical components which cannot be localized outside the venting flow.

Measures to avoid short circuits: During a Thermal Runaway, the battery cell not only emits hot venting gases but also electrically conductive particles, for example, copper and aluminum. To avoid secondary short circuits, potential-carrying components, like battery cells, busbars, and high-voltage connections should not be exposed to the venting flow. If package design permits, it can therefore be beneficial to provide dedicated venting channels connecting the cell vents to the degassing unit of the battery pack. Ideally, these venting channels do not lead the gas- and particle flow past potential-carrying surfaces. However, due to packaging-restrictions a full separation of functions is not always suitable. If exposure of potential-carrying components to the venting flow is not fully avoidable, short-circuits can be efficiently prevented by using temperature-resistant isolations. Due

to the high temperatures during Cell Thermal Runaway modern battery therefore use isolations made of Mica or polyurethan-based foams which keep their isolating properties even at high temperatures.

Functional Measures: To effectively warn and therefore protect car occupants, a cell thermal runaway must be detected. Common concepts involve the detection of a rapid rise in pressure and temperature as well as abnormal behavior of electrical cell parameters like voltage or current. Eventually, engine power can be either restricted or deactivated to prevent additional heat input from ohmic heating. Furthermore, it can be beneficial to activate cooling to dissipate heat from the Cell Thermal Runaway. To illustrate the effect of "emergency cooling", a propagation simulation was conducted with and without the cooler being a heat sink. The temperature of the cooling fluid was set to 60°C. Figure 34 shows the resulting temperatures of the battery cell next to a Thermal Runaway.
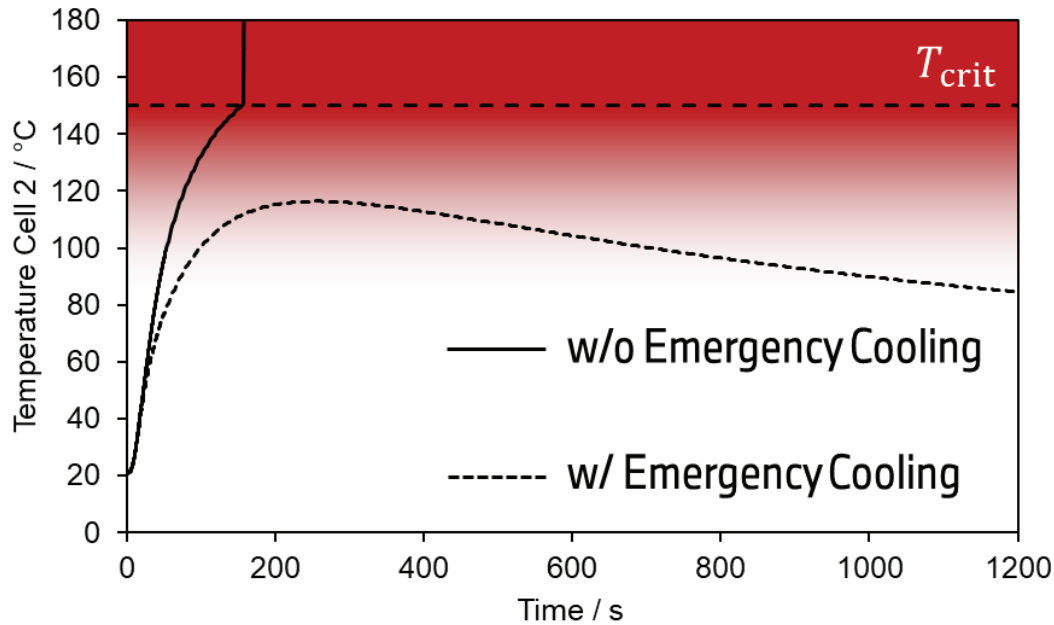

Figure 34: Temperature of the neighboring cell over time with and without "emergency-cooling".

The simulation results indicate a strong influence of the emergency cooling on the temperature of the adjacent cell. Under the chosen boundary conditions, the activation of emergency cooling increases the robustness to a level, where propagation through heat transfer can be fully prevented.

SAFETY LEVEL 4: CONTROLLED AND OPTIMIZED VEHICLE BEHAVIOR

For as long as the risk for thermal propagation cannot be fully eliminated, risk mitigation measures on vehicle level should be installed to further improve overall safety. Those measures aim at enlarging the time span between the warning of passengers, pedestrians or fire fighters and the point where the vehicle gets into a safety critical state.

Warning concept

Directly after detecting a cell thermal runaway, car occupants should be informed and urged to leave the vehicle as fast as possible. Engine power can be taken away to ensure that the warning is not dismissed by the passengers. The surrounding of the vehicle can be informed by activation of warning lights or horn. The automatic emergency call can be started with a specific note for the rescue coordination center indicating a critical status of the vehicle battery.

Protection of passenger compartment

The passenger compartment should be kept free of cell gases and smoke as well as extensive heat input for as long as possible. To achieve this, degassing units of the battery pack should be placed in a way that allows an unhindered flow away from the cabin and the exit area of the passengers. A direct flow towards the ground is preferred. Furthermore, flammable components should not be placed close to hot venting gases to prevent

secondary fires. Guide plates or profiles can be used if the degassing units cannot be placed at the bottom of the battery pack where they risk of being hit and damaged by obstacles while driving. The cabin should be by and large leak tight and temperature tolerant, especially in proximity to the gas flow. Active measures to obtain safer conditions in the cabin are a shut off of the ventilation and closing of windows upon the warning signal from the battery.

CONCLUSION

Electric Vehicle technology eliminates some of the safety concerns of conventional vehicles powered by internal combustion engines (ICE) like gasoline leakage or fuel tank bursts as a consequence of e.g. a severe vehicle crash. Yet it brings its own specific safety relevant concerns for example due to the high voltage system with 400 V or more, its energy density or a potential vulnerability of the batteries.

Safety requirements for EVs should consider the differences between the two. The selection of appropriate crash load cases for conventional ICE vehicles strives for a deformation characteristic, which allows for good restraint system performance on the one hand and a sufficient fuel system integrity to reduce the risk of car fires on the other. Some of the standard crash load cases are therefore defined to damage sensitive areas where there is a risk to penetrate fuel system components and the integrity of the fuel system is demanded. In the case of electric vehicles, the potentially critical areas may be at different locations, the possible measures to protect electric components is different to the protection of e.g. fuel pipes and specific crash tests are required to assure a comparable level of safety for these vehicles. (Plug-In) hybrid vehicles are a mix of both worlds: the safety engineers task is to protect both the gasoline as well as the electric components.

Another example is the difference in the effort necessary to de-energize the two vehicle variants: for an ICE vehicle it is sufficient to reliably empty the gasoline tank and the subsequent gas hoses from flammable liquids and vapor. In practice it is much more difficult to de-energize an electric battery on the road or in a repair shop. A clear guideline is necessary for service technicians, rescue teams, recycling mechanics or even a normal user to ensure a safe enough operation and handling of this system in every situation. Crash laboratories often handle early prototypes or other pre-production vehicles with high voltage components or systems. Also here, safety is an important aspect for everyone working in this area and specific processes and tools are used to keep a high level of safety.

With the continuous strive for higher energy densities, thermal proliferation after a malfunction cannot be fully prevented, in every case. To reach a sufficient level of passenger safety, engineers face the challenge to handle this safety threat and to at least delay the ignition of other battery cells within the pack, which is commonly referred to as thermal propagation. This Whitepaper offers a variety of measures from cell level over pack level to vehicle level to avoid or at least further mitigate such propagation.

DISCLAIMER

The exemplary solutions, described in this paper in most cases are not meant to be demanding obligations. The main intention of this publication is to demonstrate ways to improve the safety of electric vehicles. When solutions are presented, they are meant to be examples of good practice, recommendations or good engineering judgements. It well may be that the desired improvement can be achieved by alternative measures or processes. This publication shall provide possible options to achieve a higher degree of safety and the authors fully accept that alternatives exist, that might fulfil the same target.

REFERENCES

[1]   IIHS. [Online]. Available: https://www.iihs.org/news/detail/with-more-electric-vehicles-comes-more-proof-of-safety.

[2]   IIHS. [Online]. Available: https://www.iihs.org/media/ca2618fc-c875-4246-8a9f-5977f3b702f6/Ewxm_A/HLDI%20Research/Bulletins/hldi_bulletin_37-25.pdf.

[3]   J. e. al, „Sicherheit ist keine Frage des Antriebs,“ in *13. VDI-Tagung Fahrzeugsicherheit*, Berlin, 2022.

[4]   „NTSB Safety Report NTSB/SR-20/01 PB2020-101011,“ Safety risks to emergency responders from lithium-ion battery fires in electric vehicles, 2020.

[5]   UN/ECE. [Online]. Available: https://unece.org/transport/documents/2022/04/working-documents/grsp-proposal-02-series-amendments-un-regulation-no.

[6]   CARHS. [Online]. Available: https://www.carhs.de/de/companion-poster/product/safetycompanion-2022-pdf-download.html.

[7]   Argonne. [Online]. Available: https://publications.anl.gov/anlpubs/2021/06/167626.pdf .

[8]   „FMVSS 305 regulations," [Online]. Available: https://www.federalregister.gov/documents/2015/01/16/2015-00423/federal-motor-vehicle-safety-standards-electric-powered-vehicles-electrolyte-spillage-and-electrical..

[9]   „UN ECE R95," [Online]. Available: https://www.unece.org/fileadmin/DAM/trans/main/wp29/wp29regs/r095r1e.pdf.

[10] „Euro NCAP. Testing off electric vehicles, technical bulletin Nov. 2010," [Online]. Available: https://www.euroncap.com/en/for-engineers/supporting-information/.

[11] „UNECE R94," [Online]. Available: http://www.unece.org/fileadmin/DAM/trans/doc/2009/wp29grsp/ELSAsg-1-04e.pdf.

[12] „Mercedes-Benz, C-Class Model 205 sedan, 2014 – 2018," [Online]. Available: https://rk.mb-qr.com/en/205.14/.

[13] S. Hoelle, S. Scharner, S. Asanin und O. Hinrichsen, „Analysis on Thermal Runaway Behavior of Prismatic Lithium-Ion Batteries with Autoclave Calorimetry," *Journal of The Electrochemical Society,* pp. 168(12), 120515, 2021.

[14] [Online]. Available: https://www.autoinsuranceez.com/gas-vs-electric-car-fires/. [Zugriff am 12 2022].

[15] [Online]. Available: https://www.adac.de/rund-ums-fahrzeug/elektromobilitaet/info/sicherheit-elektroauto/. [Zugriff am 12 2022].

[16] P. Sun und R. Niu, „A review of battery fires in electric vehicles.," *Fire technology,* pp. 56(4), 1361-1410, 2020.

[17] E. Darcy, „Safety Benefits of the 18650 Bottom Vent for Future Space Battery Operations," *The Battery Conference (No. JSC-CN-37392) ,* p. https://ntrs.nasa.gov/archive/nasa/casi.ntrs.nasa.gov/20160011169.pdf, 2016.

[18] S. Hoelle, S. Zimmermann und O. Hinrichsen, „3D Thermal Simulation of Thermal Runaway Propagation in Lithium-Ion Battery Cell Stack – Comparison of Modeling Approaches," *Submitted in Journal of The Electrochemical Society,* 2023.

[19] S. Hoelle, F. Dengler, S. Zimmermann und O. Hinrichsen, „3D Thermal Simulation of Lithium-Ion Battery Thermal Runaway in Autoclave Calorimetry - Development and Comparison of Modeling Approaches.," *Accepted in Journal of The Electrochemical Society,* 2023.

PREDICTIVE SAFETY: TOWARDS HOLISTIC TOP-DOWN SYSTEMS ENGINEERING FOR PRE-CRASH SYSTEMS

Philipp Straßburger, Bernhard Grotz, Stefan Heiß, Bruno Arbter, Kilian Hachmann, Jürgen Metzger, Nenad Ocelić
ZF Group
Germany

ABSTRACT

Since the first equipment of vehicles with environmental sensors for driver assistance systems more than 20 years ago, engineers are working on employing this data to improve or enable the activation of existing or envisioned passive safety systems. This task is motivated by potential benefits in occupant safety. In particular by an increased robustness of activation logic or by innovative actuators which promise to enable more degrees of freedom for new vehicle interior designs and the positioning of occupants. New regulations for ADAS functionalities lead to high equipment rates with environmental sensors which can foster the integration of active and passive safety technologies. Signals with an appropriate quality can be used smart to improve occupant safety in holistic safety strategies combining active and passive safety systems still offers big potentials (see e.g., ref. [1]). In this paper we aim to detail challenges in the multidisciplinary field of "Pre-Crash", the field of using environmental sensing to improve occupant safety. This requires considering the whole functional chain: sensor – perception – prediction - function logic - actuator, and further system properties like functional safety (including SOTIF topics) or validation strategies. As an example, throughout this paper, we will use a new functionality of a reversible pretensioner to reposition a forward leaned occupant by seatbelt retraction, called Active Occupant Repositioning. By getting into details, the complexity and mutual influences becomes apparent. Discontinuous relationships and dependencies on scenario details exist. The challenge is to divide the problem into manageable tasks. To get a clear understanding and a basis for communication we classify Pre-Crash systems in different base architectures and elaborated principal differences to assess the suitable next step for Pre-Crash system development. Methodologies are reflected to develop Pre-Crash systems, and strategies are derived to adjust the variety of dependent system parameters. Therefore, properties of an electromechanical actuator are analyzed to come towards a holistic Pre-Crash system development.

HOLISTIC SAFETY STRATEGY COMBINING PASSIVE AND ACTIVE SAFETY

Passive safety, active safety, regulations, safety education, safer infrastructure among other disciplines did and will contribute to road safety. In Germany, the traffic fatalities have been reduced to 1/10 in the last 50 years although three times more motorized vehicles take part in traffic nowadays. Due to innovations, stricter regulations and a change in awareness, accidentology does not show these statistically noticeable accident use cases any more. With accident reconstructions specialists are able to analyze details on how accidents could have occurred. But complete details of the situation in the interior are highly complex to reconstruct. Preparing an occupant to be best protected and get the best performance out of the restraint system is reasonable but statistically benefits are still hard to prove with statistics from accident database. Reacting before an accident comes with a lot of other challenges.
Different studies show tremendous potential to reduce the injury risks for the driver using adaptive restraint systems in real world accident scenarios assuming it can e.g., be adapted to specific relative velocity and occupant position (by e.g. 20% to 50% [2]).
Since July 6th 2022 all new developed vehicles in Europe have to be equipped with advanced driver assisted systems. From 2024 all new registered vehicles in Europe have these additional systems. These regulations lead necessarily to a 100% equipment rate for new vehicles with environmental sensors. This opens up potential for a quick market penetration using standardized sensor sets for new functionalities.

CHALLENGES FOR PRE-CRASH

When a crash is unavoidable the gal is to protect the vehicle occupants, to mitigate the crash consequences. We define Pre-Crash systems as systems which use the information of environmental sensors before a crash to improve the occupant protection system performance. State of the art pulse-based or in-crash decision logics measure the mechanical impact and derive the decision logic for an actuator (Figure 1, pulse and pressure). The information which is collected with environmental sensors can be used with different strategies to improve occupant safety. Basic additional elements of a Pre-Crash systems are a perception and a prediction module. A perception is combining the sensor information to interpret the environment and abstract it in a model. A prediction is necessary to be able to react before something is happening or to offset latencies, depending on the application the information

is used for. With Pre-Crash systems the goal is to develop occupant safety beyond the standard load cases which leads to challenges in different fields when compared to pulse-based systems. We are working on fundamental critical challenges to enable system development

- to make the systems objectively assessable,
- to derive complete requirements,
- to develop methodologies to handle multiple result influencing parameters with complex interdependencies and uncertainties and
- to enter new ground in functional safety depending on the system parameters.

These fundamentals are further described in the following subchapters.

State-of-the-art pulse-based

Mechanical Impact → Sensing of Crash Pulse → Pulse Based Decision → Actuator activation

Pre-Crash

(detectable) Environment → Sensing → Perception → Prediction
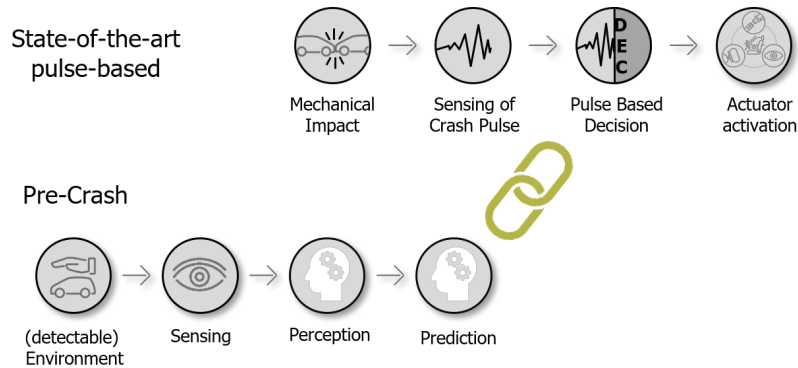
Figure 1 Basic understanding of Pre-Crash compared to state-of-the-art pulse-based decisions

Performance Assessment

The performance assessment of state-of-the-art passive safety systems only takes in-crash decisions in defined standard-load cases into account (pulse or intrusion based). To develop robust triggering algorithms a combination of fire, no-fire and so-called misuse events was established and further developed over decades with field experience. Misuse events in the field of deployment algorithms is an expression for test cases which are used to prevent unintended firing due to misinterpretation of the accelerometer-based decision. Examples are situations which result in a high acceleration peak at the beginning of pulse but do not justify a triggering signal like curbstone override or shopping cart impacts. Environmental sensing enables a safety strategy prior to an imminent collision. As the situation before the crash is not taken into account yet in legal or consumer rating test strategies, not only the system, but also the effectiveness assessment and the proof of concept has to be developed. The potential to improve vehicle safety with information gathered with environmental sensors is also in focus of consumer rating organizations. First not yet specified incentives for Pre-Crash systems are planned in the Euro NCAP Roadmap 2030 for the year 2026.

Requirement elicitation

To derive requirements for occupant safety beyond the standard load cases is a basic challenge. The relevant field of action and respective measures of effectiveness (MOEs) have to be defined. Fields of action can be defined differently, from broad and comprehensive improving restraint performance in the field to very specific improving occupant safety in defined load cases. Also, the MOEs vary from improving occupant safety for the average driver, increasing robustness to addressing specific groups like elderly driver (an example from the Euro NCAP Roadmap 2030 Milestone M7: Senior protection: low severity testing with sled). The existing standard load cases are developed for conventional in-crash systems. Pre-Crash signals are not allowed in the specification of these standard load cases and cannot be taken into account. The Pre-Crash maneuver or Pre-Crash situation e.g., influencing the occupant's position are not taken into account because the real benefits cannot be shown in the existing standard load cases. In addition, acceptance criteria for unnecessary or unintended activations are crucial aspects to be developed as well.

Enhanced system design complexity

As described conventional pulse-based decision logic, calibration and validation tests were developed and optimized over several decades. The multiple effects which can reduce the quality or level of information of environmental sensors exceed the number of cases for conventional impact pulse measuring. For existing pulse-based decisions, the pulse evolvement during the impact is not completely known at the time of an activation decision, nevertheless due to established calibration methods the severity of the impact can be judged robustly. In comparison, limits, tolerances and uncertainties for environmental sensors are numerous and the risks of misinterpretations are higher and have to be taken into account for a holistic system development. In addition, some object parameters which are necessary for crash severity estimations like e.g., mass, stiffness or fixation cannot

directly be measured and have to be estimated in advance (e.g., with object classification and corresponding accuracy). To react early enough before an impact and to compensate latencies, the vehicles trajectory and the possible bullet trajectory have to be predicted with an accuracy which is limited as any given situation can result in different impact constellations or even near misses.

Safety assessment methodology
If missed/delayed activation or unintended activation are rated "safety relevant" in terms of functional safety, a property which depends on the specific action and further actuator characteristics of the specific system, these limitations must also be regarded in the context of product safety. The well-known standard ISO 26262 addresses failures inside the (electrical control) system and will not handle performance limitations. The new standard 21448 for "safety of the intended function (SOTIF)" focuses on such safety issues which arise from "situational awareness, derived from complex sensors and processing algorithms". The application of this standard to Pre-Crash brings some further challenges. The standard was originally developed for ADAS/AD systems which take over a dynamic driving task. In its current state, SOTIF aligned to a limitation of the Operational Design Domain (ODD). The standard and specifically the idea of an ODD must be adapted for systems mitigating crash consequences. The SOTIF standard requires a full scope description of the intended function. Currently, crash mitigation systems are defined by reference load cases representing statistically relevant scenarios and describing minimal requirements extended with specific OEM requirements. A full scope specification presents unchartered waters for the field of occupant protection. Direct acceptance criteria are not defined in the SOTIF standard but must be derived with basic principles like GAMAP (Globalement Au Moins Aussi Bon), ALARP (As Low As Reasonably Practicable) or MEM (Minimum Endogenous Mortality) which are challenging to apply and break down to specific performance goals.

STRATEGIC NEXT STEP PRE-CRASH SYSTEMS

To structure the variety of possible Pre-Crash systems, we define three main base architectures (Figure 2). With "Assisted Systems", we describe systems which use the information of the environmental sensors as additional input for the decision logic to optimize in-crash activation times (after the first contact) or activation logic robustness. The weighting of the perception inputs vs. the pulse thresholds, in other words the responsibility of the perception signals can be used in a wide range. "Add-On systems" have two separated decision paths, one relying exclusively on the signals of the environmental perception with a second 'state of the art' decision path relying on conventional crash pulses as a fallback option. This architecture allows for systems with a reduced field of action comparable to an ODD for ADAS/AD systems when focusing on true positives. In the third base architecture, the decision path solely relies on environmental sensors to activate before the first contact and is "fully responsible" for any activation of the restraint system.

Most common in the market are Add-on systems with actuators bringing minimum risk of harm if activated inadvertent and bringing benefits within their limits. To minimize risks, velocities and forces of actuators are limited and the actuation like chassis lifting to improve compatibility of vehicle structures are limited to defined velocities.

ZF has already Pre-Crash assisted systems in serial production. In so-called truck underride scenarios, when the front energy absorbing structure is not in direct contact with the crash opponent, the accelerometers mounted in the front crumple zone may measure reduced deceleration levels in the early impact phase as compared to typical car-to-car crashes, introducing trade-offs in restraint deployment performance. This is a principal problem of poor crash compatibility with impact-sensing accelerometers, which can be improved by an assisted system. To recover more optimized restraint system performance, information from the environmental sensing technology is used to assist in the contact-based crash detection judgment, thereby improving deployment timing and reliability in underride impacts, while maintaining robustness in all other scenarios.

Similar strategies are being employed to assist pedestrian impact judgement in Vulnerable Road User Hood Lifter systems, to improve performance in the challenging uses cases specific to these systems. These are among the first steps being taken to integrate pre-crash sensing information into state-of-the-art restraint control systems, to further improve the safety value provided for occupants and pedestrians. ZF continues to evaluate further Pre-Crash assisted solutions across the operational domain of traditional contact-based restraint control systems, as well as for Fuel / Battery Cut Off and Emergency Call functions.

To further develop assisted systems, market entry and penetration is important to follow an evolutionary development strategy. The reasonable evolutionary next step to tackle challenges of decisions relying solely on environmental sensors is the transition to Pre-Crash actuators with fallback or also called add-on architecture. If the actuator is non-safety-relevant for unintended firing, the requirements from product safety during the development process of add-on functions are comparably low. One serial product out of this category is the ZF Active Controlled Retractor with the ability to reversible retract the seatbelt independent of the pyrotechnical activation. Its actuation is, e.g., based on vehicle dynamics information during a pre-crash phase, which has a high signal reliability.

But once an add-on function is potentially safety-relevant an adjusted development methodology is required. There it is essential to understand the parameters influencing the safety relevance and to understand the benefits and disadvantages when crossing this border in detail. To reduce complexity and to go step by step, the actuation should be flexible in timing. The actuation triggering time should be flexible in timing as well as in duration, in time of effectiveness of the actuator. In this paper we will further use a new add-on function for active controlled retractors: the Active Occupant Repositioning is a function that brings an occupant into a nominal position before an imminent collision. With the possibility to adapt force limits, define force progression and hold forces the flexibility is given to take this as an example. Details on the relevant parameters for appropriate next Pre-Crash system properties and an analyze of the pretensioner function system concept will be presented in the following.

Understand influencing parameters and effects on threshold for functional safety relevant actuation
For safety critical actuators, the requirements for the functional chain from sensing to decision logic changes. Depending on risk of harm or distracting a driver in case of a "false positive", the requirements differ compared to state-of-the-art systems like e.g., AEB. As described in SOTIF Annex C with the example of an AEB, the risk for this system to end in a hazardous event after a false positive is reduced due to the dependency of the following traffic usually keeping enough distance, and if not, it does not necessarily end in a hazardous event. If missed/delayed activation or unintended activation are rated "not safety relevant" clear testable requirements have to be derived from user acceptance criteria to be able to balance performance versus false positive rate. If a safety relevant actuation is necessary to fulfill the overall goals, then the decision is made to break new ground in several disciplines like safety, validation and beforehand requirements elicitation in a balanced development process which we describe in the next chapter.

Depending on the system requirements and the corresponding safety relevance the Pre-Crash base architecture is defined (Figure 2). There are categorical differences in these architectures with different advantages and disadvantages. As described, depending on the necessary responsibility of the perception in an assisted system also the safeguarding efforts can vary in a wide corresponding range. In an Add-On architecture, safeguarding intended activation is not necessary, because errors can be compensated by a fallback (described in the next chapter). If safeguarding unintended firing gets relevant depends on the actuator. If an actuator is rated safety relevant, a defensive decision strategy is obligatory and reduces the triggered scenarios and thus the true positive rate. For fully responsible systems safety requirements for unintended activation and intended activation exist per definition and errors in crash prediction are difficult to compensate. The parameters influencing the safety rating have to be analyzed and understood in detail and the effects on the development process and the function below and above the safety thresholds need to be known to prepare a basis for strategic decisions.
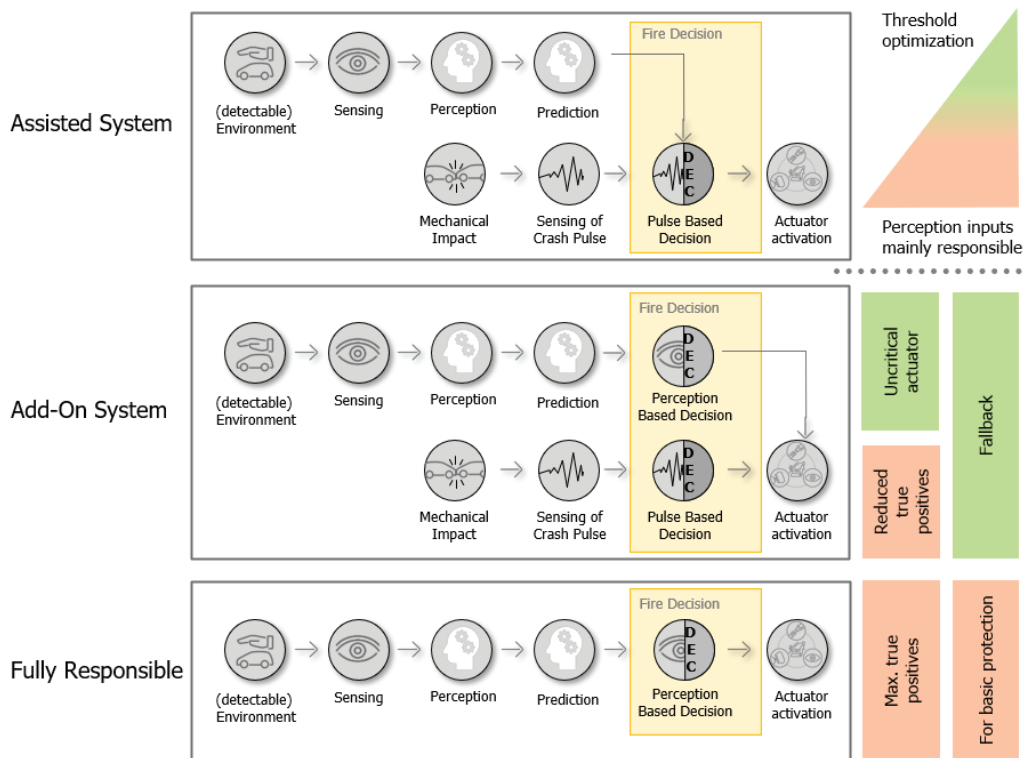

Figure 2 Pre-Crash base architectures and their categorical safety rating

Why with fallback / add-on architecture?

Pre-Crash with fallback means a system guaranteeing a basic occupant safety level even if the activation is not triggered by the Pre-Crash detection. The fallback solution can be realized with different concepts. Possible solutions are triggering a time flexible actuator with a pulse-based system if the Pre-Crash signal was not detected or triggering a different actuator with the fallback path. A special exception is guaranteeing enough basic protection (e.g. defined by legislation) without triggering a function, e.g. by the vehicle structure and interior. An occupant safety system without a fallback would end in a Pre-Crash system with the highest complexity, the fully responsible architecture (Figure 2). The challenge would be to achieve the system goals while handling the tolerances of sensing, perception and prediction while fulfilling the safety requirements.

When looking at the Active Occupant Repositioning there are no minimal safety requirements based on e.g., legislation which must be fulfilled even without a Pre-Crash detection, so no fallback for this function is necessary. On the other hand, when adding a strong electromechanical pretensioner to a belt system, the idea is obvious to try to replace the functions solved with the pyrotechnical pretensioner. This replacement leads to the requirement to ensure the same safety level in any situation, which would get challenging to prove in open world context (any scenario which can be imagined out there). Furthermore, depending on vehicle the benefits of the pyrotechnical pretensioner are necessary for legally required load cases where Pre-Crash information cannot be used nowadays, leading to further unknown requirements and validation specification until regulations are adapted.

Why an actuation that is flexible in time?

Environmental sensors are subject to tolerances and uncertainties. Prediction adds additional variations to triggering times. Some passive safety elements, for example front airbags are time critical and therefore difficult for Pre-Crash activation. They are optimized to be positioned very fast in a relevant severe impact and vents help to reduce the maximal load in the contact with the occupant to decelerate the occupant as soft as possible. That means, if an airbag is triggered too early it cannot support the occupant protection optimal. Exact triggering times are critical. Therefore, we selected the electromechanical belt pretensioner as a Pre-Crash actuator which has a higher tolerance for triggering times compared to airbag systems to further investigate principles of Pre-Crash systems. The force can be applied for a long period, disregarding dynamic effects like elevations inertias in the pretensioning system. And the belt system can be equipped with fallback solutions for basic safety requirements. Due to this flexibility and adjustability this actuator was chosen to analyze the effectiveness and the benefit with different operating strategies.

To be able to handle the development of complex systems with interdependencies between multiple domains different methodologies were analyzed according to their suitability for Pre-Crash development. Methods to include safety already in an early stage of development were applied [3]. The tailored approach based on fundamentals of systems engineering will be shown and outcomes described in the following.

MIDDLE-OUT METHODOLOGY TO DEVELOP AFFORDABLE AND EFFICIENT PRE-CRASH SYSTEM

Development of complex Pre-Crash Systems must be supported by a systems engineering process. Basis for clear top-down systems engineering are detailed system requirements which can be derived from use cases. Especially when working with environmental sensors, an unreflected application of the approach can lead to unaffordable or even not viable requirements for sensing and perception. Tolerances and insufficiencies of environmental sensors have to be reflected in the process to not derive unrealistic precise requirements. To follow the approach of bottom-up would mean to take an existing system and find out how good a function can be implemented within the given limits. The bottom-up approach will not lead to a well performing system because the development of existing components like sensors, perception and prediction was based on other system goals.

When constraints do not allow to develop all system components from scratch and the goal is to improve a system the appropriate approach is called Middle-Out in literature (e.g., [4]).

In the development approach, the already existing functions of the system (bottom up) are compared to potential beneficial field of new functions (top-down) in an iterative process (compare Figure 3). The Measures of Performance (MOP) of subsystems have to be sufficient to achieve relevant Measures of Effectiveness (MOE) of the complete system. Identified gaps can be analyzed. After a feasibility check the development effort can be estimated and discussed with stakeholders if with reasonable effort MOPs for subsystems can be improved to increase the overall MOE.
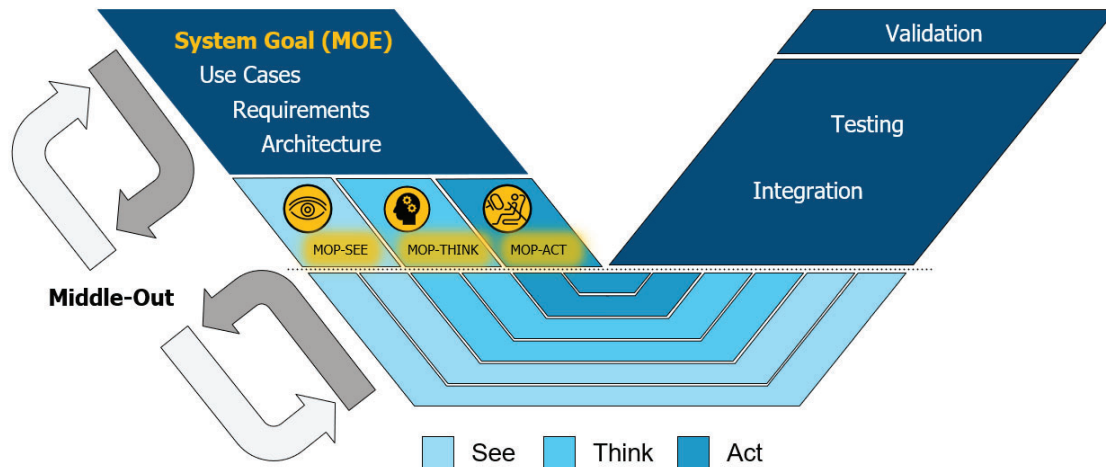
Figure 3 Middle-Out process in relation to the V-Model

CHALLENGES AND OPPORTUNITIES IN DEVELOPMENT STRATEGY WITH A HOLISTIC VIEW

When it is possible to map a system MOE to defined MOPs, next subsystem level development can start. However, when having a holistic view on the overall system effectiveness and the characteristics of one subsystem influences the MOPs of other subsystems it gets complex. If these relationships are not linear but have discontinuous jumps with different effects depending on the scenario, a holistic understanding is important. A clear understanding can only be achieved by applying the methodology to a first example otherwise it is too theoretical. For the Active Occupant Repositioning the interdependencies and discontinuities of the different subsystems - Sensing & Perception - Prediction & Decision and Act are schematically described (Figure 4).

Basic principles for discontinuous jumps
For Active Occupant Repositioning more situations in the field can be addressed (e.g., late detection times) when the actuator has the capability to provide higher forces. So in principle the field coverage over the force level is increasing (right schematic graph Figure 4). A discontinuity can be expected when the required force for Active Occupant Repositioning reaches the level necessary to overcome deceleration forces due to breaking maneuvers (simplified view excluding effects due to occupant or vehicle specific properties). Breaking before an accident is and will be an even larger proportion of remaining accidents when advanced driver assisted systems cannot completely avoided an accident or the driver is reacting too late. What must be considered is that depending on the force level, the criticality of the actuator increases. Below the distraction level, the acceptable rate of unintended activation (false positives) for the sensing - perception – prediction to decision path is defined by user acceptance. Above the distraction level the functional safety is the main stakeholder for false positive rates and SOTIF gets relevant. A defensive design strategy for sensing and perception gets necessary to achieve minimal false positives rates. For example, if difficult weather conditions might lead to a false activation these scenarios must be actively suppressed. This is one reason for the drop of the field coverage over the requirements due to force level (left schematic graph Figure 4). Not only sensing and perception strategies are influenced by functional safety ratings also uncertainties tolerated in the prediction logic is strongly dependent on the safety rating. For an actuator with a high risk of injury in case of an unintended activation, the accident must be physically unavoidable, otherwise activation could take place also in non-collision scenarios. Compared to a prediction with the most probable trajectory (this includes allowing activation in evasive maneuvers), the scenarios which can be declared as a true positive drop significantly (middle schematic graph Figure 4). The challenge is to find the right balance, the tradeoff between these divergent effects.
In general perception of objects and the prediction of their behavior cannot be executed perfectly fault free due to inevitable uncertainties. The performance of perception and prediction can be described on a statistical basis according to the "confusion matrix" by false positives (FP) and false negatives (FN). In such a constellation there is an inherited tradeoff between FPs and FNs as decreasing the one will increase the other. So there is an inevitable tradeoff between the two for all systems incorporating perception and prediction – including Pre-Crash systems [5].
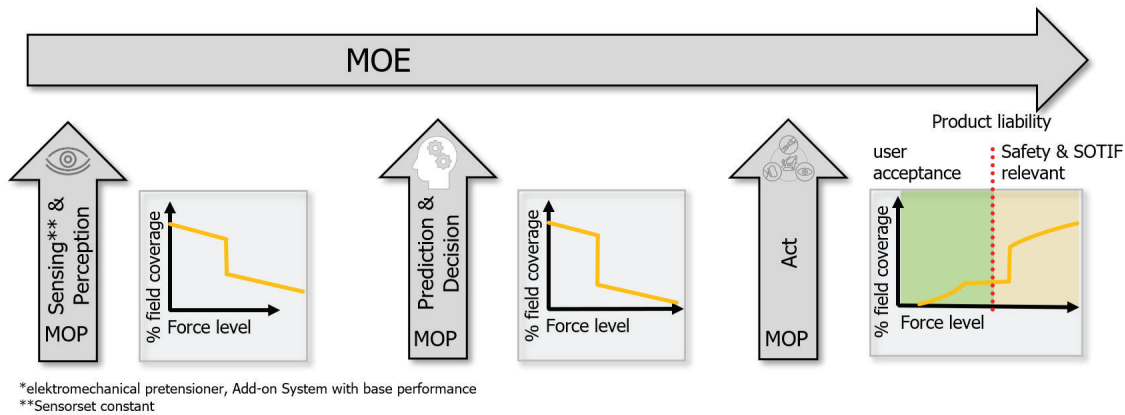
Figure 4 Simplified principles of divergent discontinuous jumps in MOPs

The next dimension to this optimization problem is that the effects of the relationship are different, depending on the scenario. One example thesis is, that in a breaking or steering maneuver, higher forces are possible before distracting a driver from the driving task (Figure 4) compared to driving on narrow lanes on construction sites.
These different theses have to be proven to be included in a final function. Obviously most important for this optimization problem is the dimension of time. When reacting before the deceleration of a breaking maneuver, lower forces are able to bring an occupant in a nominal position.
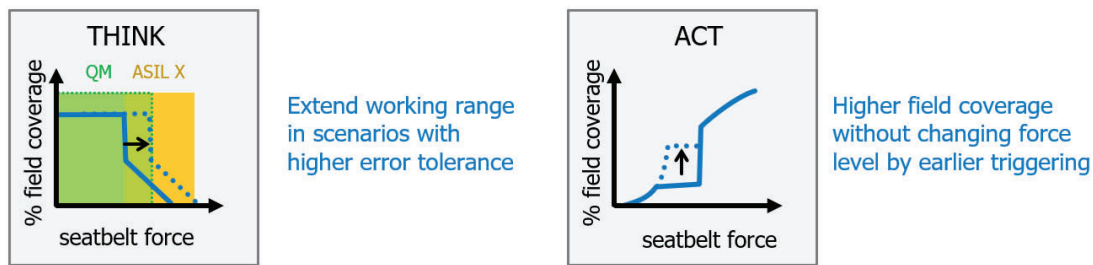
Figure 5 Parameter relationships and strategies to improve field coverage

Benefits and disadvantages of different levels supporting a common goal
The selected goal to have the occupant in a nominal position before an imminent collision cannot solely be achieved by a pure Pre-Crash function. Early, softer solutions with less side effects can support the goal. Reacting early, not even before a crash but already in critical situations are state of the art functions which contribute to the same goal to have an occupant in a nominal position before a collision. To avoid unnecessary work in developing solutions for sensing, perception and predictions on scenarios which can be detected with other sensors and furthermore be solved with different actions the first task is to understand the functions which contribute to the goal (Figure 6). It is necessary to exclude these scenarios from the Pre-Crash prediction development process but to include them into the development process of the decision logic. Their interdependencies and the effect on field coverage for the overall goal is to be considered. Typical examples are accidents which occur after driving instabilities. These scenarios do not have to be solved with a solely environmental sensor-based decision. When losing control is detected, state of the art pretensioners retract the webbing with a limited force and support the occupants to get or to stay in nominal position. Limits of this functions can be identified, and solutions must be implemented to combine vehicle sensor data and environmental sensors to address missing scenarios with a robust decision. Scenarios with driving instabilities are very challenging for state-of-the-art perceptions because they were developed for stable driving, but also are rare due to electronic stability controls systems (ESC) and anti-lock braking system (ABS). The possibility to solve these scenarios beforehand reduces the effort for the Pre-Crash function and improves the overall occupant in-position rates.
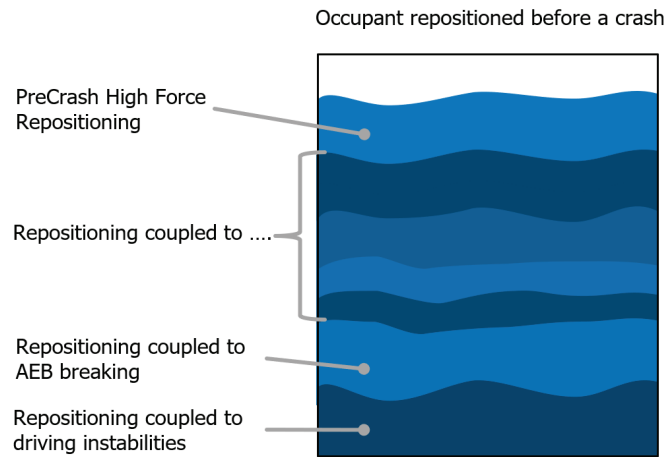
Occupant repositioned before a crash

PreCrash High Force
Repositioning

Repositioning coupled to ….

Repositioning coupled to
AEB breaking

Repositioning coupled to
driving instabilities

Figure 6 Functions contributing to the goal to reposition an occupant before a crash

After identifying the gap between the potential beneficial area and the already solved scenarios identifiable without a special Pre-Crash perception and prediction, a tool chain is necessary to be able to understand the complex interdependencies and the effects of decisions made for the different subsystems. Ideal is a tool chain, which helps to estimate the field coverage. Methods, the developed chain and an example what gets possible to analyze will be described in the next chapter.

TOOL CHAIN TO ESTIMATE FIELD COVERAGE AND OPTIMIZE SYSTEM PARAMETERS OF SEE THINK AND ACT

To assess the effectiveness of an innovative system with benefits in a complex environment in an early stage of development is a research discipline in itself, which is addressed by different collaborations. One collaboration ZF is also involved is called Prospective Effectiveness Assessment for Road Safety (P.E.A.R.S.). P.E.A.R.S. suggests four baseline approaches for the safety performance assessment (source [6]). All approaches are based on real-world scenarios. In the first approach directly, the real-world scenarios are taken to analyze the effectiveness of new or changed functions. The second approach is to add variations to this real-world scenario pool. The third and fourth approaches are based on synthetic generated cases based on parameter statistics from real world accidents with and without variations.

In accordance with the suggested second approach, we extracted relevant scenarios from GIDAS and made variations to get further scenarios ending in a crash and further near miss scenarios. These scenarios help to assess and determine the robustness of the decision logic. Further details see ref. [7].

When evaluating complex systems with several components which contribute to a final function, it is helpful to start with an ideal assumption for the components. This process was e.g., described by [8]. This process helps to learn about fundamental upper limits of components and finally assesses the performance of the complete system. The idea is to improve the assessment in the development process by adding more accurate representations in the approach. Starting with idealizations representing the different involved components in a tool chain and going over different modelling accuracies and prototype stages to the final component. This methodology can also be used to understand the effects of the discontinuous jumps described in the section "basic principles for discontinuous jumps".

We divided our system chain into sensing and perception going over into the prediction, our so-called Collision Pose Estimation, leading to a decision and finally the action of the passive safety system. The idealization of sensing and perception helps to better understand the fundamental limits of crash prediction (also shown by [9]).
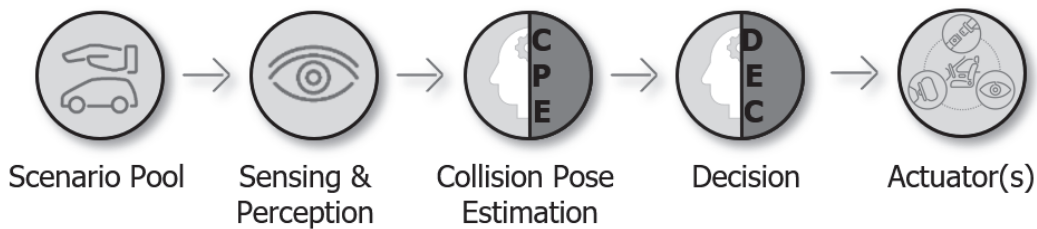
Figure 7 Main parts of involved components represented in the tool chain to analyze system performance

A big challenge is the definition of an appropriate scenario pool to assess statistically meaningful results (our approach see ref. [7]). It is challenging to include enough and the correct parameters addressing the performance limitations of the sensing and perception component. Here a reasonable approach is with the assumption of rates for example how often adverse weather conditions occur where limits of sensors are reached. Challenging no-fire scenarios must be generated and specifically selected with the knowledge on a sensor set and its limitations. To estimate the field coverage, it becomes particularly challenging when the performance assessment of the actuator is included. The evaluation of current passive safety systems is based on standard load cases representing statistically relevant accident scenarios. This is helpful to have a testable and evaluable amount of load cases but not necessarily applicable to Pre-Crash as discussed in Chapter "Challenges for Pre-Crash". For real life safety, the most appropriate choice is to define desired performance rates for the field. This definition leads to a complex assessment of the restraint system performance. The parameters to derive these rates are numerous and vary strongly. Besides the pulse direction, intensity and profile, the triggering time due to detection time is a key influencing factor for the MOP of the restraint system. Surrogate models based on carefully selected FEM simulations are an effective approach to get the number of results which are required to get to field rates [10]. Much more convenient would be to agree in collaborations on standardized procedures to judge on performance and to validate systems [11]. Due to the variant diversity and the wide range of benefits these procedures do have to be flexible enough and the fundamental knowledge on how to estimate the effectiveness in the field beforehand has to be build up.

To be able to react before an imminent collision the vehicles trajectories of the ego and the possible bullet vehicle have to be predicted. Different approaches to predict the trajectories are available with different advantages and disadvantages. Examples are suitability for time frames, needed computing power or false positive rates. To reduce false positive rates to a minimum, an accident has to be physically unavoidable. Such restrictive requirements might get important depending on the safety rating, discussed in the Chapter "Challenges for Pre-Crash".

Comparing this logic to a logic with reduced hypotheses, e.g., a no change assumption for the ego vehicle while keeping all hypotheses for the potential accident opponent. This strategy leads to much earlier actuation times. For example, in 70% of the selected scenarios the physically unavoidability of the accident is estimated 200 ms before the impact, based on ground truth. A function which could be activated already when breaking or steering and would get necessary 200 ms before the impact, would be triggered in 92% based on ground truth (Figure 8. Latencies and sensor uncertainties are possible to consider in our tool chain, but are not included in this ground truth analysis.

For the development strategy for a function and the components it is essential to get a good understanding of the consequences in the complete chain due to parameter changes in one component (see Chapter "Basic principles for discontinuous jumps"). The difference of the two prediction strategies and their effect on the triggering rates on the selected scenario pool was analyzed to give some principal insights in the possibilities with our tool chain. The comparison on detected scenarios over time shows in how many scenarios triggering of a function based on the two different defined decision parameters is possible. The change from physically unavoidable to the prediction with a reduced number of hypotheses leads to a drastic increase of the rate of early detection (Figure 8) along with not compulsory or even unintended activation. The challenge is to find the right balance for the complete system (Chapter "Basic principles for discontinuous jumps").
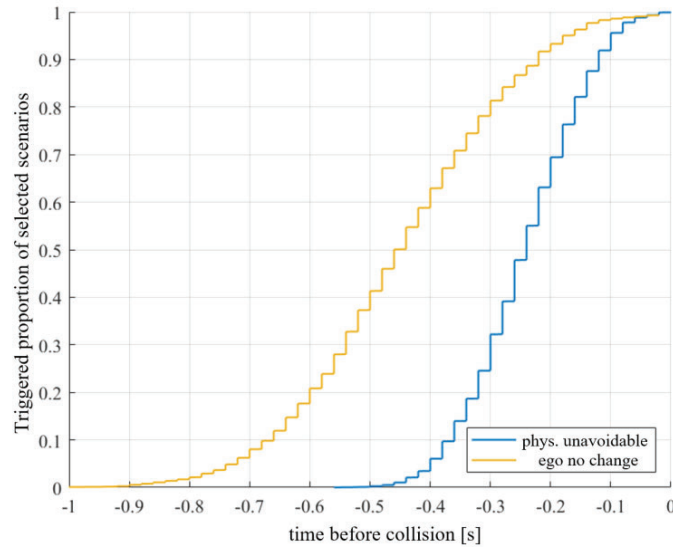
Figure 8 Influence of prediction strategy on triggering time based on ground truth information

With a reduced area of action, the true positive rates are adjustable. The area of action describes crash constellations where an action is required. For example, a minimal overlap and a May-Trigger overlap area is defined. The May-Trigger area describes the grey area where a crash or a driving constellation does not require an activation but is also not rated as a false positive. The overall number of activated scenarios of the complete selected pool can be reduced by this process, and results in a clear understanding and description of the activation characteristics of the function.

The minimum overlap for standard load cases is 25 % between barrier and the vehicle (IIHS Small Overlap). With No-Fire and misuse load cases, the lower thresholds are defined. A similar approach has to be established for environmental sensing-based restraint system triggering. The agreement on acceptance criteria is only possible in collaborative working groups.

CONCLUSION AND LIMITATIONS

We detailed the different levels and interdependencies leading to the complexity in realization of advanced Pre-Crash systems. Classifications help to understand fundamental differences and challenges in a specific system development. Active Occupant Repositioning was used to describe in detail the discontinuous relationships of different influence factors by taking safety requirements into account. We outlined a process to develop a holistic system-design for affordable and efficient Pre-Crash systems on basis of a full scope system development. On this foundation, the following basic developments steps of methodology, standards and technologies for validation, functional safety, legal and regulatory requirements as well as sensing were discussed. The complexity of this field requires collaborations to jointly develop acceptance criteria addressing performance and false positive acceptance rates. ZF actively supports these collaborations and working groups and is open for further exchange.

ACKNOWLEDGEMENTS

REFERENCES

[1] Pischinger, S., Seiffert, U. (2021). Vieweg Handbuch Kraftfahrzeugtechnik 9. Auflage, Wiesbaden, Springer Vieweg

[2] Hu, J. Flannagan C. A. (2015) Integration of Active and Passive Safety Technologies - A Method to Study and Estimate Field Capability, Stapp Car Crash Journal, Vol. 59

[3] Grotz, B. (2022) Predictive Safety: Activation of a Pre-Crash System with Fallback Option, Verkehrstechnik / Fahrzeugtechnik Band 817, VDI Verlag Düsseldorf

[4] Blanchard, B. S., Blyler J.E. (2016) System Engineering Management, John Wiley & Sons, Inc. Hoboken, New Jersey

[5] Koopman, P (2022) How safe is safe enough? Measuring and predicting autonomous vehicle safety, ISBN 9798846251243

[6] ISO. 2021j. ISO/TR 21934-1:2021 Road vehicles — Prospective safety performance assessment of pre-crash technology by virtual simulation — Part 1: State-of-the-art and general method overview.
https://www.iso.org/standard/76497.html
ISO. n.d.-k. ISO/AWI TS 21934-2: Road vehicles — Prospective safety performance assessment of pre-crash technology by virtual simulation — Part 2: Guidelines for application (under development).
https://www.iso.org/standard/81790.html

[7] Grotz, B., Straßburger, P. (2021) Predictive Safety – Perception-based Activation of Pre-crash Systems, ATZ worldwide 01|2021

[8] Siegl S., Gollewski, T. (2014) About Development Processes and Accompanying performance evauations of integral automotive safety systems, FISITA 2014 World Automotive Congress, Maastricht, Netherlands

[9] Freienstein, H., Höpfner H. (2017) Reliable pre-crash detection and decision making for accident against oncoming traffic, VDI conference for vehicle safety, VDI Verlag, Düsseldorf

[10] Hay, J. (2022). A Surrogate Model-Enhanced Simulation Framework for Safety Performance Assessment of Integrated Vehicle Safety Systems. Schriften aus dem Institut für Technische und Numerische Mechanik der Universität Stuttgart, Ph.D. Thesis, Vol. 75. Shaker, Aachen. ISBN 978-3-8440-8727-

[11] Machens, K.-U., Kübler, L. (2023): "Dynamic Testing with Pre-Crash Activation to Design Adaptive Safety Systems", International Conference on Enhanced Safety of Vehicles; ID#: 23-0067, Yokohama, Japan

RESEARCH ON V2X COMMUNICATION SYSTEM TO REDUCE PEDESTRIAN ACCIDENTS

Moriya, Horiuchi

Shigeru, Inoue

Takahiro, Kurehashi

Takashi, Oshima

Yuta, Sakagawa

Honda R&D Co

Japan

Yosuke, Komiyama

Koichi, Serizawa

SoftBank Corp.

Japan

ABSTRACT

Everyone deserves to feel safe on the road. The goal is to strive for zero traffic collision fatalities involving motorcycles and automobiles globally by 2050. Many traffic fatalities are categorized as vulnerable road users such as pedestrians and cyclists. In particular, pedestrian fatalities account for the largest portion. Pedestrian accidents have occurred not only through drivers' errors but through pedestrians' errors. Thus, in addition to advanced driver-assistance systems, safety behavior by pedestrians is effective for reducing pedestrian accidents. Research was therefore conducted on the vehicle-to-everything (V2X) communication system connecting vehicles and pedestrians to assist both drivers and pedestrians.

The system used 5G standalone mobile communication system and a cellular-V2X communication system. With an in-vehicle camera, the system detected a pedestrian walking across a street ahead and in an area that is in a blind spot for the driver. Then, the total time required for the pedestrian to receive notification after detection by the in-vehicle camera was estimated. Also, the reactions of pedestrians were observed, and the time required for pedestrians to react to notification was measured as well.

The result in the assumed use case was that the system promoted safety behavior by supporting drivers and pedestrians before collision occurred.

However, considering the reaction time of pedestrians, assisting system users before collision is a challenge if the time to the collision is extremely short. Therefore, the system is required to notify the users in plenty of time before the collision. In order to utilize the system, it is desired to promote widespread adoption by installing the system on smartphones rather than on dedicated equipment. Also, the accuracy of location ascertained using smartphone needs to be improved to establish acceptability.

The safe use of communication technologies was considered as one of the one-step-ahead integrated vehicle safety technologies. This report details the structure, results, and issues of the V2X communication system.

RESEARCH QUESTION/OBJECTIVE

According to traffic statistics from the National Public Safety Commission and the National Police Agency [1], 2839 people died in traffic accidents in Japan in 2020. The number of fatalities from traffic accidents has decreased greatly over the past decade or more, but in the past several years, that decrease has tended to slow down. In particular, a comparison of the annual incidence of accident fatalities among people riding in motor vehicles and accident fatalities among people walking shows that their levels have been about equal in recent years, which means that countermeasures against pedestrian accidents are important for reducing the number of fatal accidents. Functions that help prevent accident include, for example, advanced emergency braking systems (AEBS) and forward collision warning (FCW). As these suggest, safety technology development has been focused on the vehicle side. These functions have shown results in preventing accidents due to human error, such as inattention to the road ahead and operating errors by vehicle drivers. These are considered to have contributed to a reduction of fatal accidents among vehicle occupants. However, risks hidden in blind spots cannot readily be handled solely using information from autonomous sensors. Looking further at the number of fatalities due to traffic accidents by type of traffic violation among fatal pedestrian accidents, it can be seen that 582 out of 970 pedestrian fatalities, or 60%, involved pedestrian violations such as ignoring traffic signals or crossing violations. From this it is apparent that accidents occur not only because of human error by vehicle drivers, but also because of dangerous behavior by pedestrians. Steps to reduce accidents resulting in pedestrian fatalities will be taken, therefore, by assistance that prompts safe behavior by pedestrians before accidents occur and by assistance to notify drivers to the presence of pedestrians in blind spots.

The present research created systems using communication technology to notify pedestrians of risks and to notify drivers of risks in places that are blind spots from their vehicles, to function linked to conventional assistance functions for vehicles such as AEBS and FCW. In addition, changes in behavior by pedestrians who received assistance were verified, more effective means of notifying pedestrians of danger were explored, and a study of the acceptance of assistance while walking was conducted.

METHOD

A system was created to connect pedestrians and vehicles for the purpose of sharing their risk information. This system is an assistance system that features an in-vehicle camera and communications coordinated in an event-driven system. In the event-driven system, the occurrence of risk is a trigger that executes assistance by means of communication. Pedestrians posing a danger and blind spot areas are detected by an in-vehicle camera and the system uses communication to provide assistance to the party at risk. This method coexists with conventional support systems and provides more reliable support when risks between vehicles and pedestrians increase. This system is not only a human–machine interface (HMI) to provide the required assistance to the vehicle driver, but also a HMI directed at pedestrians. Smartphones were therefore used as the device for providing assistance to pedestrians. The reason for this is that according to a survey of smartphone ownership in recent years [2], 80% or

more of the world population has a smartphone, and so it is likely that pedestrians will be holding one. As smartphones are equipment for individuals, it is also possible to provide assistance only to the party at risk. Notification by smartphone informs recipients about circumstances in their surroundings without interfering with their walking, and prompts pedestrians to take action themselves to avoid danger.

Verification of V2X System in Actual Vehicles

For the verification of V2X system in actual vehicles, cellular V2X (C-V2X) was adopted as the method of communication [3]. Figure 1 shows the C-V2X communication interfaces. In direct communication among V2X-special user equipment by means of the C-V2X PC5 interface, assistance information is broadcast from the vehicle, and traffic participants in the surrounding area that have communications equipment receive the information. Communication via base station (BS)/core network (NW) by means of the Uu interface uses the cellular network to conduct communication through the server. In communication via BS/core NW, information from the vehicle is used by the server to identify the party targeted to receive assistance. For this reason, it is necessary for the MEC server to have a grasp of traffic participant location information. The cellular network was implemented by means of 5G standalone (5GSA). In 5GSA, the use of 5G core equipment achieves ultra-high speed and high capacity. It is a communication service that enables ultra-low delay and high reliability by means of network slicing technology and multi-access edge computing (MEC), which suits it for use in vehicle automated driving and safety [4].
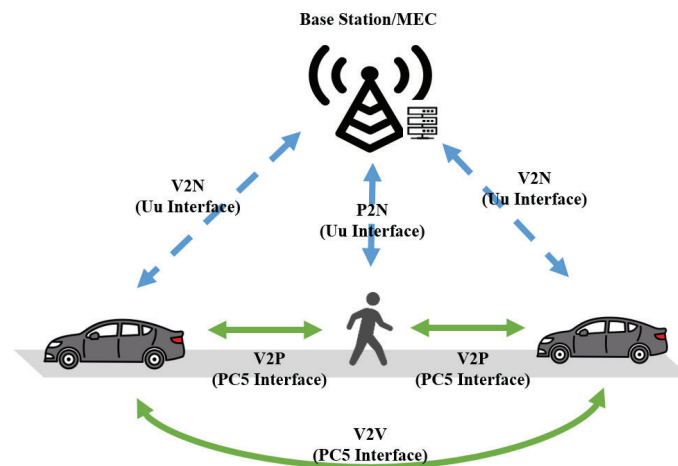

Figure 1. C-V2X Interfaces

Figure 2 shows an overall view of the actual vehicle system that was created. This system comprises three elements: the vehicle, the pedestrian, and the MEC server. The vehicle system is made up of global navigation satellite system (GNSS) equipment for acquiring location information, a radio for conducting communications, a recognition processing unit that performs object recognition using the in-vehicle camera, and an in-vehicle unit that, based on recognition results, manages calculation and communication regarding the possibility of collision with pedestrians and areas with blind spots due to occluding objects. The pedestrian system is made up of a portable terminal that acquires location information and a pedestrian unit that processes communications by radio. The MEC server manages location information regarding traffic participants and manages transmission and reception

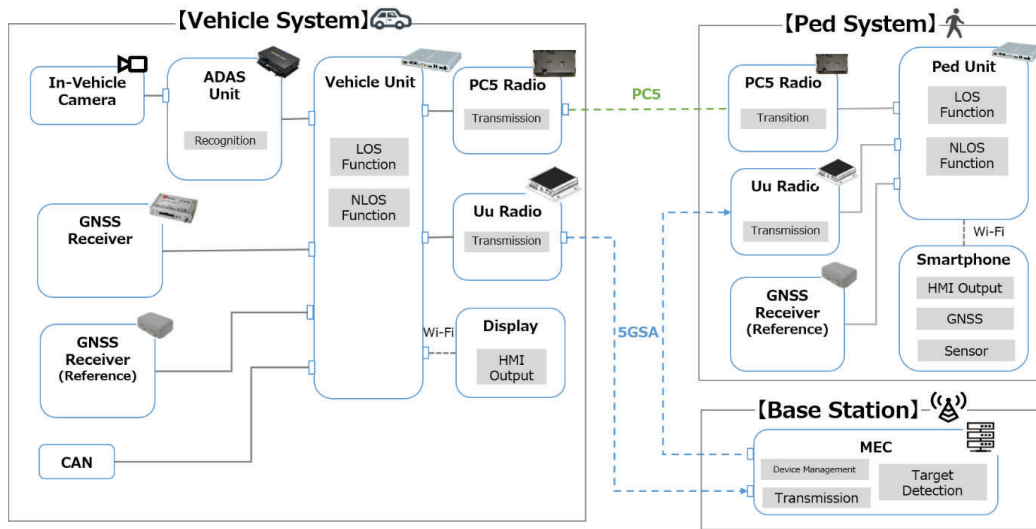of information to and from parties that require assistance.

Figure 2.V2X System for Pedestrians

For verification in actual vehicles, two use cases were prepared and verified. Testing of verification in actual vehicles was conducted in open sky with GNSS receivable, with the number of server connections with units limited to the traffic participants appearing in the particular use case and with dedicated communication circuits. Figure 3 shows the first line-of-sight (LOS) use case. The LOS use case was implemented in an environment where there were no occluding objects between the vehicle and pedestrian. The case recreated a scene in which a vehicle was moving straight ahead, and pedestrians crossed ahead of it.
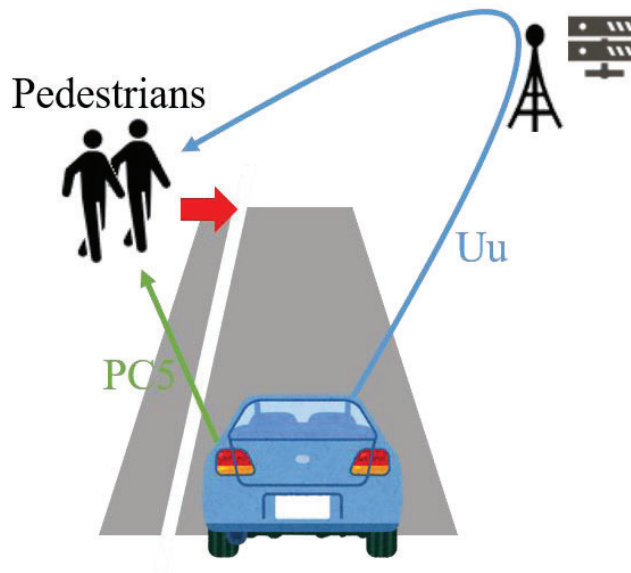
Figure 3. LOS Use Case

Figure 4 shows the processing sequence in verification of the LOS use case. The vehicle system uses the in-vehicle camera to detect the pedestrian crossing the road ahead, judges the possibility of collision with the subject vehicle, and calculates the time to collision. When this time to collision is at or lower than a certain threshold value,

assistance information is transmitted from the vehicle. For this verification, this threshold value was set to 2 seconds and verification was carried out uniformly with that setting. Assistance information was transmitted simultaneously by direct communication and by communication via BS/core NW. In the case of communication via BS/core NW, processing by the MEC server is added to the time until the party targeted to receive assistance is notified. In this verification, the arrival rate of the transmitted information at the party targeted to receive assistance, the vehicle system processing time, the server processing time, and the communication time were calculated to obtain the total time the system took to provide assistance.
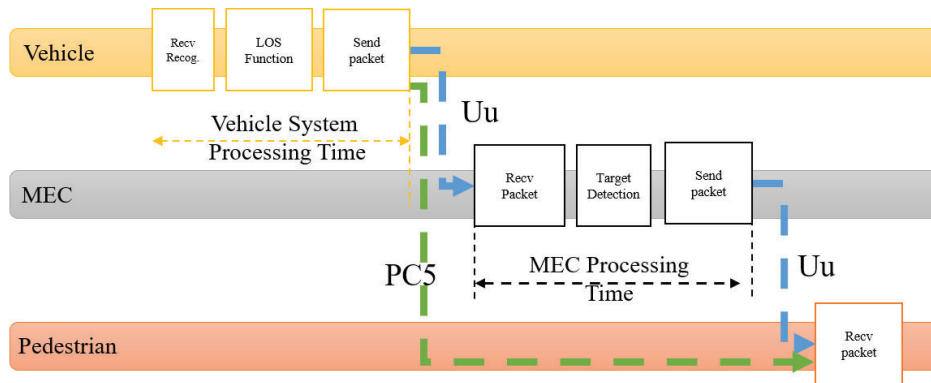
Figure 4. LOS Use Case Sequence

Next, the second non-line-of-sight (NLOS) use case is shown in Fig. 5. In this use case, a vehicle with high vehicle height was prepared to function as an occluding object between the subject vehicle and the crossing pedestrian such that the subject vehicle driver and the pedestrian were unable to see each other. With the present system, communication is used to check whether or not a pedestrian is present in a blind spot from the vehicle, and when a pedestrian is present, assistance is provided to the vehicle driver and the pedestrian.
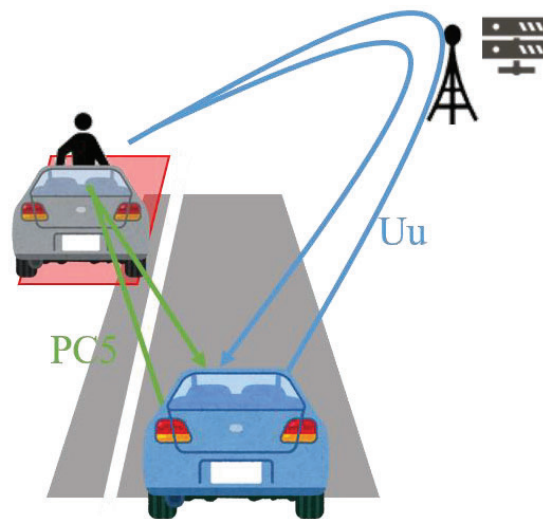

Figure 5. NLOS Use Case

In the NLOS use case, the in-vehicle camera is used for object recognition of an occluding object ahead of the vehicle, and the system calculates the risk area that includes the blind spot as viewed by the vehicle driver. Figure

6 shows an example of the risk area that is calculated. With this system, the risk area is a quadrangle, and each side is calculated as parallel or perpendicular to the subject car's direction of movement. The purpose of this is to reduce the calculation cost, as the area that is a blind spot is by its nature polygonal. In the present verification, when the time headway to the calculated area became 2.5 seconds or less, the area up to the point that would be arrived at in 3.8 seconds was taken to be the risk area, and a request for information about the area was made using communications.
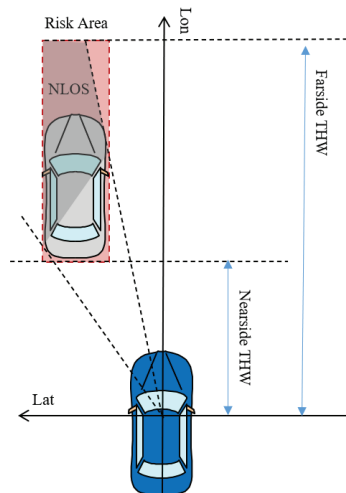
Figure 6. NLOS Risk Area Detection

Next, the processing sequence in verification of the NLOS use case is shown in Fig. 7. In the case of direct communication, the risk area information broadcast from the vehicle is received directly by the pedestrian. At this time, the pedestrian judges on the basis of their own location information whether or not they are in a risk area, and they send back that result. In the case of communication via BS/core NW, the received risk area information was used by the MEC server as the basis for identifying pedestrians in the surrounding area and distributing that area information by multicasting. Pedestrians who receive the information would judge whether they are in that area and send back their reply. The MEC server would then notify the vehicle that made the information query whether or not there are pedestrians in the area. For the verification conducted here, measurements were made of the communication time taken from when the query information was transmitted from the vehicle to when the reply was received and of the processing time.
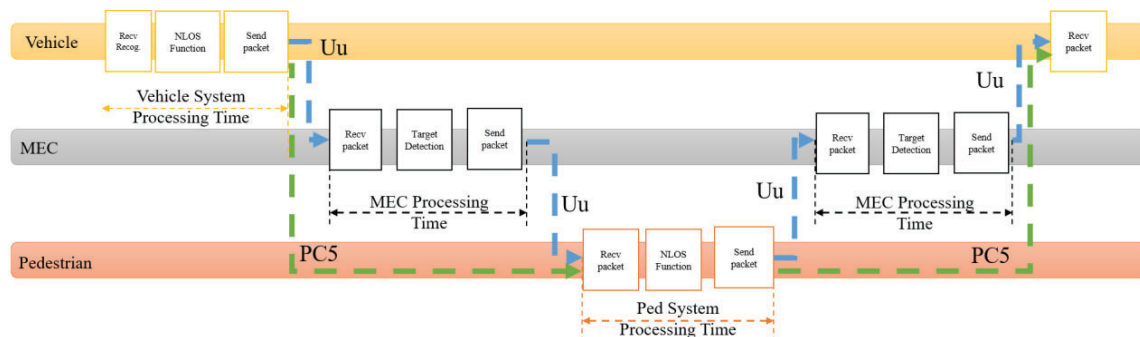

Figure 7. NLOS Use Case Sequence

Verification of Pedestrian-Oriented HMI

With this system, the subject pedestrians themselves are prompted to avoid danger. When the lines of movement of pedestrians and vehicles overlap so that the risk of collision is heightened, the smartphones that pedestrians possess are used to convey that "a vehicle is approaching, and caution is necessary" by sound, vibration, and display. The effectiveness and acceptance of this HMI were confirmed by verification using the below procedure.

As testing with actual vehicles is dangerous, a simulator using the head-mounted display (HMD) shown in Fig. 8 was created and used. The simulator uses the HMD and motion trackers in an arrangement that coordinates the test subject's actual actions with actions within the virtual space. The test subjects were instructed to cross a street. At that time, a vehicle approaches, recreating a scene of increasing risk. The results of these actions are analyzed together with questionnaires of subjective evaluations collected after completion. Test subjects were selected from among employees who responded to an in-house call for applications and who were not aware of the content of the research. Prior to the start of the experiment, all participants received an explanation of the contents and risks of the experiment as well as their rights and voluntarily signed a participation agreement. This study was approved by the Ethical Committee of the Honda Motor Co., Ltd.
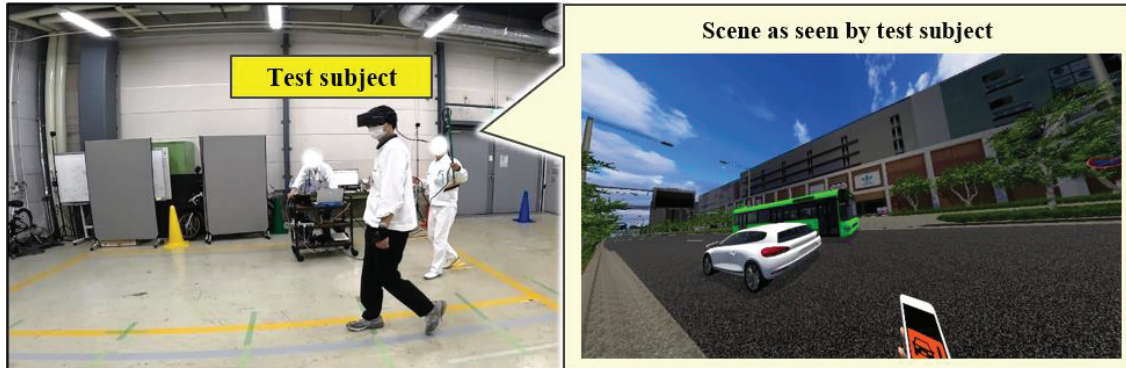

Figure 8. Simulator Using HMD

An overview of the test scenario is shown in Fig. 9. The test subject would repeatedly cross the street, and some of those times, the subject vehicle would approach from the right side. When the risk from this vehicle rises, a warning is issued by means of the HMI. In addition, a sub-task was assigned that would tend to draw attention toward the left side in order to induce subject vehicle recognition error. Test subjects would cross the street a total of nine times. If they learn when doing this that a vehicle will approach from the right each time, it will not be possible to confirm the aimed-for effect. Therefore, the number of times that a vehicle would approach was limited to three out of that total number of times. To check whether or not the behavior of test subjects would change according to whether or not they understood the purpose of this in advance, the test was conducted so that during the first vehicle approach and up to the time the alarm was issued, the test subjects were not told of the aim of the HMI.
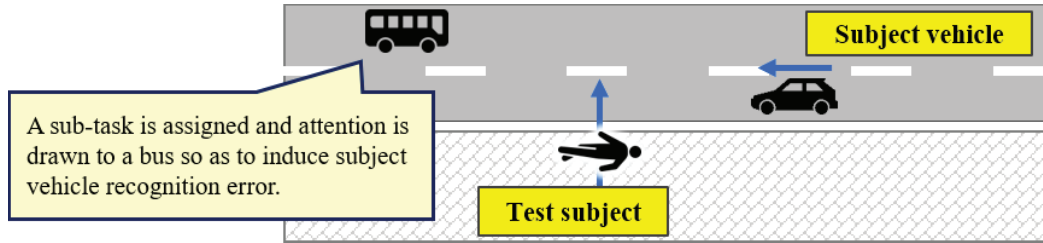
Figure 9. Overview of Test Scenario

The testing was conducted with three patterns each of where the pedestrian kept the smartphone and what notification sound was made by the HMI. The specifics are shown in Fig. 10.
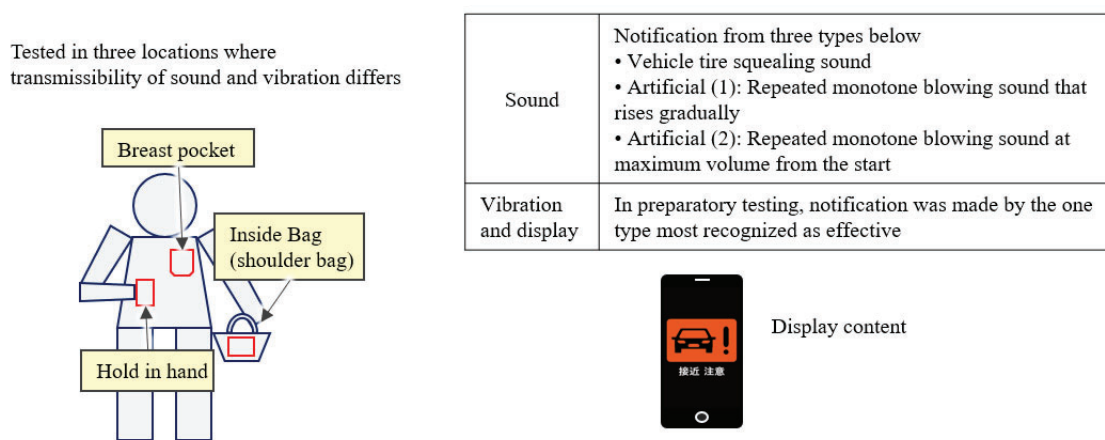

Figure 10. Location Where Smartphone is Kept and HMI Specification

After the testing ended, analysis of the filmed images that had been acquired and of the system log confirmed that behavior change, and reaction time change effects did occur. The subjective questionnaire responses also confirmed awareness, degree of understanding, and acceptance.

RESULT

Results from Verification of Actual Vehicle V2X System

In verification of the LOS use case with direct communication, the assistance information arrival rate was 100% and with communication via BS/core NW, the arrival rate was 95%. In the tests in which assistance information from the vehicle to the pedestrian through communication via BS/core NW did not arrive, the assistance information arrival rate at the MEC server was 100%. However, large discrepancies occurred in the location information used by the server to identify the party targeted to receive assistance, as a result of which the system was not able to identify the target.

Figure 11.1 shows the vehicle system processing time in validation of the LOS use case. The average time from reception of recognition results to transmission of assistance information was 38 ms. Figure 11.2 shows the total time of risk information reception processing at the MEC server, identification of the target, and transmission

processing during communication via BS/core NW. The average processing time was 16 ms. Figures 11.3 and 11.4 show the communication time for direct communication and for communication via BS/core NW, respectively. Direct communication took an average of 25 ms, whereas communication via BS/core NW took 39 ms. The results show that the time taken by communication is shorter in direct communication than in communication via BS/core NW, and there was also less variation.
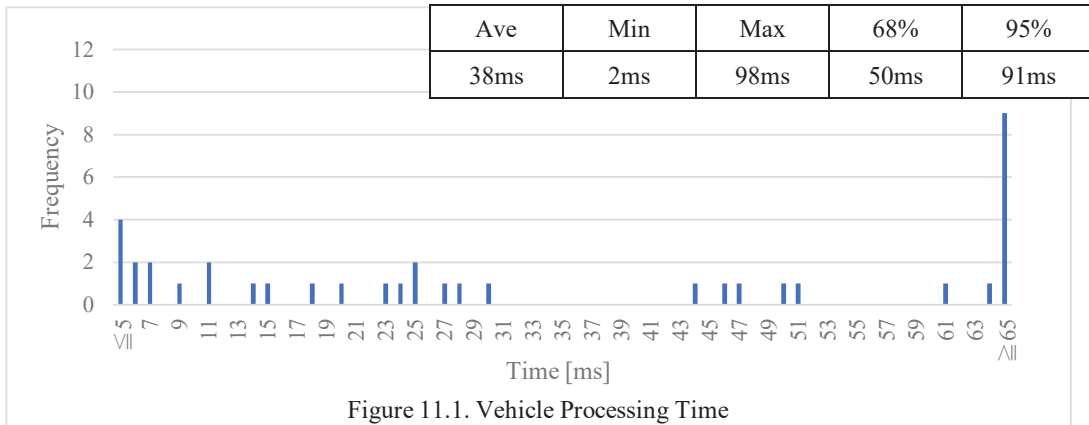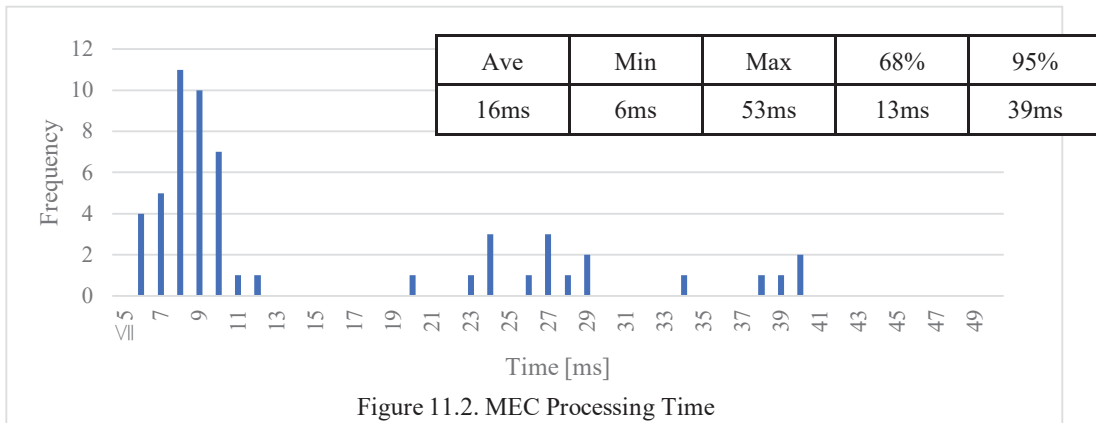
Ave	Min	Max	68%	95%
38ms	2ms	98ms	50ms	91ms

Figure 11.1. Vehicle Processing Time

Ave	Min	Max	68%	95%
16ms	6ms	53ms	13ms	39ms

Figure 11.2. MEC Processing Time

Ave	Min	Max	68%	95%
25ms	16ms	34ms	26ms	31ms

Figure 11.3. PC5 Communication Time

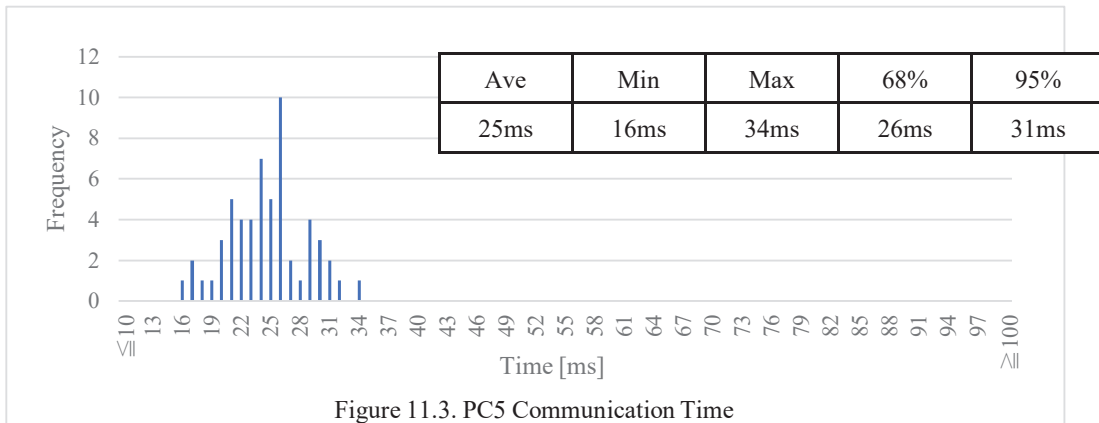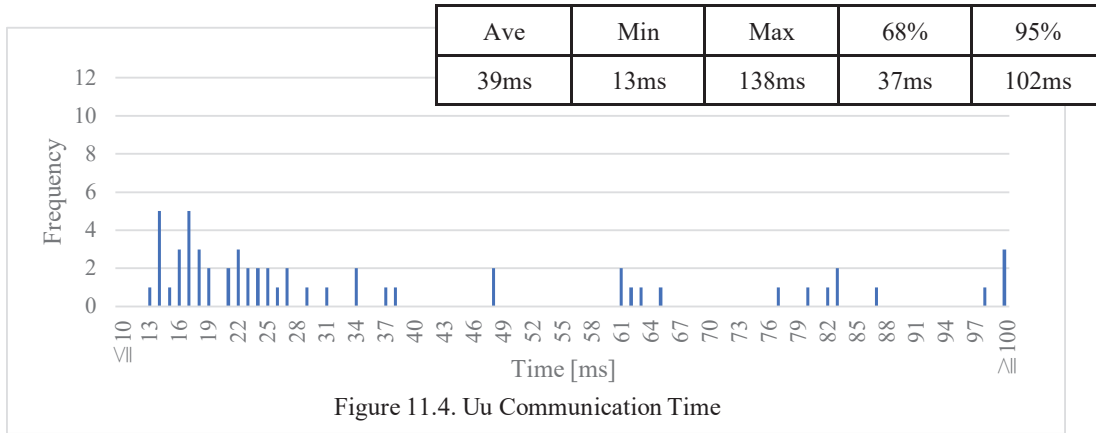|	Ave	Min	Max	68%	95%
	39ms	13ms	138ms	37ms	102ms

Figure 11.4. Uu Communication Time

In verification of the NLOS use case, in cases when a pedestrian was present in an area that was a blind spot for the vehicle driver, it was possible to convey assistance information to the driver of the vehicle before the vehicle arrived at that area. Table 1 presents the average time taken for the system to provide support during verification. The average time taken for the vehicle driver to receive information by direct communication was 79 ms, and the average time by communication via BS/core NW was 131 ms. In the case of communication via BS/core NW, it is necessary for the MEC server to mediate each communication, and thus it required more time than direct communication.

Table 1 NLOS Use Case Average Required Time

	Total System Required Time	Communication Time	MEC Processing Time
PC5	79ms	26ms	
Uu	131ms	58ms	32ms

Results from Verification of Pedestrian-Oriented HMI

The results regarding whether or not test subjects perceived the notifications are shown in Fig. 12. Note that these are the results immediately after the first tests ended and the test subjects did not understand that they would be notified by HMI from a smartphone. Notification by sound was perceived by all test subjects regardless of where the smartphone was kept. Next, regarding notification by vibration, half of the test subjects did not perceive it when the smartphone was in the breast pocket or a bag, which are not in direct contact with the body. Regarding display, even among test subjects who were holding the smartphone in their hand, only half perceived it. Test subjects who were not holding the smartphone in their hand did not bring the smartphone out when the notification was issued. These results suggest that in order to notify pedestrians of a risk by means of smartphone, it is important to obtain their perception of it by sound.

HMI type	Location where smartphone is kept	N*	Not perceived / Perceived
Sound	Held in hand	11	100% (Perceived)
Sound	In breast pocket	11	100% (Perceived)
Sound	In bag	11	100% (Perceived)
Vibration	Held in hand	11	9% / 91%
Vibration	In breast pocket	11	45% / 55%
Vibration	In bag	11	45% / 55%
Display	Held in hand	11	45% / 55%
Display	In breast pocket	11	100% (Not perceived)
Display	In bag	11	100% (Not perceived)

*Total number in test: 33 people (held in the hand: 11 people; breast pocket: 11 people; bag: 11 people)
(Test subjects experienced only one location where smartphone is kept. Notifications by sound, display, and vibration issued simultaneously.)

Figure 12. Perception or Otherwise of Notification by Sound, Vibration, and Display Without Advance Explanation

Next, the results regarding whether the purpose of notification by smartphone was successfully understood, as tested without informing the test subjects of the purpose in advance, are shown in Fig. 13. Of the test subjects who perceived the notification for the first time, 70% or more understood that the purpose was to convey that a vehicle was approaching and that therefore caution was necessary. Also, all of those in the group of test subjects who perceived the display responded that the display was most helpful to their understanding of the purpose. The above suggests that adding use of the display together with sound could heighten the degree of understanding on first notification.

Was the purpose of notification understood?

Unable to understand the purpose 27% (9)

Understood the purpose 73% (24)

Checked with the 24 people who understood the purpose 24

What was the most helpful for understanding the purpose?

Vibration 13% (3)
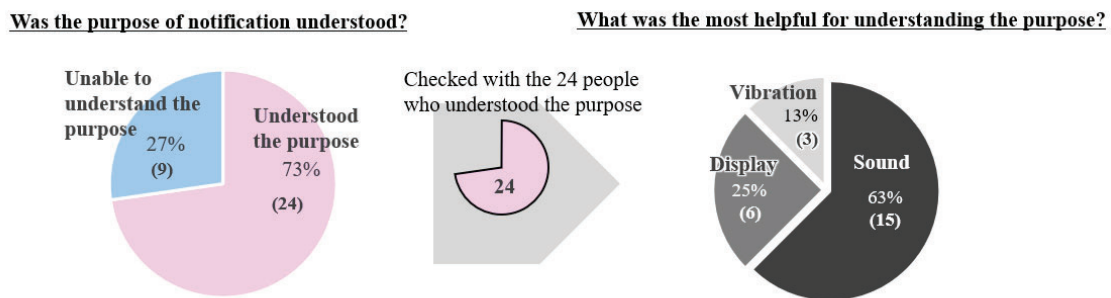
Display 25% (6)

Sound 63% (15)

Figure 13. Whether the Purpose of Notification was Understood

Figure 14 shows changes in test subject behavior due to notification. From the images and system logs, we confirmed changes in the subject's behavior before and after the notification. In addition, the subjects who confirmed the right side before the notification and were aware of the approaching vehicle were excluded from the results. As a result, after the notification, 97% of the subjects stopped after checking the surroundings or

stopped immediately to avoid accidents. Also, the average time from the notification to the subject's cessation was 1250ms.
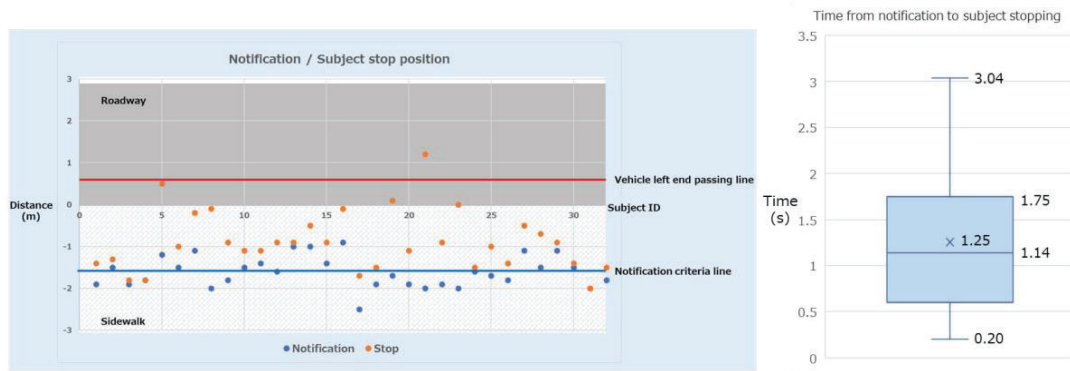

Figure 14. Notification/Subject stop position / Time from notification to subject stop

Finally, Fig. 15 shows the results from checking whether the test subjects' feeling of security would change when they go walking outside, on the assumption that this system would be present on their smartphone. The test subjects who replied that their feeling of security would increase amounted to 84%, and no test subjects replied that their feeling of insecurity would increase. The above confirms that there is acceptance of the use of smartphones to convey to pedestrians that a vehicle is approaching.
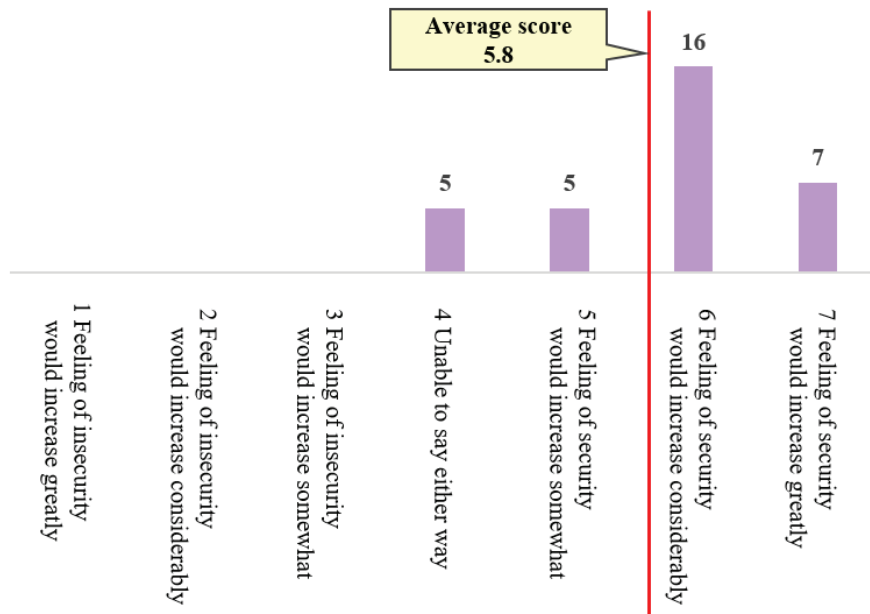

Figure 15. Whether the Sense of Security Would Change
When the HMI Experienced Here is Present While Out Walking

Total Required Time for Pedestrian Assistance

The processing time taken by this system, including the time taken for communication segments, to notify pedestrians of risk and the reaction time taken by pedestrians who received the notification until a behavior change occurred, were learned from the two verifications conducted to this point, that of the V2X system in actual vehicles

and that of the pedestrian-oriented HMI. The average times required for assistance in the case of direct communication and the case of communication via BS/core NW, respectively, are presented in organized form in Fig. 16. The result was that the time taken by this system to provide assistance in the case of direct communication was an average of 1313 ms, and in the case of communication via BS/core NW it was an average of 1343 ms. The greatest amount of time taken was the pedestrian reaction time, which took up 90% or more of the total time to provide assistance.
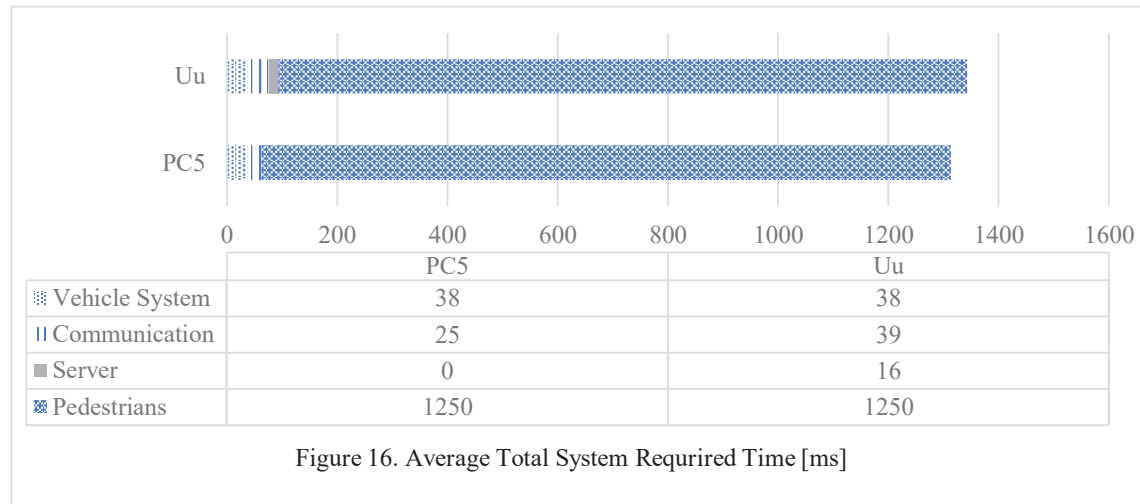

	PC5	Uu
Vehicle System	38	38
Communication	25	39
Server	0	16
Pedestrians	1250	1250

Figure 16. Average Total System Requrired Time [ms]

DISCUSSION and LIMITATIONS

The present research created a system that coordinates between vehicles and pedestrians by means of communication. This yielded findings regarding a number of issues. First, there is a limit to assistance that comes from the time required by the system to provide assistance. An average of 1.3 seconds was required from when a pedestrian crossing the street was detected until assistance resulted in a behavior change by the pedestrian. In an environment where a greater number of units are connected by communication, however, constraints on bandwidth and increasing load on the server are expected to further increase the time taken. In cases where pedestrians dash out into the street very close to the vehicle, it is possible that assistance cannot be provided before collision is avoided. In order to deal with such cases, it will be necessary to predict the behavior of pedestrians and provide assistance before they start to cross the street. Also, GNSS location information is key information for assistance in the present system, but when the influence of multipath or other such factors cause conspicuous degradation of location accuracy, there is a possibility that assistance by the system will no longer be possible. In order to maintain a high level of acceptance and promote widespread adoption of the system even when systems like this one end up with degraded location accuracy, it will be important to clarify the conceptual approaches to providing mistaken assistance and not providing assistance. There is also the fact that the perceptibility of the HMI can differ according to the location where the smartphone is kept. For this reason, it is necessary to use auditory information, which was the most effective means of notification, as the main approach regardless of where the smartphone is kept, and to use tactile information and visual information as supplementary means, so as to convey the risk to the intended subject intuitively.

CONCLUSION

The present research focused on the fact that fatal accidents for pedestrians are caused not only by drivers of vehicles but also by unsafe behavior by pedestrians and created a system to provide assistance both to the drivers of vehicles and to pedestrians. Measurement of the processing time necessary to provide assistance in an actual vehicular environment successfully confirmed the feasibility of assistance systems that make use of communication. Also, verification of the pedestrian-oriented HMI through the use of a simulator successfully confirmed the signs change in behavior toward safety as a result of assistance, thereby successfully indicating the usefulness of assistance to pedestrians. Going forward, the aim will be to realize cooperative safety that can enable the coexistence of all traffic participants by the use of communication technology, and to realize a world that is safe and sound, with no risk caused by mobility.

REFERENCES

[1] National Public Safety Commision and National Police Agency, Traffic accident situation, 2021, http://www.npa.go.jp/publications/statistics/koutsuu/index_jiko.html, 2022-11

[2] BankMyCell, "HOW MANY SMARTPHONES ARE IN THE WORLD?", 2022, https://www.bankmycell.com/blog/how-many-phones-are-in-the-world, 2022-11

[3] ITS Info-communications Forum, "Issue Survey Report on Advanced ITS and Automated Driving Using Cellular Communications Technologies", 2021, https://itsforum.gr.jp, 2022-11

[4] SoftBank Corp., "SoftBank Corp. First Carrier in Japan to Provide 5G Standalone Commercial Services", 2021, https://www.softbank.jp/en/corp/news/press/sbkk/2021/20211019_01/, 2022-11

INTEGRATED SAFETY FOR OCCUPANT PROTECTION

Simona Roka, Clara Cabuti, Pablo Lozano, Cristina Periago, Alessandro Gravina, James Jackson, Genís Mensa, Maria D'Odriozola, Eduard Romero
IDIADA Automotive Technology
Spain

ABSTRACT

Integrated vehicle safety aims to connect active and passive safety technologies and has the potential to go far beyond what each can achieve separately. Improving integrated vehicle safety has become highly relevant for the development of automated vehicles.

The goal of the ISOP project is to investigate whether applying active safety features and manoeuvres during the pre-crash phase can negatively influence the performance of the vehicles' restraint systems in a way that the state-of-art passive safety systems are no longer as effective in preventing fatalities and avoiding or mitigating injuries in road accidents.

A couple of test protocols have been defined within the project to analyse the effects of pre-crash manoeuvres on the initial occupant posture. The data from the tests with volunteers in proving ground performing cut-out manoeuvres have been collected and have been used as input database for the simulations with the Human Body Models (HBM). Due to the limitations of the Anthropometric Test Devices (ATD) in responding to a pre-crash manoeuvre, the effectiveness and sensibility of the restraint systems has been evaluated by HBM.

In contrast to ATDs, virtual Human Body Models (HBM) represent the anatomic structure of human beings including bones, flesh, skin, fat, and soft tissue. The high model detail allows a direct assessment of the injury risk based on the damage applied to the respective body region (e.g., in form of stress or strain), assuming a correct damage prediction of the model.

Integrated safety enhances comfort, convenience and can help assist in critical driving situations and in protecting occupants. However, the state-of-the art restraint systems need to be evaluated in such novel load cases including the activation of vehicle active safety systems and the pre-crash manoeuvres.

This paper focuses on the influence of active safety systems towards the protection of vehicle occupants in the event of a crash that has not been avoided, by developing a combined series of test protocols, performing volunteer tests and HBM simulations.

INTRODUCTION

One of the main objectives of vehicle safety engineers is to protect occupants when there is a risk of crash event, either by means of pre-crash safety systems or by means of in-crash performance of the restraint systems and vehicle structure once the crash is unavoidable. The motivation of the ISOP project, and of this paper, is the study how the pre-crash safety manoeuvres affect the position of the occupant in the initial phases of the crash and; therefore, influence the effectiveness of the state-of-the-art restraint systems.

Anticipation and a braced response can change the kinematics of the vehicle's passenger and have an effect on the outcome of the injury mechanism [1]. At T0, moment of the crash, not only the change of position is of importance but also the muscular activity. Occupants' response to the threat, plays an important role in the final performance of the restraint systems and consequently the injuries provoked by the accident.

To study the pre- and in- crash phase, Anthropometric test devices (ATDs) and Human Body Models (HBMs) have been evaluated. ATDs used in occupant safety testing represent a limited application regarding the pre-crash active responses of the occupant to the upcoming impact scenario. The main application of these devices is in medium- to high-severity impacts and the negative aspect of them is that they are only passive and mechanically stiff compared to other technologies. To evaluate the pre-crash response properly and to be able to mimic the response of volunteer testing, virtual testing using HBMs has been considered to be the correct approach for this study.

Four available human body models were evaluated and compared based on the different characteristics that each one had. The four models chosen were the THUMS (Total HUman Model for Safety) from Toyota, the active HBM from Simcenter Madymo, the ViVA human body model (Virtual Vehicle-safety Assessment), and the Active HBM from SAFER.

The vehicle model which will be used in the next phase of the ISOP study will be the CUPRA Formentor FE model. THUMS and ViVA models were selected as main models to be used in the next phase of the project. This decision was given by analysing the variables included in the HBM comparison study that was conducted in parallel to ISOP by means of an internal project in IDIADA (HBM_in_AV) (see Table 1).

Table 1
HBM Comparison for ISOP study

	THUMS	MADYMO	ViVA	SAFER
Active/Passive model	Active/Passive	Active/Passive	Passive	Active/Passive
Available body sizes (percentiles)	5th, 50th, and 95th	5th, 50th, and 95th and children	Female 50th	50th percentile only. Female 50th in the process
License	Open Source	Tokens	Open Source	Need to be a partner of the SAFER investigation group
Partner that uses it	TOYOTA, general use	Siemens, general use	Volvo Cars, The Swedish National Road and Transport Research Institute (VTI)	Volvo, SAFER, Autoliv
Software	LSDYNA	MADYMO	LSDYNA	LSDYNA
Positioning tool	Not a specific one. Need to perform a simulation for adjusting the posture of the model	Manual definition of the initial angles of the joints	Not a specific one. Need to perform a simulation for adjusting the posture of the model	Not a specific one. Need to perform a simulation for adjusting the posture of the model. NEW TOOL INCOMING
Injury reports	Bone fracture, ligament rupture, brain injury, and internal organ injury	Injury criteria related to accelerations and forces	Not sure	Rib cage fracture model, Brain strain model, Spine model. Not sure if it has ligament or muscle rupture predictors.
Validation	Reports with PMHS for both the mechanical model and the active muscle model, not real motion with volunteers	PMHS	Female PMHS tests	Validation with real volunteers was developed. Originally based on THUMS.

In order to be able to study the load cases with the selected HBMs, the testing subjects were selected by the specific anthropometry criteria which represents a 50th -percentile male THUMS HBM and 50th -percentile female ViVA HBM as follows:

- 50% male THUMS HBM = height: 178.6 cm and weight=78.5 kg
- 50% female VIVA HBM = height: 161.6 cm and weight=62.7 kg

To be able to identify the most relevant and most frequently occurring accidents and to still focus on the standardised protocols, an accidentology study and a review of the Euro NCAP protocols has been performed. From the created database [3], [4], two load cases have been studied (Figure 1):

- Urban Rear-end: Target vehicle braking in front of the following EGO (vehicle to be affected, studied) vehicle on a straight road.
- Urban Crossing: Target vehicle crossing in front of EGO vehicle at a junction from the right side.

Figure 1: Load cases: rear-end (left; EGO vehicle - black) and crossing (right; EGO vehicle - black)

The ISOP project is focused on a combination of all of the above-mentioned aspects with the goal of understanding the influence of the occupant's repositioning and muscle activation response on the safety of today's vehicles by means of a series of volunteer tests which will be compared with THUMS and ViVA human body models in the next project phase.

METHODOLOGY

Safety feasibility study

To analyse the safety conditions of the testing environment, a simulation-based feasibility study was completed. The first part of the study consisted of the definition of the braking manoeuvre deceleration pulse. It was estimated that a current modern car can generate a maximum sustained braking force of around 1g [9.8 m/s2]. Some even more advanced models can reach 1.1g by helping the occupant to brake by increasing the hydraulic braking pressure when a hard braking manoeuvre is detected. For simplification and to ensure the repeatability of the tests, the maximum deceleration for this analysis was set at 1g. In addition, the deceleration jerk or brake gradient was set at 66 m/s3 representing the average deceleration jerk for a generic AEB pulse. The resulting pulse is shown on Figure 2.

For simulation purposes, pre-crash manoeuvres are defined in negative time as the theoretical crash is defined to start at time 0. The test is estimated to be performed at around 70 km/h. If a car applies the mentioned deceleration pulse at that velocity, the evolution of the velocity can be seen on Figure 3.
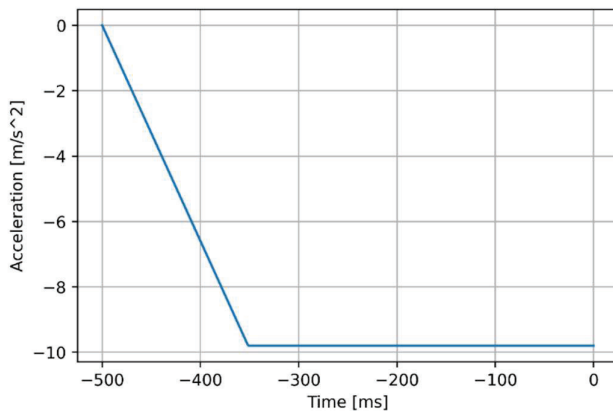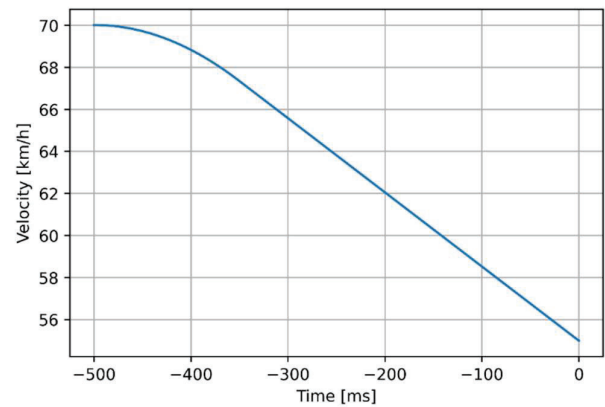

Figure 2: Deceleration pulse

Figure 3: Braking velocity from 70km/h

To simulate the full 3-second pre-crash manoeuvre without using excessive computational resources, a Madymo model was used. [2] Madymo is a multibody-based simulation software designed for developing crash simulation analysis. The software also counts with HBMs with active musculature that make it possible to recreate real human behaviour during a pre-crash or in-crash phase using less computational time than a finite element solver like LS-Dyna. The model used for this study was developed in the OSCCAR project in which a generic car environment was developed [2].

The HBM was placed on the passenger side to recreate the volunteer tests and the deceleration pulse was applied to study the displacement of the body of the model and the possible injuries that could be produced due to the braking manoeuvre. In these conditions, the maximum head displacement was 16.5 cm forward and it occurred at -2.28s. The maximum knee forward displacement was 2cm and occurred at -2.61s.
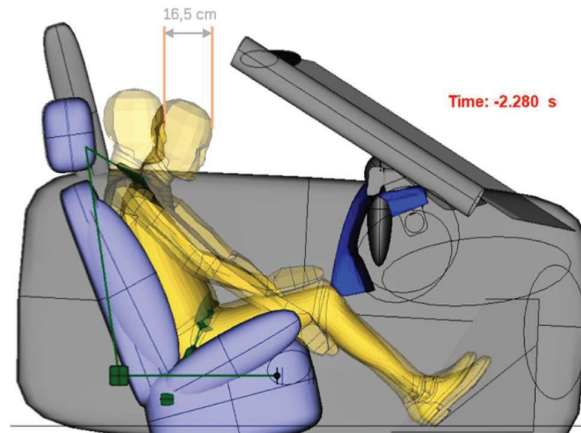

Figure 4: Madymo feasibility study. Head maximum forward displacement 16.5 cm.

Regarding injury criteria, no relevant injuries were found during the simulation. The following table summarises the most relevant injury risk predictors obtained from simulation.

Table 2.
Predicted injury for the AEB manoeuvre

Injury criteria	Value	Probability of AIS2+ injury
HIC15	0,04438	0,00%
Head 3 ms (m/s^2)	15,21	-
Neck peak tension (N)	98,139	-
Chest deflection (m)	0,00276	0,02%
Shoulder belt B3 (N)	382,81	-
Lap belt B5 (N)	208,68	0,00%
Lap belt B6 (N)	201,96	0,00%

According to the predicted values, if the passenger is properly seated and enough room for head and knee displacement is provided, hard impact against the car interior is unlikely to happen, resulting in no injury. This result is as expected as active safety systems have been designed to not generate any injuries and concentrate in avoiding or mitigating the crash event.

Definition of the test
In the first stage of the study, the frontal impact load case was selected (Figure 1). The volunteer tests were conducted at IDIADA's proving ground facility which can be seen on Figure 5.

Figure 5: IDIADA Headquarters Proving ground (L'Albornar, Spain)

The main goal of these volunteer tests was to create a database of EMG (Electromyography) signals and tracking information relative to the unexpected reaction of the participants to the frontal impact which later will be analysed by means of simulations using HBM. In order to achieve a "surprise" reaction from the participants, the test was set up as a test of comfort and confidence in an automated car depending on the distance between vehicles.

In the test, two consecutive cars made laps in the area shown in the Figure 5. At each lap, the distance between these cars varied, while the participant reported the safety and comfort feelings. The EGO vehicle was driven on the proving ground by professional driver and the volunteer was positioned in the front passenger seat. The volunteer was instrumented with EMG sensors and was being tracked by a series of 2 cameras in order to calculate the final occupant position just before the crash event.

A visual obstacle, balloon car, was placed in the way of the EGO vehicle's route. On the fourth/fifth lap the cut-out maneuver was performed and close to crash event took place. The maneuver can be seen in the Figure 6. The safety of the volunteers was studied by means of feasibility study as previously described.
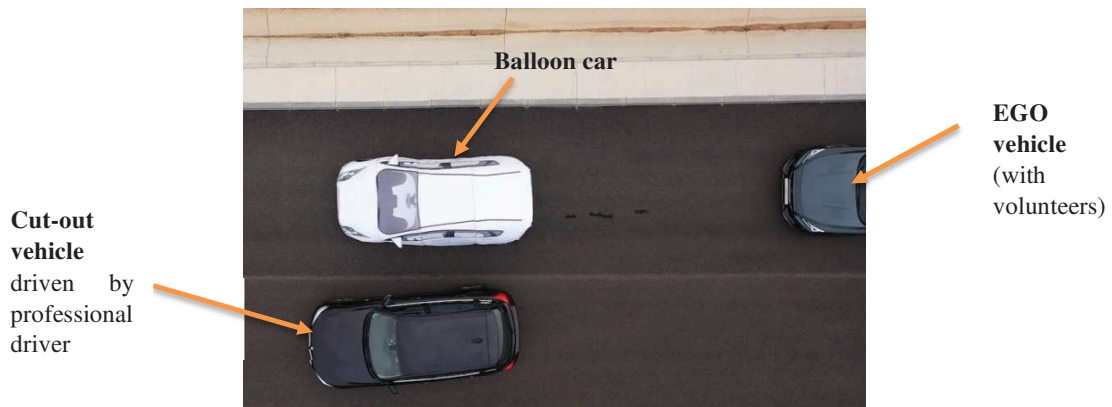

Figure 6: Cut-out manoeuvre

The initial velocity of the vehicle was set to 70km/h. A generic deceleration pulse was generated based on three parameters as described in Figure 7:

- A = Pulse activation time. A time of 500 ms was used for the generic pulse as shown in Figure 2.
- B = Brake gradient. A value of 66 m/s^3 was used.
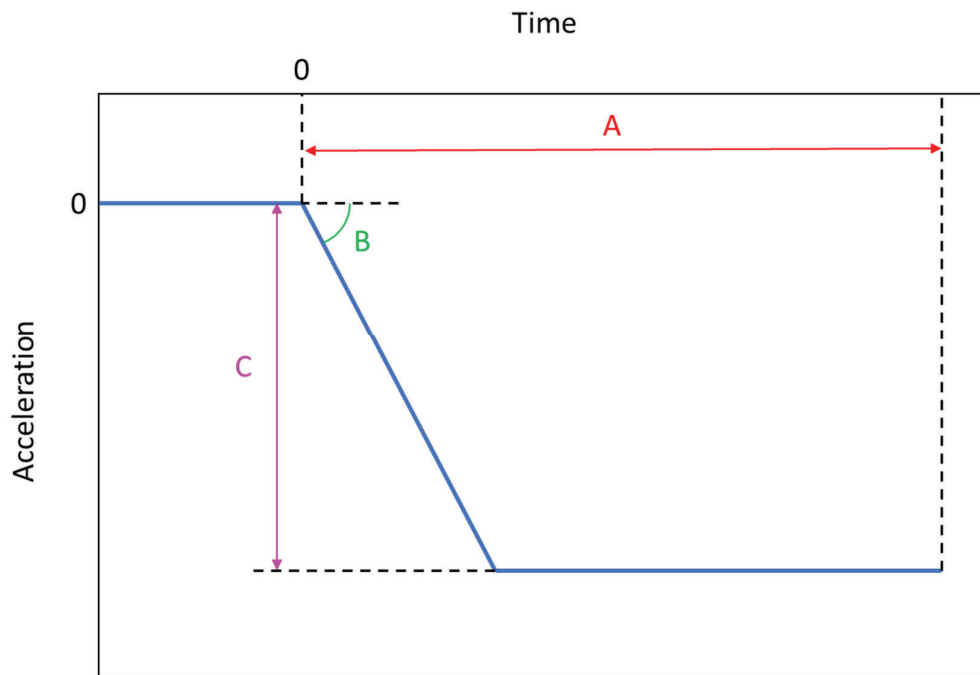- C = Maximum brake acceleration. 1 g was used as described previously.

Figure 7: Generic braking pulse diagram

An important factor in the tests, to be able to compare the participants' reactions, both in terms of motion tracking and muscle activation, was the repeatability of the braking manoeuvre.

In order to achieve similar deceleration values, the driver of the test vehicle practised the manoeuvre several times until the differences between rounds were reduced as much as possible. In addition, visual reference points were installed on the proving ground to facilitate this task.

Test preparation
Electromyography

EMG sensors are designed to monitor muscular activity. In the case of the ISOP study, the muscle activation of a volunteer was measured during the pre-crash event. The sensors and the methodology applied were in accordance with the European SENIAM project [5].

EMG sensors connected to electrodes placed on the skin surface over the corresponding muscle were used to collect the physiological signals. These were connected to the Channel Hub device, with capacity for 8 inputs. A total of 2 Channel Hubs and 16 EMG sensors were being used in all volunteer tests.

Figure 8: EMG sensors placement on neck

Table 3 lists the 16 muscles being monitored in the trunk and neck region, which were considered to be the most significant muscles for this type of study, according to the study done with active HBM subjected to a pre-crash scenario simulation. Upper and lower extremities were not included in the study due to the test limitations.

Table 3.
Muscle selection for the study

Body part	Sensor	Muscle	Primary motion	Secondary motion
Trunk	1	Erector spinae left	Spinal column extension	
	2	Erector spinae right	Spinal column extension	
	3	Rectus abdominis right	Spinal column flexion	
	4	Rectus abdominis left	Spinal column flexion	
	5	Medial external obliques right	Spinal column flexion	Lateral trunk flexion
	6	Medial external obliques left	Spinal column flexion	Lateral trunk flexion
	7	Lateral external obliques right	Lateral trunk flexion	Spinal column flexion
	8	Lateral external obliques left	Lateral trunk flexion	Spinal column flexion
Neck	9	Splenius Capitis left	Neck extension	Lateral neck flexion
	10	Splenius Capitis right	Neck extension	Lateral neck flexion
	11	Splenius Cervicis left	Neck extension	Lateral neck flexion
	12	Splenius Cervicis right	Neck extension	Lateral neck flexion
	13	Sternocleidomastoid left	Neck anterior flexion	Lateral neck flexion
	14	Sternocleidomastoid right	Neck anterior flexion	Lateral neck flexion
	15	Scalenus anterior/posterior right	Lateral neck flexion	
	16	Scalenus anterior/posterior left	Lateral neck flexion	

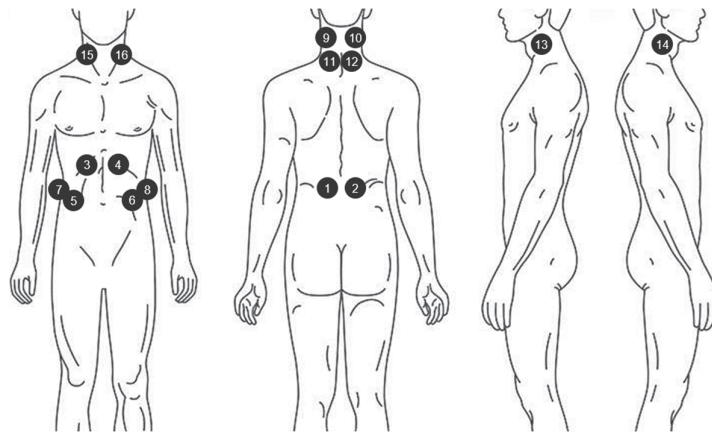Placement of the sensors is shown in Figure 9.

Figure 9: Volunteer EMG instrumentation

A calibration process was done with each participant to find the Maximal Voluntary Contraction (MVC) levels. To find the MVC value of each muscle group, specific physical exercises were performed. Figure 10 shows the calibration exercises for the trunk muscles and Figure 11 shows the calibration exercises for the neck muscles.

Figure 10: Calibration exercise for MVC of rectus abdominis (a), obliquus externus (b) and erector spinae (c)

Figure 11:Calibration exercises for MVC of splenius capitis, splenius cervicis, sternocleidomastoid and scalenus

Trunk contraction exercises lasted 3 to 5 seconds and were repeated four times. Each exercise analyses a single muscle.

For the neck, the procedure was the same, but all the muscles were analysed simultaneously in each exercise. In this case, the help of a person was needed to make the different points of force with the hands so that the participant could apply resistance and activate the musculature.

From the obtained values, the highest value in each case was marked as MVC. To be able to make a later comparison with the HBM this value corresponds to a number 1, being the maximum muscular activation and 0 the total relaxation.

For further analysis, data was exported, and the transfer function was applied (Equation 1).

$$EMG(V) = \frac{\left(\frac{ADC}{2^n} - \frac{1}{2}\right) * VCC}{G_{EMG}}$$ Equation 1 [14]

- ADC   Raw data imported
- n = 16   Number of channel bits
- VCC = 3 V   Operating voltage
- GEMG = 1000   Sensor gain

The results are shown in mV which is just multiplication of the EMG(V) by 1000.

iMotions
iMotions software was installed for data collection in the vehicle during the testing with participants. iMotions is an integrated analysis platform made to execute human behaviour research. In this project it served to process and synchronize all data from Open Signals and camera signals.

Open Signals software reads data collected from 16 EMG sensors. This software was integrated into iMotions. Although iMotions displays plotted data at a frequency of 20Hz it recorded it at a frequency of 1000Hz. Sensor cables and Channel Hubbs were taped to the participant's body with medical tape to minimize noise. The data obtained were consistent and synchronized with the recordings obtained by AXIS cameras and can be seen in Figure 12.
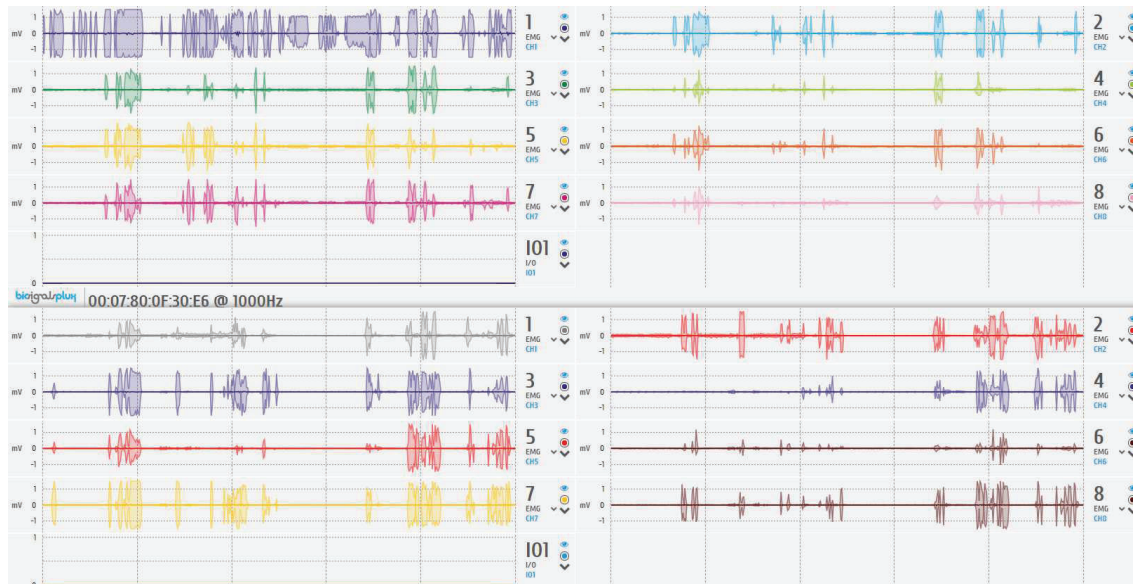
Figure 12: Example of Open Signals data collection from 16 EMG sensors

Tracking

To be able to obtain the exact position of the critical body regions at T0, a tracking system was implemented in the vehicle. The interior of the vehicle was measured with Krypton measuring system and targets were put to the key points for tracking as can be seen in Figure 13.

A system of 2 high-speed cameras was placed in the interior of the vehicle in order to video record the following targets: shoulder, elbow, wrist, hip, knee and head on the left side of the participant. The targets were white ping pong balls placed on the exact location. The cameras were synchronized with the EMG data by triggering a flash.
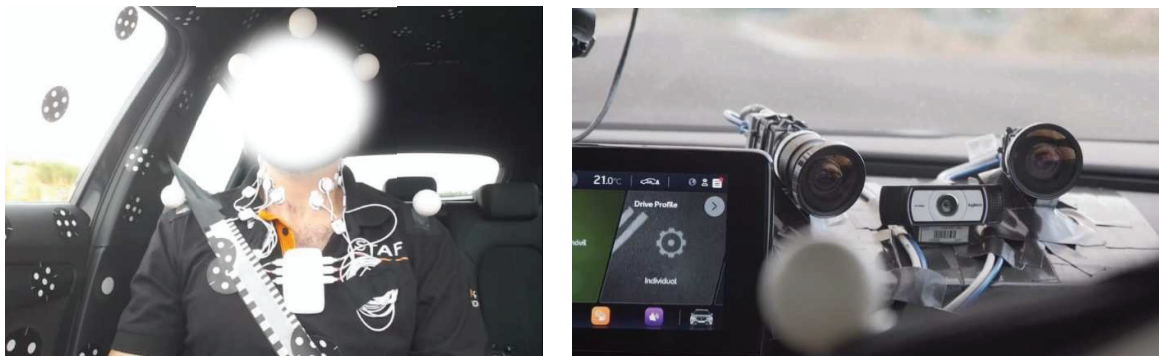

Figure 13: Right: Tracking targets on vehicle, seat belt and volunteer; left: system of 2 high-speed cameras

Key points:
- Head: 3 tracking balls (2 lateral, 1 front of the head)
- Shoulders: left and right
- Lap belt: left and right (submarining analysis)
- Wrist: left and right (global movement analysis)

Figure 14: Tracking targets on volunteer

CANape
GPS data from the EGO vehicle and the support vehicle were collected in both iMotions and CANape. CANape allows exporting mf4 files for analysis with the ADAS department tools.
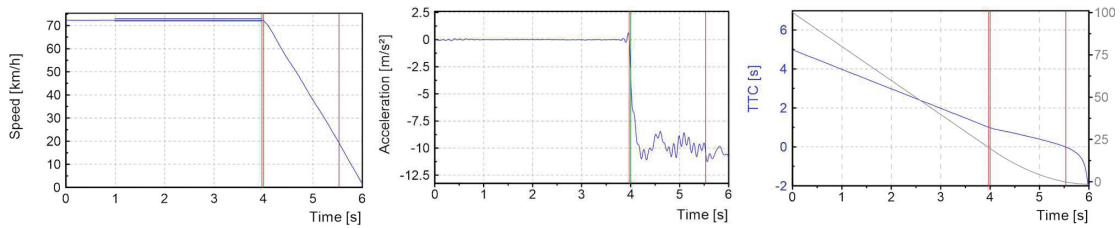

Figure 15: CANape signals (left: speed; middle: acceleration; right: TimeToCollision)

Positioning of the seat and volunteers
The seat was adjusted to a position which was considered to be the most common and still comfortable for both 50% male and 50% female occupant. This position was measured, and the seat was put on exact point by means of 3D positioning tools. The seat back angle was not altered neither the fore-aft position of the seat during or between the tests. The seat back angle was set to a standard 22.5° and the seat was set to the mid-fore-aft position and mid-height. The correctness of the testing position was controlled visually by checking the marking on both seat and floor as can be seen on Figure 16.

Figure 16: Fixed seat adjustment: mid-mid, 25° seat back angle

TEST RESULTS
The participants were selected according to the anthropometry which would be the most suitable to represent the THUMS 50% male HBM and ViVA 50% female HBM. The tolerance was set to +/-2kg of weight and +/-5cm of height. Table 4 represents the volunteer selection for the study.

	Sex	Weight	Height
Participant 1	M	OK	OK
Participant 2	M	OK	OK
Participant 3	F	OK	OK
Participant 4	M	OK	OK
Participant 5	M	OK	OK
Participant 6	M	OK	OK
Participant 7	F	OK	OK
Participant 8	M	OK	OK
Participant 9	M	OK	OK
Participant 10	M	OK	OK

Each test was performed with the 3 main investigation points: muscle activation, tracking and information about the vehicle. Table 5 shows the evolution of the tests, where some of the measured quantities failed.

Table 5: Tests database

	Sex	iMotions	CANape	Tracking
Participant 1	**M**	NOK	NOK	NOK
Participant 2	**M**	OK	OK	OK
Participant 3	**F**	OK	OK	NOK
Participant 4	**M**	OK	OK	OK
Participant 5	**M**	OK	NOK	NOK
Participant 6	**M**	OK	OK	NOK
Participant 7	**F**	OK	OK	NOK
Participant 8	**M**	OK	OK	OK
Participant 9	**M**	OK	OK	OK
Participant 10	**M**	NOK	NOK	NOK

Out of the 10 volunteer tests, only 4 could be subjected to the whole spectrum analysis.

EMG analysis
Muscle activation data was collected during the braking manoeuvre. The following graphs show an example of the muscle activation collected from Participant 3.
In Figure 17 can be seen the activation of the neck and activation of the trunk. Analysing the EMG signals together with the video / tracking analysis, the following could be concluded. During the first moments of the braking event, the volunteer was moved towards the interior of the vehicle, activating the neck muscles. Following movement was bracing towards the seat back activating the trunk muscles. The whole sequence can be seen on Figure 18.
All participants showed consistency in the muscle activation with what is perceived through the video, so with this preliminary analysis, we can consider that the data acquired will be able to provide valuable information on the occupant's behaviour.
One drawback that was observed is that the muscle activation arrived with a delay of approximately 1 second. This problem will have to be solved in further tests in order to have an exact synchronisation.
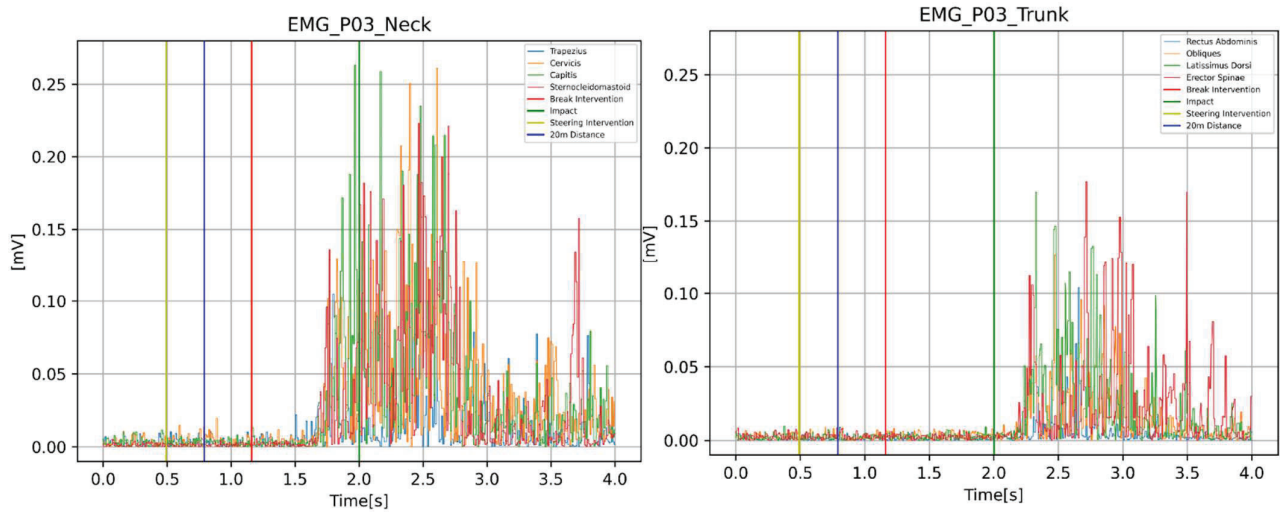
Figure 17: EMG neck and trunk signals from volunteer n.3

T = 0s   T = 2s   T=3s

Figure 18: Video sequence analysis of volunteer n.3: left = relaxed, middle = neck activation + forward movement, right = trunk activation + rearward movement

Video tracking analysis

The Tracking analysis consisted in a dynamic photogrammetry measurements, a mathematical calculation methodology using images from video as source of information. For the 3D analysis, 2 calibrated cameras were needed, measuring 3D reference and targets. The camera calibration transformed the image into a bounded plane where all the pixels/image points were geometrically controlled.
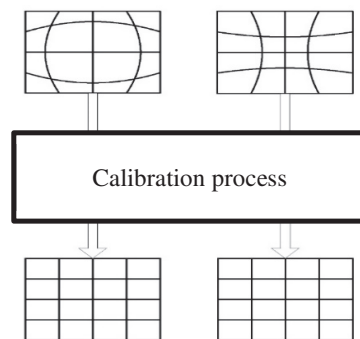

Figure 19: Video calibration process

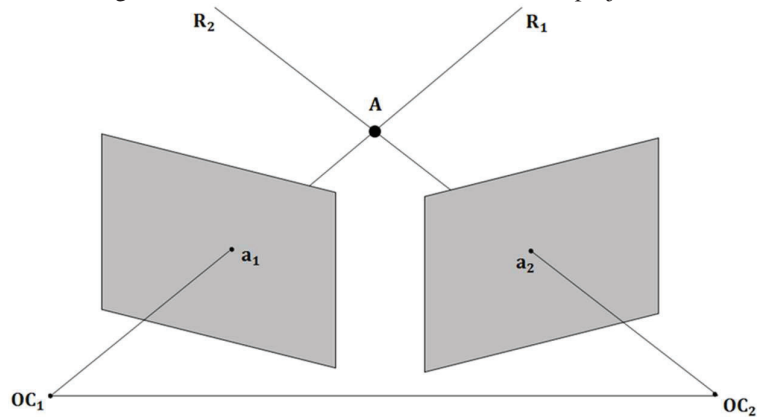Those cameras need 15-30 degrees between them in order to intersect their projections onto the image plane.

Figure 20: Projection onto the image plane

OC1:   Optical center of camera 1
OC2:   Optical center of camera 2
R1:   Target projection from optical center onto image planes
R2:   Target projection from optical center onto image planes
A1:   2D position in camera 1 plane
A2:   2D position in camera 2 plane
A: Target 3D position

The interior of the car was full of measured 3D targets to be used as reference, defining the coordinate system and avoiding the camera vibrations because those targets were also tracked.

Figure 21: Measurement of the hard points (in the vehicle interior) and movable targets (on participant)

The final step of this phase of the project is to combine the EMG data with the video analysis and calculate the maximum displacement of the volunteer after applying the pre-crash braking.

NEXT STEPS
All the data from the volunteer testing will be analyzed in next months and from the preliminary analysis already done, the need of more statistically significant valid test sample has been identified.
The scope of the project ISOP is not limited only to the volunteer testing, but as was mentioned earlier in the paper, simulations with THUMS and ViVA HBMs are on-going and the results will be available in following months. The goal is to understand the influence of the pre-crash maneuvers on the safety of the current state-of-the art restraint systems.
In the previous phase of the project, several tests were performed in IDIADA's driving simulator which will be analyzed and compared with the volunteer testing in the proving ground. Both testing protocols are following the same methodology.

LIMITATIONS

Injury risk evaluation with ATDs (Anthropometric Test Devices) is being used in crash testing protocols and for the development of safety systems for decades and builds a common and accepted base in the industry as well as legislation for the assessment of occupant safety.

However, ATDs are not validated nor developed for being subjected to the pre-crash manoeuvres or new seating configurations such as reclined positions. Moreover, there doesn't exist any ATD with muscle activation, which is essential while investigating engagement of the occupant in the pre-crash and in-crash phase.

In contrast to ATDs, some virtual HBMs (human body models) realistically represent the anatomic structure of the human including bones, flesh, skin, fat, and soft tissue. The high model detail allows a direct assessment of the injury risk based on the damage applied to the respective body region (e.g., in form of stress or strain), assuming a correct damage prediction of the model. However, human body models are not yet validated and are still under the study and development.

During the study, several limitations connected to the methodology were identified, such as reliable tracking system, data collection system, etc. and therefore for the next volunteer testing, new systems will be evaluated and selected.

CONCLUSIONS

Nowadays, the emphasis is done not only to minimize the fatalities or to lower the severity of the injuries during the crash events but also to prevent the impacts from occurring at all. These pre-crash systems and manoeuvres however are altering the optimal position of the occupant to which the state-of-the art restraint systems are developed.

The active response of the occupant to unexpected impact can result in decreasing the effectiveness of the state-of-the art restraint systems. Therefore, it is essential to understand the scope of this influence.

IDIADA has been working on creating the protocols for testing with volunteers in proving ground as well as in the driving simulator in order to create a database with information from EMG data collection, tracking data and vehicle manoeuvre data. Once the protocols have been created and validated, several tests have been performed with volunteers representing 50% male and 50% female occupants.

The project ISOP has established a methodology for pre-crash manoeuvre testing which could be later used to enlarge the database and to add even more anthropometries in order to cover most of the population.

A safety feasibility study using MADYMO HBM showed that with the deceleration of 1g, the expected forward displacement of the passenger is about 17cm. This value will be compared in the next phase of the study with the data from tracking analysis.

From the performed test it is clear that new technologies need to be explored for more reliable data acquisition.

ACKNOWLEDGEMENTS

REFERENCES

[1] Krašna, Simon; Dordevic, Srdan. Estimating the Effects of Awareness on Neck-Muscle Loading in Frontal Impacts with EMG and MC Sensors. Sensors, 2020.

[2] Jakobsson L., F. A. (2018). Test Case Matrix and selecting Demonstrator Test Cases; Deliverable D2.1, OSCCAR Project, Grant Agreement No. 768947.

[3] IDIADA Human Factor. Accidentology study. Proyecto EVADE, 2021.

[4] Scanlon JM, Kusano KD, Gabler HC Analysis of Driver Evasive Maneuvering Prior to Intersection Crashes Using Event Data Recorders Traffic Inj Prev 2015 16 Suppl 2 S 182 S 189 doi 10 1080 15389588 2015 1066500

[5] Dr. ir. H.J. Hermens; ir. B Freriks. Seniam Project. <http://www.seniam.org/>

[6] Toyota Motor Corporation. THUMS. Toyota. <https://www.toyota.co.jp/thums/about/>

[7] Kato, Daichi; Nakahira, Yuko; Atsumi, Noritoshi; Iwamoto, Masami. Development of human-body model THUMS Version 6 containing muscle controllers and application to injury analysis in frontal collision after brake deceleration. A: IRCOBI Conference, 2018.

[8] Lara, Antonio; Skvarce, Jeffrey; Feifel, Harald; Wagner, Michael; Tengeiji, Toshihisa. Harmonized pre-crash scenarios for reaching global vision zero. 26th International Technical Conference on the Enhanced Safety of Vehicles, 2019. <https://www-esv.nhtsa.dot.gov/Proceedings/26/26ESV-000110.pdf>

[9] Robles Pérez, Juan Miguel. Investigació d'accidents de circulación. Barcelona: Diputació de Barcelona. https://repositori-dsf.diba.cat/public_resources/wiki_prod/manuals_basics/091IAC/003.html>

[10] Krašna, Simon; Dordevic, Srdan; Hribernik, Marija; Trajkovski, Ana. A novel approach to measuring muscle mechanics in vehicle collision conditions. *Sensors*, 2017.

[11] Hu, Jingwen, Zhang, Kai; Fanta, Abeselom; L.H. Jones, Monica; P. Reed, Matthew. Stature and body shape effects on driver injury risks in frontal crashes: a parametric human modelling study. A: *IRCOBI Conference Proceedings*. 2017.

[12] Huber, Ludwig. *Validation and qualification in analytical laboratories*. Informa healthcare, 2007.

[13] Gallagher, Sean; Pollard, Jonisha; Porter, William L. Electromyography of the thigh muscles during lifting tasks in kneeling and squatting postures. *Ergonomics*, 2011.

[14] https://support.pluxbiosignals.com/wp-content/uploads/2021/10/biosignalsplux-Electromyography-EMG-Datasheet.pdf